Manipulating Sodium Caseinate Behaviour at the Interface:

Applications for

Concentrated Emulsion Formulation

By

Mario Jesús Alayón Marichal

A thesis
submitted to Victoria University of Wellington
in fulfilment of the requirement for the degree of
Doctor of Philosophy
in Chemistry

Victoria University of Wellington

2014

Abstract

The effect of ionic strength, pH and droplet size distribution on the stability and rheological properties of concentrated emulsions formed using sodium caseinate was investigated. The emulsions were formulated with soybean oil concentration between 50 and 70 wt% and 1 wt% protein. In order to understand the role and response of the sodium caseinate interfacial thin film to physicochemical changes to the continuous phase the behaviour of sodium caseinate at the air-water and oil-water interfaces, as a function of pH and ionic strength, was studied using Langmuir trough, surface potential and pendant drop methods. Changes in measured system response can be explained by considering changes to protein conformation. Upon increasing ionic strength the data fit with the protein conformation changing from those states where the protein extends into the aqueous phase to those where it essentially lies flat on the interface. Aggregation and dispersion of the protein at the interfaces were detected at different pH values. Also, the buffer capacity of sodium caseinate was evaluated by preparing protein solutions at different pH and ionic strengths. Bridging flocculation and creaming occurred in the emulsions investigated, evaluated via static light scattering and Cryo-SEM. Emulsions with the appearance and texture of liquid-like through to gel-like were formulated by seemingly small changes to the ionic strength and pH of the aqueous phase. Shear-thinning was the flow behaviour of the emulsions with a shear dependent flow response that was function of the parameters evaluated. Time-dependent flow behaviour was detected for the emulsions at a low shear rate and they showed rheopexy behaviour. Viscoelastic properties of the emulsions and the interaction between the droplets were evaluated by strain sweep and creep-recovery tests.

Acknowledgements

While I am the author of this thesis, and I am academically responsible for its contents and conclusions, I did not get to this point by myself. There are many people I want to thank for their support since I arrived in New Zealand in 2010.

I want to begin by thanking the Riddet Institute at Massey University for providing me with the scholarship that allowed me to study in New Zealand. I particularly want to thank my supervisor, Professor Kate McGrath, for her considerable support and for giving me the opportunity to study in her research group at the MacDiarmid Institute for Advanced Materials and Nanotechnology at Victoria University of Wellington. I also want to acknowledge the assistance of my co-supervisor, Dr Aiqian Ye. I am also grateful for the assistance of the staff at the English language programme at Victoria University whose course allowed me to complete this research in English. I want to thank my PhD friend Daniel Fernandez who helped me with the statistical analysis of my data.

I have used numerous different pieces of equipment in many laboratories, particularly at Victoria University. I am grateful for the assistance of David Flynn, EMF Technician, who showed me how to use the scanning electron microscope. Sally Wiseheart and Liza Meredith have unfailing ordered all the chemicals I needed for my research. Dr Olly Pantoja, Research Fellow at Victoria University, helped me with the use of the ellipsometer, and Professor Peter Munro, from Massey University and Dr Marisabel Briceño, from Venezuela, for their suggestions about rheology.

As I carried out my work, I was aided by the support of others in my research group: Davoud Zare, Saeedeh Afsar, Natasha Munro, Riyad Mucadam, Marjorie Griffiths, William Greenbank, Mehrdad Ghahraee, Nurul Che Zaudin, Christina Efthymiou, Graham Fairweather and all the PhD student I had the opportunity to meet. Thank you especially to Davoud and Saeedeh for the Iranian tea and food every time I visited them and for their helpful advice, support and friendship.

This new goal in my live is offered to my son Gabriel Alejandro Alayon Blanco. I want to thanks all my family in my home country and my Venezuelan fiends here in Wellington, Latin community and salsa dancers for their friendship and support. Also, my kiwi friends from the running and swimming team.

Finally, I want to especially thank Antony Paltridge, who read every chapter, checked my grammar and did many of the countless corrections suggested by Professor McGrath as I kept writing in the crazy last weeks before I submitted this thesis. Many thanks for all your support during all my time here in this new land....

And finally I offer my best wishes to everyone and anyone who supported me in finishing this project: ¡Muchas gracias a todos!

Mario Alayón
March 2014

Table of contents

Chapter 1 Introduction

The formulation of emulsions requires knowledge of their components, i.e. the composition and physicochemical properties, and the interactions between them. In a basic emulsion with only three components; non-polar phase (oil), polar phase (water) and surfactant (emulsifier), its properties can be predicted once their components are characterised. For the characterisation of the oil phase it is common to use the equivalent alkane carbon number (EACN), while for the aqueous phase it is necessary to know the ionic strength and pH. Finally, surfactants can be described by their hydrophile lipophile balance (HLB) that is the affinity of the surfactant molecules for the polar or non-polar phase. When proteins are used as emulsifiers, their characterisation is complex because their conformation and properties are very sensitive to the environment in which they are located. The characterisation of protein molecules is crucial when they are used to formulate concentrated emulsions; this is because the interactions between droplets from a practical perspective control the properties of the system. The interactions between droplets are a consequence of the protein molecules adsorbed at the interface and their properties. Consequently, a systematic study of the protein molecule at the interface is required to predict and control the properties of the concentrated emulsions to be formulated.

Investigation of the protein molecules at the oil-water interface in an emulsion has a major limitation in that there are not techniques that allow the interface to be studied directly in situ. Therefore, different interfacial techniques have to be used to gain information about the conformation and properties of the protein at the interface so that this information can be used to understand and control the properties of a concentrated emulsion. The work outlined in this thesis seeks to understand the conformation and properties of sodium caseinate at the interfaces (air-water and oil-water) under different ionic strength and pH conditions. Also, investigation of the behaviour of sodium caseinate with buffer solutions at different ionic strength and pH values was undertaken. Subsequently, sodium caseinate concentrated emulsions were formulated and their stability and rheological properties understood using information about sodium caseinate at the different interfaces and their behaviour

when different buffer solutions with different ionic strength and pH values were used in their formulation.

Outlined below is the key known information described and discussed in this thesis.

1.1 Emulsions

An emulsion is a system that consists of two immiscible phases, where one phase is dispersed in a second phase by adding energy and emulsifier molecules. One of the phases exists as discrete droplets in suspension (dispersed phase) in the second continuous phase. The interfacial layer between the two phases is stabilised by the presence of surface active molecules known as emulsifiers such as surfactants, polymers, proteins, solid particles or their mixtures [1, 2]. Figure 1.1 represents the formation of an emulsion, where water and oil are the continuous and dispersed phases respectively.

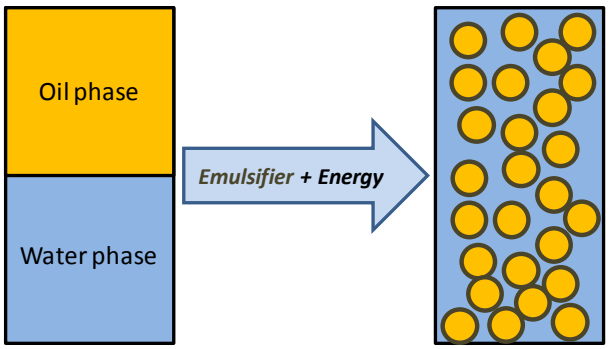

Figure 1.1 Schematic diagram of the formation of an oil-in-water emulsion.

1.1.1 Emulsion classification

Emulsions can be classified by their oil and water configuration and the concentration of the internal phase. There are three main configurations of the oil and water phase that are important in the food industry, as shown in Figure 1.2. The first configuration is oil-in-water (o/w) emulsions, where droplets of oil are suspended in an aqueous continuous phase. These o/w emulsions are the most versatile type of emulsions and their properties can be controlled by varying the emulsifiers, the components present in the aqueous phase and the oil. By way of comparison, water-in-oil (w/o) emulsions consist of droplets of water suspended in an oil phase. The

third configuration of emulsions is water-in-oil-in-water emulsions (w/o/w), which are in effect, an o/w emulsion whose droplets themselves contain water droplets. Milk, butter and some trans-dermal medicines are respectively examples of the three different emulsion configurations [1].

Depending on the volume fraction of the internal phase, emulsions can be classified as being of low internal phase ratio, where the internal phase is less than 20 wt%; medium internal phase ratio, where the internal phase is between 20 wt% and 65 wt%; and those above 70 wt% of internal phase, which are called high internal phase ratio emulsions (HIPRE) .

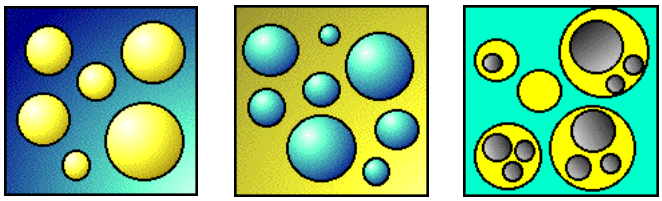

Figure 1.2 Schematic diagrams of the three emulsion configurations.

1.1.2 Emulsifiers

Emulsifiers are molecules with a structure that basically consists of two parts: one part that has a strong affinity for a polar phase, known as the hydrophilic group when the polar phase is water; while the other part has attraction for the non-polar phase (hydrophobic group). Molecules with both affinities are known as amphiphilic and their representation, as can be seen in Figure 1.3, consists of a head group (the hydrophilic part) with a tail group (the hydrophobic part).

Figure 1.3 A representation of an amphiphilic molecule at the oil-water interface.

Amphiphilic molecules have two main properties: adsorption and association (see Figure 1.4). When amphiphilic molecules are added to a system, which consists of two immiscible phases (oil-water), they have the capacity to adsorb at the interface,

forming a monolayer that is able to reduce the energy between the two phases (interfacial tension). If the quantity of amphiphilic molecules is higher than the amount necessary to saturate an interface, the excess molecules migrate to one of the phases forming associations known as micelles. The preference of amphiphilic molecules to migrate to the oil or water phase depends on the balance between the hydrophilic and hydrophobic portions of the molecules, i.e., if the major proportion of the molecules is hydrophilic the micelles will form in the water phase. On the contrary, if the major proportion of the molecules is hydrophobic, the micelles will from in the oil phase.

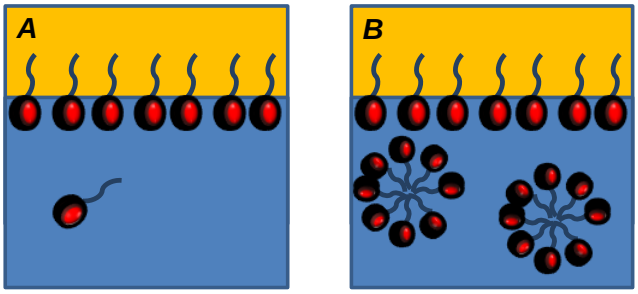

Figure 1.4 Schematic diagrams showing the properties of amphiphilic molecules. (A) Adsorption and (B) association (micelles).

In emulsions, the emulsifier is present at the interface between the droplet and the continuous phase, and the properties of the bulk system depend on the characteristics of the emulsifier and the physicochemical environment of the continuous phase [4]. The emulsifiers can be non-ionic, cationic, anionic, polymers and proteins. Some of the physicochemical parameters that can be changed in an emulsion are pH, ionic strength and temperature.

Two methods can be used to evaluate the behaviour of the emulsifier at the air-water and oil-water interfaces: Langmuir monolayer and interfacial tension, respectively.

1.2 Langmuir monolayers

When monomolecular insoluble films are formed on the surface of a liquid, they are known as Langmuir monolayers. Amphiphilic molecules are essentially the kind of compounds used to produce monolayers and they can adsorb at the interface where they are located to satisfy their double affinity for both phases, polar (water) and non-polar (air or oil) phases respectively [5].

Langmuir monolayers are excellent model systems for investigating amphiphilic molecules in two dimensions. When the interfaces are air and water, the condensed phase surface (water) provides an ideal smooth substrate while two thermodynamic variables, temperature and surface pressure, can be directly controlled. The interfacial area, where the molecules are adsorbed, can be modified by moving a barrier along the surface. As a consequence, the surface pressure is varied and the different phases of the monolayers can be studied, i.e. gas, liquid and solid. Moreover, the intra-monolayer and the monolayer-subphase interactions can be varied significantly by changing the chemical structure of the head or tail parts of the amphiphilic molecule, or by changing the physicochemical properties of the aqueous subphase such as pH and ionic strength [5].

The direct information obtained by studying Langmuir monolayers is the determination of surface pressure-area isotherms. The surface pressure (π) is the difference between the surface tension of the aqueous phase (γ_0) and the surface tension of the surface covered by the monolayer (γ).

$$\pi = \gamma_0 - \gamma. \qquad 1.1$$

1.2.1 States of a Langmuir monolayer

Considering the inset diagram, (Figure 1.5) the sharp break at the first plateau is the onset of condensation into a liquid. The plateau represents two-phase co-existence, i.e., gas plus liquid. Further compression of the monolayers results in the formation of the liquid expanded phase (denoted LE or L_1). The LE one-phase region extends from the end of the first plateau to the start of the second. At this point, a phase transition takes place into another condensed phase known as the liquid-condensed phase (LC or L_2).

A plateau indicates a first-order phase transition where the LE and LC phases co-exist. The plateau is not perfectly horizontal in many systems and for many monolayers the LE-LC transition is lost when the temperature decreases as Gehlert *et al*.[6], and others have shown [7, 8].

Increasing the surface pressure of the monolayer after the LC state produces a change in the slope or a small kink. This feature can be interpreted as a transition

from the LC phase to a solid phase. In smaller areas, the monolayer is a two-dimensional crystalline solid with a structure related to that of the three-dimensional crystal [9].

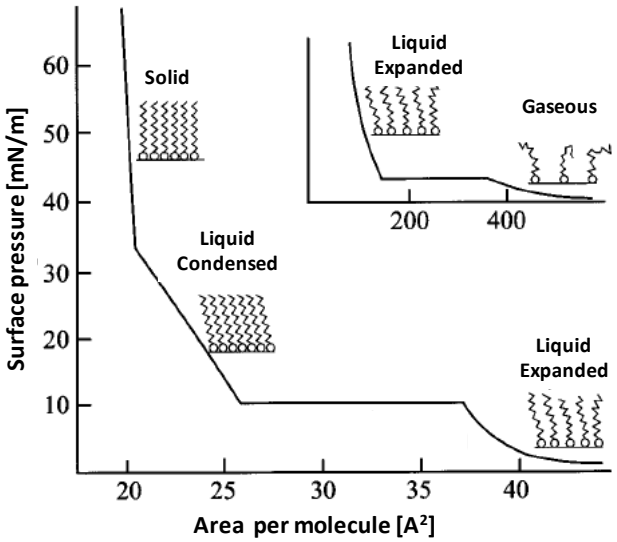

Figure 1.5. Generalised isotherm of a Langmuir monolayer [5].

When macromolecules, such as polymers and proteins, are used to produce Langmuir monolayers, commonly horizontal transition is not observed. Theoretical considerations of this behaviour have included the formation of small molecular aggregates of surface micelles. A number of monolayer studies by Zhu *et al*., [10-13] and Hanley *et al*. [14], have been undertaken with block polyelectrolytes in order to understand surface micelle formation. For small molecular weight amphiphiles a first-order phase transition is almost always observed in the liquid state of the film with this transition being ascribed to a LE-LC process. This transition can be viewed as an incremental change in the orientation of the alkyl chains from horizontal, water-adsorbed state to a vertical, air-solubilised state.

However, this is not a realistic mechanism for macromolecules such as block polyelectrolytes and proteins [10, 15]. For these compounds a possible mechanism is the incremental increase in solubilisation of the polar part of the macromolecule into the aqueous subphase as the surface area is steadily reduced. The LE-LC transition for block polyelectrolytes has been associated with the “starfish-jellyfish” model proposed by Zhu *et al.* [11, 12]. Their starfish-jellyfish model illustrates the block copolymer shape transformation at the air-water interface with changes in the surface film. At low surface pressures, the starfish surface micelles consist, at the

core, of an aggregate of the hydrophobic part of the block copolymer with the hydrophilic part of the molecule's arms radiating outward from the core on the surface of the water. With an increase in the surface concentration via compression of the dilute surface film, the first detectable rise in pressure above baseline is observed at the point at which the branches from different surface aggregates begin to interact electrostatically or sterically. As surface compression continues, all the unoccupied space on the water surface is gradually eliminated as the hydrophilic arms are compressed. At a high surface compression, the ionic branches in the hydrophilic arms submerge into the water subphase and the surface micelles form the jellyfish shape. The starfish-jellyfish model is shown in Figure 1.6.

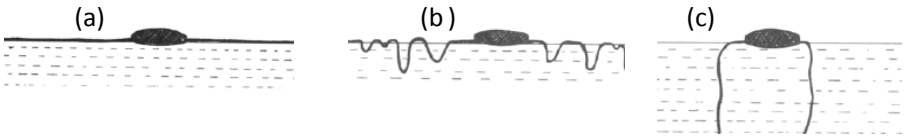

Figure 1.6. Schematic representations of a (a) starfish surface micelle, (b) partial jellyfish surface micelle, and (c) complete jellyfish surface micelle [12].

Fainerman *et al.* [16] and Israelachvili [17] presented mathematical models to predict surface micelle formation using an aggregate number as one of the variables. They demonstrated that the absence of a plateau in the phase transition of some molecule isotherms was a consequence of the aggregation of molecules at the interphase (micelles). They compared results using block polymers with their mathematic models, and found satisfactory adjustments between them. Considering that proteins are constituted by amino-acid groups, which give them the character of biological polymers, not only the aggregation of proteins can be expected at the air-water interface, but also the absence of a plateau during the transition of phases.

1.2.2 Monolayers of proteins

Monolayers of proteins at the air/water interface have been widely investigated because of their significant importance in the stabilisation of foams and emulsions in areas such as cosmetics, coating processes, pharmaceuticals, biotechnology and food technology [18]. Proteins are the most important class of food colloids and understanding their structure and physicochemical characteristics are important in food formulation. In the formulation of concentrated emulsions, the characteristics of

the emulsifier adsorbed at the interface practically controls their stability and rheology. As a consequence, a systematic study of the Langmuir monolayer of proteins with changes in the parameters that affect the chemical composition in the continuous phase could assist in understanding the interfacial behaviour of absorbed proteins, and on elucidating the relationship between interfacial characteristics and the properties of concentrated emulsions.

The capacity of protein molecules to adsorb at interfaces and produce films is a consequence of their hydrophilic-hydrophobic nature. This characteristic is due to the different residual groups that constitute the protein structures and their large size. When protein molecules are located at an interface, they achieve configurations that allow them to minimise the energy of the system. The conformation of protein molecules at the interface decreases the interfacial tension (oil/water) or superficial tension (air/water). The reduction in the tension between the two phases is basically because the non-polar side chains are predominantly directed toward the non-polar phase and the polar side chains to the aqueous phase thereby avoiding the contact between the two immiscible phases. This conformation confers a great stability on protein monolayers, since desorption of a whole molecule requires simultaneous removal of a large number of segments from the interface [19].

Using proteins as emulsifiers requires an understanding of their behaviour in different physicochemical environments. A large number of studies have been undertaken with different proteins [20-29]. Rodriguez Ma *et al.* [30-33] among others [34, 35] have presented results of the influence of pH and ionic strength on the behaviour of monolayers. Their data shows that the ionic strength and pH affect the protein and the structural and interfacial properties of the Langmuir monolayers, because of changes in the electrostatic properties of the molecules.

Surface pressure-area isotherms provide evidence of changes in monolayer structure when different subphase pH and ionic strengths are used. Complementary techniques have to be used to corroborate the surface pressure-area results, including surface potential, transmission electronic microscope (TEM) and Brewster angle microscopy. Rodríguez J *et al.* [28, 32, 33, 36] among others have used some of these techniques and they have found adequate correlative information for the surface pressure-area isotherm results.

1.3 Interfacial tension

The capacity to produce an emulsion is related to the reduction of the interfacial tension between the immiscible phases by an emulsifier. The interfacial tension can be defined as the perpendicular force that operates inwards from the boundaries of a surface to each phase, tending to decrease the area of the interface [37]. When two liquid phases separated by an interface exist, the cohesive forces between molecules in a liquid are shared with all the other molecules and the net force on the molecule is zero. The molecules at the interface do not have other like molecules surrounding them on all sides and as such they display stronger attractive forces than their similar neighbours. This imbalance of forces obliges the molecules at the interface to decrease the contact area at the interface, as shown in Figure 1.7.

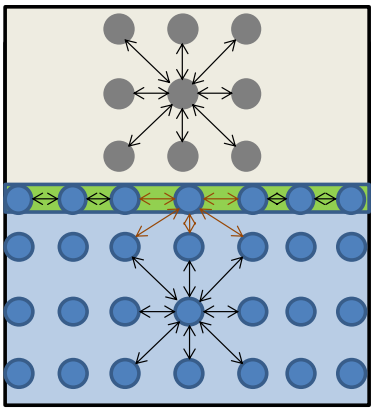

Figure 1.7. Distribution of forces on molecules inside liquid faces and interfaces (interfacial tension).

The interfacial tension values depend on the similarity between the molecules in the different phases. When the molecules are extremely similar, the interaction between them is significant and as a consequence the interfacial tension between the phases is small. In contrast, the greater the difference between the molecules in the phases, the smaller the interaction between them and the interfacial tension between the phases is bigger.

When amphiphilic molecules are added to a system of two immiscible phases the interfacial tension is reduced. The amphiphilic molecules are adsorbed at the interface and they will specifically orient themselves there. The hydrophilic group comes into the polar phase, while the hydrophobic group will move toward the non-polar phase (see Figure 1.3). When the amphiphilic molecules replace the polar/non-

polar molecules at the interface, the interactions between molecules are altered and now consist of the polar phase/hydrophilic amphiphilic part and the non-polar phase/hydrophobic amphiphilic part [38].

1.4 The properties of emulsions

Emulsions have several distinctive properties, which depend, among other parameters, on the droplet size distribution, the volume fraction of the dispersed phase, the physicochemical properties of the phases, the amphiphilic agent and method used to formulate the emulsion. Stability and rheology are the most common properties to characterise emulsions, and these properties depend on the interaction between the droplets in the system. Formation of stable emulsions requires an adequate selection of emulsifiers which create a strong and uniform layer around the droplets. Additionally, this layer has to provide the droplets with sufficient repulsive forces to keep them separated.

1.4.1 Stability of protein-based emulsions

The droplets of dispersed liquid in an emulsion are in constant motion, resulting in them undergoing frequent collisions. If on collision the interfacial film surrounding the two colliding droplets ruptures, the two droplets can coalesce to form a larger droplet, resulting in a decrease in the energy of the system. If this process continues, the dispersed phase will separate from the emulsion; in other words, it will break. The mechanical strength of the interfacial film is therefore one of the prime factors determining the stability of emulsions. For maximum mechanical stability, the interfacial film resulting from the adsorbed emulsifiers should be condensed, with strong lateral intermolecular forces, and should exhibit high film elasticity [38].

Emulsions are thermodynamically unstable and tend to decrease their energy over time by reducing the total interfacial area [39]. The lifetime of emulsions can vary considerably from one system to another; ranging from minutes to many years depending on the nature of the emulsifiers, the two phases, and their volume ratio [40]. The difference in density between the continuous and dispersed phases, the interaction between droplets, and the structure and quantity of the emulsifier are physical parameters that affect the stability of emulsions. Stable emulsions require repulsive forces to prevent droplet growth, the origin of which is the thin film residing

on the surface of the droplets. The strength of this repulsive force depends on the physical properties of the inter-droplet film, such as viscosity, or on the interfacial phenomena that occurs whenever two interfaces approach each other in the sub-micrometre range. The first class of interfacial phenomena deals with static, attractive or repulsive forces, like electrical, steric and generic entropic repulsions, while the second has to do with dynamic processes such as the streaming potential and interfacial viscosity effects, as well as more classical hydrodynamic considerations [3, 41]. These interfacial phenomena influence the rate of various processes of instability, such as creaming or sedimentation, flocculation, coalescence, Ostwald ripening, bridging and depletion flocculation. These phenomena (shown in Figure 1.8) will be described in the following sub-sections.

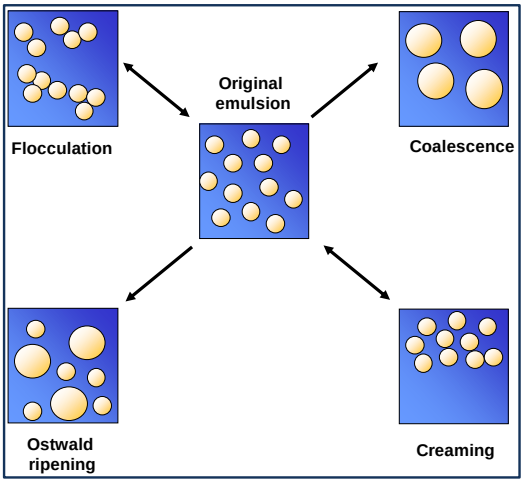

Figure 1.8.Four processes of emulsion destabilisation

1.4.1.1 Creaming

Creaming takes place when the density of the dispersed phase is lower than that of the continuous phase, and against gravity the droplets rise to the top of the system. The rate of creaming is related to Stoke's law:

$$v = \frac{2r^2(\Delta\rho)g}{9\eta_0} \qquad 1.2$$

where r is the radius of the oil droplets, $\Delta\rho$ is the difference in the densities of the phases, g is the acceleration due to gravity, η_0 is the viscosity of the medium and v is the settling velocity. Equation 1.2 can be applied to dilute emulsions with monodisperse droplets. For dilute emulsions with polydisperse droplets, the following equation can be used [42]:

$$\nu = \frac{(r^2+\sigma^2)g\Delta\rho}{18\eta_0} \quad 1.3$$

where σ is the droplet size standard deviation. Both Equations 1.2 and 1.3 can only be correctly applied to dilute emulsions where the interactions between the droplets are almost negligible. However, Equations 1.2 and 1.3 can provide information about how to change the rate of creaming in emulsions; increasing the viscosity of the medium, reducing droplet size and reducing the density difference all reduce the rate of creaming in an emulsion.

In the formulation of many emulsions droplet size and the viscosity of the medium are manipulated to reduce the rate of creaming, although of these parameters droplet size has the major influence (square factor) rather than linear as shown in equations 1.2 and 1.3. The ideal reduction of the droplet size is achieved when the creaming rate is similar to that of Brownian motion. Reducing the size of the droplets to achieve this requires the input of enormous amounts of energy [42]. Changes in the viscosity of the medium can be achieved by using thickening agents such as polysaccharides (starch, alginin, guar gum and xanthan gum) or some proteins (collagen, egg white and gelatine).

1.4.1.2 Flocculation

Flocculation is defined as the process where two or more droplets come together to form a floc. This process is facilitated by the net force of inter-droplet attraction and can generally be reversed. The properties and structure of the floc depend on the net attractive force between the droplets and the fraction of the dispersed phase, i.e., more flocs can be formed if the fraction of the dispersed phase increases. Two effects can be observed from flocculation: I) an increase in the rate of creaming because of the size of the aggregate and II) the probability of coalescence because this process is preceded by flocculation[43].

The noncovalent interactions which contribute to flocculation are van der Waals forces, electrostatic forces and steric forces. The last two are repulsive forces while the first is attractive. In o/w emulsions, the contribution of these forces depends on the kind of emulsifier and the physicochemistry of the continuous phase.

The stability of the dispersion can be estimated according to the Derjaguin, Landau, Verwey and Overbeek theory (DVLO). This theory is based on the balance between attractive van der Waals forces and the repulsive electrostatic forces. The van der Waals attraction between two oil droplets (U_{vdW}) follows the relation[42]:

$$U_{vdW} = \frac{A_H a}{12d} \qquad 1.4$$

where A_H is the Hamaker constant, a is the radius of the colloidal droplet and d is the distance between the two droplets. Note that this form of the van der Waals attraction is for two identical droplets.

The presence of a charge on the dispersed droplets constitutes an electrical barrier resisting the close approach of the two droplets to each other [38]. The electrical barrier is related to the electrostatic double-layer forces that are always present between charged particles or emulsion droplets in electrolyte solutions. Counter-ions to the emulsion droplets are attracted to the surfaces and co-ions are repelled [44]. Hence, outside the charged emulsion droplet, in the so-called diffuse layer, the concentration of ions will be different than in the bulk solution and the charge volume density of the diffuse layer balances the surface charge.

An electrostatic double-layer interaction arises when two charged droplets are so close together that their diffuse layers overlap. The electrostatic double-layer interaction, U_{dl}, for two identical charged droplets with a small electrostatic surface potential and large radius compared to their separation is approximately given by

$$U_{dl} = 2\pi r \varepsilon \varepsilon_0 \psi_0^2 \exp(-\kappa d) \qquad 1.5$$

where r is the radius of the droplets, ε_0 is the permittivity of vacuum, ε is the static dielectric constant of the medium, ψ_0 is the surface potential, d is the distance between the droplets , and κ^{-1} is the Debye screening length. The Debye screening length is given by:

$$\kappa^{-1} = \sqrt{\frac{\varepsilon_0 \varepsilon \kappa T}{1000 N_A e^2 \sum_i c_i z_i^2}} \qquad 1.6$$

where e is the charge of the electron, N_A is Avogadro's number, c_i is the concentration of ion i, T is the absolute temperature, and z_i is the valency of ion i.

The double layer interaction is repulsive and it decays exponentially with surface separation and a decay length proportional to the Debye length. Further, the Debye length, and consequently, the range of the double layer force decreases with increasing salt concentration and the valency of the ions present [45].

The net force between two droplets is given by the sum of the van der Waals and electrostatic forces. The typical shapes of attractive, repulsive and net energy between two droplets as a function of droplet separation are shown in Figure 1.9.

As can be seen in Figure 1.9 when the droplets are far enough apart there is no interaction between them. Once they start to approach each other up to a distance where the first attractive minimum exists, known as the secondary minimum, the attractive force is slightly higher than the repulsive force and the droplets form weak flocs (flocculation process). In this step, gentle shaking of the system is more than enough to separate the droplets, i.e., the process is reversible. The obstacle to forming irreversible flocs or inducing coalescence is the primary maximum. At the primary maximum the electrostatic repulsive force dominates the system and the capacity to achieve a primary minimum depends on the ionic strength of the continuous phase and the charge on the droplets. If the attractive force between droplets is higher than the primary maximum, they will reach the primary minimum and coalescence might occur if the emulsifier layer around the droplets is not significantly strong [42, 43].

The second major kind of repulsion, so-called steric repulsion, is associated with the concept of a volume or three-dimensional effect of the layer of the emulsifier that covers the droplets. Steric repulsion occurs when the emulsifiers are macromolecules such as polymers and proteins. Here the macromolecule projects loops and tails into the continuous phase and the interaction of these projections hinders the approach of emulsion droplets to each other. When two interfaces approach each other, these "protective" layers bump against each other, and the actual distance between the droplets can never reach the minimum required for the cohesion/adhesion force to take over [46].

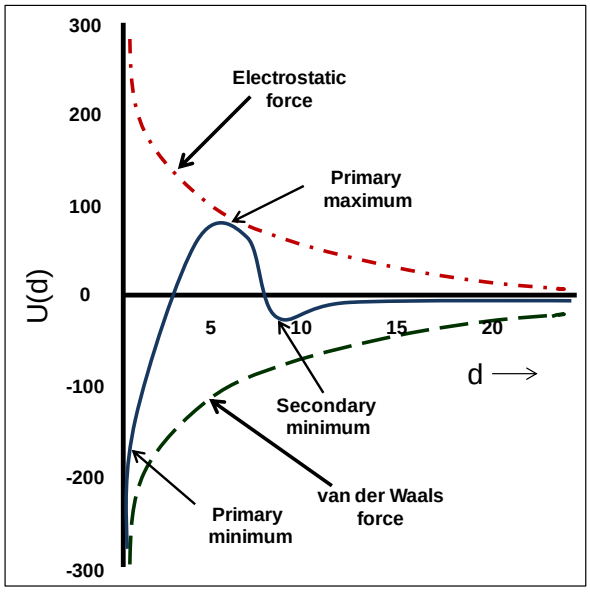

Figure 1.9. Representative form of interactions between two droplets in an emulsion.

The third generic entropic repulsion is related to the molecular organisation or degrees of freedom with respect to interactions of surfactant or polymer molecules with the solvent that changes as the two interfaces come closer. Entropic repulsions occur, for example, when polymeric amphiphilic molecules are forced to rearrange and sometimes to loose solvation as they are compressed [22].

Steric and entropic forces do not produce any effects until contact takes place between absorbed antagonist layers, at which point they can increase slowly or rapidly depending on the compressibility or elasticity of the adsorbed layer on the droplet [46].

The use of biopolymers as an emulsifier may generate two kinds of additional flocculation: depletion and bridging.

1.4.1.3 Depletion flocculation

When the quantity of an emulsifier exceeds that required to be adsorbed by the interface droplets, the non-adsorbing emulsifier in the continuous phase produces an increase in the attractive force between the droplets. The attractive force is a consequence of the osmotic pressure effect related to the exclusion of the emulsifier in excess from a narrow region around each droplet. If this force overcomes the repulsive force between the droplets, as a consequence of an increment in the

emulsifier concentration, flocculation will occur. This is the process known as depletion flocculation[47].

1.4.1.4 Bridging flocculation

Bridging flocculation can occur when the emulsifier is a biopolymer adsorbed at the droplet interface and parts of its conformation consists of loops and tails. The loops and tails can make contact with the surface of the different droplets when they are in close proximity, creating a bridge between the particles. Formation of multiple contacts of this nature will produce flocculation and increase the rate of creaming [42], Figure 1.10.

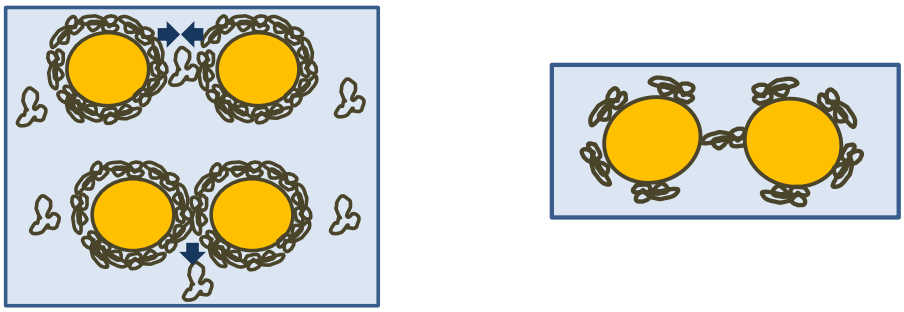

Figure 1.10.Schematic diagram of depletion (left) and bridging flocculation (right).

1.4.1.5 Coalescence

Coalescence of droplets takes place when the energy of attraction between the droplets is higher than the primary maximum energy and there is no steric repulsive force between the droplets. The first step in the coalescence process is collision of the droplets, followed by droplet deformation which produces a flat contact zone between the droplets. In the contact zone a thin liquid film exists, the properties of which control the stability of the droplets. In addition to repulsive forces, the attractive van der Waals forces are also an influencing factor.

When the attractive forces are predominant, the liquid present in the thin film drains until the film achieves a critical thickness and the droplets join together. If the repulsive forces are predominant, the droplets repel each other. The coalescence process is a function of the viscosity of the medium, the volume fraction of the dispersed phase, and the hydrodynamics of the system [48].

1.4.1.6 Ostwald ripening

Ostwald ripening consists of the preferential diffusion of the dispersed fluid out of smaller droplets into larger ones, driven by the higher Laplace pressure of small droplets [49]. Additionally, from the thermodynamic point of view, increasing the size of droplets reduces the energy of the system because of the destruction of the interfacial area [50]. The rate of droplet growth may be determined by the molecular diffusion across the continuous phase and/or by permeation across the surfactant film. Ostwald ripening can occur in two ways; constant volume rate Ω_3 (diffusion-controlled ripening) [51] or a constant surface rate Ω_2 (surface-controlled ripening) [52], depending on the origin of the transfer mechanism:

$$\frac{d\delta^{\alpha}}{dt} = \Omega_{\alpha} \qquad 1.7$$

where δ is the average droplet diameter. Diffusion-controlled ripening (α = 3) has been recognised in sub-micrometre dilute emulsions stabilised by ionic or non-ionic surfactants; so far, permeation-controlled ripening (α = 2), has been proposed to account for the coarsening of concentrated air foams.

1.4.2 Rheology of emulsions

Rheology is the study of the flow and deformation of matter. The rheological properties of materials provide information from both theoretical and practical points of view. From the theoretical point of view, rheological measurements, allied with hydrodynamic theory, can provide useful information about the structure of emulsions, and clues to their stability [53].

The practical considerations with regard to the rheological behaviour of emulsions have been motivated by the problems of industry. Industrial processes produce and consume hundreds of thousands of tonnes of emulsions annually which have different characteristics and functions. In food industries, for example, the rheological response of the products is important with respect to their appearance and texture, which are essential considerations for a consumer product [53, 54].

In Figure 1.11 is a classical example used to explain the response of a fluid to shear. Layers of fluid are contained between two solid plates that have a contact area with

the fluid represented by A. After a force (F) is applied to the upper plate the system reaches a steady condition where the layer of fluid next to the upper plate moves with the same velocity as that of the upper plate (V_2). On the contrary, in the case that slip is not present, the layer of fluid close to the lower plate is stationary. The intermediate layers move as if they were sliding on each other, and the velocity decays from the upper plate to the lower plate producing a velocity gradient, that is also known as the shear rate, or more commonly as the shear strain. The shear strain ($\dot{\gamma}$) is expressed as

$$\dot{\gamma} = \frac{dv_x}{dy} \qquad 1.8$$

where $dv_x$is the differential of velocity and dy is the differential of distance related to the layer distribution.

At the same time the plate starts to move, momentum is transferred to the fluid under the plate inducing the former to flow. The amount of momentum transferred per unit area and unit time is known as shear stress (τ), and it is written as

$$\tau = \frac{mv_x}{At} \qquad 1.9$$

where m is the mass of the layer, v_x is the velocity in the direction of the force, A is the area of the layers and t is time.

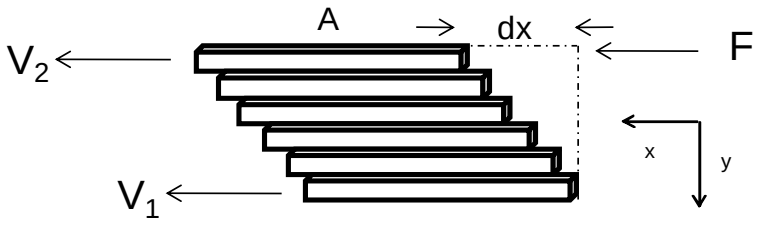

Figure 1.11. Flow velocity of a fluid when a shear is applied.

For some fluids, the amount of momentum produced by the force applied to the system is proportional to the shear strain. The constant of proportionality is called the viscosity (η). Viscosity is interpreted as the internal resistance to flow that some

fluids display under shear. The shear stress and viscosity are related in the following manner:

$$\eta = \frac{\tau}{\dot{\gamma}} \ . \qquad 1.10$$

Equation 1.10 is well-known as Newton's law. Fluids that behave according to this equation exhibit a linear relationship between τ and $\dot{\gamma}$ and they are called Newtonian fluids.

Homogeneous liquids with a low molecular weight dilute polymer solutions, dilute emulsions and dilute suspensions all obey Newton's law. On the contrary, concentrated polymer solutions or concentrated emulsions do not act according to Newton's law and they are called non-Newtonian fluids.

Elasticity is a property of solids: it describes the capacity of matter to recover its structure once the applied shear stress is withdrawn. In Figure 1.12 elastic solid behaviour is depicted.

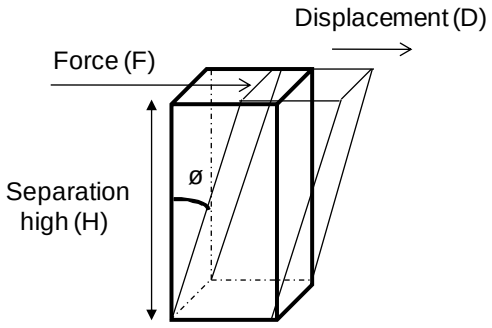

Figure 1.12. Deformation of an elastic solid as a consequence of an applied shear stress.

The relation between the displacement (D), which is produced by the shear stress, and the separation of the upper and lower part of the solid (H) is called strain (γ). The strain equation is

$$\gamma = \frac{D}{H} = \tan \emptyset. \qquad 1.11$$

The proportionality relation between shear stress and strain is characteristic of elastic solids and such solids obey Hooke's law.

$$\tau = G\gamma \qquad 1.12$$

where G is the elastic modulus.

For non-Newtonian fluids, viscosity is no longer a sufficient property to describe and understand their response to deformation because it is no longer dependant on temperature alone. The viscosity of the system now depends on factors such as strain rate, shear stress, strain, time, and confinement geometry. Under shear conditions the flow response is now called the "apparent viscosity" $\eta(\dot{\gamma})$ and it is defined as

$$\eta(\dot{\gamma}) = \frac{\tau}{\dot{\gamma}} \qquad 1.13$$

Equation 1.13 does not imply a linear relationship between shear stress τ and strain rate $\dot{\gamma}$, it only suggests that a given shear rate will bring about a given shear stress and that the viscosity for this given shear rate is calculated as in Equation 1.13.

There are five general types of flow behaviour used to describe fluids (see Figure 1.13) [44]: shear-thinning, shear-thickening, viscoplastic, thixotropic and viscoelastic. While shear-thinning or pseudoplastic fluids exhibit a decrease of viscosity under shear, shear-thickening or dilatant fluids exhibit an increase of viscosity under shear. In these fluids the intermolecular structure of the material is apparently altered under the influence of the shearing force.

The flow behaviour of viscoplastic fluids is identified by the appearance of a yield stress (τ_y), i.e., the fluid flows in a viscous manner only after a threshold has been exceeded. Below this threshold, or yield stress, the behaviour of the fluid is similar to an elastic solid and should obey Equation 1.12 when subjected to a strain or stress sweep. Concentrated emulsions and suspensions often exhibit more complex viscoplastic behaviour, without a well-defined yield. Cheng [55] mentions that the values of the yield stress depends on the observation time and shear rate applied. For thixotropic fluids the flow properties depend not only on the shear rate, but also on the length of time that the shear stress is applied. In thixotropic flow, viscosity decreases with time, and vice versa for rheopectic flow.

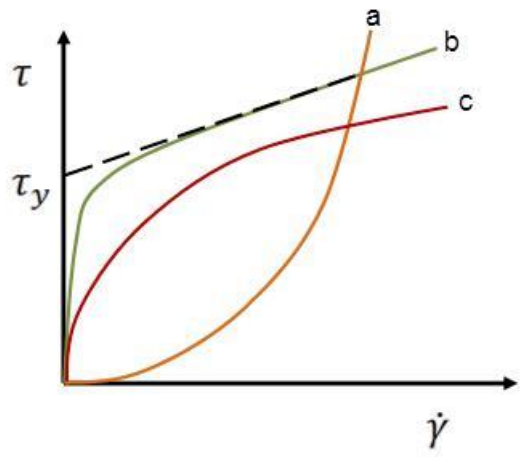

Figure 1.13. Flow behaviour. (a) Shear thickening, (b) Viscoplastic and (c) Shear thinning.

The word “viscoelastic” encompasses many fluids with behaviour which falls between the classical extremes of a Hookean elastic response and Newtonian viscous behaviour [56]. Most concentrated pastes, emulsions and gels are viscoelastic. Under minimal deformation, viscoelastic fluids behave like elastic solids but under higher deformation they flow like liquids. They can develop a variety of different behaviours as a function of shear rate.

The dispersed phase volume fraction is an important parameter for defining the viscosity of emulsions. Several equations have been developed for the prediction, for example, of the viscosity with the internal phase content. The first of these equations, used to predict the viscosity of dilute emulsions is Einstein’s law:

$$\eta(\varphi) = \eta_0(1 + 2.5\varphi) \qquad 1.13$$

where φ is the fraction of the dispersed phase and η_0 is the viscosity of the continuous phase. This equation may be rewritten in terms of the reduced viscosity, η_r:

$$\eta_r = \frac{\eta - \eta_0}{\eta_0} = 2.5\varphi \ . \qquad 1.14$$

Equations 1.13 and 1.14 are exact for very dilute emulsions (φ<0.01) when fluid dynamics or any interactions between droplets can be negligible[57].

With an increase in the volume of dispersed phase, more complex equations are necessary. Phan-Thien [58] presented a version of the generalisation of the Taylor model:

$$\left(\frac{\eta}{\eta_0}\right)^{2/5}\left[\frac{2\eta+5\eta_{dr}}{2(\eta_0+\eta_{dr})}\right]^{3/5}=(1-\varphi)^{-1} \qquad 1.15$$

where η_{dr} is the viscosity of the liquids forming the droplets. Pal [59] proposed another equation that uses the limit of the closest packing of droplets factor, φ^*, which corresponds to the volume fraction where the droplets are close packed without deforming.

$$\eta_r\left[\frac{2\eta_r+5\lambda}{2+5\lambda}\right]^{1/2}=[1-(\varphi/\varphi^*)]^{-2.5\varphi^*} \qquad 1.16$$

where λ is the ratio of the viscosity of liquid forming the droplets.

The previous equations and others proposed by researchers, as well as results obtained with real emulsions [54, 57, 60-62], clearly show a direct relationship between the viscosity of the emulsions (η) and the fraction of the dispersed phase (φ).

The distribution of droplet sizes is another factor that affects the rheology of emulsions, particularly as they become more concentrated. When the volume fraction of the dispersed phase is greater than 0.6, the viscosity of the emulsion is inversely proportional to the mean diameter of the droplets. Equations 1.15 and 1.16 do not show any dependence of the viscosity on droplet size. The size of the droplet and the degree of polydispersity of the droplet sizes affects the distance between the droplets, according to Equation 1.17, resulting in a change in the rheological behaviour of the emulsions. At a critical distance of separation between droplets the viscosity rapidly increases [57].

$$h_m=\delta\left[\left(\varphi^*/\varphi\right)^{1/3}-1\right] \qquad 1.17$$

where h_m is the average distance of separation between the droplets and δ is the diameter of the droplet. Such a dependence of the viscosity on droplet size has been reported by Pal [63] .

The numerical value of the viscosity of an emulsion does not provide sufficient information, not only about the viscoelastic properties of the system, i.e. the viscous or elastic component, but also the structure and interactions between the droplets. Also, many of the rheological equations have been developed using suspensions as models and their application for emulsions is not accurate. As a consequence, a complete characterisation of viscoelastic fluids requires other parameters such as complex modulus, storage modulus, loss modulus, creep compliance and creep recovery.

1.4.2.1 Rheology of concentrated emulsions

The term “concentrated emulsion” covers the wide range of intermediate concentrations. The boundaries are, at one end, the limit of dilute emulsions where there is a linear dependence of viscosity on concentration (ignoring inter-droplet interactions), and at the other end, the concentration of closely packed spherical droplets (droplets remain spherical but it is not possible to add more dispersed phase without deformation of the droplets). Droplet interactions dominate concentrated emulsions, which display non-Newtonian behaviour, and the extent of these interactions dictate the complex flow behaviour of the emulsions [54].

Droplet interactions are dominated by the properties of the continuous phase and the interfacial film. Ionic strength and pH, controlled by the chemical composition of the continuous phase, and the chemical functionality of emulsifier and oil, are all factors that affect the behaviour and hence inter-droplet interactions of emulsions [57, 64]. For instance, some researchers have used a protein as an emulsifier, and their results show the effect of pH and ionic strength on the rheological behaviour of concentrated and highly concentrated emulsions [65-68]. van der Waals, electrostatic double-layer, hydration and steric forces not only control the stability of the emulsions, but also their rheological properties.

For concentrated emulsions, emulsifiers play an important role in their rheological behaviour. The interactions between droplets are determined by the nature and concentration of the surfactant as well as by the physicochemical properties of the continuous phase. As a consequence, the emulsifier has an important function in controlling the properties of the system [54].

The chemical structure of emulsifiers is the primary practical interest, and this provides information related to their capacity of adsorption at the oil-water interface and the properties of emulsions [54]. However, the adsorption and emulsification capacity not only depend on the hydrophilic–lipophilic balance in the emulsifier, but also on the quantity of the oil and aqueous phases, the nature of the oil and the physicochemical characteristics of the aqueous phase [69].

Wulff-Pérez *et al*. [70] and Masalova *et al*. [71] studied the role of the emulsifier in the rheological properties of emulsions. Their results show that they depend on the chemical structure of the emulsifier, and the rheological properties of the systems studied were totally different.

Currently no mathematical equations exist that are suitable to be applied to the rheological data obtained from investigations of concentrated emulsions that encompass all the major parameters that influence their behaviour. Some of these parameters include: droplet size distribution, concentration of the dispersed phase, kind of emulsifier, physicochemical properties of the continuous phase (for O/W emulsions) and temperature.

Some equations have been developed to estimate the viscosity of concentrated emulsions. For example, in some equations the concentration of the dispersed phase and the maximum packing concentration are used [72, 73] or, those parameters plus the ratio of viscosities between the dispersed and continuous phase [54]. Also, there are equations that estimate the viscosity of concentrated emulsions using parameters such as the phase volume of the dispersed phase at zero and infinite stress [73] or electrostatic parameters, in the case of O/W emulsions with charged droplets [74]. Besides the parameters cited previously, the interfacial film also strongly affects the behaviour of concentrated emulsions and for this reason characterisation of the thin film structure is vital. A major limitation, however, is that

there are no adequate methods to study the adsorbed layers within an emulsion directly. Therefore, the standard methods applied in investigations of interfacial thin films are model systems at stationary flat interfaces. Isotherm Langmuir monolayer films are one example of a model system that can be used to obtain information about the structure and physicochemical characteristics of emulsifiers. The relationships between the structural characteristics of emulsifier monolayers at the air-water interface and the dispersion stability have been established, as well as between condensed film formation and emulsifier association in the bulk phase [22, 75, 76].

1.5 Milk proteins

The ability of milk proteins to adsorb at interfaces producing a strong barrier between dispersed phase domains by a combination of electrostatic and steric mechanisms, in systems such as emulsions and foams, are characteristics that the food industry exploits in the formulation of stable products. Furthermore, because of their nutritional values, milk proteins are widely used in the manufacture of medical food, dietary formulations and pharmaceutical products.

There are two main classes of milk proteins: caseins and whey proteins. Caseins can be divided into four distinct proteins, α_1, α_2, β and κ caseins, with percentages of 40, 8, 40 and 10, respectively [77], all of them with phosphoseryl fractions. Whey proteins can be divided into β-lactoglobulin, bovine serum albumin, α-lactalbumin and immunoglobulin. β-lactoglobulin represents about 50 percent of the total whey protein in bovine milk [78].

The presence of the phosphoseryl residues in the caseins gives them the ability to bind calcium ions. The tendency to bind calcium ions is related to the number of these residues in the molecule. The binding of calcium to caseins reduces the electrostatic repulsion between the casein molecules and promotes interactions between hydrophobic domains, leading to the formation of aggregates[65]. The descending order of calcium sensibility is, α_2 (11 or 12 phosphoserine residues), α1 (8 phosphoserine residues), β (5 phosphoserine residues) and κ (1 phosphoserine residue) [79, 80].

Various models of casein micelles have been developed in the form of polydisperse spherical complexes containing casein proteins and colloidal calcium phosphate (CCP). These structures are known as casein micelles with an average radius of approximately 100 nm [81, 82]. The function of the colloidal calcium phosphate is to induce clustering for α_1, α_2 and β caseins. Interactions between the α_1, α_2 and β caseins include the formation of calcium or calcium apatite bridges, hydrophobic interactions or perhaps both [83].

Horne [79] refers, in his review about casein micelle structure, that in the Holt model the calcium phosphate is in the form of nanoclusters and the interaction sites on the caseins are the phosphoseryl clusters of the calcium-sensitive caseins (Figure 1.14). The 3-dimensional network structure for Holt model (Figure 1.15) is due to α_1 and α_2 caseins that have more than two such clusters.

Using field emission scanning electron microscopy, Dalgleish *et al*.[84] suggested that the surface of the casein micelles could have a more complex structure than previous models suggested, including the absence of κ caseins in the structure of casein micelles. Additionally, their results indicated that the submicelles are not spherical and, that the interior of the casein is of tubular structure.

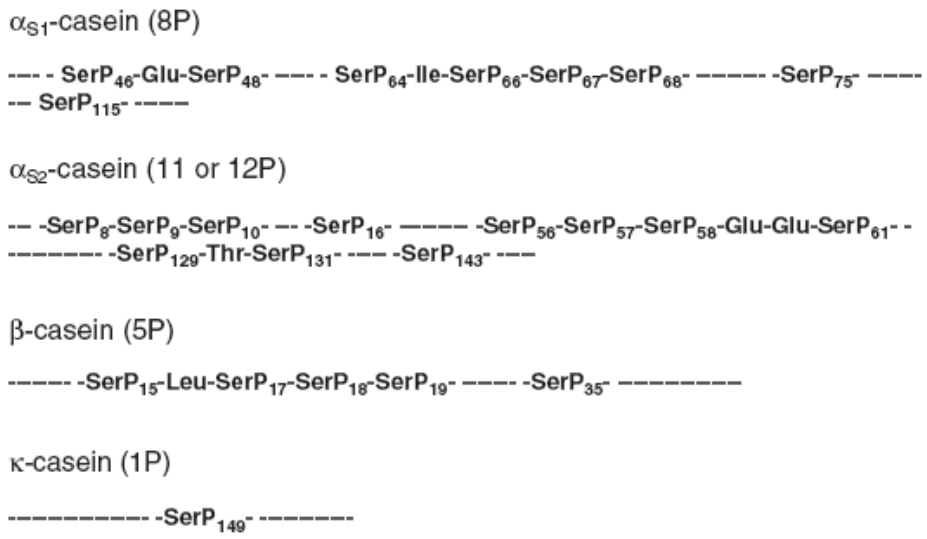

Figure 1.14. Phosphate residue positions in the bovine caseins, indicating the phosphoseryl clusters [79].

The previous models proposed that the κ casein is present on the surface of casein micelles, and the hydrophilic C-terminal part of κ casein protrudes from the micelle surface into the surrounding solvent, giving it a “hairy” or “brush” appearance. As a result, the approach and interactions of hydrophobic regions of the casein molecules are avoided [78, 82, 85].

Another previous model of the casein micelles is known as the submicelle model [79]. In this model, the caseins first aggregate through hydrophobic interactions into subunits of 15-20 molecules each. The pattern of interaction is such that it brings about a variation in the κ casein content of these submicelles. Those submicelles that are rich in κ casein congregate on the micelle surface, while submicelles that lack or are poor in κ casein are located in the interior of the micelles as illustrated in Figure 1.16 [79].

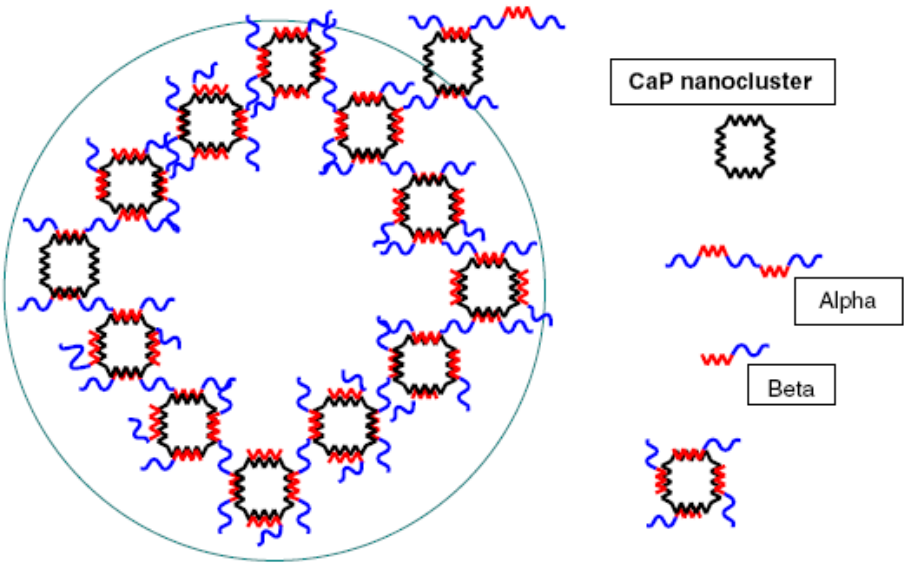

Figure 1.15 Illustration of network formation in the Holt model[79].

Holt [79] suggests that because recent research has shown that micelle formation can occur without calcium phosphate, a new model should be able to explain how this occurs. In order to achieve new models, he proposed the use of new and powerful techniques such as cryo-transmission electron microscopy to improve the existing models or assist in developing new ones.

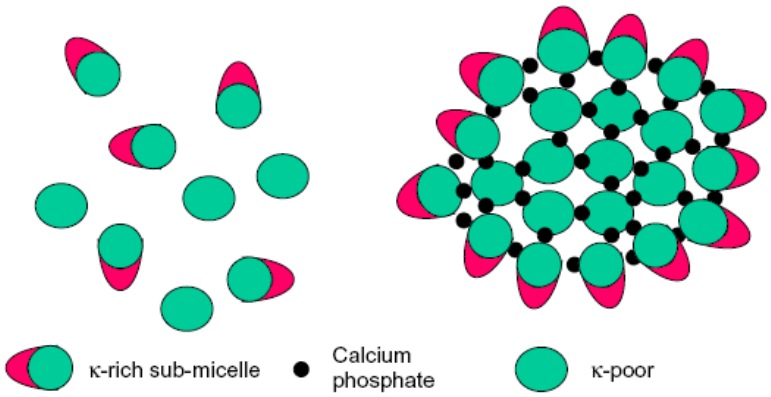

Figure 1.16. The schematic of the submicelle model of the casein micelle [79].

1.5.1 Sodium caseinate

Sodium caseinate is an excellent emulsifying agent and is a common ingredient in a wide range of emulsions [86]. Sodium caseinate is obtained after removing the colloidal calcium phosphate (CCP) from native casein, yielding a mixture of individual α_1, α_2, β and κ casein proteins. Caseins are converted to sodium caseinate to increase their water-solubility [87]. Sodium caseinate is produced using skim milk by (1) raising the acidity to pH 4.6 to solubilise the CCP, (2) washing to remove the soluble salts, lactose and whey proteins and (3) re-neutralisation to a pH of approximately 7 with sodium hydroxide [88].

Despite removing the colloidal calcium phosphate to yield individual α_1, α_2, β and κ casein proteins, some researchers have shown the presence of small aggregates in sodium caseinate solutions [89, 90]. The small aggregates have a radius of about 11 nm and contain about 15 molecules, probably due to the association of the hydrophobic parts of the casein molecules [91]. The behaviour of the small aggregates and casein proteins in sodium caseinate is strongly affected by physicochemical parameters such as pH and ionic strength.

HadjSadok *et al*. [92] among others [77, 87, 88, 91, 93, 94], have shown the effect of pH, ionic strength and temperature on the properties of sodium caseinate. Generally the results suggest that near and below the isoelectric point (IP), (pH 4.6 to 5), the solubility of the sodium caseinate decreases and the quantity and size of the aggregations increases. On the contrary, the solubility of sodium caseinate increases with a pH above the IP as the quantity and size of sodium caseinate aggregates

decreases. With respect to the ionic strength, the formation of the aggregates depends on the concentration and charge of the cation.

1.5.1.1 Emulsions with sodium caseinate

In the food industry, proteins are the main emulsifier agents. Most proteins in their native states possess specific three-dimensional structures that are maintained in solution, unless they are subjected to denaturation parameters such as heating. When a protein adsorbs at the oil-water interface, the hydrophobic regions of their structures (created by clusters of appropriate amino acid side chains) lie on, or possibly partially dissolve in, the oil phase. This kind of change in protein structure is known as surface denaturation [1].

When proteins are located at an interface, they are capable of changing structural arrangement either as they adsorb or shortly afterward. Once the proteins are adsorbed at the interface they form a protective membrane. In the case of emulsions, this membrane not only generates repulsive interactions (e.g., steric and electrostatic) between oil droplets, but also plays an important role in stabilising the droplets against flocculation and coalescence during long-term storage [47].

Sodium caseinate can easily form films from aqueous solutions because of its random coil nature and its ability to form extensive intermolecular hydrogen, electrostatic and hydrophobic bonds, resulting in an increase of the interchain cohesion [95]. Additionally, the excellent adsorption of sodium caseinate at the interface is a consequence of its flexibility and the considerable numbers of hydrophobic residues present in these proteins [96].

Experimental studies based on the influence of parameters such as the pH, ionic strength, protein concentration, internal phase concentration and calcium ion concentration in emulsions with sodium caseinate have provided useful information about their formulation and properties. However, the majority of the research was based on dilute and intermediate emulsions.

Research by Sirinivisan *et al.* [86] has shown a direct relationship between the concentration of sodium caseinate in the system and the surface concentration of protein on the droplets. Moreover, they observed that the addition of calcium chloride

results in the formation of casein aggregates that are adsorbed on the droplet surface increasing the barrier between the droplets, as well as improving the stability of the emulsion. The effect of increasing the concentration of calcium chloride in the formulation of emulsions and its effect on the stability of emulsions was corroborated by Sirinivasn *et al.* [97].

Srinivasan *et al.* [86, 98] and Dickinson *et al.* [99] studied the competitive adsorption of the different caseins present in sodium caseinate. Their results showed the preference of β casein to adsorb at the interface in comparison with the rest of the caseins. Sirivasan *et al.* found that when the sodium caseinate concentration is below 2%, β casein preferably adsorb at the interface of the droplets. Dickinson *et al.* found a similar result using different interface geometries; droplet (spherical) and planar.

The influence of the pH in emulsions with sodium caseinate was evaluated by Perrechi *et al.* [68] and their results show an increase in the stability of emulsions in systems with a pH between 2.7 and 6.6, with the exception of a pH close to the isoelectric point.

Carrero *et al.* [100] studied the influence of the sodium caseinate concentration on emulsion stability. They showed that a low concentration of sodium caseinate coalescence is induced and increasing the sodium caseinate concentration results in flocculation and creaming.

Dickinson *et al.* [101] used the rheological properties of emulsions prepared with sodium caseinate to predict the flocculation effect with different fractions of protein and oil. They found that there are two flocculation processes. The first, when the fractions of protein and oil are low is bridging flocculation. In this type of flocculation macromolecules on one droplet become shared, through partial adsorption, with the initially uncoated surface of another droplet. The second occurs when the fractions of protein/oil are high, and depletion flocculation occurs. In this flocculation the emulsion droplets may be driven to form a concentrated emulsion phase, distinct from the aqueous phase containing the sodium caseinate protein. Bridging flocculation is irreversible, while depletion flocculation is partially reversible. In order

to confirm their results, similar studies were undertaken using different microscopic techniques to investigate the structures of the floccules [102, 103].

An interesting study by Ma *et al.* [104] was based on determining the stability of emulsions as a function of aqueous phase pH using sodium caseinate and sodium caseinate that had been chemically modified. They chemically modified the sodium caseinate by adding carboxylic groups to decrease the isoelectric point of the sodium caseinate and amine groups to produce the reverse effect. They found good emulsion stability far from the isoelectric point of the sodium caseinate. The modifications they made in the structure of the sodium caseinate allowed them to formulate stable emulsions at a pH when the sodium caseinate, without modifications, was not able to produce a stable emulsion.

The effect of calcium ions on the properties of sodium caseinate emulsions is a consequence of the anionic phosphoseryl residues clustering in the casein molecules [96]. The process of calcium ions binding to the caseins has been suggested to occur over several stages depending on the concentration of the ions. At a molecular level, low concentrations of calcium ions produce conformational changes occurring to the protein structure without precipitation. Increasing the concentration of calcium ions reduces intermolecular electrostatic repulsion, while hydrophobic interactions produce the aggregation and finally the precipitation of the molecules [96, 105]. An illustration of this process is shown in Figure 1.17. Dickinson *et al.* [80, 106] studied the effect of calcium ions on the rheology and stability of sodium caseinate emulsions. They found that changes in the stability of the emulsions depend on the amount of calcium ions added. They also showed that the addition of calcium ions increases the bounding of sub-micelles into large aggregates, which reduce depletion flocculation, producing emulsions with a rheological behaviour similar to low-viscosity Newtonian liquids. On the contrary, the absence of calcium ions produces pseudoplastic emulsions as a result of depletion flocculation.

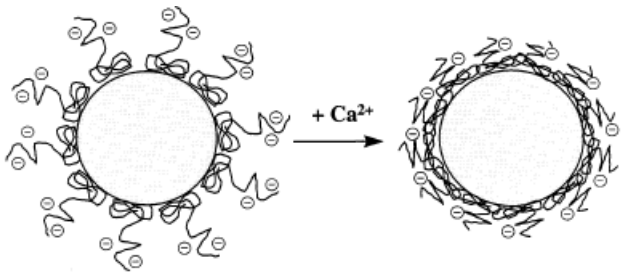

Figure 1.17. Illustration of the influence of Ca^{+2} on sodium caseinate emulsion stability [106].

The real effect of calcium ions on the properties of sodium caseinate emulsions depends not only on the quantity of this ion, but also on the physicochemical parameters of the aqueous phase such as pH and ionic strength.

Therefore, the characteristics of sodium caseinate protein in different physicochemical environments are vital to deal with the formulation and properties of emulsions that use this protein as an emulsifier. In the next chapter, a brief description of the equipment and techniques used to characterise sodium caseinate at different interfaces and the formulation and evaluation of some properties of sodium caseinate concentrated emulsions are shown.

1.6 References

1. Dalgleish, D.G., *Food Emulsions*, in *Food Emulsion*2004, Marcel Dekker: London.
2. Mittal, K.L.a.P.K., *Emulsions, foams and thin films*2000, New York Marcel Dekker.
3. Lissant, K.J., *The geometry of high-internal-phase-ratio emulsions.* Journal of Colloid and Interface Science, 1966. **22**(5): p. 462-468.
4. Robins, M.M., A.D. Watson, and P.J. Wilde, *Emulsions--creaming and rheology.* Current Opinion in Colloid & Interface Science, 2002. **7**(5-6): p. 419-425.
5. Kaganer, V.M., et al., *Structure and phase transitions in Langmuir monolayers.* Reviews of Modern Physics, 1999. **71**(3): p. 779.
6. Gehlert, U., G. Weidemann, and D. Vollhardt, *Morphological Features in 1-Monoglyceride Monolayers.* Journal of Colloid and Interface Science, 1995. **174**(2): p. 392-399.
7. Vollhardt, D. and V.B. Fainerman, *Progress in characterization of Langmuir monolayers by consideration of compressibility.* Advances in Colloid and Interface Science, 2006. **127**(2): p. 83-97.
8. Lin, B., et al., *Phase diagram of a lipid monolayer on the surface of water.* Physical Review Letters, 1990. **65**(2): p. 191.
9. Knobler, C.M., *Recent developments in the study of monolayers at the air-water interface.* Advances in Chemical Physics, 1990: p. 397-449.
10. Zhu, J., A. Eisenberg, and R.B. Lennox, *Interfacial behavior of block polyelectrolytes. 1. Evidence for novel surface micelle formation.* Journal of the American Chemical Society, 1991. **113**(15): p. 5583-5588.

11. Zhu, J., R.B. Lennox, and A. Eisenberg, *Interfacial behavior of block polyelectrolytes. 2. Aggregation numbers of surface micelles.* Langmuir, 1991. **7**(8): p. 1579-1584.
12. Zhu, J., A. Eisenberg, and R.B. Lennox, *Interfacial behavior of block polyelectrolytes. 5. Effect of varying block lengths on the properties of surface micelles.* Macromolecules, 1992. **25**(24): p. 6547-6555.
13. Zhu, J., A. Eisenberg, and R.B. Lennox, *Interfacial behavior of block polyelectrolytes. 6. Properties of surface micelles as a function of R and X in P(S260-b-VP240/RX).* Macromolecules, 1992. **25**(24): p. 6556-6562.
14. Li, S., et al., *Surface micelle formation at the air/water interface from nonionic diblock copolymers.* Langmuir, 1993. **9**(8): p. 2243-2246.
15. Birdi, K., *The determination of work of compression of protein monolayers at the air-water interface.* Colloid & Polymer Science, 1972. **250**(3): p. 222-226.
16. Fainerman, V.B., D. Vollhardt, and V. Melzer, *Equation of State for Insoluble Monolayers of Aggregating Amphiphilic Molecules.* The Journal of Physical Chemistry, 1996. **100**(38): p. 15478-15482.
17. Israelachvili, J., *Self-Assembly in Two Dimensions: Surface Micelles and Domain Formation in Monolayers.* Langmuir, 1994. **10**(10): p. 3774-3781.
18. Alahverdjieva, V.S., et al., *Adsorption behaviour of hen egg-white lysozyme at the air/water interface.* Colloids and Surfaces A: Physicochemical and Engineering Aspects, 2008. **323**(1-3): p. 167-174.
19. MacRitchie, F., *Spread monolayers of proteins.* Advances in Colloid and Interface Science, 1986. **25**: p. 341-385.
20. Krägel, J., et al., *Consistency of surface mechanical properties of spread protein layers at the liquid-air interface at different spreading conditions.* Colloids and Surfaces B: Biointerfaces, 1999. **12**(3-6): p. 391-397.
21. Fadeev, A., et al., *Collagen denaturation in spread monolayers at the air-water interface: Experiments and a possible model of the process.* Biochemistry (Moscow) Supplemental Series A: Membrane and Cell Biology, 2008. **2**(1): p. 62-72.
22. Rodríguez Patino, J.M. and M.R. Rodríguez Niño, *Interfacial characteristics of food emulsifiers (proteins and lipids) at the air-water interface.* Colloids and Surfaces B: Biointerfaces, 1999. **15**(3-4): p. 235-252.
23. Innocente, N., et al., *Langmuir Film Balance Study of the Surface Properties of a Soluble Fraction of Milk Fat-Globule Membrane.* Journal of Agricultural and Food Chemistry, 1997. **45**(5): p. 1559-1563.
24. Rodríguez Patino, J.M., M.R. Domínguez, and J. de la Fuente Feria, *Monostearin monolayers spread on aqueous solutions containing ethanol.* Journal of Colloid and Interface Science, 1992. **154**(1): p. 146-159.
25. Chang, S.-H., L.-Y. Chen, and W.-Y. Chen, *The effects of denaturants on protein conformation and behavior at air/solution interface.* Colloids and Surfaces B: Biointerfaces, 2005. **41**(1): p. 1-6.
26. Dauphas, S., et al., *The supramolecular organisation of [beta]-casein: effect on interfacial properties.* Food Hydrocolloids, 2005. **19**(3): p. 387-393.
27. Krause, J.P. and K.D. Schwenke, *Behaviour of a protein isolate from rapeseed (Brassica napus) and its main protein components -- globulin and albumin -- at air/solution and solid interfaces, and in emulsions.* Colloids and Surfaces B: Biointerfaces, 2001. **21**(1-3): p. 29-36.
28. Sánchez, C.C., et al., *Soy globulin spread films at the air-water interface.* Food Hydrocolloids, 2004. **18**(2): p. 335-347.
29. Rodríguez Patino, J.M., et al., *Structural and shear characteristics of adsorbed sodium caseinate and monoglyceride mixed monolayers at the air-water interface.* Journal of Colloid and Interface Science, 2007. **313**(1): p. 141-151.

30. Caro, A.L., M.R.R. NiÃ±o, and J.M.R. Patino, *The effect of pH on structural, topographical, and rheological characteristics of Î²-casein-DPPC mixed monolayers spread at the air-water interface.* Colloids and Surfaces A: Physicochemical and Engineering Aspects, 2009. **332**(2-3): p. 180-191.
31. Niño, M.R.R., C.C. Sánchez, and J.M.R. Patino, *Interfacial characteristics of [beta]-casein spread films at the air-water interface.* Colloids and Surfaces B: Biointerfaces, 1999. **12**(3-6): p. 161-173.
32. Rodríguez Niño, M.R., et al., *Milk and soy protein films at the air-water interface.* Food Hydrocolloids, 2005. **19**(3): p. 417-428.
33. Rodríguez Patino, J.M., C.C. Sánchez, and M.R. Rodríguez Niño, *Structural and morphological characteristics of [beta]-casein monolayers at the air-water interface.* Food Hydrocolloids, 1999. **13**(5): p. 401-408.
34. Balla, A., et al., *Interfacial Properties of Gluten Monolayers Spread on Various Chloride Salt Solutions. Effects of Electrolytes, Salt Concentrations, and Temperature.* Journal of Agricultural and Food Chemistry, 1998. **46**(9): p. 3535-3539.
35. Nieto-Suárez, M., N. Vila-Romeu, and I. Prieto, *Behaviour of insulin Langmuir monolayers at the air-water interface under various conditions.* Thin Solid Films, 2008. **516**(24): p. 8873-8879.
36. RodrÃ-guez Patino, J.M., C.C. SÃ¡nchez, and M.R. RodrÃ-guez NiÃ±o, *Morphological and Structural Characteristics of Monoglyceride Monolayers at the Airâˆ'Water Interface Observed by Brewster Angle Microscopy.* Langmuir, 1999. **15**(7): p. 2484-2492.
37. Erbil, H.Y., *Surface Chemistry: Of Solid and Liquid Interfaces*2009: Blackwell Publishing Ltd. 364
38. Rosen, M., *Surfactants and Interfacial Phenomena* 2004, Ney York John Wiley & Sons.
39. Kabalnov, A., *Thermodynamic and theoretical aspects of emulsions and their stability.* Current Opinion in Colloid & Interface Science, 1998. **3**(3): p. 270-275.
40. Bibette, J., et al., *Stability criteria for emulsions.* Physical Review Letters, 1992. **69**(16): p. 2439.
41. Kizling, J., B. Kronberg, and J.C. Eriksson, *On the formation and stability of high internal phase O/W emulsions.* Advances in Colloid and Interface Science, 2006. **123-126**: p. 295-302.
42. Benkeblia, N., et al., *Variation of Fructooligosaccharides and their Metabolizing Enzymes in Onion Bulb (Allium cepa L. cv. Tenshin) During Long-term Storage.* Journal of Food Science, 2005. **70**(3): p. S208-S214.
43. Borwankar, R.P., L.A. Lobo, and D.T. Wasan, *Emulsion stability -- kinetics of flocculation and coalescence.* Colloids and Surfaces, 1992. **69**(2-3): p. 135-146.
44. Briceno, M.I., *Rheology of Suspensions and Emulsions*, in *Pharmaceutical Emulsions and Suspensions*2000, Marcel Dekker, Inc. : New York
45. Claesson, P.M., E. Blomberg, and E. Poptoshev, *Surface Forces and Emulsion Stability*, in *Food Emulsion*2004, Marcel Dekker: London.
46. Salager, J.-L., *Interfacial phenomena in dispersed systems*, in *FIRP Booklet # E120-N*1994, Universidad de los Andes. Facultad de Ingenieria. Escuela de Ingenieria Quimica: Merida, Merida, Venezuela
47. McClements, D.J., *Protein-stabilized emulsions.* Current Opinion in Colloid & Interface Science, 2004. **9**(5): p. 305-313.
48. *Food Colloids*. 1 ed. Fundamentals of Formulation, ed. E. Dickinson and R. Miller2001: The Royal Society of Chemistry.
49. Bibette, J., *Stability of thin films in concentrated emulsions.* Langmuir, 1992. **8**(12): p. 3178-3182.
50. Taylor, P., *Ostwald ripening in emulsions.* Advances in Colloid and Interface Science, 1998. **75**(2): p. 107-163.

51. Kabalnov, A.S., et al., *Ostwald ripening in emulsions : 2. Ostwald ripening in hydrocarbon emulsions: Experimental verification of equation for absolute rates.* Journal of Colloid and Interface Science, 1990. **138**(1): p. 98-104.
52. Durian, D.J., D.A. Weitz, and D.J. Pine, *Scaling behavior in shaving cream.* Physical Review A, 1991. **44**(12): p. R7902.
53. Becher, P., *Emulsions Theory and Parctice*2001, London: Oxford University Press.
54. Derkach, S.R., *Rheology of emulsions.* Advances in Colloid and Interface Science, 2009. **151**(1-2): p. 1-23.
55. Cheng, D.C.H., *Yield stress: A time-dependent property and how to measure it.* Rheologica Acta, 1986. **25**(5): p. 542-554.
56. Barnes, H.A., J.F. Hutton, and K. Walters, *An Introduction to Rheology*1996, New York: Elsevier Science.
57. Tadros, T.F., *Fundamental principles of emulsion rheology and their applications.* Colloids and Surfaces A: Physicochemical and Engineering Aspects, 1994. **91**: p. 39-55.
58. Phan-Thien, N. and D.C. Pham, *Differential multiphase models for polydispersed suspensions and particulate solids.* Journal of Non-Newtonian Fluid Mechanics, 1997. **72**(2-3): p. 305-318.
59. Pal, R., *Influence of interfacial rheology on the viscosity of concentrated emulsions.* Journal of Colloid and Interface Science, 2011. **356**(1): p. 118-122.
60. Pal, R. and E. Rhodes, *A novel viscosity correlation for non-newtonian concentrated emulsions.* Journal of Colloid and Interface Science, 1985. **107**(2): p. 301-307.
61. Buffo, R.A. and G.A. Reineccius, *Modeling the rheology of concentrated beverage emulsions.* Journal of Food Engineering, 2002. **51**(4): p. 267-272.
62. Pal, R., *Relative Viscosity of Non-Newtonian Concentrated Emulsions of Noncolloidal Droplets.* Industrial & Engineering Chemistry Research, 2000. **39**(12): p. 4933-4943.
63. Pal, R., *Shear Viscosity Behavior of Emulsions of Two Immiscible Liquids.* Journal of Colloid and Interface Science, 2000. **225**(2): p. 359-366.
64. Gallegos, C. and J.M. Franco, *Rheology of food, cosmetics and pharmaceuticals.* Current Opinion in Colloid & Interface Science, 1999. **4**(4): p. 288-293.
65. Martínez, I., M. Angustias Riscardo, and J.M. Franco, *Effect of salt content on the rheological properties of salad dressing-type emulsions stabilized by emulsifier blends.* Journal of Food Engineering, 2007. **80**(4): p. 1272-1281.
66. Romero, A., F. Cordobés, and A. Guerrero, *Influence of pH on linear viscoelasticity and droplet size distribution of highly concentrated O/W crayfish flour-based emulsions.* Food Hydrocolloids, 2009. **23**(2): p. 244-252.
67. Dickinson, E., M.G. Semenova, and A.S. Antipova, *Salt stability of casein emulsions.* Food Hydrocolloids, 1998. **12**(2): p. 227-235.
68. Perrechil, F.A. and R.L. Cunha, *Oil-in-water emulsions stabilized by sodium caseinate: Influence of pH, high-pressure homogenization and locust bean gum addition.* Journal of Food Engineering. **97**(4): p. 441-448.
69. Salager, J.-L., et al., *Current Phenomenological Know-How and Modeling of Emulsion Inversion.* Industrial & Engineering Chemistry Research, 2000. **39**(8): p. 2665-2676.
70. Wulff-Pérez, M., et al., *Bulk and interfacial viscoelasticity in concentrated emulsions: The role of the surfactant.* Food Hydrocolloids. **25**(4): p. 677-686.
71. Masalova, I., R. Foudazi, and A.Y. Malkin, *The rheology of highly concentrated emulsions stabilized with different surfactants.* Colloids and Surfaces A: Physicochemical and Engineering Aspects. **375**(1-3): p. 76-86.
72. Campanella, O.H., N.M. Dorward, and H. Singh, *A study of the rheological properties of concentrated food emulsions.* Journal of Food Engineering, 1995. **25**(3): p. 427-440.
73. Barnes, H.A., *Rheology of emulsions — a review.* Colloids and Surfaces A: Physicochemical and Engineering Aspects, 1994. **91**(0): p. 89-95.

74. Pal, R., *Effect of droplet size on the rheology of emulsions.* AIChE Journal, 1996. **42**(11): p. 3181-3190.
75. Pearson, J.T., *The application of monolayer techniques to a study of protein-surfactant interaction : II. Interactions in adsorbed films at the air/water interface and in oil-in-water emulsions.* Journal of Colloid and Interface Science, 1968. **27**(1): p. 64-74.
76. Murray, B.S., R. Xu, and E. Dickinson, *Brewster angle microscopy of adsorbed protein films at air-water and oil-water interfaces after compression, expansion and heat processing.* Food Hydrocolloids, 2009. **23**(4): p. 1190-1197.
77. Pitkowski, A., D. Durand, and T. Nicolai, *Structure and dynamical mechanical properties of suspensions of sodium caseinate.* Journal of Colloid and Interface Science, 2008. **326**(1): p. 96-102.
78. Singh, H., *Aspects of milk-protein-stabilised emulsions.* Food Hydrocolloids. **In Press, Corrected Proof**.
79. Horne, D.S., *Casein micelle structure: Models and muddles.* Current Opinion in Colloid & Interface Science, 2006. **11**(2-3): p. 148-153.
80. Dickinson, E. and M. Golding, *Influence of calcium ions on creaming and rheology of emulsions containing sodium caseinate.* Colloids and Surfaces A: Physicochemical and Engineering Aspects, 1998. **144**(1-3): p. 167-177.
81. Holt, C., et al., *Substructure of bovine casein micelles by small-angle X-ray and neutron scattering.* Colloids and Surfaces A: Physicochemical and Engineering Aspects, 2003. **213**(2-3): p. 275-284.
82. de Kruif, C.G., *Casein micelle interactions.* International Dairy Journal, 1999. **9**(3-6): p. 183-188.
83. Slattery, C.W., *Model calculations of casein micelle size distributions.* Biophysical Chemistry, 1976. **6**(1): p. 59-64.
84. Dalgleish, D.G., P.A. Spagnuolo, and H. Douglas Goff, *A possible structure of the casein micelle based on high-resolution field-emission scanning electron microscopy.* International Dairy Journal, 2004. **14**(12): p. 1025-1031.
85. de Kruif, C.G. and E.B. Zhulina, *[kappa]-casein as a polyelectrolyte brush on the surface of casein micelles.* Colloids and Surfaces A: Physicochemical and Engineering Aspects, 1996. **117**(1-2): p. 151-159.
86. Srinivasan, M., H. Singh, and P.A. Munro, *Sodium Caseinate-Stabilized Emulsions:â€‰ Factors Affecting Coverage and Composition of Surface Proteins.* Journal of Agricultural and Food Chemistry, 1996. **44**(12): p. 3807-3811.
87. Carr, A.J., P.A. Munro, and O.H. Campanella, *Effect of added monovalent or divalent cations on the rheology of sodium caseinate solutions.* International Dairy Journal, 2002. **12**(6): p. 487-492.
88. O'Kennedy, B.T., et al., *Factors affecting the acid gelation of sodium caseinate.* International Dairy Journal, 2006. **16**(10): p. 1132-1141.
89. Nash, W., et al., *Dynamic light scattering investigation of sodium caseinate and xanthan mixtures.* International Journal of Biological Macromolecules, 2002. **30**(5): p. 269-271.
90. Chu, B., et al., *Laser Light Scattering of Model Casein Solutions: Effects of High Temperature.* Journal of Colloid and Interface Science, 1995. **170**(1): p. 102-112.
91. Pitkowski, A., T. Nicolai, and D. Durand, *Stability of caseinate solutions in the presence of calcium.* Food Hydrocolloids, 2009. **23**(4): p. 1164-1168.
92. HadjSadok, A., et al., *Characterisation of sodium caseinate as a function of ionic strength, pH and temperature using static and dynamic light scattering.* Food Hydrocolloids, 2008. **22**(8): p. 1460-1466.
93. Jahaniaval, F., et al., *Soluble protein fractions from pH and heat treated sodium caseinate: physicochemical and functional properties.* Food Research International, 2000. **33**(8): p. 637-647.

94. Ruis, H.G.M., P. Venema, and E. van der Linden, *Relation between pH-induced stickiness and gelation behaviour of sodium caseinate aggregates as determined by light scattering and rheology.* Food Hydrocolloids, 2007. **21**(4): p. 545-554.
95. Khwaldia, K., et al., *Properties of Sodium Caseinate Film-Forming Dispersions and Films.* Journal of Dairy Science, 2004. **87**(7): p. 2011-2016.
96. Swaisgood, H.E., *Review and Update of Casein Chemistry and.* Journal of Dairy Science, 1993. **76**(10): p. 3054-3061.
97. Srinivasan, M., H. Singh, and P.A. Munro, *The effect of sodium chloride on the formation and stability of sodium caseinate emulsions.* Food Hydrocolloids, 2000. **14**(5): p. 497-507.
98. Srinivasan, M., H. Singh, and P. A. Munro, *Adsorption behaviour of sodium and calcium caseinates in oil-in-water emulsions.* International Dairy Journal, 1999. **9**(3-6): p. 337-341.
99. Dickinson, E., S.E. Rolfe, and D.G. Dalgleish, *Competitive adsorption of [alpha]s1-casein and [beta]-casein in oil-in-water emulsions.* Food Hydrocolloids, 1988. **2**(5): p. 397-405.
100. Sánchez, C.C. and J.M.R. Patino, *Interfacial, foaming and emulsifying characteristics of sodium caseinate as influenced by protein concentration in solution.* Food Hydrocolloids, 2005. **19**(3): p. 407-416.
101. Dickinson, E. and M. Golding, *Rheology of Sodium Caseinate Stabilized Oil-in-Water Emulsions.* Journal of Colloid and Interface Science, 1997. **191**(1): p. 166-176.
102. Dickinson, E. and M. Golding, *Depletion flocculation of emulsions containing unadsorbed sodium caseinate.* Food Hydrocolloids, 1997. **11**(1): p. 13-18.
103. Dickinson, E., M. Golding, and M.J.W. Povey, *Creaming and Flocculation of Oil-in-Water Emulsions Containing Sodium Caseinate.* Journal of Colloid and Interface Science, 1997. **185**(2): p. 515-529.
104. Ma, H., et al., *Sodium Caseinates with an Altered Isoelectric Point As Emulsifiers in Oil/Water Systems.* Journal of Agricultural and Food Chemistry, 2009. **57**(9): p. 3800-3807.
105. Ho, C. and D.F. Waugh, *Interactions of Bovine Caseins with Divalent Cations1.* Journal of the American Chemical Society, 1965. **87**(4): p. 889-892.
106. Dickinson, E. and E. Davies, *Influence of ionic calcium on stability of sodium caseinate emulsions.* Colloids and Surfaces B: Biointerfaces, 1999. **12**(3-6): p. 203-212.

Chapter 2 Experimental

2.1 Introduction

This chapter presents a description of the materials, equipment and techniques used to investigate the behaviour of sodium caseinate at the air-water and oil-water interfaces by changing ionic strength and pH values. It also explains the methods used to prepare the concentrated emulsion samples whilst the evaluation of their stability and rheological properties is also shown.

2.2 Materials

The milk protein used in this study was sodium caseinate powder from bovine milk that was obtained from Sigma-Aldrich. Buffer solutions of different pH and ionic strength were prepared using sodium hydrogen carbonate (Panreal, 99.7%), sodium carbonate (Pure science), disodium hydrogen orthophosphate (BDH Chemicals, AnalaR grade, 99%), potassium dihydrogen orthophosphate (BDH Chemicals, AnalaR grade, 99%), glacial acetic acid (Pure science) and sodium acetate (Scientific Supplies). All chemicals were used as received. Milli-Q ultrapure water (resistivity 18.2 MΩ cm) was used in the preparation of all solutions. pH measurements were performed using a Mettler Toledo Seven Easy pH meter.

For the study of the sodium caseinate at the air/water and oil/water interfaces, the concentration of the protein solutions were 0.15 % w/v and 0.05 % w/v respectively. Sodium caseinate powder was dissolved in Milli-Q water or buffer under continuous stirring for two hours, and then the solution was rested for 24 hours at 4ºC to ensure the total hydration of the protein. The non-polar phases used for the interfacial tension tests were soybean oil (Sigma-Aldrich), and normal-Dodecane (Sigma-Aldrich reagent plus).

For the study of the concentrated emulsions the concentrations of oil were between 50 and 70 wt% and 1% wt of sodium caseinate. Soybean oil (Sigma-Aldrich) was the non-polar phase used. The sodium caseinate powder was dissolved in the buffer solution under continuous stirring for 2 hr, then the oil was added and finally the system was rested for 24 hr at 4ºC to ensure the total hydration of the protein. After

24 hr the phases were premixed at 22,000 rpm for 15 s using a blender, Waring model HGB2WTS3, and then the emulsification process was done using a homogeniser at a pressure of 2500 psi and five pass through. For all the systems studied 0.01% w/v of sodium azide, respect of the aqueous phase, was used as a biocide. All experiments were replicated to ensure reproducibility and for each repetition a fresh sample was made to avoid protein degradation.

2.3 Equipment used for the conformation of Na-Ca at the air-water and oil-water interfaces

General information about the techniques used and the experimental parameters for the investigation of sodium caseinate conformation at the air-water and oil-water interface will be explained here. For additional information, further references are listed at the end of this chapter.

2.3.1 Surface Pressure-Area Isotherms

The surface pressure-area isotherm data were acquired using a Langmuir trough, a rectangular tray made from teflon with movable teflon barriers. The trough was filled with the substrate liquid; this constitutes the “subphase”. A Wilhelmy plate (typically a rectangular piece of chromatography paper) (Figure 2.1) was allowed to have contact with the subphase. The Wilhelmy plate, completely wetted by the subphase, was suspended from a pressure sensor. This device automatically measures the mass variation and the software of the equipment converts this into a surface tension. The relationship between the mass differential and the surface tension is given by

$$\gamma = \frac{F}{l \cos \theta} \qquad 2.1$$

where, F is the force exerted on the plate, l is the wetted perimeter of the plate and θ is the contact angle between the subphase and the plate. Because the complete wetting occurs the contact angle is taken to be zero and Equation 2.1 is simplified to

$$\gamma = \frac{F}{l} \qquad 2.2$$

Once the trough is filled with the substrate liquid (normally an aqueous solution), a solution of an insoluble substrate molecule in a volatile solvent is added drop wise onto the subphase using a micro syringe. Spreading occurs, the solvent evaporates and a monolayer is formed. In order to prevent changes in protein structure, water was used as the solvent [1, 2]. Thirty minutes were allowed to elapse before measurements were taken; this time having been suggested in other studies [3, 4] and was considered as appropriate for obtaining reproducible data in preliminary tests. After 30 minutes had elapsed, the area of the monolayer was varied by moving the barriers across the subphase surface. The surface tension was measured using the pressure sensor and the surface pressure calculated by software using Equation 2.2.

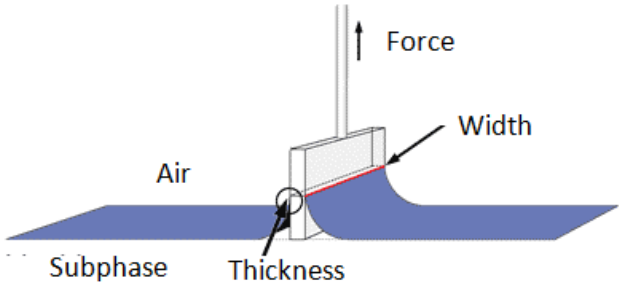

Figure 2.1 Schematic description of surface tension measurement using the Wilhelmy plate method.

2.3.1.1 Experimental Parameters

Surface pressure isotherms were measured using a NIMA 702 PTFE trough (area 700 cm^2) at room temperature (21°C). Before doing each experiment the trough and barriers were cleaned with AR grade chloroform, in order to avoid contamination in the system, and then rinsed with buffer solution. Whatman chromatography paper (Char 1) was used for the Wilhelmy plate. With the barriers open at 535 cm^2 and using a Hamilton microsyringe, volumes of sodium caseinate solution (1.554 mg/mL) were spread onto the surface of the buffer solution. The volumes used were between 50 and 20 μL and the quantity depended on the ionic strength of the subphase.

The changes in the ionic strength subphase for a formed monolayer were done by using a syringe with a long needle. The volumes of buffer solution required to change the ionic strength were injected outside of the barriers to prevent adsorption

of the protein molecules at the needle. After 30 minutes, which was the time set to allow casein molecules to achieve the equilibrium, the barriers were compressed until an area of 70 cm^2 at a speed of 115 cm^2 min^{-1}.

2.3.2 Surface Potential

The change in electrical potential between two electrodes (one in the aqueous subphase and the other in the air above the surface) when a monolayer is spread on the surface is called the surface potential (ΔV) of the film. Surface potential measurements provide a rather simple, traditional tool to probe molecular orientation and changes at interfaces. The potential difference is attributed to the film and is generally given a qualitative interpretation in terms of the analogy with a condenser according to the Helmholtz equation,

$$\Delta V = \frac{4\pi\tilde{\mu}n}{\sigma} \qquad 2.3$$

where $\tilde{\mu}$ is the effective surface dipole moment in the perpendicular direction, n is the number of dipoles (usually number of molecules) per unit area and σ is the dielectric constant. The effective surface dipole moment in the perpendicular direction is expressed as:

$$\tilde{\mu} = \mu \cos\theta \qquad 2.4$$

where μ is an intrinsic moment making an angle θ with the vertical. Generally, it is assumed that σ is unity and the equation 2.3 could be rewritten as:

$$\Delta V = 4\pi n\mu \cos\theta. \qquad 2.5$$

Surface potential measurements on protein monolayers can give information on the homogeneity of the film and the orientation of dipoles within the film. In principle, they can also be used in conjunction with surface pressures to follow the structure changes occurring at the interface [5-7].

2.3.2.1 Experimental Parameters

The surface potential of the sodium caseinate monolayer was investigated using a Trek Electrostatic Voltmeter (320C) and a 3250 high-sensitivity vibrating-plate probe from Treck INC, Medina NY, USA. For all the measurements the null voltage was established on the bare subphase and the data were processed by the NIMA software.

The procedure used was similar to that described to the surface pressure area isotherm with some exceptions: the final area was 140 cm^2 and the volumes of sodium caseinate used t were between 27 and 15 μL.

2.3.3 Pendant drop

The imbalance of cohesive forces at the oil-water interface produces an interfacial tension, as shown in Figure 1.7. The interfacial tension depends on the similarity of the molecules between the phases in contact. Therefore, similar phases produce low values of interfacial tension, while high interfacial tension values are obtained when the two phases differ greatly. If amphiphilic molecules are added at the interface between two immiscible liquids, they will adsorb there and reduce the interfacial tension between the phases. One technique that is used to measure the kinetic adsorption and reduction of the interfacial tension is the pendant drop method, as shown in Figure 2.2.

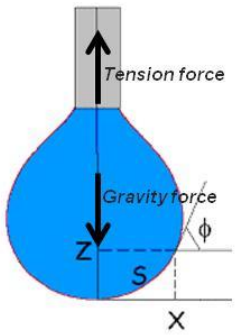

Figure 2.2 Schematic diagram of a pendant drop and the forces acting on the drop.

When a drop hangs from a syringe tip, it has a geometry that depends on the equilibrium between gravity and tension forces, as shown in Figure 2.2. Gravity tries to elongate the drop, while the tension force opposes this by shrinking the drop. Tate

[8] developed an equation that relates the weight of the drop and the interfacial tension at equilibrium, assuming that the contact angle between the syringe tip and drop is zero. The equation at equilibrium is:

$$mg = 2\pi r_w \gamma \qquad 2.6$$

where m is the mass of the drop and r_w is the radius of the dropping tip. Harkins and Brown added a shape factor (β) to the previous equation and the difference of density between the two phases (Δ_ρ), becoming the equation as follows:

$$\gamma = \frac{\Delta_\rho g}{r_w \beta} \qquad 2.7$$

The shape factor (β) is determined by using the first-order Young-Laplace equation [9] and the parameters shown in Figure 2.2:

$$d_x/d_s = \cos\phi \quad 2.8$$

$$d_z/d_s = \sin\phi \quad 2.9$$

$$d_\phi/d_s = 2 + \beta z - \sin\phi/x \quad 2.10$$

where s is part of the drop curvature and ϕ is the angle between the x axis and the end of the curvature evaluated. Computational tools can be used to calculate the shape factor and then the interfacial tension.

2.3.3.1 Experimental Parameters

Interfacial tension between non-polar phases (soybean oil and n-dodecane) and sodium caseinate buffer solutions (0.05-2% w/v) was investigated using a computer controlled KSV CAM 101 instrument with software to calculate the parameters for the Young-Laplace equation. A sodium caseinate stock solution (4% w/v) was prepared in Milli-Q ultrapure water, using the same procedure as for the protein solution used in the Langmuir trough, and then diluted in buffer solutions as required. For each experiment plastic cuvettes were filled with the non-polar phase and a drop of the sodium caseinate solution was set into the non-polar phase using a syringe. The

camera was set to take 600 photos in frame intervals of two seconds, for a total time of 20 minutes. The interfacial tension data was returned directly in the software.

2.4 Equipment used for the emulsion properties

2.4.1 Light scattering

Information regarding the droplet size distribution of the emulsions is of considerable importance because droplet size and polydispersity impact on the stability and rheology of emulsions [10]. Different techniques are used to determine droplet size distribution such as Coulter-counting, light scattering, turbidimetry, photosedimentation, and various types of microscopy.

Light scattering is one of the most common methods to characterise macromolecules and colloids [11]. When a beam of light is directed at a colloidal solution or dispersion, some of the light may be adsorbed, some is scattered and the remainder is transmitted undisturbed through the sample. Light scattering, which is based on the Tyndall effect, results from the electric field associated with the incident light inducing periodic oscillations of the electron clouds of the atoms of the material in question. These then act as secondary sources and radiate scattered light.

All materials are capable of scattering light to some extent. The noticeable turbidity associated with most colloidal dispersions is a consequence of intense light scattering. The phenomenon of light scattering may be viewed as arising from reflections at the interface between two media of differing refractive indices. Furthermore, the intensity, polarisation and angular distribution of the light scattered from a colloidal system also depend on the size and shape of the scattering particles and the interactions between them [12].

The pattern of light scattering varies with the size range of particles: Rayleigh scattering dominates with particles that are small relative to the wavelength of light whilst Mie scattering occurs when the particles are of a similar size to the wavelength of light. For Rayleigh scattering, the intensity of light scattered at right angles to the incident light is measured. This is proportional to the number and concentration of scatterers (in this size range each droplet is a single scatterer) so if the concentration of dispersed material is known the average droplet size can be calculated. With

larger particles, Mie scattering occurs and there are multiple scatterers within each particle and optical interference yields a complex pattern of scattering intensity with angle of observation. In dispersed systems such as emulsions, the diffraction angle increases as the droplet size decreases, and the relation, although complex, is well known [13]. Comparison of the observed pattern with that generated by computer software using Mie theory gives the particle size distribution with good accuracy if the particles are spherical. For Mie theory it is necessary to know the refractive index of the particle and medium in order to obtain the value of the equivalent sphere.

Two kinds of light scattering can be used depending on the size range of particles. In static light scattering (SLS), measurement of the scattering intensity at many angles allows calculation of the radius of the particles or droplets a range of 0-02 to 2000 μm. On the other hand, dynamic light scattering (DLS) is applied for particles undergoing Brownian motion, particles below 1 nm, where the intensity of the scattered light fluctuates at a rate that is dependent upon the size of the particles, and their size is calculated using the Stokes-Einstein relationship.

Normally the distribution of the droplet size is reported by the equipment as the distribution frequency in volume. This distribution represents the proportion of droplets in a volume class with respect to the whole internal phase volume [10]; Figure 2.3 shows a unimodal and bimodal distribution. Other parameters that are common in the droplet size characterisation are: mode, median ($D_{(v,0.5)}$), mean of distribution in volume or mass (D(4,3)) and mean of the distribution in surface (D(3,2)). This last mean diameter is the diameter of the sphere that has the same surface/volume ratio as the whole population. This is also known as the Sauter mean diameter and it is commonly used in surfactant adsorption and catalysis applications.

2.4.1.1 Experimental Parameters

The droplet size distribution of the concentrated emulsions were obtained using a MALVERN Mastersizer 2000 with a 45 mm lens and a sample unit container (800 mL beaker), containing a pump, ultrasound probe and stirrer. Droplet size in the range of 0.02 and 2000 μm can be measured using incident light with wavelengths of 663 and 452 nm generated by a He-Ne laser.

The model used in the Mastersizer software was Mie-Theory with refractive indices for the droplets and dispersant of 1.45 and 1.33 respectively. The obscuration value for all the samples was between 14 and 17%.

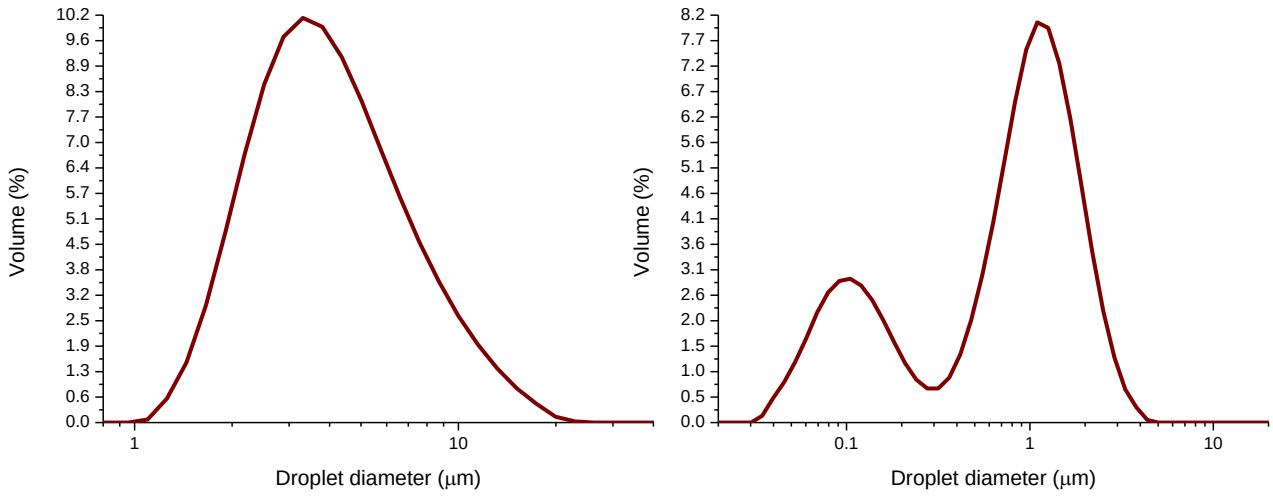

Figure 2.3 Examples of unimodal (left) and bimodal (right) drop size distributions.

2.4.2 Rheology

Investigating rheological behaviour of concentrated emulsions provides information about the structure of the system and the interactions between droplets. There are physical factors that influence the rhelogical properties of concentrated emulsions including: internal phase content; droplet size; droplet size distribution; emulsifier concentration and emulsifier characteristics. When the emulsifier is a protein, additional physicochemical factors such as pH and ionic strength have to be considered.

Concentrated emulsions have viscoelastic behaviour and they exhibit both elasticity (solid-like behaviour) and flow (liquid-like behaviour) when a shear is applied. A simple description of ideal viscoelastic behaviour in a system is afforded by the Maxwell model. This consists of an elastic spring and a dashpot in series. The spring represents the elastic response of the system and the dashpot the viscous response. When a strain is applied, the first to respond is the spring, followed by movement of the dashpot. Once the strain is released the spring recovers its original size, while the dashpot is not able to recover its original size. The spring and dashpot represent

the stored energy and dissipated energy, respectively. In Figure 2.4 the Maxwell model before and after a strain is applied is shown.

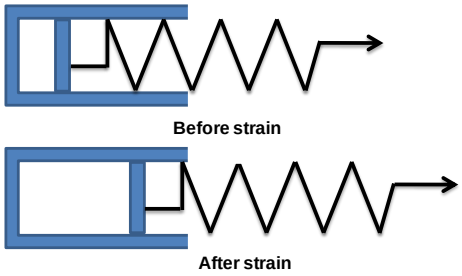

Figure 2.4. Maxwell model for viscoelastic systems.

The viscoelastic behaviour is evaluated using two types of experiments: dynamic and static tests, while the flow behaviour is evaluated using the steady state test. The dynamic tests involve the imposition of an oscillatory strain or stress and the complex shear modulus, storage modulus, loss modulus and loss factor are determined. On the contrary, in the static test a step change of stress or strain is applied and the stress or strain response is recorded as a function of time; stress relaxation, creep compliance and creep recovery are static methods. In the steady state test, a shear rate ramp is applied to a sample and the shear stress response is obtained. Each test done during this research will be described briefly below.

2.4.2.1 Dynamic test (oscillation experiments)

An oscillation experiment consists in applying a fluid to a sinusoidal strain or stress for a period of time. For tests with controlled shear strain in the form of oscillatory sine functions the time varying strain is:

$$\gamma(t) = \gamma_0 \sin \omega t \qquad 2.11$$

where γ_0 is the amplitude and ω is the angular frequency. If the test is with controlled oscillatory shear stress, the sine function is written as:

$$\tau(t) = \tau_0 \sin \omega t \qquad 2.12$$

where $\tau_0$is the shear stress amplitude.

When the test is done with controlled strain the shear stress is written as:

$$\tau(t) = \tau_0 \sin(\omega t + \delta) \qquad 2.13$$

where δ is the phase angle or loss angle. The phase angle is zero (0°) for elastic solids and ninety (90°) for Newtonian fluids. A viscoelastic fluid exhibits a phase angle between these values. The graphic relation between shear stress and shear strain is shown in Figure 2.5.

The elastic and viscous components of a viscoelastic fluid when an oscillatory test is applied are known as the storage modulus (G') and the loss modulus (G''), respectively, their equations are:

$$G' = (\tau_0/\gamma_0)\cos\delta \qquad 2.14$$

$$G'' = (\tau_0/\gamma_0)\sin\delta \ . \qquad 2.15$$

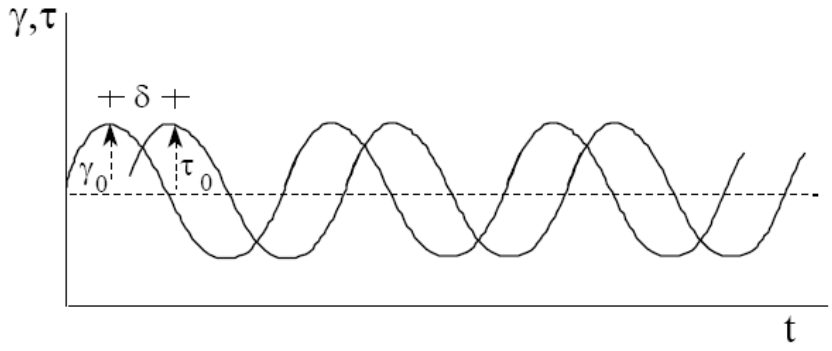

Figure 2.5. Graphic description of an oscillatory experiment with a controlled strain applied.

The relationship between $G'$and G'' allows calculation of the loss factor:

$$\tan\delta = {}^{G''}/_{G'} \ . \qquad 2.16$$

Elastic behaviour can be specified in terms of $\tan\delta$ equal to zero since here, G' completely dominates G''. Viscous behaviour can be expressed as $\tan\delta$ equal to infinite since here, G''completely dominates G'. If viscous and elastic behaviour exactly balance, then $\tan\delta$ is equal to one. This behaviour is characterised as the cross over point.

2.4.2.1.1 Strain sweep

A strain sweep is a dynamic test where the strain amplitude is varied, while the frequency and temperature are held constant [14].

2.4.2.1.2 Frequency sweep

A frequency sweep is a dynamic test where a constant strain is applied and the frequency is varied, during this test the temperature is also constant [14].

2.4.2.2 Static methods

2.4.2.2.1 Creep and recovery tests

This test consists basically in applying a constant stress τ_0 for a specific time (t_0) and the correspondent deformation (strain) is recorded as a function of time. Depend on the fluid and the stress applied the responses can be Newtonian, elastic solid or viscoelastic as shown in Figure 2.6. The elastic solid shows a short deformation and once the stress is removed the sample goes back to its original conformation. For the viscoelastic fluid, because of its elastic and viscous components, a continuous deformation occur until a steady rate of strain (γ_∞) is achieved and after the stress is removed the system exhibits only a small recovery (γ_r). In the case of a Newtonian fluid, the energy is lost during the application of the stress and the fluid lost entirely its original conformation.

Creep and recovery test allows obtaining quantitative information about the viscous and elastic components of a viscoelastic fluid. Also, in fluids that show structure and interactions this test provides information about how strong are them.

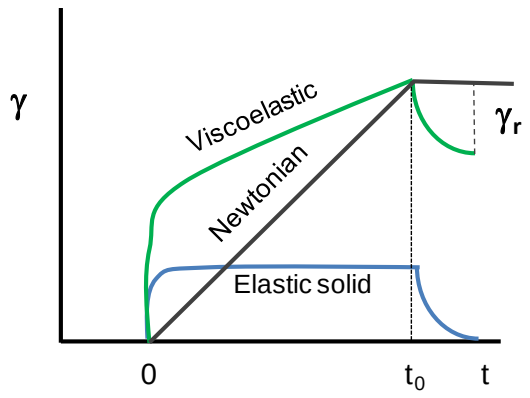

Figure 2.6. Creep and recovery for different materials.

2.4.2.3 Steady state test

This test gives information about the response of a material when the flow rate is varied by applying a shear rate [15]. Using the flow curve it is possible to characterise the flow behaviour as Newtonian, shear thinning, shear thickening and it is also possible to determine if a yield stress exists.

2.4.2.4 Experimental Parameters

All rheological tests were performed using a stress-controlled TA Instrument AR2000 and plate-and-plate geometry (diameter 40 mm, angle 0° and gap 1 mm). The plate-plate geometry was selected because of its flexibility with regard to the types of samples that can be used, i.e. it can be used with samples that vary from viscous through to those with samples having a high elastic component. Also, this geometry offers the versatility to be used for emulsions with different droplet sizes because the gap can be adjusted. Whilst all geometry measuring systems have disadvantages, the only principal disadvantage with plate-plate geometry is that shear condition is not constant through all the sample.

Dynamic strain and frequency sweep tests were performed at a frequency of 1 Hz for strain amplitudes from $1x10^{-3}$ to 100 and from 0.1 to 10 Hz for strain amplitudes below 0.02, respectively.

Creep and recovery tests were performed for a total time of 3 minutes and torque values located before the cross over point; the torque selection depended on the oil concentration and droplet size.

The flow curve was characterised by varying the shear rate from $1x10^{-3}$ to 100 s^{-1} with 10 steps per decade and three minute times for the steady state condition. For all tests the temperature was 25°C.

2.4.3 Cryo-Scanning Electron Microscope (cryo-SEM)

In a scanning electron microscope the energy provided by the electron beam is used to release atomic electrons present in the sample. The samples are scanned horizontally and vertically, producing images of the sample topography.

Egerton [16] explains SEM function as follows: an electron gun emits an electron beam that is focused by one or two condenser lenses above the sample. The incoming electrons (known as primary electrons) provide energy to the atomic electrons that are present in the sample, which can then be released as secondary electrons. These electrons are emitted with a range of energies, making it more difficult to focus them into an image by electron lenses. However, the SEM uses the principle of scanning to produce the image. Primary electrons are focused into a small-diameter electron probe that is scanned across the sample, making use of the fact that electrostatic or magnetic fields, applied at right angles to the beam, can be used to change its travelling direction. By scanning simultaneously in two perpendicular directions, a square or rectangular area of sample (known as a raster) can be covered and an image of this area can be formed by collecting secondary electrons from each point of the sample. The technique is widely used and is termed raster scanning.

The spatial resolution of the SEM depends on the size of the electron spot, which in turn depends on both the wavelength of the electrons and the electron-optical system which produces the scanning beam. The resolution is also limited by the size of the interaction volume, or the extent to which the material interacts with the electron beam. The spot size and the interaction volume are both large compared to the distances between atoms, so the resolution of the SEM is not high enough to image individual atoms. Depending on the instrument, the resolution can fall somewhere between less than 1 nm and 20 nm.

Cryo-SEM is a technique that allows the use of liquid samples to obtain images from the SEM. The preparation of the sample requires cryogenic temperatures, when liquid nitrogen is used as the cryogenic environment the temperature achieved is about -160°C. This instantaneous freezing process avoids crystal formation ensuring the real structure of the liquid sample is maintained.

2.4.3.1 Experimental Parameters

The equipment used was a Joel JSM_6500F with a Gatan Alto 2500 cryo mechanism, operated at 5 kV and $3x10^{-11}$ A. For the sample preparation, a special

cylindrical metallic device was used to load the sample. The sample was frozen in a cryogenic unit, under vacuum conditions, using liquid nitrogen. The sample was transferred to the cryo-preparation chamber and fractured using a cold knife. The sample was submitted to sublimation at -110°C for 20 minutes and coating with platinum to allow high resolution detection. Finally, the sample was transferred to the SEM chamber.

2.4 References

1. Niño, M.R.R., C.C. Sánchez, and J.M.R. Patino, *Interfacial characteristics of [beta]-casein spread films at the air-water interface.* Colloids and Surfaces B: Biointerfaces, 1999. **12**(3-6): p. 161-173.

2. Mingins, J. and N.F. Owens, *Experimental considerations in insoluble spread monolayers.* Thin Solid Films, 1987. **152**(1-2): p. 9-28.

3. Sánchez, C.C., et al., *Soy globulin spread films at the air-water interface.* Food Hydrocolloids, 2004. **18**(2): p. 335-347.

4. Rodríguez Patino, J.M., C.C. Sánchez, and M.R. Rodríguez Niño, *Structural and morphological characteristics of [beta]-casein monolayers at the air-water interface.* Food Hydrocolloids, 1999. **13**(5): p. 401-408.

5. Pearson, J.T., *The application of monolayer techniques to a study of protein-surfactant interaction : II. Interactions in adsorbed films at the air/water interface and in oil-in-water emulsions.* Journal of Colloid and Interface Science, 1968. **27**(1): p. 64-74.

6. Pearson, J.T. and A.E. Alexander, *The application of monolayer techniques to a study of protein-surfactant interaction : I. Interactions in spread films at the air/water interface.* Journal of Colloid and Interface Science, 1968. **27**(1): p. 53-63.

7. Mohwald, H., *Phospholipid and phospholipid-protein monolayers at the air/water interface.* Annual Review of Physical Chemistry, 1990. **41**: p. 441-476.

8. Garandet, J.P., B. Vinet, and P. Gros, *Considerations on the Pendant Drop Method: A New Look at Tate's Law and Harkins' Correction Factor.* Journal of Colloid and Interface Science, 1994. **165**(2): p. 351-354.

9. Yakhshi-Tafti, E., R. Kumar, and H.J. Cho, *Measurement of Surface Interfacial Tension as a Function of Temperature Using Pendant Drop Images.* International Journal of Optomechatronics, 2011. **5**(4): p. 393-403.

10. Briceño, M.I., *Rheology of suspensions and emulsions*, in *Pharmaceutical Emulsions and Suspensions*, F. Nielloud and G. Marti-Mestres, Editors. 2000, Marcel Dekker: NY, USA. p. 557–607.

11. Bloomfield, V.A., *Static and dynamic light scattering from aggregating particles.* Biopolymers, 2000. **54**(3): p. 168-172.

12. Wyatt, P.J., *Light scattering and the absolute characterization of macromolecules.* Analytica Chimica Acta, 1993. **272**(1): p. 1-40.

13. Link, S. and M.A. El-Sayed, *Shape and size dependence of radiative, non-radiative and photothermal properties of gold nanocrystals.* International Reviews in Physical Chemistry, 2000. **19**(3): p. 409-453.

14. Mezger, T.G., *The Rheology Handbook*. 3 ed 2011: Vincentz Network.

15. *Practical Food Rheology*. An Interpretive Approach, ed. I.T. Norton, F. Spyropoulos, and P. Cox2011: Wiley-Blackwell.

16. Egerton, R.F., *Physical Principles of Electron Microscopy. An Introduction to TEM, SEM, and AEM.*2005, United States of America: Springer.

Chapter 3 Sodium caseinate at air/water and oil/water interfaces

3.1 Introduction

The formulation of emulsions that have a target quality profile requires an understanding of the interfacial behaviour of the emulsifier adsorbed at the oil/water interface. In the food industry many proteins are used as emulsifiers because they have the capacity to facilitate the formation of oil-in-water (o/w) emulsions and produce different physicochemical properties of the dispersed phase [1].

The capacity of proteins to adsorb and produce a monolayer at the air/water or oil/water interface is a consequence of their hydrophilic-hydrophobic nature [2]. The amphiphilic character of proteins and their three-dimensional structure depends on the sequence of amino-acids. When protein molecules reside at an air/water or oil/water interface their three dimensional structure changes with their hydrophobic residues or domains orienting towards the non-polar phase and the hydrophilic parts to the polar phase. This re-orientation produces a process whereby proteins partially or totally unfold. The amino-acid residues and their interactions can be strongly affected by the pH and ionic strength of the system, resulting in alterations to the three-dimensional structure and self-assembly of the protein and therefore its surface activity and function.

Sodium caseinate is widely used in food technology to produce dispersed systems such as emulsions and foams because of its interfacial activity and nutritional properties [3]. The constituents of sodium caseinate (α_1, α_2, β and κ) are very flexible molecules, without tertiary structure, and as such many possible interfacial conformations exist due to the large variety of inter- and intra-molecular interactions [4]. Despite the significant use of, and applications for, sodium caseinate in the food and pharmaceutical industries, studies of sodium caseinate at the air-water or oil-water interface have not been reported. Several investigations have been reported for β-casein, one of the major constituent parts of sodium caseinate (40%), at the air-water interface using different techniques. Niño *et al.* [5] investigated the interfacial characteristics of β-casein at the air-water interface as a function of temperature and

subphase pH (pH 5 and 7) using a Langmuir-type balance. They reported that the β-casein films present two structures and that the transition between them depends on the pH and temperature. Additionally, they found that the film structure is more condensed at pH 5 than at pH 7. Atkinson *et al.* [6] studied the adsorption of β-casein and β-lactoglobulin at the air-water interface using neutron reflectivity. They found that at neutral pH β-casein forms a boundary monolayer that can be divided into a protein-rich (hydrophobic) region close to the interface and a diffuse part (hydrophilic) extending into the aqueous phase region. They also explained that the amount of β-casein adsorbed at the interface increases as the pH of the subphase is close to the isoelectric point.

The structural and morphological characteristics of β-casein monolayers, at the air-water interface, as a function of subphase pH (pH 5 and 7) were examined by Patino *et al.* [7]. They used Brewster angle microscopy (BAM) and a Langmuir-type balance to evaluate the structure of β-casein at the air-water interface. Their results confirmed those reported by Rodriguez *et al.* [8]. Ellipsometry was used by Russev *et al.* [9] to study the β-casein adsorption kinetics at air-water and oil-water interfaces. They affirmed that the β-casein adsorption process is not influenced by the type of hydrophobic phase used. Moreover, they found that a dense protein layer is initially formed and then the adsorption continues producing a more diffuse thinner layer, which is related to the extension of the protein in the interfacial domain that is finally produced.

The behaviour of sodium caseinate at two interfaces; air/water and oil/water, was investigated by changing the ionic strength and pH of the aqueous phase. With regard to changing the ionic strength, the purpose was to investigate how at a specific hydrophilic-hydrophobic balance on the casein molecules (constant pH) the ion concentration in the aqueous phase influences sodium caseinate behaviour at the interfaces. The pH of the aqueous phase was changed to study how variations in the hydrophilic-hydrophobic balance and the charge of the casein molecules affect their behaviour at an interface. It is important to state that the study of sodium caseinate at an interface at very low ionic strengths (below 20 mM) changes to the ionic strength of the buffer solutions were made without adding ions other than those that make up the buffer. This approach has not been used previously, to the best of

my knowledge, in any research where proteins at an interface has been studied. The aim of this work was to develop a model that described how the different conformations of sodium caseinate at the air/water and oil/water interfaces could be altered when the ionic strength and pH of the aqueous phase were changed. This information will be used to elucidate how the different conformations of sodium caseinate at an interface can be related to the behaviour of oil/water sodium caseinate concentrated emulsions when the ionic strength and pH of the continuous phase is changed.

3.2 Results and discussion

Prior to exploring the monolayer isotherm behaviour, it was necessary to determine the quantity of protein needed to produce a representative monolayer (here defined as one which exhibits the gas phase at maximum trough area) and the time required for the protein monolayer to achieve structural equilibrium. To determine the quantity of protein required to form a representative monolayer at different subphase pH and ionic strengths, the amount of protein was varied until a gas phase was formed at the maximum trough area while still detecting the collapse of the monolayer upon monolayer compression. An estimate of the time to equilibrium was obtained by placing a specified amount of sodium caseinate at the air-water interface and monitoring the π-area of isotherms as a function of time. Once the mean deviation was reduced to ± 0.1 mN/m for successive time runs the system was defined to be at equilibrium. The data deviation, for all the systems investigated, was calculated using the procedure shown in Appendix A1. In Figure 3.1 are shown representative examples of both procedures.

For both figures on the x axis, the lowest and highest areas (68 and 540 cm^2) correspond to the minimum and maximum apertures of the barriers respectively. In Figure 3.1 (top), it is demonstrated how the surface pressure increased with the mass of sodium caseinate at the air-water interface. For sodium caseinate mass above $1.09x10^{-1}$mg, it can be seen that the gas phase is almost absent and this condition is not desired. On the other hand, very low mass of sodium caseinate will produce a long gas phase without the possibility to detect representative liquid or solid phases. Considering the detection of the different phases on Figure 3.1 (top), $8.55x10^{-2}$ mg of sodium caseinate was the mass limit used to produce a

representative isotherm. With regards to the time necessary for the system to achieve equilibrium at the air-water interface (Figure 3.1 bottom), it can be seen that 30 minutes is adequate. The procedures described previously were the same as used by Niño *et al.* [5] in their study of the β-casein at the air-water interface.

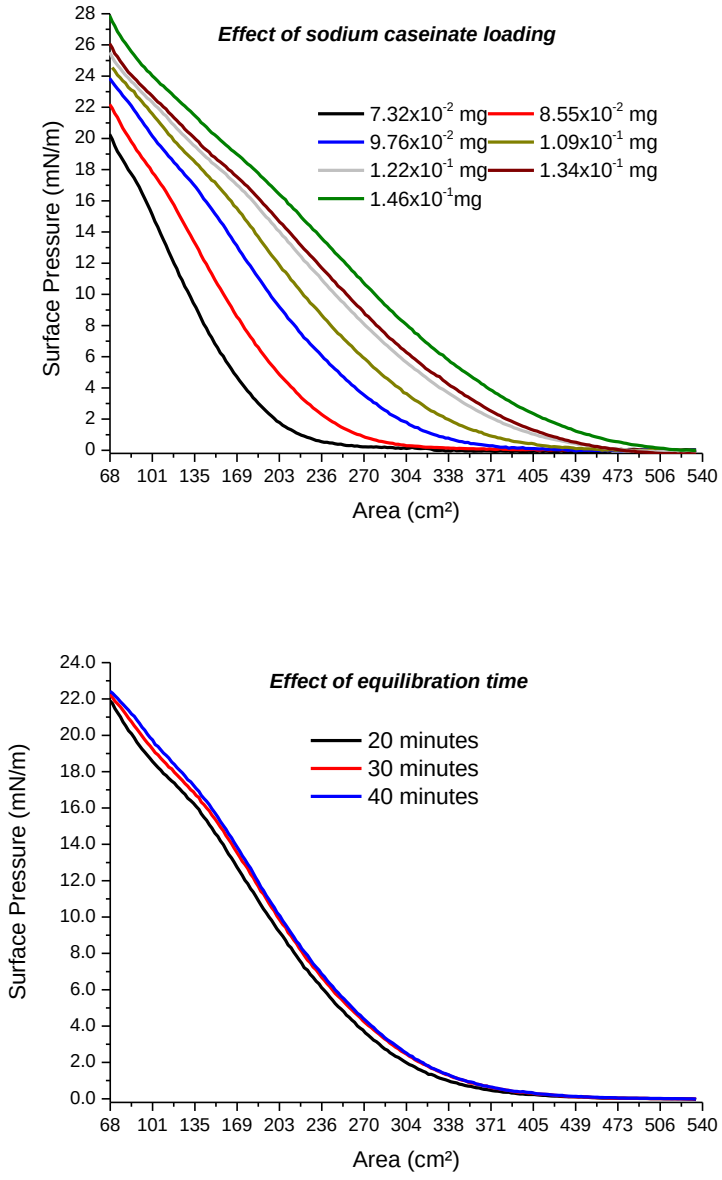

Figure 3.1 π-A isotherms for sodium caseinate films at the air-water interface to establish the quantity of sodium caseinate (top) and the equilibrium time (bottom). Phosphate subphase buffer, pH 6.8 and ionic strength 0.5 mM.

When isotherms of sodium caseinate at different pH and ionic strength values were compared, a criterion had to be used to select the mass of protein required for the different conditions. The criterion used consisted of choosing the lowest quantity of

sodium caseinate necessary to produce a representative isotherm for one of the systems and then comparing all the others with this.

3.2.1 Sodium caseinate π-A isotherms

Measurement of surface pressure-area isotherms (π-A) is a well-known method for obtaining thermodynamic data about monolayers [10]. Generally, different phases of the monolayer, such as gaseous (G), liquid-expanded (LE), liquid-condensed (LC) and solid (S) can be detected upon changing the area for a fixed quantity of molecules on the surface at a constant temperature. The changes in the area generate variations in the surface pressure and with this data the isotherm can be obtained. In Figure 3.2 representative pressure-area isotherms are shown for sodium caseinate monolayers for two of the subphases investigated here.

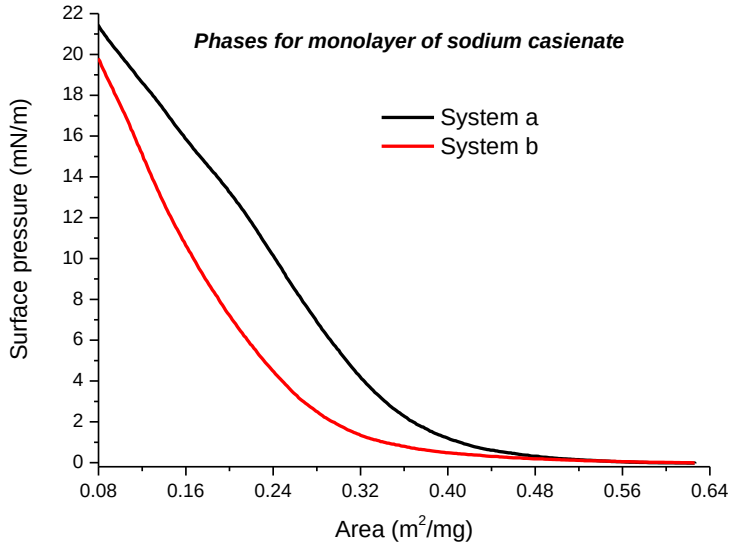

Figure 3.2 π-A isotherms for sodium caseinate films at the air-water interface (Mass of protein 8.55 x 10^{-2} mg). a) pH 6.8 and ionic strength 0.5 mM. b) pH 10 and ionic strength 1.4 mM.

Sodium caseinate monolayer isotherms have a liquid-expanded-like structure for all the systems studied; a similar result was reported by Rodriguez *et al.* for β-casein [7, 11]. The sodium caseinate isotherms show multiple phases and one plateau that depends on the physicochemistry of the subphase. The isotherms shown in Figure 3.2 display a plateau representing the gas-liquid two phase region at areas of 0.48-0.64 m^2/mg and 0.37-0.64 m^2/mg, for pH 6.8 (a) and 10 (b), respectively.

Upon decreasing the area, the monolayer advances into an LE phase. The LE phase spans from the end of the gas-liquid plateau (0.48 m^2/mg) to an area around 0.22 m^2/mg for pH 6.8. At pH 10 the LE phase is from 0.37 m^2/mg to 0.108 m^2/mg. For the sodium caseinate isotherms, the LE-LC transition takes place without the occurrence of a plateau which corresponds to a first-order transition. The absence of a plateau for the LE-LC transition is frequently observed for macro polymer and protein monolayers, and this kind of transition is known as a second order phase transition. Second order phase transitions are associated with the formation of aggregates, i.e., protein self-assembly, at the interface. Support for the formation of aggregates has been observed in some recent studies [7, 12]. The phase transition points LE-LC and LC-S in the isotherms were estimated by fitting the different phases to a linear equation and then finding the intersection point between the two consecutive phases. For the gas phase, the end of the plateau was reported as the transition between Gas-LE and the curvature between this point (Gas-LE) and the line of the LE phase was the phase change (Gas-LE). Figure 3.3 displays an example of the estimation of the phases in an isotherm and the Appendix A2 shows the procedure used to obtain the transition phases.

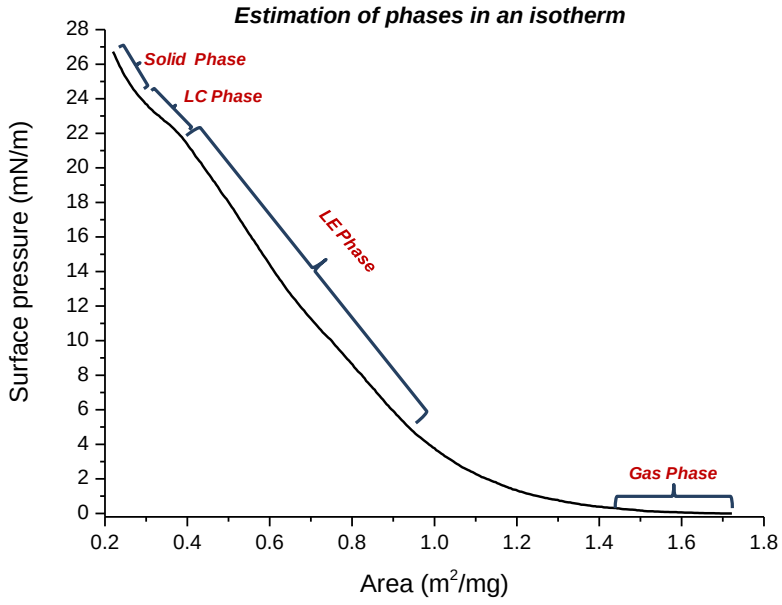

Figure3.3. Estimation phases for a π-A isotherm for sodium caseinate spread at the air/water interface: subphase pH 6.7, phosphate buffer. Ionic strength 63 mM and 0.031 mg of sodium caseinate present at the interface.

3.2.2 Effect of aqueous phase pH on protein conformation

In the food industry, proteins can be in contact with different physicochemical environments (pH and salinity) during food processing. Understanding their behaviour in the different environments is essential to control the properties of the final product, especially when they are used as an interfacial agent to produce dispersed systems.

The aqueous subphase pH, where the protein is located, has an effect on the charge of the protein and its hydrophobic-hydrophilic ratio. The transition between positive to negative charge defines the isoelectric point of the protein, i.e., at pH values below its isoelectric point (IP) a protein will have a net positive charge. In contrast, at pH above the IP the protein will have a net negative charge [13]. The values of the isoelectric point of the caseins, α_1 , α_2 , β and κ are around 4.93, 5.33, 5.24 and 5.76, respectively [14]. Sodium caseinate, which is a mixture of the caseinates, has an isoelectric point between pH 4.6 and 5. As a result, an overall positive charge of the sodium caseinate mixture is expected below pH 4.6 and a negative charge above pH 5. As a consequence, protein molecules at different subphase pH not only present diverse conformations and interactions between them, but also functionality.

The different charges and IP of proteins depend on their amino-acid sequence. Hence, knowledge of type, quantity and sequence of the amino acids in proteins is crucial to understand their properties. In Table 3.1 is given the amino-acid composition of the caseins and their pKa [14, 15] and an estimation of the number of amino-acids located at the interface for the pH values evaluated. For the estimation of the amino-acids located at the interface, it was supposed that for a specific pH the amino-acids without charge (hydrophobic groups) were at the interface and the amino-acids with charge (hydrophilic groups) were into the aqueous phase.

The π-A isotherms of sodium caseinate monolayers as a function of subphase pH were studied. Four subphase pH domains were considered: acid pH (below the isoelectric point), the isoelectric point (pH 4.6-5), neutral pH and basic pH (see Figures 3.4 and 3.5). Also, an estimation of the proportion of the caseins that could be located at the interface was done using the information provided in Table 3.1.

Residual group pKa values (Table 3.1) were used to establish changes between hydrophobic-hydrophilic characters of the amino-acids. For this estimation, it was assumed that not only the hydrophilic amino-acid residual groups were immersed into the aqueous phase, but also the rest of their amino-acid components. This simplification was used considering the high flexibility of the caseins and their similarity to long linear polymers.

In Figure 3.4 the sodium caseinate isotherms at four different pH subphases; 1.9, 4.8, 6.7 and 9.6 are shown as representatives of the pH range investigated. A subphase ionic strength of 63mM was required in order to achieve the lowest pH using a HCl/KCl buffer solution. For all pH values used the sodium caseinate isotherms have a liquid-expanded-like structure. At subphase pH 1.9 and 6.7 the isotherms show four phases: gas, liquid-expanded (LE), liquid-condensed (LC) and solid. Three phases are observed at subphase pH 4.8 and 9.6: gas, liquid-expanded (LE) and liquid-condensed (LC). In Table 3.2 the quantitative analysis of the phase transitions observed in the π-A isotherms are summarised.

The number of phase transitions observed for the sodium caseinate monolayers for the different subphase pH values is associated with the changes in the hydrophobic-hydrophilic balance of the proteins resulting in different conformations and the subsequent multiplicity of inter and intramolecular interactions [16]

At subphase pH 1.9, it can be predicted that casein molecules will have enhanced high hydrophobicity (see Table 3.1) with the highest ratio of amino-acids located at the interface. The net charge is positive due to the lysine and arginine residual groups. As a result, a large proportion of the protein molecules avoid the aqueous phase by altering their conformation in an attempt to be located at the air/water interface while the hydrophilic part is immersed into the aqueous phase. The net positive charge on the proteins creates an electrostatic repulsion that keeps the molecules apart. Therefore, the G-LE transition for sodium caseinate monolayers at subphase pH 1.9 occurs on a large area on the Langmuir trough and four phases are detected (see Table 3.2).

Table 3.1. Amino-acid composition of caseins and their typical pK values of the ionisable groups and an estimation of the amino acids located at the interface at different pH values

Amino-acids	***α_1 (%)***	***α_2 (%)***	***β (%)***	***κ (%)***	***pK***	***pH = 1.9***	***pH = IP***	***pH = 6.7***	***pH = 9.6***
Asp	3.66	2.06	1.96	1.82	2-5.5	9.5			
Asn	4.19	7.22	2.45	4.85		18.71	18.71	18.71	18.71
Thr	2.62	7.73	4.41	8.48		23.24	23.24	23.24	23.24
Ser	4.19	3.09	5.39	7.27		19.94	19.94	19.94	19.94
Glu	13.09	12.37	9.31	7.27	2-5.5	42.04			
Gln	7.33	8.25	9.8	8.48		33.86	33.86	33.86	33.86
Pro	8.9	5.15	17.16	12.12		43.33	43.33	43.33	43.33
Gly	4.71	1.03	2.45	1.21		9.4	9.4	9.4	9.4
Ala	4.71	4.12	2.45	9.09		20.37	20.37	20.37	20.37
Val	5.76	7.22	9.31	6.67		28.96	28.96	28.96	28.96
Met	2.62	2.06	2.94	1.21		8.83	8.83	8.83	8.83
Ile	5.76	5.67	4.9	7.88		24.21	24.21	24.21	24.21
Leu	8.9	6.7	10.78	4.85		31.23	31.23	31.23	31.23
Tyr*	5.24	6.19	1.96	5.45	9-12.1	18.84	18.84	18.84	
Phe	4.19	3.09	4.41	2.42		14.11	14.11	14.11	14.11
Trp	1.05	1.03	0.49	0.61		3.18	3.18	3.18	3.18
Lys	7.33	12.37	5.39	5.45	9.5-10				
His*	2.62	1.55	2.45	1.82	5-8.1	8.44	8.44		
Arg	3.14	3.09	1.96	3.03	12.5				
Amount of amino-acids presumably located at the air-water interface						348.69	306.65	298.21	279.37
Ratio of amino-acids located at the air-water interface/amount total of amino-acids *						0.89	0.79	0.76	0.72

****The amount total of amino-acids was 390.45 that correspond to the addition of the total amino-acids of each casein.***

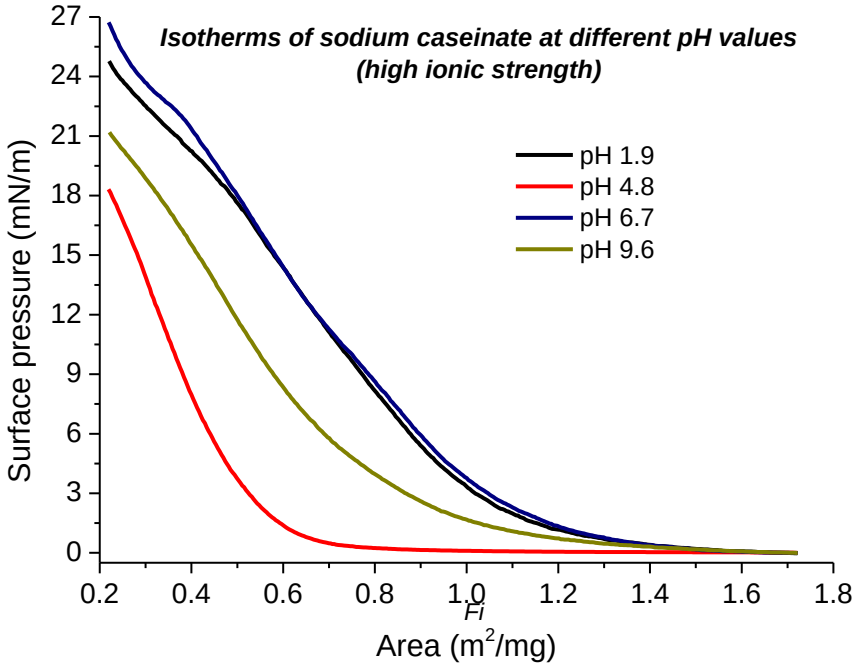

gure3.4. π-A isotherms for sodium caseinate spread at the air/water interface: subphase pH 1.9, buffer HCl/KCl; pH 4.8, acetate buffer; pH 6.7, phosphate buffer; and pH 8.9, phosphate buffer. Ionic strength for all subphases: 63mM, 0.031 mg of sodium caseinate present at the interface.

At subphase pH 4.8 the G-LE phase transition is detected at the lowest trough area for all pH values studied, despite that the ratio of amino-acids located at the interface is the second in decreasing order (see Figure 3.4 and Tables 3.1 and 3.2). This result is associated with the attraction between the protein molecules because their total charge equals or is around zero, i.e., the isoelectric point. Aggregation of sodium casein protein molecules at the air-water interface is expected at pH values near its isoelectric point.

Table 3.2 Phase transition areas for sodium caseinate monolayers spread on aqueous subphases.

pH (Not units)	Gas-LE (m^2/mg)	LE-LC (m^2/mg)	LC-S (m^2/mg)
1.9	1.56 ±0.01	0.46 ±0.07	0.26 ±0.23
4.8	0.99 ±0.01	0.27 ±0.05	Not detected
6.7	1.54 ±0.01	0.33 ±0.05	0.28 ±0.31
9.6	1.42 ±0.01	0.35 ±0.04	Not detected

Subphase ionic strength 63mM

For neutral subphase pH the G-LE phase transition is detected at a large trough area and four phases are distinguished (see Figure 3.4 and Table 3.2), in similarity with subphase pH 1.9. At neutral pH the charge density of the sodium caseinate protein molecules is elevated [17]. As a result, the protein molecules are dispersed at the air/water interface because of the electrostatic repulsions and a large area at the interface is covered by protein molecules. Additionally, the hydrophobic fraction of the casein molecules is contributing to the large interfacial area covered by the protein molecules.

Basic subphase pH produces a slight decrease in the area at which the G-LE phase transition takes place and three phases are identified: gas, liquid expanded and liquid condensed (see Figure 3.4 and Table 3.2). At subphase pH 9.6 the protein molecules show two characteristics: significant hydrophilic character (see Table 3.1) and a large negative charge density. These are both a consequence of the lysine and arginine deprotonation. Cross *et al.* [18] showed that increasing the subphase pH increases the capacity to bind calcium and phosphate due to the rise in the negative charge of the casein molecules. The strong charge density of the protein molecules produces a large electrostatic repulsion between them preventing the formation of the solid phase.

The values of the measured surface pressures as a function of pH provide information on the conformation of the protein molecules at the air interface and the interactions between them. Low surface pressure values are a consequence of the attraction between the protein molecules (isoelectric point), or high hydrophilic fraction in the protein molecules which decrease the interfacial area that can be covered by the protein molecules (basic pH). On the contrary, high surface pressure values are related to high electrostatic repulsion within and between protein molecules or protein molecules which have a large hydrophobic fraction, therefore covering a large area at the interface.

Sodium caseinate monolayers with different pH values were also studied at low ionic strengths, except for the pH domain below the isoelectric point. This exception is because no acid buffers could be formulated at a very low ionic strength. The sodium caseinate isotherms for the subphase pH values 4.5, 6.9 and 9.8 are shown in Figure 3.5.

The pH effect on the behaviour of the sodium caseinate molecules at the air-water interface at a low ionic strength is similar to that observed at a high ionic strength, and the isotherms also show a liquid-expanded-like structure. It is important to point out that the quantity of sodium caseinate protein used for the low ionic strength experiments (0.085 mg) was approximately three times the quantity used for the high ionic strength experiments (0.031 mg). The reason for the difference in the quantities of sodium casein mass is explained below.

At subphase pH 4.5 the G-LE phase transition occurs at the lowest trough area (see Figure 3.5 and Table 3.3). This result corroborates the effect of the isoelectric point on the aggregation of the sodium caseinate protein molecules at the air-water interface. Additionally, the isotherm only shows two phases: gas and liquid expanded.

The G-LE phase transition for subphase pH 6.9 was detected at the largest trough area (see Table 3.3) and four phases were detected: gas, LE, LC and solid. Furthermore, at this pH the value of the surface pressure is the highest, suggesting high electrostatic repulsion and the considerable hydrophobic character of the protein molecules (Table 3.1).

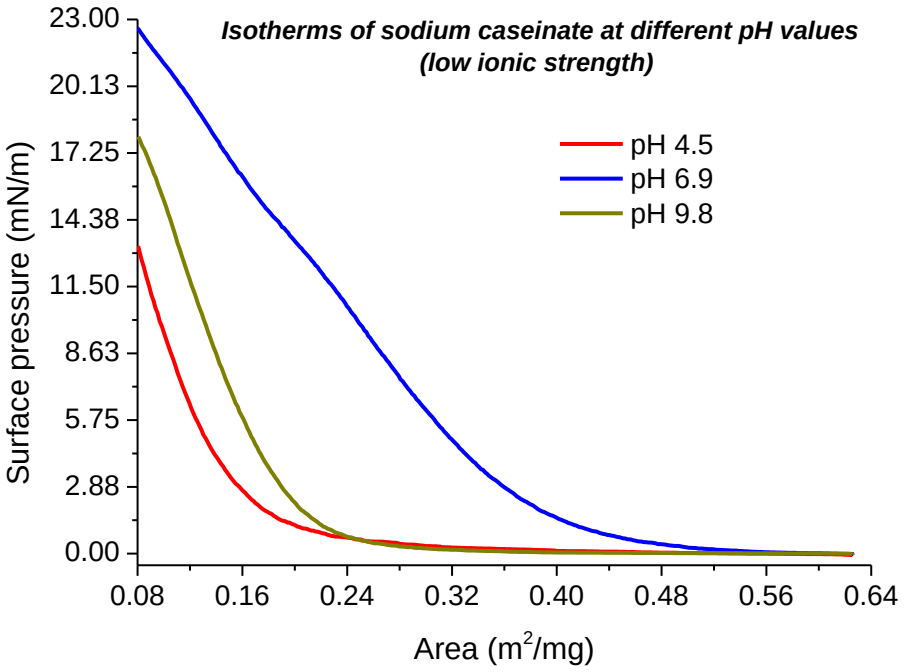

Figure3.5. π-A isotherms for sodium caseinate spread at the air/water interface: subphase pH 4.5, acetate buffer; pH 6.9, phosphate buffer; and pH 9.8, phosphate buffer. Ionic strength of all subphases: 2mM, 0.085 mg of sodium caseinate present at the interface.

Table 3.3 Phase transitions areas of sodium caseinate monolayers spread on aqueous subphases

pH (Adim)	Gas-LE (m^2/mg)	LE-LC (m^2/mg)	LC-S (m^2/mg)
4.5	0.36 ±0.01	Not detected	Not detected
6.9	0.54 ±0.01	0.26 ± 0.05	0.18 ±0.21
9.8	0.42 ±0.01	0.11 ± 0.04	Not detected

Subphase ionic strength 2mM

Finally, at subphase pH 9.8 a decrease in the transition area of the G-LE phase transition is shown and three phases detected (see Figure 3.5 and Table 3.3). At this pH, a large fraction of the protein molecules are immersed in the aqueous phase; thereby reducing the area at the interface that is covered by the protein molecules.

3.2.3 Effect of aqueous phase pH on monolayer elasticity

The phase transitions and the cohesive or disperse structure of the monolayer can be quantitatively determined from analysis of the elasticity of the monolayer. Monolayer elasticity, which is a measure of the resistance of the interfacial film to a change in area, can be extracted from the isotherm data. The elasticity of a monolayer, E, at zero deformation rate, is estimated from the slope of the surface pressure-area isotherm at a constant temperature, according to the equation

$$E = -A\left(\frac{\delta\pi}{\delta A}\right)_T \qquad 3.1$$

where A is the surface area and π is the surface pressure

In Figures 3.6 and 3.7 the elasticity versus superficial density for sodium caseinate spread on subphases of different pH values at 25°C are shown.

On the basis of the results shown in Figures 3.6 and 3.7, it is evident that the elasticity of the sodium caseinate monolayer depends on the pH of the aqueous phase. The general behaviour for all monolayers studied is that the elasticity of the monolayer increases as a function of the superficial density until reaching a maximum, after which the elasticity decreases. The superficial density at which the maximum in the elasticity is achieved depends on how disperse or compact the protein molecules are at the interface.

For subphase pH values of 1.9 and 6.7 and ionic strength 63 mM (Figure 3.6) the maximum elasticity is achieved at a lower superficial density than for a subphase pH of 4.8 and 9.6. These results are in concordance with their corresponding isotherms, where a large area at the interface is occupied by the sodium caseinate proteins because of their high hydrophobic character and the electrostatic repulsion between the protein molecules. Additionally, two maxima are detected which is consistent with the number of phase transitions observed to take place at these subphase values (see Table 3.2).

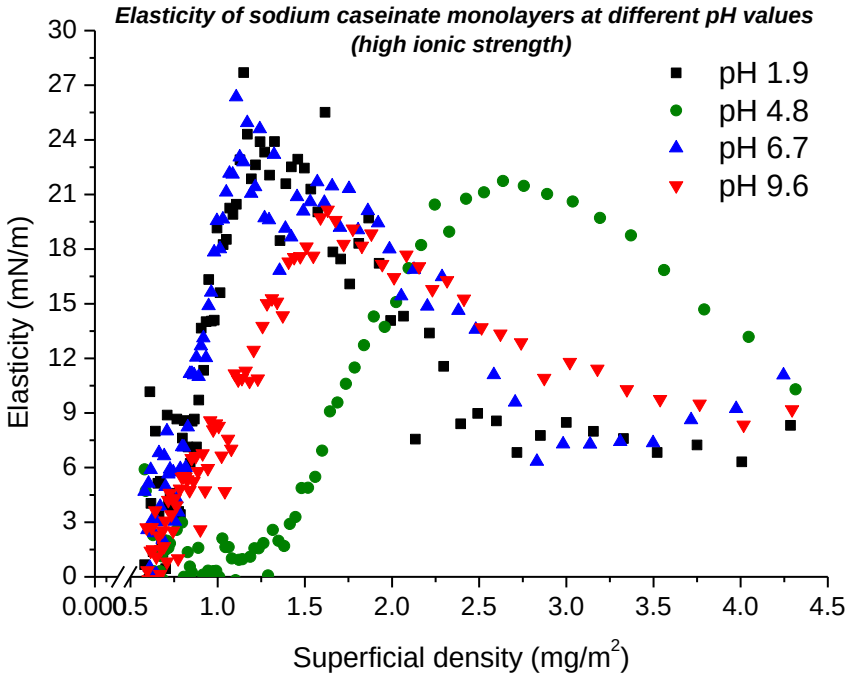

Figure3.6. Elasticity vs. surface concentration for sodium caseinate spread at the air/water interface: subphase pH 1.9, buffer HCl/KCl; pH 4.8, acetate buffer; pH 6.7, phosphate buffer; and pH 8.9, phosphate buffer. Ionic strength 63mM for all subphases and 0.031 mg of sodium caseinate used to form the monolayers.

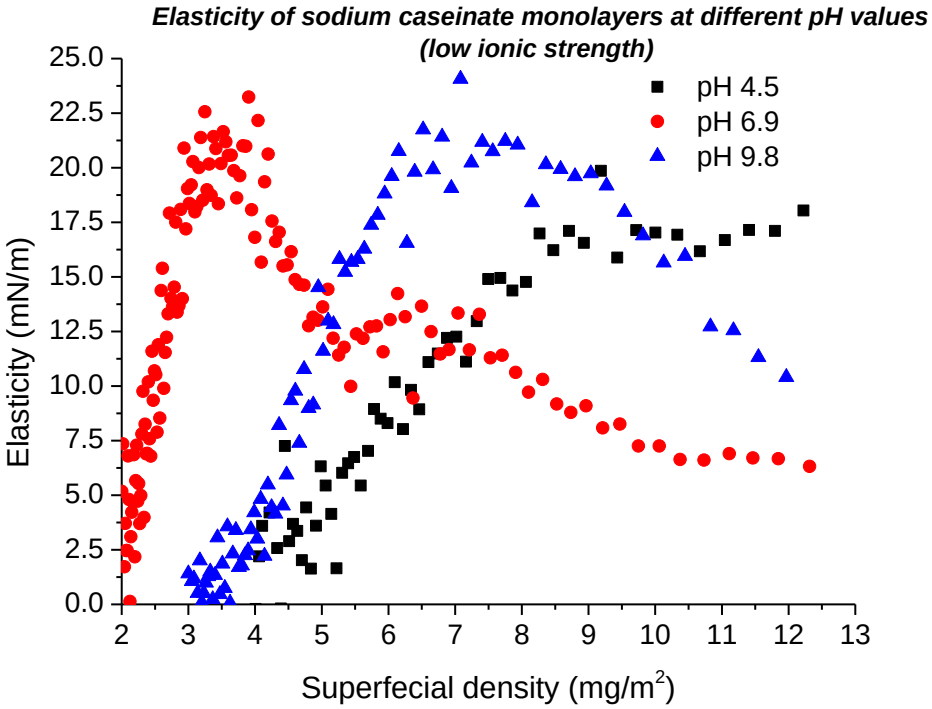

Figure3.7. Elasticity vs. surface concentration for sodium caseinate spread at the air/water interface: subphase pH 4.5, acetate buffer; pH 6.9, phosphate buffer; and pH 9.8, phosphate buffer. Ionic strength of all subphases: 2mM and 0.085 mg of sodium caseinate used to form the monolayers.

The elasticity curves for subphases at pH 4.8 and 9.6 show only one maximum and it is achieved at high values of superficial density, around 2.75 and 1.5 mg/m^2 respectively. At subphase pH 9.6, the maximum in the elasticity is at a large superficial density due to a significant amount of the individual protein molecules

immersed in the subphase. Hence, the interfacial area covered by the protein is small. When the subphase pH is 4.8 the maximum elasticity is achieved at the highest value of superficial density. This result is expected because of protein aggregation occurring for pH values at the isoelectric point.

When the monolayer is contained within a small area on the Langmuir trough, i.e. high superficial density, the following decreasing trend in the measured elasticity is observed with respect to subphase pH: 4.8, 9.6, 1.9 and 6.7 (see Figure 3.6). This result is a consequence of cohesion between the protein molecules. At pH 4.8, which is around the isoelectric point, the attractive forces dominate the interactions between protein molecules and aggregation occurs. As a result, the density of molecules per area is large. At pH 9.6, a large proportion of the protein is immersed into the aqueous phase and therefore more molecules can be located at the interface. However, the electrostatic repulsion impedes strong cohesion between protein molecules.

Low values of elasticity are evident at pH values 1.9 and 6.7. This behaviour is associated with the large proportion of hydrophobic amino-acid groups in the protein molecules being located at the interface. Also, the charge of the protein molecules generates electrostatic repulsion that keeps the molecules apart from each other. As a result, few protein molecules can be located at the air-water interface thereby reducing the elasticity.

Decreasing the ionic strength to 2 mM, produced similar results to those for an ionic strength of 63 (see Figure 3.7). The highest values of elasticity at low superficial density, i.e. large trough areas, are achieved at a neutral pH. This result is associated with the large proportion of the protein molecules located at the interface and the electrostatic repulsion between them. On the contrary, at high superficial density the monolayer at subphase pH 4.5 shows higher elasticity values than for subphases at pH 6.9 and 9.8. Also, the decreasing order of elasticity at ionic strength 2 mM is the same as the order reported at ionic strength 63mM: pH 4.5, pH 9.8 and pH 6.9. Thus, the cohesion between the protein molecules of sodium caseinate at the air-water interface at high values of superficial density depends on the similarity of the pH of the subphase to the isoelectric point, and how small the proportion of the

protein molecules that resides at the interface compared with that in the aqueous phase.

3.2.4 Effect of ionic strength on protein conformation

Proteins have a large number of possible conformations due to the rotational mobility of many of the individual bonds present in their covalent backbone. Their possible conformations are a consequence of the environment in which they are located. Some factors that produce changes in protein conformation include: temperature, pH, electrolyte chemistry and added surfactants. Once the physicochemistry of the environment is altered, the protein molecules adopt the conformation that offers the most stable thermodynamic condition and the lowest Gibbs energy [19].

The chemical identity of the electrolytes and their concentration have a remarkable effect on conformation, stability, solubility and biological activity of proteins, as well in their electrostatic interactions [20]. Electrolytes can influence the stability and solubility of proteins through effects known as salting-in and salting-out, which are highly ion specific [21].

The salting-in effect consists of the binding of charged groups in the protein by electrolytes added to the water-protein system, promoting the destabilisation of the proteins. Electrolytes that promote salting-in are called chaotropic ions. The salting-out effect is related to the dramatic decrease in the solubility of protein molecules due to the presence of strongly hydrated electrolytes which attract water molecules from the hydrophilic groups of the protein. These electrolytes are known as komostropes. The effects of specific electrolytes on protein properties have been investigated for many years and the effects have shown a reoccurring trend summarised in the Hofmeister series [22]. To the best of knowledge of this researcher the majority of studies on the effect of ionic strength on protein conformation have been performed using a buffer plus additional electrolytes (salts) to increase the ionic strength. The mixture of electrolytes can produce effects on the protein conformation which make it complex to understand as to whether the effect is due to changes in the ionic strength or the effect of the specific electrolytes present in solution.

In this research, the evaluation of the effect of ionic strength on the protein conformation of sodium caseinate monolayers at the air-water interface was done by progressively changing the buffer concentration without adding any additional electrolyte. This method was used in order to study the specific effect of the ionic strength on the sodium caseinate conformation. The effect of different ions, according to the Hofmeister series, was not evaluated in this research. The procedure used to formulate the buffers with the different ionic strengths is given in the Appendix A3.

The monolayers of sodium caseinate were evaluated at three different pH values: the isoelectric point, neutral pH and basic pH. The different buffer solutions used for the different pH values were: acetate, phosphate and carbonate respectively. Acetate buffer solutions were made by mixing sodium acetate and acetic acid solutions, while phosphate and carbonate buffer solutions were prepared by combination of disodium hydrogen orthophosphate-potassium dihydrogen orthophosphate and sodium hydrogen carbonate-sodium carbonate, respectively. Six ionic strengths were investigated: 4mM, 8mM and 12mM, the so-called low ionic strength range, and 35mM, 40mM and 45mM, for the high ionic strength range. The mass of the sodium caseinate used to produce the monolayers for the low and high ionic strength ranges were 0.034 and 0.023mg respectively. These quantities were selected in order to compare the sodium caseinate isotherms at all the pH values studied, not only for a specific ionic strength range but also between low and high ionic strength ranges. The experiences were repeated three times and the deviation was calculated according to the procedure shown in the Appendix A1. Sodium casein isotherms at the air-water interface at different pH and ionic strength values are shown in Figures 3.8-3.13.

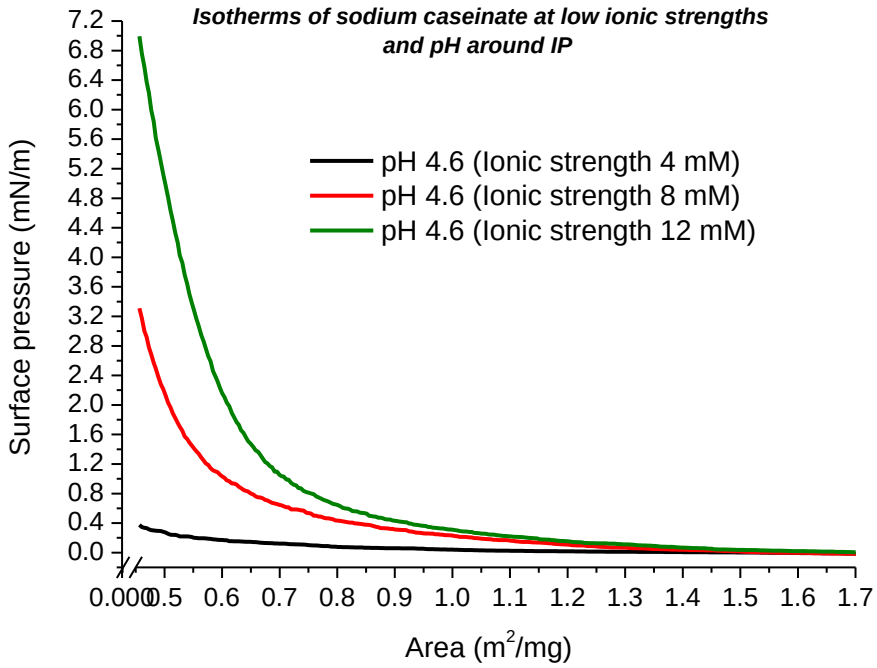

Figure3.8. π-A isotherms for sodium caseinate spread at the air/water interface. Subphase: acetate buffer, pH 4.6, low ionic strengths and 0.034 mg of sodium caseinate.

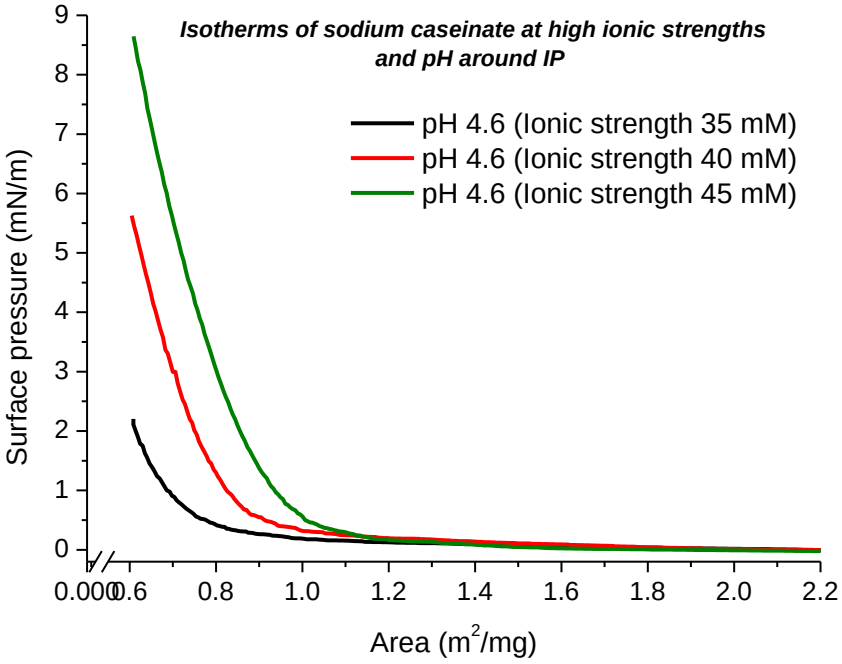

F*igure3.9. π-A isotherms for sodium caseinate spread at the air/water interface. Subphase: acetate buffer, pH 4.6, high ionic strengths and 0.023 mg of sodium caseinate.*

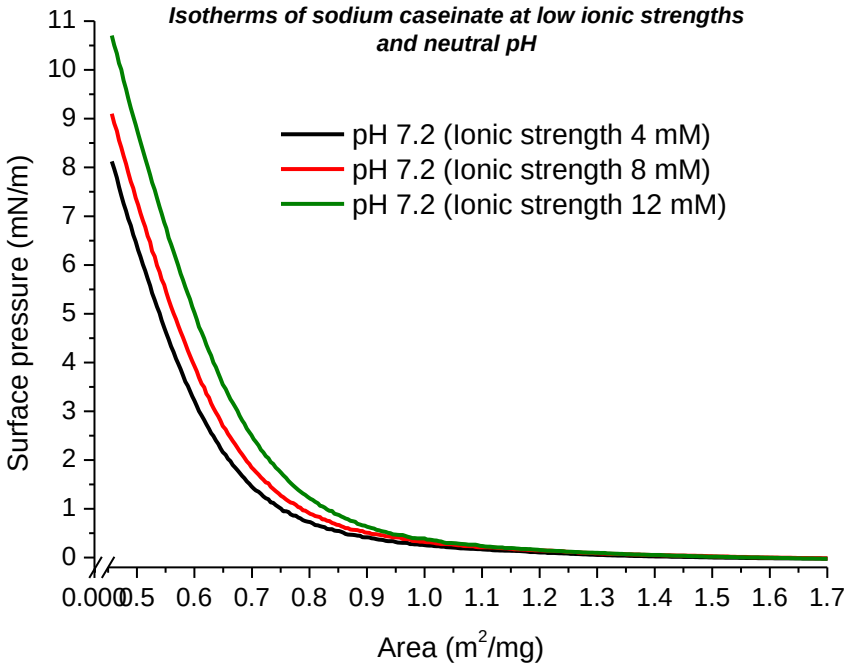

Figure3.10. π-A isotherms for sodium caseinate spread at the air/water interface. Subphase: phosphate buffer, pH 7.2, low ionic strengths and 0.034 mg of sodium caseinate.

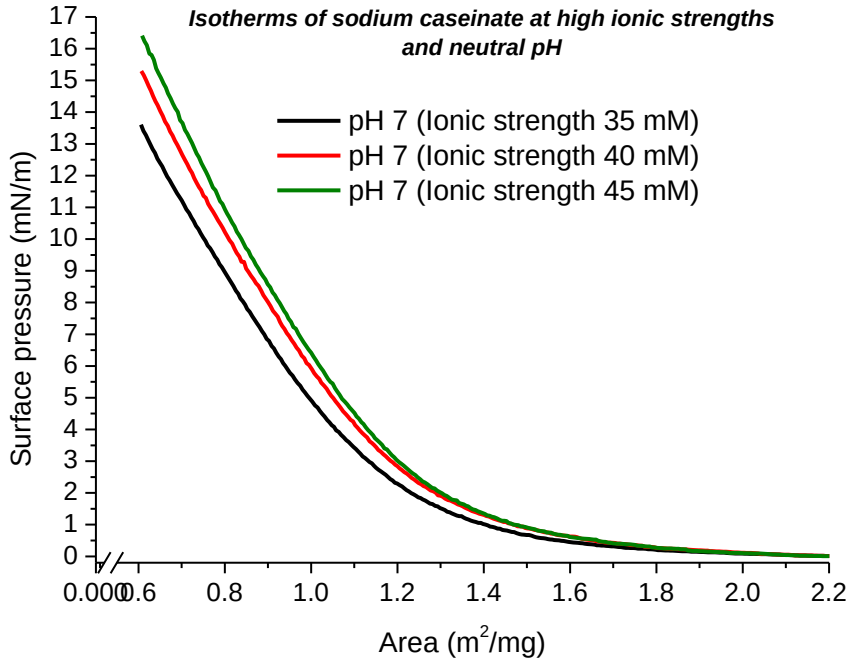

Figure3.11. π-A isotherms for sodium caseinate spread at the air/water interface. Subphase: phosphate buffer, pH 7, high ionic strengths and 0.023 mg of sodium caseinate.

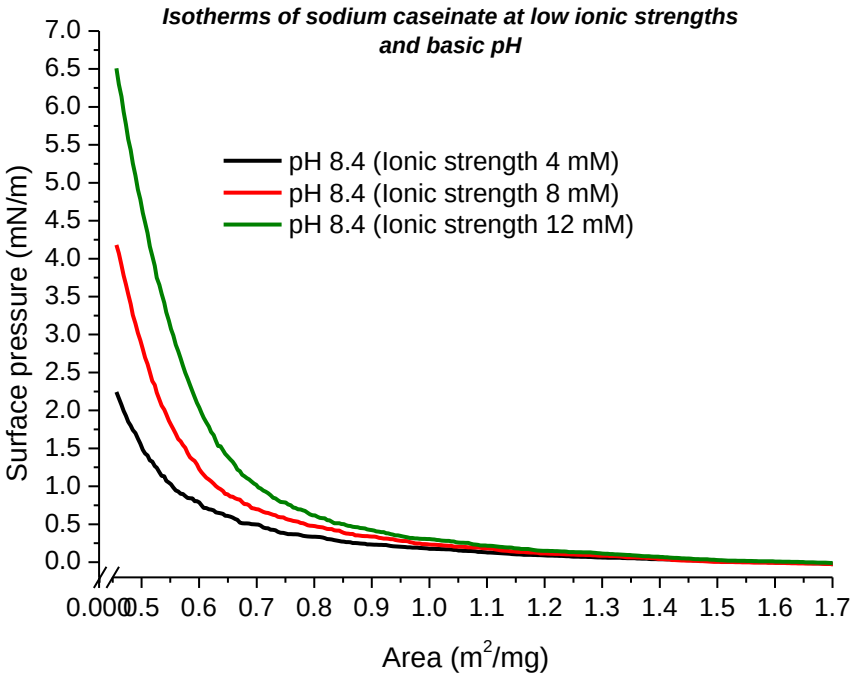

Figure3.12. π-A isotherms for sodium caseinate spread at the air/water interface. Subphase: carbonate buffer, pH 8.4, low ionic strengths and 0.034 mg of sodium caseinate.

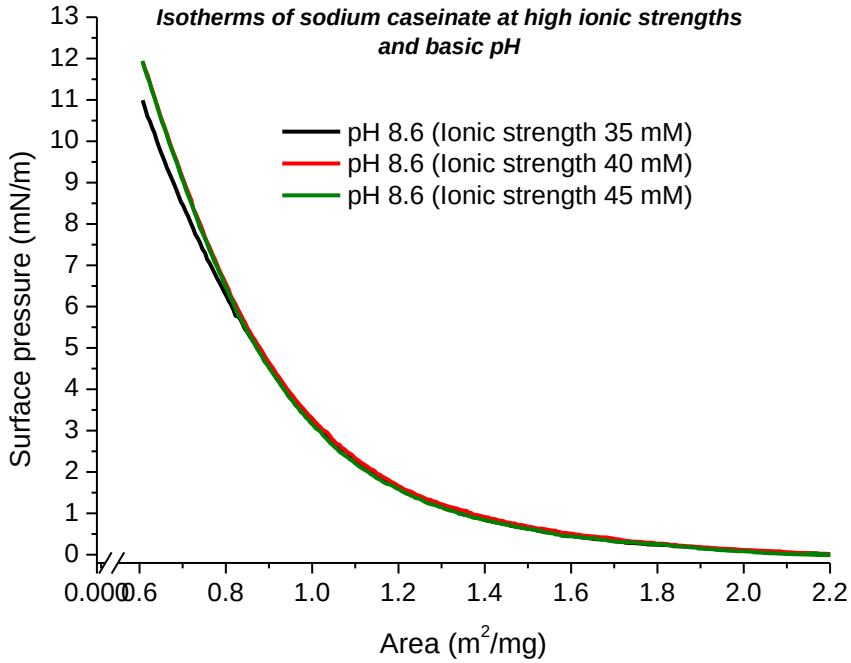

Figure3.13. π-A isotherms for sodium caseinate spread at the air/water interface. Subphase: carbonate buffer, pH 8.6, high ionic strengths and 0.023 mg of sodium caseinate.

A general trend for all the subphase pH values studied, retaining a constant mass of protein for both ionic strength ranges, was an increment in the surface pressure and the interface area covered by protein molecules on increasing the ionic strength.

Similar results were reported by Nieto Suarez *et al*. [12], Miñones Conde *et al.* [23] and Phillips *et al*. [24] using insulin, lysozyme and block co-polypeptide monolayers of protein at the air-water interface respectively. Additionally, the changes in these parameters are more significant at low ionic strengths (4-12 mM) than at high ionic strengths (35-45 mM).

To compare the capacity of protein molecules to cover the air-water interface, a specific surface density was set (0.7 m^2/mg) and its corresponding surface pressure was measured for different ionic strength and pH values (Tables 3.4-3.6). This specific surface density was chosen, because measurements of the surface pressure could be performed at either low or high ionic strength values. Also, in Tables 3.4-3.6 the maximum surface pressure is displayed at the minimum area at the trough.

Table 3.4 Maximum surface pressure and surface pressure at (0.7m^2/mg) for sodium caseinate monolayers spread on aqueous subphases with different ionic strengths and pH 4.6

Ionic strength (mM)	Maximum surface pressure (mN/m)	Surface pressure (mN/m)
4	0.37 ± 0.25	0.12 ± 0.02
8	3.31 ± 0.31	0.64 ± 0.02
12	6.90 ± 0.28	1.03 ± 0.03
35	2.20 ± 0.30	0.91 ± 0.02
40	5.63 ± 0.22	2.99 ± 0.01
45	8.64 ± 0.30	5.47 ± 0.02

Table 3.5 Maximum surface pressure and surface pressure at (0.7 m^2/mg) for sodium caseinate monolayers spread on aqueous subphases with different ionic strengths and pH ≈ 7

Ionic strength (mM)	Maximum surface pressure (mN/m)	Surface pressure (mN/m)
4	8.12 ± 0.29	1.41 ± 0.02
8	9.10 ± 0.25	1.80 ± 0.01
12	10.70 ± 0.28	2.42 ± 0.01
35	13.60 ± 0.23	11.21 ± 0.02
40	15.29 ± 0.24	12.65 ± 0.03
45	16.40 ± 0.25	13.65 ± 0.02

Table 3.6 Maximum surface pressure and surface pressure at (0.7 m^2/mg) for sodium caseinate monolayers spread on aqueous subphases with different ionic strengths and pH ≈ 8.5

Ionic strength (mM)	Maximum surface pressure (mN/m)	Surface pressure (mN/m)
4	2.24 ± 0.28	0.49 ± 0.01
8	4.18 ± 0.23	0.69 ± 0.01
12	6.51 ± 0.19	0.98 ± 0.02
35	10.99 ± 0.22	8.43 ± 0.01
40	11.90 ± 0.23	9.03 ± 0.03
45	11.94 ± 0.25	9.14 ± 0.01

The variation in the quantity of sodium caseinate required to produce the monolayers, at low and high ionic strengths is associated with the capacity of the ionic strength to weaken the non-covalent interactions between the amino-acids present in the protein molecules. In fact, under physiological conditions, the difference in the free energy between native protein conformation (folded) and unfolded conformation is only about 5-20 kcal/mol. As a result, moderate changes in physicochemical parameters such as, temperature, pH or ionic strength can destabilise the protein structure, i.e., its unfolding.

In the case of the caseins that comprise sodium caseinate, i.e., α_1, α_2, β and κ caseins, modifications in the physicochemical parameters of the aqueous phase can produce considerable changes in the protein conformation. Substantial changes in the conformation of caseins can be expected due to the absence of a tertiary structure which permits casein molecules to have a relatively open configuration. At a low ionic strength it is possible that non-covalent interactions, such as hydrogen bonding van der Waals interactions and hydrophilic interactions induce loop formation in a fraction of the protein molecule which reduces the interfacial area able to be covered by the protein molecules. Clearly then, more molecules of protein are necessary to produce a monolayer at the air-water interface. Raising the ionic strength weakens the non-covalent bonds and reduces the protein solubility inhibiting the loop formation and producing an increase in the interfacial area covered by the molecules. Hence, more protein molecules are required to produce a monolayer.

An alternative explanation with regard to monolayer expansion upon increasing ionic strength for all the pH values studied is related to the salting-in or salting-out effects

of the ions present in the buffer solutions. The real effect of the ions on protein conformation is still controversial. This debate is because it is difficult to quantify the extent of ion-ion vs. ion-water interactions and their effect on protein conformation [25]. Generally, at very low ion concentrations (< 0.1 M) electrostatic interactions between charged residual groups of protein molecules and ions dominate. At high ion concentrations (> 2 M) ions can modify water structure which affect the non-covalent bonds present in protein molecules [25, 26]. However, the effects of ion concentration on protein conformation depend on the kind of ions and proteins.

For all the pH values investigated, the expansion of the isotherms with an increase of the ionic strength may be associated with the salting-out effect produced by the ions present in the different buffer solutions. Ions that induce the salting-out effect (kosmotropes) attract water molecules from the protein, such that they are strongly hydrated with several layers of water molecules organised around them [21]. As a result, the solubility of the hydrophilic parts of the protein molecules decrease and they have to migrate from the aqueous phase to the air-water interface covering more interfacial area. The migration of the hydrophilic part of the protein molecules from the water to the interface reduces the superficial tension of the air-water interface and because of this the surface pressure of the monolayer rises. Since the hydrophobic-hydrophilic nature of the protein molecules depends on the pH, and the specific ion effects are a function of its concentration, different changes in the sodium caseinate monolayer structure and behaviour were expected because of the diverse pH buffer solutions used.

At pH 4.6 (sodium acetate buffer) for both ionic strength ranges, the results show a dramatic change in the surface pressure and the trough area covered by the protein molecules upon changing the ionic strength (Figures 3.7 and 3.8). Furthermore, the isotherms at this pH show the largest gas phase regions and the lowest maximum surface pressures for the pH values studied. The values of the maximum surface pressure and the surface pressure at a specific superficial density ($0.7 m^2/mg$) for all ionic strengths studied are shown in Table 3.4. The large gas phase region and low maximum surface pressure are a consequence of sodium caseinate aggregation at the interface, as was explained above. With respect to the remarkable expansion of the isotherm with changing ionic strength, these results could be related to the

specific ions present in the buffer solution at pH 4.6. According to the Hofmeister series sodium ions (Na^+) and acetate ions (CH_3COO^-) are ranked as a high and medium kosmotropes anion and cation respectively. Thus, sodium and acetate ions are able to attract a large number of water molecules reducing the solubility of the hydrophilic residue groups of the protein molecules and forcing them to migrate to the interface. In fact, the dramatic change in the sodium casein solubility upon increasing ionic strength and low pH can be rationalised if the surface pressures at different ionic strengths are compared at a specific surface density. In Table 3.4 the values of surface pressure at a specific surface density (0.7 m^2/mg) as a function of ionic strength are given. For a fixed mass of protein and interfacial area, the observed direct relationship between the surface pressure and ionic strength is due to transfer of the protein residual groups located in the water phase to the interface as a result of the increasing ion concentration; with subphases at neutral and basic pH values showing the same behaviour.

Upon changing the buffer pH to approximately 7 (phosphate buffer) a moderate expansion in the measured isotherms is seen with a variation in the ionic strengths for both ranges (see Figures 3.9 and 3.10). At this pH, the isotherms present the highest maximum surface pressures, the highest surface pressure values at the specific surface density (see Table 3.5) and the largest expanded liquid phase for the pH values investigated. This behaviour concurs with the results above, where the effect of the pH on sodium caseinate monolayers was evaluated. The moderate expansion in the isotherms may result for two reasons. Firstly, it is possible that a large proportion of the protein molecules are located at the interface, i.e. high hydrophobicity. Secondly, this may be due to the presence of the sodium (Na^+), potassium (K^+) and hydrogen phosphate (HPO_4^{-2}) ions in the buffer solution used. All these ions are ranked highly as the most kosmotropes cations and anions in the Hofmeister series. Because of this, it is possible that the lowest ionic strength concentration, for both ranges studied, is sufficient to considerably decrease the solubility of the hydrophilic residual groups of the proteins. As a consequence, an additional increase of ionic strength produces only a slight expansion in the isotherm generating moderate changes in the surface pressure.

Upon increasing the subphase pH to about 8.5 (carbonate buffer), the sodium caseinate isotherms show antagonistic behaviour which depends on the ionic strength range used. At a low ionic strength, a dramatic expansion of the isotherms occurs with an increase in the ion concentration. On the contrary, at a high ionic strength an insignificant expansion takes place (see Figures 3.12 and 3.13). The notable difference in the isotherm expansion for the two ionic strength ranges used could be due to ions present in the buffer solution. The ions present in the carbonate buffer have a salting-out effect on the protein molecules, similar to the behaviour seen for subphase pH 4.6 and around 7. Sodium and carbonate ions are between the first komostrope cations and anions in the Hofmeister series. Because of this, it is possible that the solubility of the hydrophilic residual groups decreases significantly with a slight increase in the concentration of these ions at a low ionic strength. The irrelevant isotherm expansion at ionic strengths above 35 mM, could be associated with a limit being reached whereby at ionic strengths greater than 35 mM the quantity of ions is more than enough to make the hydrophilic residual groups of the protein molecules move to the interface, and adding more ions has no further effect. The intermediate values of the maximum surface pressure and surface pressure at a specific area density (see Table 3.6), compared with the previous buffer solutions, agree with the effect of pH on sodium caseinate monolayers, as described previously.

3.2.5 Surface potential of sodium caseinate monolayers

The surface potential technique provides information about the molecular orientation and structure of the monolayer at the air-water interface. When a Langmuir monolayer is spread on an aqueous phase, it is able to change the potential of the air-water interface. The surface potential, ΔV, is the difference in the potential between the interface covered by the monolayer and the clean interface [27]. This difference is a consequence of the normal molecular dipoles of the monolayer.

Applying the surface potential technique to protein monolayers yields information on their conformation at the air-water interface. It is suitable technique due to the large dipole moments of the protein molecules. The large dipole moments of proteins result from the high numbers of amino acids. Additionally, the protein dipole moments vary with the pH of the aqueous phase [28].

In a Langmuir trough the progressive change of the interfacial area, by moving the barriers, generates changes in the normal dipole at the interface. For large interfacial areas the normal dipoles result from the water molecules. As the interfacial area decreases the normal dipoles increasing are a consequence of the floating monolayer at the interface [29]. The surface potential is the result of three dipolar contributions of the regions in the monolayer-subphase system: reorientation of the water molecules due to the monolayer; hydrophilic head groups; and hydrophobic tail groups [29]. The equation for this model is,

$$\Delta V = \frac{1}{A\varepsilon_0}\left[\frac{\mu_1}{\varepsilon_1} + \frac{\mu_2}{\varepsilon_2} + \frac{\mu_3}{\varepsilon_3}\right] \quad 3.2$$

where μ_i is the normal component of the dipole moment and ε_i is the effective dielectric constant of the respective regions of the monolayer at the subphase.

When some of the groups in the monolayer molecules can be ionized, the contribution of the resulting double-layer is considered according to the Gouy-Chapman theory. The equation for this theory is:

$$\psi_0 = \frac{2\kappa T}{e} sinh^{-1}\left[\frac{e\alpha}{A\left((5.88\ x10^{-7})c\varepsilon T\right)^{1/2}}\right] \quad 3.3$$

where ψ_0 is the double layer potential, α is the degree of dissociation of the monolayer headgroups, e is the protonic charge, k is the Boltzmann constant, T is the absolute temperature, c is the ionic concentration, A is the area per molecule and ε is the dielectric constant of the subphase. The Demchak-Fort model has been applied satisfactorily for many monolayers of simple amphiphilic molecules. However, the quantitative application of this model for monolayers of macromolecules, such as polymers and proteins, to correlate group dipole moments and surface potential values, is impossible because of the random orientation of the polymer chains or residual groups (proteins) within the Langmuir film [27].

In order to evaluate the effect of the pH and ionic strength on the surface potential of sodium caseinate monolayers, six different systems were studied. The systems were the same as those used to study the effect of the ionic strength on the sodium

caseinate isotherms (Section 3.2.4) in order to be able to correlate the results. Surface potential data are given in Figures 3.14-3.19.

The results show a strong effect of the pH and ionic strength on the surface potential of sodium caseinate monolayers. Additionally, two general behaviours for the monolayers studied were observed: the non-zero value of surface potential at the initial area and the detection of the monolayer by the surface potential technique at larger areas than the surface pressure technique. According to Oliviera *et al.* [30], there are two reasons why the surface potential at large areas is non-zero. The first reason is the formation of aggregates at the interface when the molecules are spread on the subphase. The second is the strong contribution to the surface potential of the double-layer formed by the monolayer. Thus, the non-zero value of the surface potential for sodium caseinate proteins should be expected because of first, their trend to produce aggregates at the air-water interface, secondly the occurrence of a second order phase transition, and thirdly the contribution of the ionisable residual groups to the double layer.

When the interfacial area was decreased by the barriers of the trough, the detection of the gas-liquid phase transition was at different interfacial area depending on the techniques used. In the systems investigated the surface potential technique detected the gas-liquid phase transition at larger areas than the Wilhelmy plate using for the surface pressure measurement. Similar behaviour was reported by Oliviera *et al.* [30] using dipalmitoyl phosphatidyl glycerol and Vogel *et al.*[31] using different lipids. Generally, techniques such as ellipsometry, Brewster angle microscope (BAM) and surface potential are able to provide information at larger areas than the surface pressure.

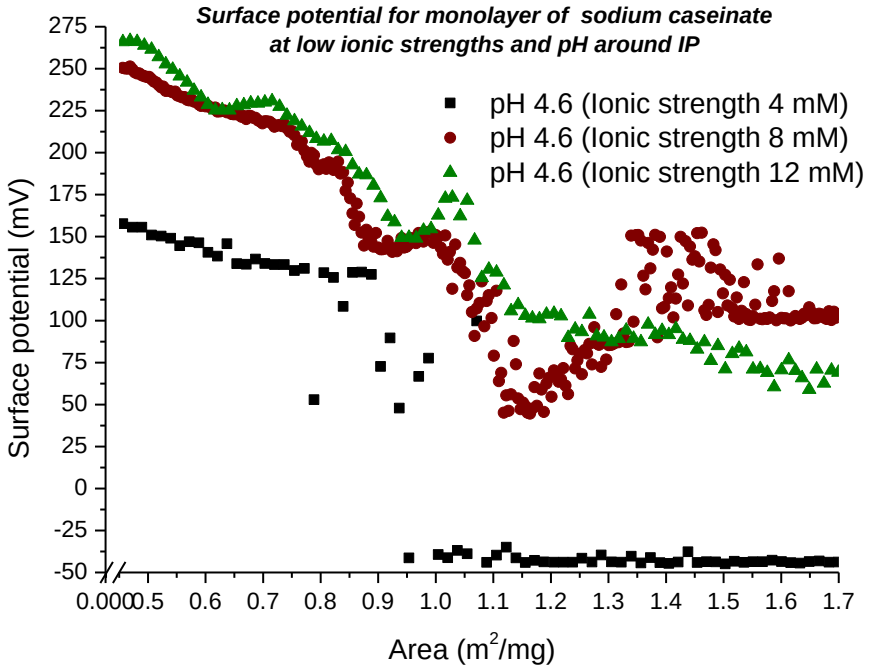

Figure3.14. Surface potential for sodium caseinate Langmuir monolayers spread at the air/water interface. Subphase: acetate buffer, pH 4.6, low ionic strengths and 0.034 mg of sodium caseinate.

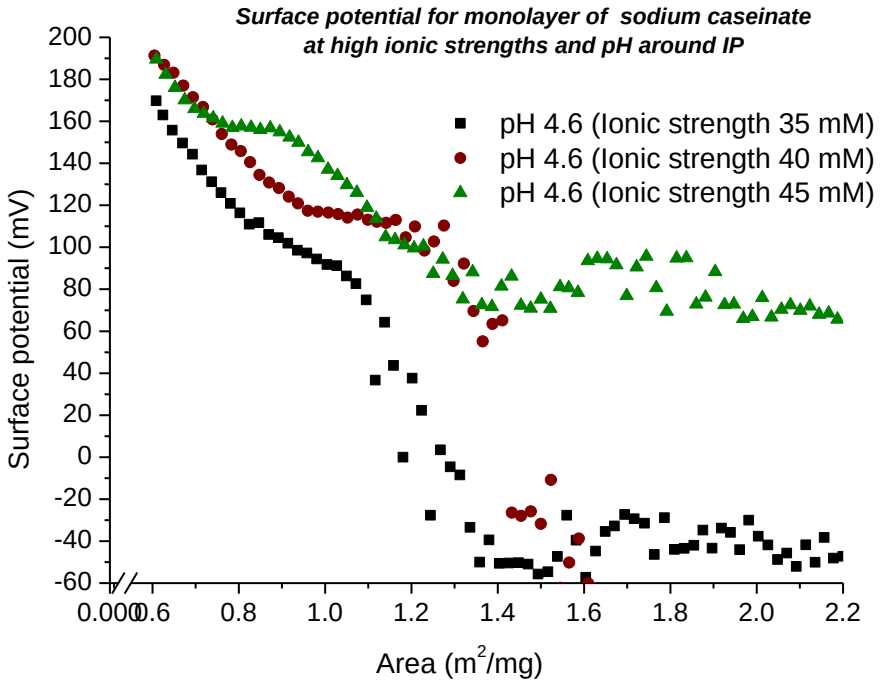

Figure3.15. Surface potential for sodium caseinate Langmuir monolayers spread at the air/water interface. Subphase: acetate buffer, pH 4.6, high ionic strengths and 0.023 mg of sodium caseinate.

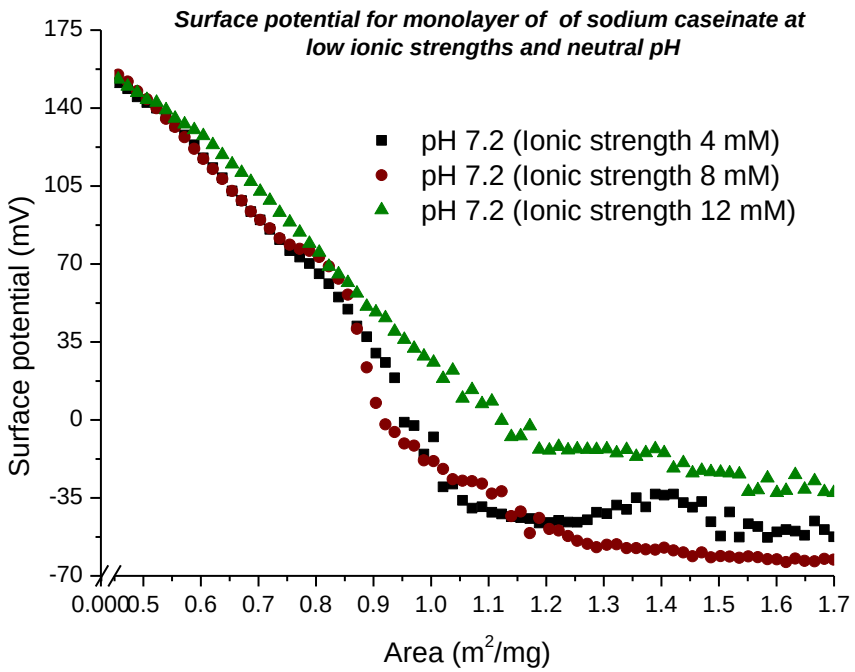

Figure3.16. Surface potential for sodium caseinate Langmuir monolayers spread at the air/water interface. Subphase: phosphate buffer, pH 7.2, low ionic strengths and 0.034 mg of sodium caseinate.

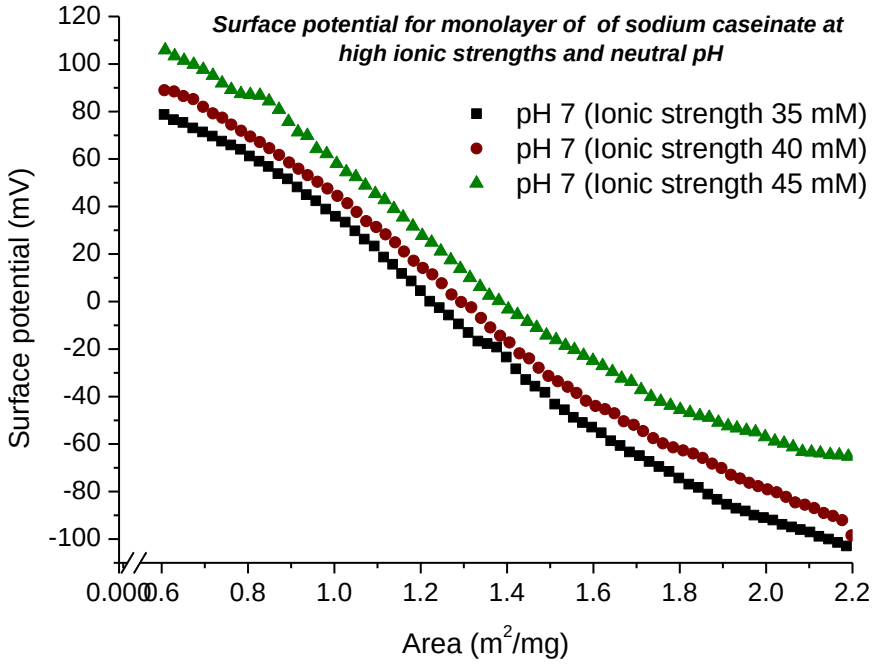

Figure3.17. Surface potential for sodium caseinate Langmuir monolayers spread at the air/water interface. Subphase: phosphate buffer, pH 7, high ionic strengths and 0.023 mg of sodium caseinate.

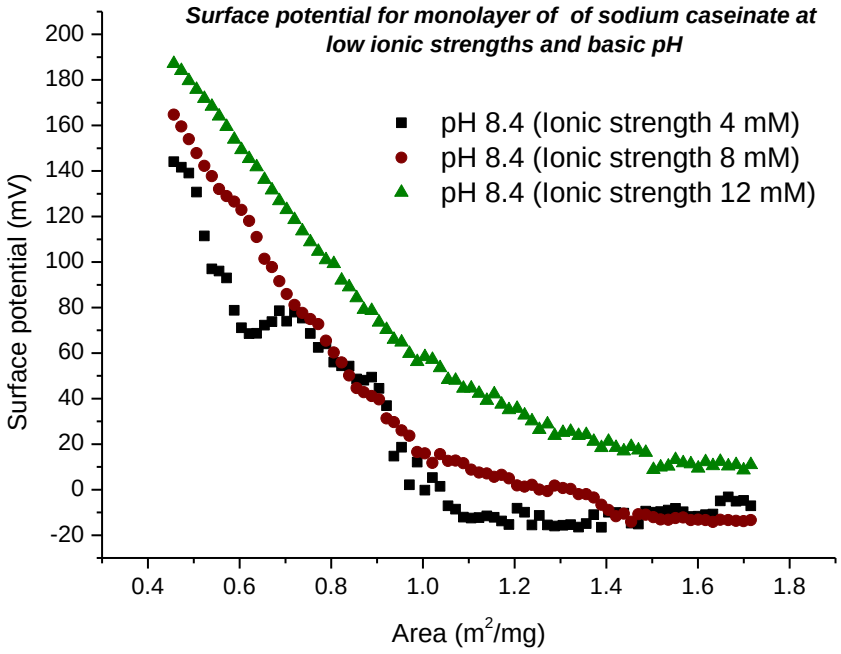

Figure3.18. Surface potential for sodium caseinate Langmuir monolayers spread at the air/water interface. Subphase: carbonate buffer, pH 8.4, low ionic strengths and 0.034 mg of sodium caseinate.

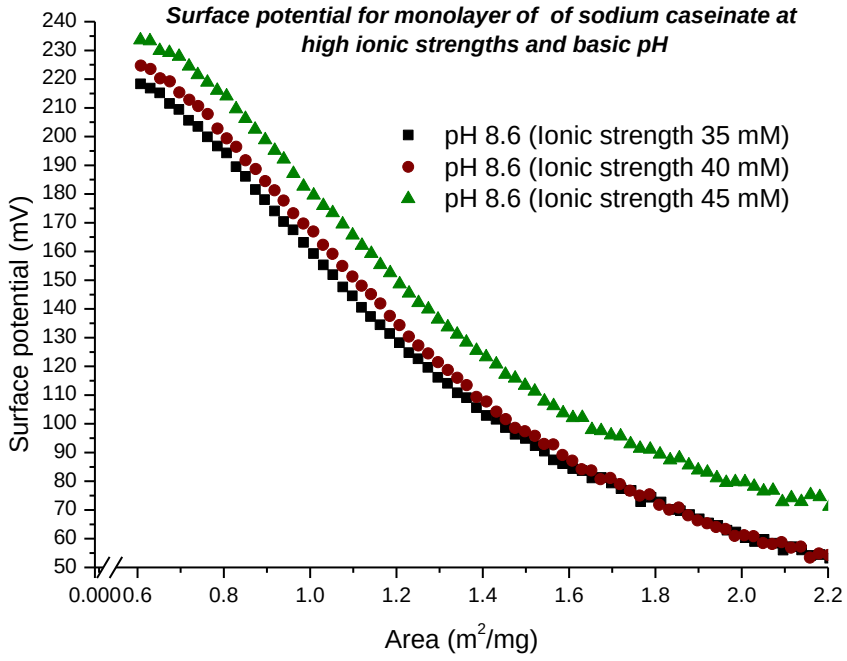

Figure3.19. Surface potential for sodium caseinate Langmuir monolayers spread at the air/water interface. Subphase: carbonate buffer, pH 8.6, high ionic strengths and 0.023 mg of sodium caseinate.

At a subphase pH 4.6, approximately the isoelectric point, there is a notable effect of the ionic strength on the surface potential of the sodium caseinate monolayer (see Figures 3.14-3.15). These results are a consequence of the salting-out effect, as well

as a decrease in the solubility of the hydrophilic groups of the protein molecules upon increasing the ionic strength of the buffer subphase. A similar trend was observed when the isotherms of the sodium caseinate monolayers were evaluated with respect to changing the ionic strength (Figures 3.8 and 3.9). In Figures 3.14 and 3.15 it is clear that at large interfacial areas, 1-1.7 m^2/mg and 1.1-2.2 m^2/mg for low and high ionic strength ranges respectively, the measured surface potential values show significant fluctuations. As the interfacial area is decreased the fluctuations decrease and a sharp increase in the surface potential occurs. Fluctuations in the surface potential are associated with protein molecule aggregation at the air-water interface forming a series of separated islands. Cockbain and Shulman [32] reported similar results using gliadin, which is a protein present in cereals. Thus, the heterogeneous distribution of protein molecules at the interface produces different normal dipole moments which are associated with the surface potential fluctuations.

Further reduction of the interfacial area, below 1 m^2/mg and 1.1 m^2/mg for low and high ionic strength ranges respectively, force the aggregates closer together thereby increasing the surface potential values, and all fluctuations disappear. This is due to the formation of a homogeneous monolayer of sodium caseinate at the air-water interface that generates large normal dipolar moments.

The results for neutral pH (Figures 3.16 and 3.17) show only slight fluctuations of the surface potential for low ionic strengths, and they are at a smaller interfacial area (1.2-1.7 m^2/mg) than seen when the pH was maintained close to the isoelectric point pH (1-1.7 m^2/mg). The surface potential values increase significantly and they are very similar upon decreasing the area values for ionic strengths investigated. In contrast, for the high ionic strength range (Figure 3.17) no fluctuations of the surface potential values are seen, and the effect of the concentration of ions on the surface potential of the sodium caseinate monolayer is minimal. These results are in agreement with the measured π-A isotherms, which revealed a uniform monolayer associated with a large proportion of the amino acid groups of the proteins at the interface and strong electrostatic repulsion between the protein molecules. The large proportion of protein molecules at the interface generates considerable normal dipolar moments, which produce a significant increase in the surface potential when the interfacial area is reduced.

When the subphase pH is around 8.5 the surface potential curves, for both ionic strength ranges, are similar to the case for neutral pH. In the low ionic strength range (Figure 3.18) there are some fluctuations, especially at an ionic strength of 4 mM. However, consequential increments of the ionic strength produce attenuation of the surface potential fluctuations until these disappear, as can be seen in Figure 3.19. Like the previous subphase pH values, there is a clear relationship between the measured sodium caseinate isotherms and their surface potential values at a given pH and ionic strength of the subphases. The ions present in the subphase buffer at pH around 8.5, i.e., sodium and carbonate are extreme kosmotropes. Thus a dramatic reduction of the protein solubility is to be expected, which induces migration of the hydrophilic part of the protein molecules from the aqueous phase to the interface producing large numbers of normal dipole moments.

3.3 Sodium caseinate at the oil-water interface

The interfacial behaviour of proteins at the oil-water interface has been previously investigated. Proteins of significant interest have been those used as emulsifying agents [33]. The rheological properties and stability of emulsions are strongly related to the protein conformation at the oil-water interface [9]. Thus, information regarding the adsorption and conformation of proteins at the interface is crucial to enable control over emulsion properties [34].

In the food industry, milk proteins are commonly used to produce dispersed systems such as emulsions, foams, suspensions or a mixture of these, due to their excellent interfacial affinity. The two milk proteins that have been widely investigated, at the oil-water interface, are β-casein and β-lactoglobulin [35].

Thermodynamically [36], protein molecules absorb spontaneously at an interface to decrease the energy of the system according to the following equation:

$$\Delta G_{ads} = \Delta H_{ads} - T\Delta S_{ads} \qquad 3.4$$

where ΔG_{ads} is the Gibbs energy change of adsorption, ΔH_{ads} is enthalpy change of adsorption, T is the absolute temperature and ΔS_{ads} is the entropy change of adsorption. The process of protein adsorption at an interface is spontaneous because the contribution of the positive entropy change in the system is much bigger

than the enthalpy change. The significant contribution of the entropy of adsorption is due to a reduction of the hydrophobic interactions in the interior of the protein, which produces ordered secondary structures, generating the total or partial unfolding of the protein (disorder) to adsorb at the interface.

Dickinson [36] explains that proteins adsorb spontaneously at an interface because the hydrophobic residual groups of the molecules move away from the aqueous phase of the protein solution looking for a non-polar phase (air or oil). He considered that molecular factors contributing to protein adsorption include: 1) dehydration of hydrophobic regions of the interface; 2) changes in protein secondary and tertiary structure; 3) charge distribution arising from the interaction of electric fields of protein interface; 4) changes in the environment of ions on transference from solution to protein layer; changes in the degree of protonation of amino-acid side groups, and 5) the van der Waals interactions between protein molecules and the interfacial oil and water molecules. Protein adsorption is favoured by factors 1 and 2 while factors 3 and 4 oppose the adsorption; the remaining factors have little effect.

In this research a study of sodium caseinate at the oil-water interface upon varying the pH and ionic strength of the aqueous phase is reported. The purpose of the oil-water interfacial test was to corroborate the results obtained from the Langmuir trough (air-water interface). It is important to note that the kinetics of casein adsorption at the oil-water interface to achieve equilibrium was not investigated. Macritchie [37] showed that changes in the interfacial tension occur upon changes in proteins and that reaching equilibrium takes place over a long period of time; the total time depends on the structural complexity of the proteins. Because the investigation of sodium caseinate at the oil-water interface was confirmatory with regard to the results of caseins at the air-water interface and because caseins are very flexible with small amounts of secondary structure, the time set to measure changes in the interfacial tension was 20 minutes, which was the same time used at the Langmuir trough tests.

Before evaluating the effect of the pH and ionic strength on the conformation of sodium caseinate at the oil-water interface, it was necessary to study the effect of the mass of sodium caseinate on the interfacial tension to select the quantity of protein to be used. The mass of protein to be used had to be able to produce a

considerable decrease in the interfacial tension, and not to have a strong buffer effect on the buffer solution to be used. (The investigation on the buffer capacity of sodium caseinate is shown in the next chapter). Two concentrations were evaluated (0.05% and 2% w/v) with the results are shown in Figure 3.20.

From the results given in Figure 3.20 there is an effect of sodium caseinate concentration on the interfacial tension. At 0.05% of sodium caseinate concentration, the initial interfacial tension was 9.8 mN/m and this dropped to 8.6 mN/m when the concentration was increased to 2%. By comparing the slope of the curves it can be seen that the velocity of absorption at the oil-water interface is higher from sodium caseinate concentration of 2% than 0.05 w/v%.

Two distinct regions can be distinguished in the data shown in Figure 3.20: the first is characterised by a dramatic reduction in the interfacial tension with the time, followed by the second more gradual decrease of the interfacial tension. Equilibrium values of interfacial tension were not achieved for either sodium caseinate concentrations for the 20 minutes of monitoring.

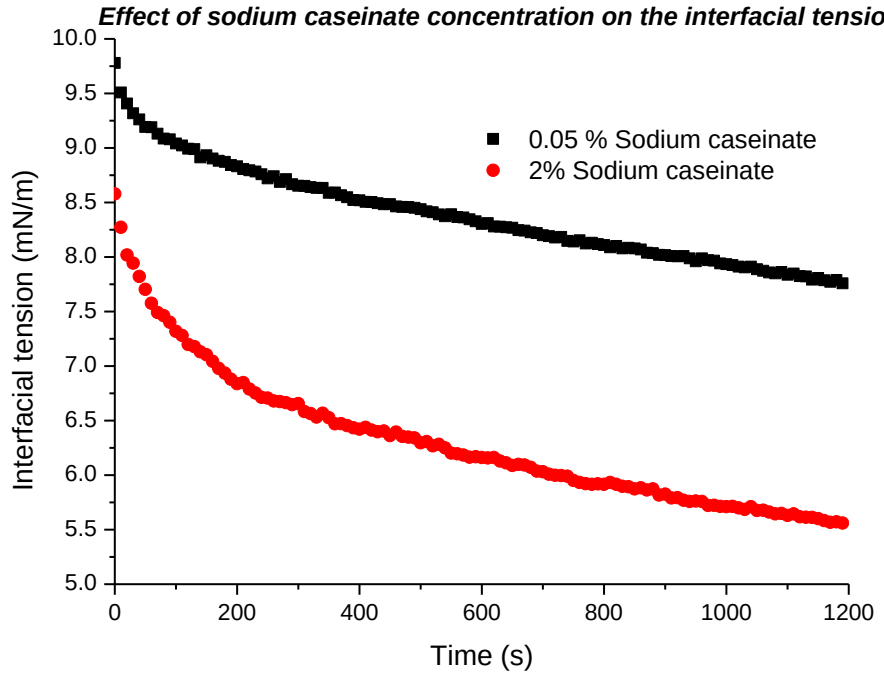

Figure3.20. Dynamic interfacial tension of sodium caseinate at the soy bean oil / aqueous interface. Aqueous phase: phosphate buffer, pH 6.8 and ionic strength 50 mM.

Dickinson [36] suggested that the first region relates to the point when diffusion of protein molecules occurs, while the second one is related to the arrival of new molecules at the interface and conformational changes in previously adsorbed molecules. A model that is used to describe the protein adsorption is the random sequential adsorption model (RSA) [38]. In this model a protein molecule hits the interface, sticks and defines a zone around it where any additional molecule can be located. After that, progressive changes of the interfacial tension occur because of variations in the protein conformation and orientation.

A sodium caseinate concentration of 0.05% was chosen to study the effect of the pH and ionic strength because this protein concentration does not produce dramatic changes in the buffer pH and a considerable reduction of the interfacial tension is produced.

3.3.1 Effect of aqueous pH on the oil-water interfacial tension in the presence of Na-Ca

Protein charge, hydrophobicity and conformation can all be manipulated by changing solution pH. Solution pH establishes whether protein molecules are overall positive, negative or zero charged affecting the electrostatic interactions between and within proteins. Also, pH changes affect the charge density of the protein molecules modifying their hydrophilic/hydrophobic balance and interactions with the oil and water phases. Thus, changes in the interfacial tension have to be expected when sodium caseinate is adsorbed at the oil-water interface at different pH values of the aqueous phase. Initially, soy bean oil was selected as the oil phase to investigate the effect of the pH on the interfacial tension. However, at basic pH some of the fatty acids that are present in the oil were deprotonated [39] decreasing dramatically the interfacial tension (see Figure 3.21). Because the interfacial tension was extremely low, it was impossible to keep a droplet pending for 20 minutes (see Figure 3.21). As a consequence, N-dodecane was used as the non-polar phase.

The results of the change of the interfacial tension at n-dodecane/water interface with pH are shown in Figure 3.22. A notable effect of the pH on the initial interfacial tension and its change with time is evident in the data shown in Figure 3.22. Differences in the initial tension are a consequence of the different buffers used, as

was previously explained. The highest initial interfacial tension was for the carbonate buffer (pH 8.9); follow by acetate (pH 5.2) and phosphate (6.2 and 6.9) buffers (see Table 3.7).

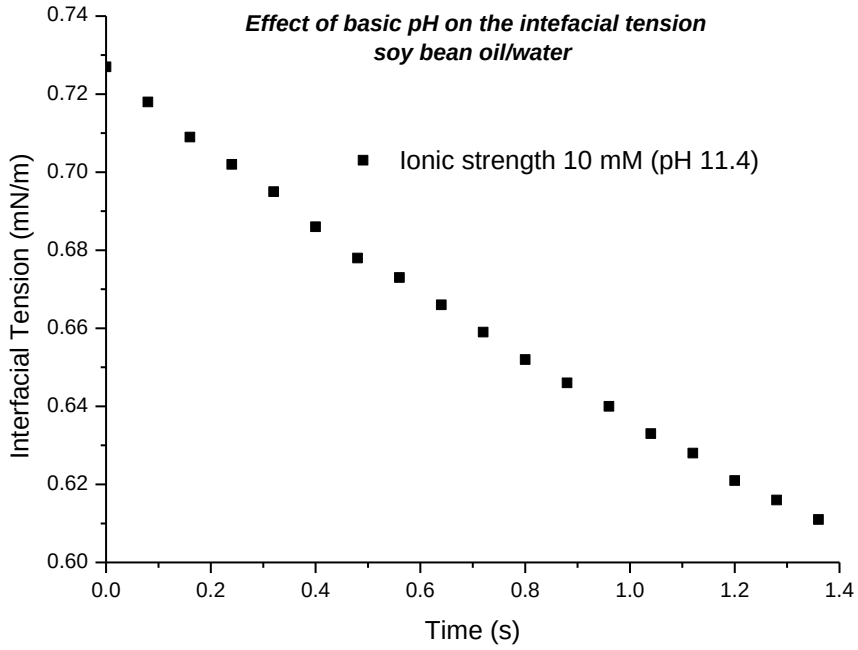

Figure3.21. Dynamic interfacial tension of sodium caseinate at the soy bean oil/aqueous interface. Aqueous phase: pH 11.4, carbonate buffer. Ionic strength: 10 mM and 0.05% of sodium caseinate.

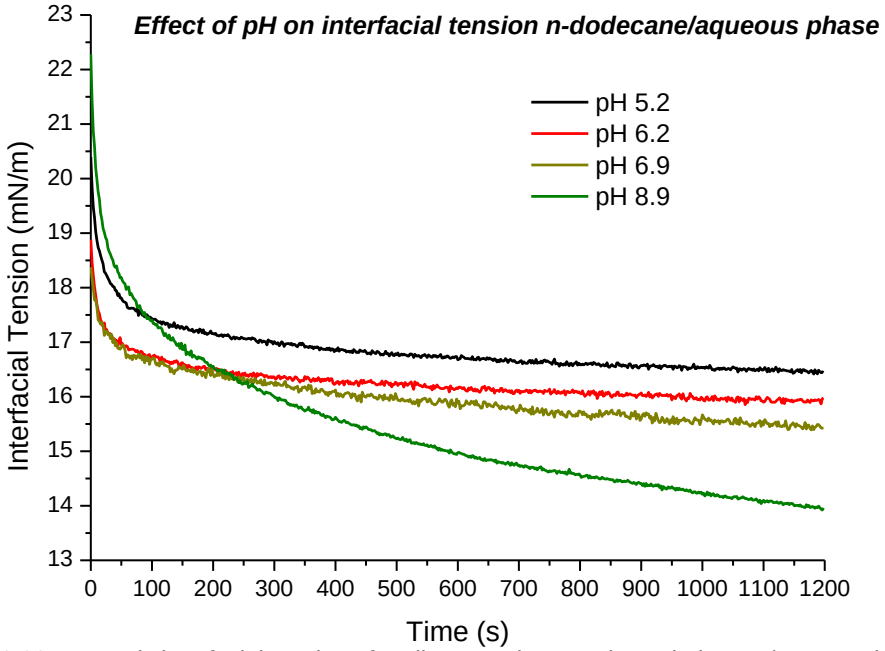

Figure3.22. Dynamic interfacial tension of sodium caseinate at the n-dodecane/aqueous interface. Aqueous phase: pH 5.2, acetate buffer; pH 6.2, phosphate buffer; pH 6.9, phosphate buffer; and pH 8.9, carbonate buffer. Ionic strength of all subphases: 20 mM and 0.05% of sodium caseinate.

Variations of the interfacial tension with the pH are a consequence of hydrophobicity changes in the amino-acid groups in the protein molecules. These changes modify the interactions within and between protein molecules, as well as interactions of the protein molecules with the oil and aqueous phases. The values of the interfacial tension show an inverse relationship with the pH (see Table 3.7).

At a pH value around the isoelectric point (pH 5.2) the interactions between the protein molecules and the oil and water domains are reduced in favour of greater attractive interactions between the protein molecules at the interface. As a consequence, the interfacial area that can be covered by the molecules is reduced, counteracting the capacity of caseins to decrease the oil-water interfacial tension. It is important to note that a similar result was obtained at the air-water interface when the pH value was around the isoelectric point. For sodium caseinate at the air-water interface with pH around the isoelectric point, the lowest surface pressure values were obtained (see Figure 3.3) implicating high superficial tension. Also, aggregations of protein molecules were detected at the air-water interface by the surface potential technique (Figures 3.13 and 3.14).

Table 3.7 Variation of interfacial tension soy bean oil-aqueous phase at different pH buffers with sodium caseinate. Ionic strength of the buffers 20 mM

Buffer pH	Initial interfacial tension [mN/m]	Final interfacial tension [mN/m]
5.2	20.42 ± 0.12	16.41 ± 0.14
6.2	18.87 ± 0.16	16.01 ± 0.12
6.9	18.41 ± 0.10	15.42 ± 0.16
8.9	22.33 ± 0.12	14.38 ± 0.13

In Figure 3.23 the turbidity of the protein solutions at different pH values is shown. This illustrative example provides evidence about the capacity of the pH to modify the interactions between the protein molecules. It is clear that at pH 5.2 (around the isoelectric point) the opaque colour is due to high attraction between protein molecules, producing aggregations of protein molecules without precipitation. For acetate and carbonate buffers, clear solutions are due to protein molecules having a negative total charge that repels each other and increases the protein-aqueous phase interactions.

Considering the amino-acid composition of caseins shown in Table 3.1, at pH 6.2 the protein molecules become increasingly negative charged (due to deprotonation of

aspartic and glutamic acid groups) inducing repulsion between the protein molecules. These deprotonated residual groups interact with the aqueous phase reducing the oil-aqueous interfacial tension. Increasing the pH favours the deprotonation of some of the amino acids in the protein molecules augmenting the negative charge of them. Hence, the interfacial tension decreases due to the increase of the interaction between the polar part of the protein molecules and the aqueous phase.

Figure3.23. From left to right, 0.05 p/v% sodium caseinate solutions at pH 5.2 (acetate buffer); pH 6.2 (phosphate buffer) and pH 8.9 (carbonate buffer). Ionic strength of all solutions 20 mM

Comparing interfacial tension results at neutral and basic pH values with respect to the results obtained at similar conditions at the air-water interface (Figure 3.3), it is clear that the results depend not only on the interactions between protein molecules and the capacity to cover the interfacial area, but also on the interactions between protein molecules and condensed phases (polar and non-polar). When the pH of the aqueous phase is changed, the effect on the interactions between protein molecules and water are the most affected. This is basically because of the protonation and deprotonation of the residual groups in the protein molecules structure. Thus, changes in the interfacial tension upon varying the pH of the aqueous phase will be referred to in terms of protein molecule-water interactions.

At neutral pH, casein molecules have a total negative charge and a considerable portion of the molecules is hydrophobic. This condition allows protein molecules to cover large areas at the air-water interface, because of the electrostatic repulsion and the location of the hydrophobic fraction of the protein molecules at the interface,

producing large surface pressure values. At the oil-water interface, the negative charge of the protein molecules augments the interaction between the water phase and the protein, reducing the interfacial tension. When the aqueous pH is basic, the hydrophobic proportion of the protein molecules are reduced due to the deprotonation of some of their residual groups and their negative charge increases. Thus, the protein molecules at the air-water interface are separated by electrostatic repulsion and a significant proportion of them are immersed into the water phase. The strong electrostatic repulsion between protein molecules and the significant proportion of their structure submerged in the water phase reduces the interfacial area that can be covered by protein molecules, decreasing the surface pressure. At the oil-water interface, the long hydrophilic portion of the protein molecules dangling into the water propitiates the interaction between the hydrophilic part of the molecules and the water, decreasing the interfacial tension.

3.3.2 Effect of the ionic strength on the oil-water interfacial tension in the presence of Na-Ca

The effect of electrolytes on protein molecules is complex; this is because the electrolytes are able to modify protein properties such as conformation, solubility (salting-in and salting-out) and aggregation. Additionally, cations and anions have different effects on protein stability. Their relative chaotropic and kosmotropic characteristics are summarised as the Hofmeister series. Chi *et al.* [40] explained that electrolytes affect not only the electrostatic interactions between the charged groups within the protein, but also electrostatic interactions between protein molecules. Thus, intramolecular charge-charge interactions affect protein conformation, while intermolecular electrostatic interactions affect the kinetics and thermodynamics of protein aggregation. The ionic strength effect of the interfacial tension was investigated using different ionic strength buffer solutions. Neutral and close to the isoelectric point pH values were evaluated using soy bean oil as a non-polar phase. A basic pH could not be used with soy bean oil, because some of the fatty acids were deprotonated and affected the interfacial activity. Also, two different sodium caseinate mass quantities were used (0.01 and 0.05 wt/v % for pH 5.2 and 7 respectively) because of the sodium caseinate capacity to change the pH of the buffer solutions at low ionic strength and pH values different than neutral, and this will be explained later. The results are shown in the Figures 3.23 and 3.24.

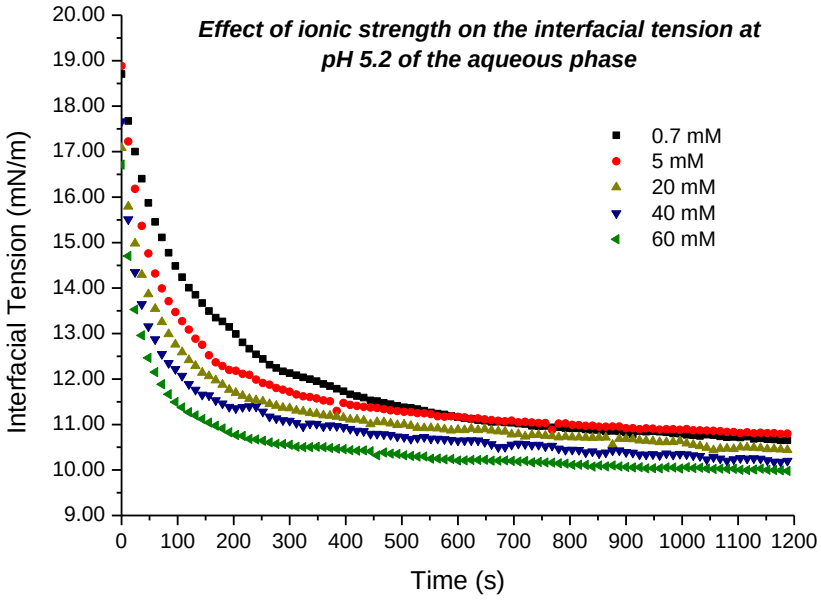

Figure3.23. Dynamic interfacial tension of sodium caseinate at the soybean oil / aqueous interface as a function of ionic strength. Aqueous phase acetate buffer pH 5.2 and 0.01 wt/v% of sodium caseinate.

Increasing the ionic strength produces a reduction of the oil-aqueous interfacial tension for the pH values investigated (Figures 3.23-3.24). Hence, the reduction in the interfacial tension observed here is due to changes in the conformation of the protein molecules between the two phases. In non-polar/electrolyte solution systems without amphiphilic molecules and increasing the ionic strength, the results contrast to what was observed here. Some investigations have reported that the interfacial tension generally increases upon increasing electrolyte concentration (dos Santos *et al.* [41] and Lima *et al.* [42]).

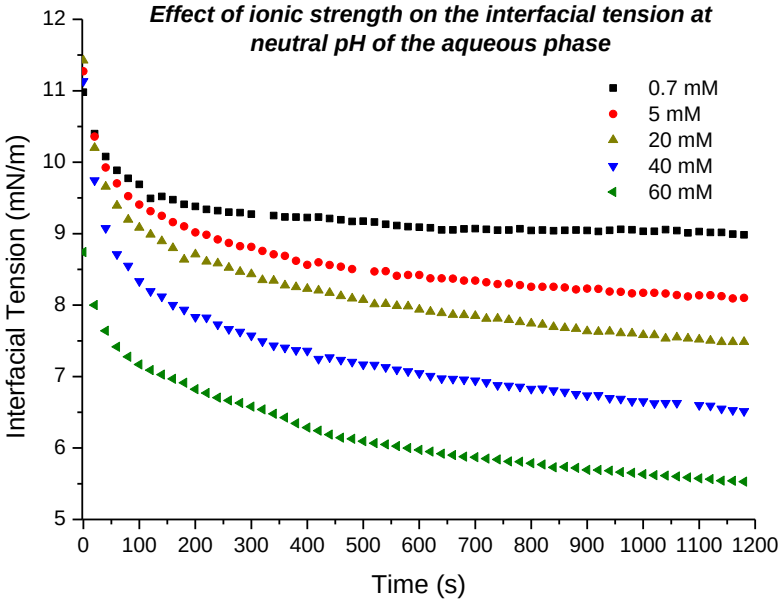

Figure3.24. Dynamic interfacial tension of sodium caseinate at the soybean oil / aqueous interface as a function of ionic strength. Aqueous phase acetate buffer pH 7 and 0.05 wt/v% of sodium caseinate.

It can be seen from the data shown in Figure 3.23 that there is an inverse relationship between the interfacial tension and the ion concentration when sodium caseinate is present. The decrease of the interfacial tension, upon increasing the ionic strength, can be associated with two factors. First, the weakness of the intramolecular interactions which drives increased interactions between the hydrophobic and hydrophilic residual groups of the protein molecules with the oil and aqueous phases respectively. Secondly, the solubility of the hydrophilic residual groups of the proteins is reduced (salting-out effect). This forces the migration of these groups to the interface increasing the interfacial area that is covered by protein molecules. Both factors reduce the interfacial tension.

At pH 7 there is a significant reduction of the interfacial tension when incrementally increasing the ionic strength (see Figure 3.24). At this pH the net charge on the protein molecules is negative and as such it is possible that there is less interaction within the residual groups of the protein with different charges to produce salt bridging. Thus, the interactions between the charged residual groups of the protein and the aqueous phase increase, thereby reducing the interfacial tension. Similar to pH 5.2, increasing the ionic strength reduces the solubility of the polar residual groups of the proteins forcing these groups to locate at the interface, thereby decreasing the interfacial tension.

Figures 3.23 and 3.24 show that a rapid decrease in the interfacial tension occurs around the first 100 s, for both values of pH investigated, followed by two different behaviours that depend on the ionic strength. The first behaviour occurs for low ionic strengths, i.e. ≤ 5 mM, where the interfacial tension reaches a plateau after 700 - 1200 s. The second behaviour is at ionic strengths above 5 mM, where a gradual reduction of the interfacial tension is observed without levelling out during the test time. Beverung *et al.*[43] considered that the capacity of the caseins to significantly and rapidly decrease the interfacial tension is because of their lack of ordered structure, which allows them to adsorb at the interface and interact with the phases easily. The two different behaviours are a consequence of the balance of energy between interactions within the protein molecules and interactions of the protein molecules with the non-polar and polar phases.

According to the conformation of the β-casein presented by Dalgleish and Leaver [44] and considering that the rest of the caseins have a similar random coil structure to β-casein, it is possible that at low ionic strength the train part of the protein molecules adsorb at the interface keeping their loops because the ionic strength is not strong enough to overcome the weak interactions between some residual groups within the protein molecules. Thus, once the protein molecules are adsorbed at the interface, after a rapid decrease in the interfacial tension, a very slight reduction in the interfacial tension occurs because of the small variations on the protein conformation and orientation at the interface. On the contrary, if the ionic strength is strong enough to be able to disrupt weak interactions within the proteins once they are adsorbed at the interface, a progressive reduction of the interfacial tension occurs due to the orientation and interaction of the residual groups with the phases.

3.4 Model of conformation of sodium caseinate at the interfaces

Considering the combined data pertaining to the behaviour of sodium caseinate at the air-water and oil-water interfaces, it is evident that the conformation of the sodium caseinate molecules responds to changes in the pH or ionic strength in the aqueous phase. Despite that the two interfaces studied were different not only because of their components, but also the geometry (being flat for air-water and curve for oil-water) similar trends were found. A proposed model for the conformational state of sodium caseinate as a function of pH and ionic strength is shown in Figure 3.25.

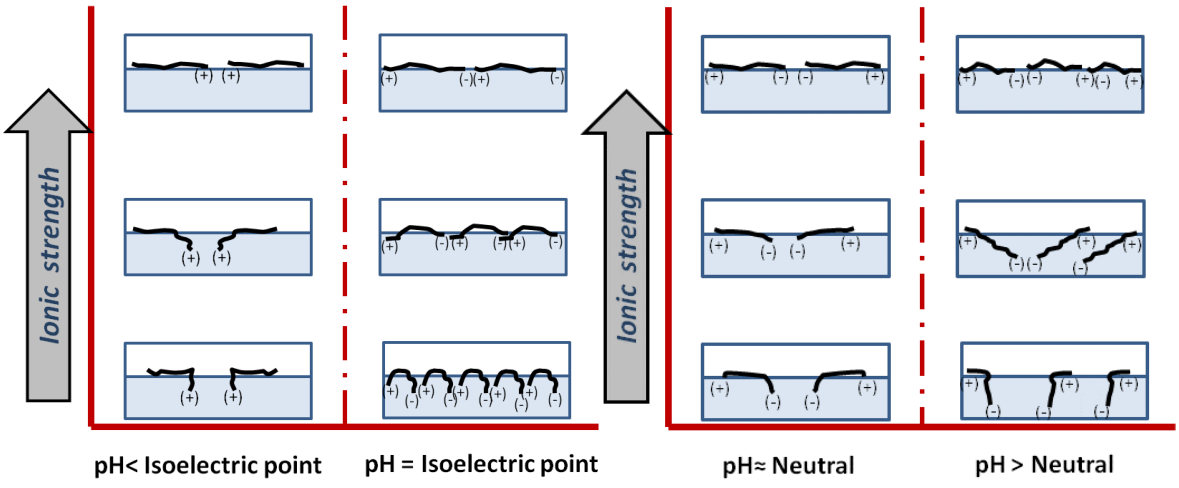

Figure3.25. Schematic representation of sodium caseinate at the air-water or oil-water interfaces by changing pH or ionic strength in the aqueous phase.

The change in the sodium caseinate conformation can be explained by considering the following criteria: i) the flexibility and lack of tertiary structure of the casein molecules that are symbolised as long linear polymers; ii) the polar amino-acid residual groups are represented with positive and or negative charges that depend on the composition of amino-acid groups in their structure (Table 3.1) and the pH of the aqueous phase; iii) the proportion of the individual molecules that are located in the water phase (hydrophilic) vs. lying (hydrophobic) on the interface (results shown in Sections 3.2.4 and 3.2.5; and iv) the high capacity of the casein molecules to hold water molecules which enables the hydrophilic part of the casein molecules to be immersed into the aqueous phase at a low ionic strength. Four conformations will be described: pH at less than the isoelectric point, at the isoelectric point, at neutral, and at basic pH.

For the pH below the isoelectric point, the casein molecules have a positive charge and they repel each other. At a low ionic strength, the short hydrophilic residual groups are immersed into the aqueous phase while the hydrophobic residual groups lie on the interface. Compared to all the other examples at a low ionic strength, the casein molecules cover the largest interfacial surface only with a pH below the isoelectric point. When the ionic strength is increased, the solubility of the hydrophilic residual groups is reduced and they migrate to the interface and cover an even larger interfacial surface.

At the isoelectric point, the total charge on the molecules is zero and the casein molecules are electrically attracted to each other. Positive and negative amino-acid residual groups are immersed into the aqueous phase. The interfacial surface with the least coverage is achieved at low ionic strength, due to the attraction between the casein molecules. Increasing the ionic strength moves the hydrophilic residual groups to the interface, again increasing the interfacial surface covered by the proteins.

When the pH is neutral, the casein molecules have a mild negative charge that repels them from each other. With a low ionic strength the hydrophilic residual groups are immersed in the water phase and a considerable interfacial area is covered by the casein molecules. Raising the ionic strength reduces the solubility of the polar groups in the casein molecules and they migrate to the interface.

For the system with a basic pH, casein molecules have a strong negative charge with a short hydrophobic proportion of the molecule located at the interface. The strong negative charge strongly repels the molecules and forces the molecules further apart. Adding ions in the aqueous phase reduces the solubility of the hydrophilic groups of the casein proteins, forcing them to move to the interface.

3.4 Conclusion

Sodium caseinate monolayers at the air-water interface are strongly affected by changes to the pH and ionic strength of the aqueous phase. The pH defines the charge and hydrophilic-hydrophobic balance of the casein molecules, while the ionic strength controls the interaction between the casein molecules and the aqueous phase.

The evolution of the isotherms, for the sodium caseinate monolayer, is liquid-expanded-liquid and the number of phases formed depends on the subphase pH. For pH values below the isoelectric point and neutral, four phases were detected: G, LE, LC and S. While at pH subphases near the isoelectric point and basic, three phases were indentified: G, LE and LC. The detection of the different phases is a function of the conformation and interaction between the casein molecules.

The capacity of the casein molecules to cover the air-water interfacial area (superficial density) depends on their electrostatic interaction and hydrophobicity. Low superficial densities were found for casein molecules at acidic and neutral pH subphases (high electrostatic repulsion and high hydrophobicity). However, basic subphase pH (low hydrophobicity and high electrostatic repulsion) and subphase with pH near the isoelectric point (low electrostatic repulsion and moderate hydrophobicity) showed high superficial density.

Monolayers of sodium caseinate at the air-water interface show elasticity and its magnitude depends on the pH of the subphase. The decreasing trend at high superficial density was as follows: isoelectric, basic, acid and neutral.

Increasing the ionic strength in the subphase increased the surface pressure for all pH values studied. The increase in the surface pressure with the ionic strength is related to the reduction in the solubility of the hydrophilic residual groups of the

casein molecules, and the weakness of the intramolecular non-covalent interactions. The increase in the ionic strength also decreased the superficial density of the sodium caseinate. As a consequence, the mass of sodium caseinate necessary to produce a monolayer decreases as the ionic strength increases.

Despite the interfaces investigated being different, similar results were found by changing ionic strength and pH values. The interfacial tension between the oil and water phases can be decreased by changing the pH in the following decreasing order: basic, neutral and near isoelectric point. The decrease in the interfacial tension is associated with the reduction of the hydrophilic portion of the casein molecules as the pH is reduced.

Increasing the ionic strength reduces the interfacial tension for all pH values, which is related to the increase of the interfacial area covered by the casein molecules.

3.5 References

1. McClements, D.J., *Protein-stabilized emulsions.* Current Opinion in Colloid & Interface Science, 2004. **9**(5): p. 305-313.

2. MacRitchie, F., *Spread monolayers of proteins.* Advances in Colloid and Interface Science, 1986. **25**: p. 341-385.

3. Corzo-Martínez, M., et al., *Effect of glycation on sodium caseinate-stabilized emulsions obtained by ultrasound.* Journal of Dairy Science. **94**(1): p. 51-58.

4. Marinova, K.G., et al., *Physico-chemical factors controlling the foamability and foam stability of milk proteins: Sodium caseinate and whey protein concentrates.* Food Hydrocolloids, 2009. **23**(7): p. 1864-1876.

5. Niño, M.R.R.g., C.C. Sánchez, and J.M.R.g. Patino, *Interfacial characteristics of β-casein spread films at the air–water interface.* Colloids and Surfaces B: Biointerfaces, 1999. **12**(3–6): p. 161-173.

6. Atkinson, P.J., et al., *Neutron reflectivity of adsorbed [small beta]-casein and [small beta]-lactoglobulin at the air/water interface.* Journal of the Chemical Society, Faraday Transactions, 1995. **91**(17): p. 2847-2854.

7. Rodríguez Patino, J.M., C.C. Sánchez, and M.R. Rodríguez Niño, *Structural and morphological characteristics of [beta]-casein monolayers at the air-water interface.* Food Hydrocolloids, 1999. **13**(5): p. 401-408.

8. Rodríguez Patino, J.M. and M.R. Rodríguez Niño, *Interfacial characteristics of food emulsifiers (proteins and lipids) at the air-water interface.* Colloids and Surfaces B: Biointerfaces, 1999. **15**(3-4): p. 235-252.

9. Russev, S.C., T.V. Arguirov, and T.D. Gurkov, *β-Casein adsorption kinetics on air–water and oil–water interfaces studied by ellipsometry.* Colloids and Surfaces B: Biointerfaces, 2000. **19**(1): p. 89-100.

10. Kaganer, V.M., et al., *Structure and phase transitions in Langmuir monolayers.* Reviews of Modern Physics, 1999. **71**(3): p. 779.

11. Niño, M.R.R., C.C. Sánchez, and J.M.R. Patino, *Interfacial characteristics of [beta]-casein spread films at the air-water interface.* Colloids and Surfaces B: Biointerfaces, 1999. **12**(3-6): p. 161-173.

12. Nieto-Suárez, M., N. Vila-Romeu, and I. Prieto, *Behaviour of insulin Langmuir monolayers at the air-water interface under various conditions.* Thin Solid Films, 2008. **516**(24): p. 8873-8879.

13. Andrews, B.A., D.L. Pyle, and J.A. Asenjo, *The effects of pH and ionic strength on the partitioning of four proteins in reverse micelle systems.* Biotechnology and Bioengineering, 1994. **43**(11): p. 1052-1058.

14. Swaisgood, H.E., *Review and Update of Casein Chemistry.* Journal of Dairy Science, 1993. **76**(10): p. 3054-3061.

15. FauchÈRe, J.-L. and V. Pliska, *Hydrophobic parameters pi of amino acid side chains from partitioning of N-acetyl-amino-acid amides.* European Journal of Medicinal Chemistry, 1983. **18**: p. 369-375.

16. Wüstneck, R., et al., *Surface dilatational behavior of β-casein at the solution/air interface at different pH values.* Colloids and Surfaces A: Physicochemical and Engineering Aspects, 2012. **404**(0): p. 17-24.

17. Baumy, J., J. and G. Brule, *Effect of pH and ionic strength on the binding of bivalent cations to β-casein.* Lait, 1988. **68**(4): p. 409-417.

18. Cross, K.J., et al., *Physicochemical Characterization of Casein Phosphopeptide-Amorphous Calcium Phosphate Nanocomplexes.* Journal of Biological Chemistry, 2005. **280**(15): p. 15362-15369.

19. Nelson, D.L. and M.M. Cox, *Lehninger Principles of Biochemistry*. 4 ed2004: Freeman, W. H. & Company. 1100.

20. Arakawa, T. and S.N. Timasheff, *Mechanism of protein salting in and salting out by divalent cation salts: balance between hydration and salt binding.* Biochemistry, 1984. **23**(25): p. 5912-5923.

21. Jungwirth, P. and B. Winter, *Ions at Aqueous Interfaces: From Water Surface to Hydrated Proteins.* Annual Review of Physical Chemistry, 2008. **59**(1): p. 343-366.

22. Zhang, Y. and P.S. Cremer, *Interactions between macromolecules and ions: the Hofmeister series.* Current Opinion in Chemical Biology, 2006. **10**(6): p. 658-663.

23. Miñones Conde, M., et al., *How to obtain a well-spread monolayer of lysozyme at the air/water interfaces.* Journal of Colloid and Interface Science, 2011. **361**(1): p. 351-360.

24. Phillips, M.C., et al., *Monolayers of block copolypeptides at the air—water interface.* Journal of Colloid and Interface Science, 1979. **72**(1): p. 98-105.

25. Kunz, W., *Specific ion effects in colloidal and biological systems.* Current Opinion in Colloid & Interface Science, 2010. **15**(1–2): p. 34-39.

26. Lawal, O.S., *Kosmotropes and chaotropes as they affect functionality of a protein isolate.* Food Chemistry, 2006. **95**(1): p. 101-107.

27. Dynarowicz-Łątka, P., A. Dhanabalan, and O.N. Oliveira Jr, *Modern physicochemical research on Langmuir monolayers.* Advances in Colloid and Interface Science, 2001. **91**(2): p. 221-293.

28. Berg, J.M., J.L. Tymoczko, and L. Stryer, *Biochemistry* 6ed2006: W. H. Freeman.

29. Andrade, C.A.S., et al., *Dielectric properties of Bauhinia monandra and Concanavalin A lectin monolayers, part I.* Journal of Colloid and Interface Science, 2005. **289**(2): p. 371-378.

30. Oliveira Jr., O.N., A. Riul Jr., and V.B.P. Leite, *Water at interfaces and its influence on the electrical properties of adsorbed films.* Brazilian Journal of Physics, 2004. **34**: p. 73-83.

31. Vogel, V. and D. Möbius, *Local surface potentials and electric dipole moments of lipid monolayers: Contributions of the water/lipid and the lipid/air interfaces.* Journal of Colloid and Interface Science, 1988. **126**(2): p. 408-420.

32. Cockbain, E.G. and J.H. Schulman, *On the structure of protein films.* Transactions of the Faraday Society, 1939. **35**(0): p. 1266-1276.

33. Zhai, J.l., et al., *Protein folding at emulsion oil/water interfaces.* Current Opinion in Colloid & Interface Science, 2013. **18**(4): p. 257-271.

34. Dalgleish, D.G., *Conformations and structures of milk proteins adsorbed to oil-water interfaces.* Food Research International, 1996. **29**(5–6): p. 541-547.

35. Dickinson, E., *Milk protein interfacial layers and the relationship to emulsion stability and rheology.* Colloids and Surfaces B: Biointerfaces, 2001. **20**(3): p. 197-210.

36. Dickinson, E., *An Introduction to Food Colloids*1992, Oxford Oxford University Press. 207.

37. Macritchie, F., *Proteins at Interfaces.* Advances in Protein Chemistry, 1978. **32**: p. 283-326.

38. Talbot, J., et al., *From car parking to protein adsorption: an overview of sequential adsorption processes.* Colloids and Surfaces A: Physicochemical and Engineering Aspects, 2000. **165**(1–3): p. 287-324.

39. Kanicky, J.R. and D.O. Shah, *Effect of Degree, Type, and Position of Unsaturation on the pKa of Long-Chain Fatty Acids.* Journal of Colloid and Interface Science, 2002. **256**(1): p. 201-207.

40. Chi, E.Y., et al., *Physical Stability of Proteins in Aqueous Solution: Mechanism and Driving Forces in Nonnative Protein Aggregation.* Pharmaceutical Research, 2003. **20**(9): p. 1325-1336.

41. dos Santos, A.P. and Y. Levin, *Ions at the Water–oil Interface: Interfacial Tension of Electrolyte Solutions.* Langmuir, 2011. **28**(2): p. 1304-1308.

42. Lima, E.R.A., et al., *Specific ion effects on the interfacial tension of water/hydrocarbon systems.* Brazilian Journal of Chemical Engineering, 2013. **30**: p. 55-62.

43. Beverung, C.J., C.J. Radke, and H.W. Blanch, *Protein adsorption at the oil/water interface: characterization of adsorption kinetics by dynamic interfacial tension measurements.* Biophysical Chemistry, 1999. **81**(1): p. 59-80.

44. Dalgleish, D.G. and J. Leaver, *The possible conformations of milk proteins adsorbed on oilwater interfaces.* Journal of Colloid and Interface Science, 1991. **141**(1): p. 288-294.

Chapter 4 Buffer effect of sodium caseinate

4.1 Introduction

Sodium caseinate has wide use in the food and pharmaceutical industries including its use as a nutritional ingredient, stabiliser, emulsifier, thickener and texture modifier. For all these applications, the sodium caseinate molecules are in contact with the aqueous phase, either within the final product or during its processing. The aqueous phase can have different pH and ionic strength values that produce different protein conformations and properties. This was shown in the previous chapter where the effect of the ionic strength and pH on the conformation and interfacial tension between different phases was investigated. If sodium caseinate is used as the emulsifier in the formulation of emulsions, it is extremely important to know its properties in the aqueous phase to elucidate the final properties of the emulsion.

Variations in ionic strength and pH are frequent in the processing and formulation of milk products such as yoghurt, fermented milk and cheese. Salaun *et al.* [1] state that in the dairy industry the buffer capacity of milk products depends on numerous compositional factors including the salts, organic acids and milk proteins (caseins and whey protein).

The amphoteric properties of protein molecules, i.e. the capacity to react as an acid or a base, are a consequence of the basic amino group ($-NH_2$), the acidic carboxyl group (-COOH) and the ionisable residual groups such as aspartic acid, glutamic acid, lysine and tyrosine. Thus, protein molecules can react as an acid or base depending on the pH of the aqueous phase.

In the formulation of emulsions using proteins, it is common to use a buffer as the aqueous phase. Hence, the conformation of protein molecules at the interface, the interactions between proteins and the phases and the interactions within and between them depend on the final pH of the protein-buffer solution.

The buffer behaviour of sodium caseinate was investigated using ranges of ionic strength and pH similar to the values that were used in the study of the sodium

caseinate at the air-water and oil-water interfaces. Also, the grams of sodium caseinate and buffer solution used were the quantities appropriate to formulate emulsions with oil concentrations from 30 to 70 wt% and sodium caseinate concentration of 1 wt%. These quantities were stated as ratios between sodium caseinate and the buffer solution mass (mP/mB). The novel approach taken in this study was the use of very low ionic strengths, below 20 mM, and the increase of the ionic strength using only the components of the buffer solutions, i.e. by not adding salt. Additionally, the information obtained about the buffer behaviour of sodium caseinate was used to formulate stable concentrated emulsions.

Two procedures were used to evaluate the buffer effect of sodium caseinate: the first was the evaluation of the buffer index or buffer capacity by titration with a strong acid and a strong base. The second was the buffer effect of sodium caseinate with different buffer solutions at different ionic strength and pH values. The results obtained were used to display formulation maps that represent ionic strength and pH conditions where emulsions can be made.

4.2 Results and discussion

Sodium caseinate solutions were made to evaluate its buffer capacity at different concentrations. Titrations were made against a strong acid (HCl) and a strong base (NaOH). The titration curves were obtained and from this data the buffering capacity was estimated.

The capacity of the sodium caseinate to control the final pH of the sodium caseinate solutions, using aqueous phases of different buffer solutions, was studied at different pH and ionic strength values. The ratio of sodium caseinate to buffer evaluated in these experiments correlates to the effective ratio used for oil in water emulsions (O/W) with 30-70 wt% oil and 1 wt% sodium caseinate. This ensures that the information obtained provides an insight into whether the sodium caseinate or the buffer controls the final pH of the emulsions.

4.2.1 Buffer capacity of sodium caseinate

Buffer capacity is an important physicochemical parameter that quantifies the capacity of a solution to resist variations in pH when a strong acid or base is added

[2]. Evaluation of the buffer capacity is undertaken by adding acid or base to a solution and measuring the pH.

The buffer capacity can be determined using the resulting titration curve; molar concentration of strong acid or base in the solution versus pH, and then evaluating the slope of the tangent (dB/dpH) at each pH value. This ratio is expressed as [3]:

$$\frac{dB}{dpH} = \frac{(volume\ of\ acid\ or\ base\ added)(molarity\ of\ acid\ or\ base)}{(volume\ sample)(pH\ change\ produced)} \quad 4.1$$

A diverse range of titration protocols have been used [1], including: acidification alone, acidification and then alkalization, alkalization alone or alkalization and then acidification. The buffer capacity of the proteins may be dependent on the protocol used.

In order to obtain the buffer capacity of sodium caseinate, two solutions were investigated; 25 and 50 g/L sodium caseinate to water. Hydrochloric acid and sodium hydroxide at 0.5 M were used as the strong acid and base respectively. The rate of titrant addition was 0.2 mL/min and the titration final points were pH 3 (acid region) and pH 12 (base region). The titration curves are shown in the Figures 4.1-4.4.

Acidification-alkalization (Figures 4.1 and 4.2) and alkalization-acidification (Figures 4.3 and 4.4) were the protocols used according with the procedure suggested by Salaün *et al.* [1]. For both protocols the volume of acid or base used (titrant) for the titration is a function of the sodium caseinate concentration. It can be seen in the vertical axis where the concentrations of HCl or NaOH (mM) required for the titration are shown, that more volume of titrant for the sodium caseinate solution at concentration 50 g/L is required than 25 g/L.

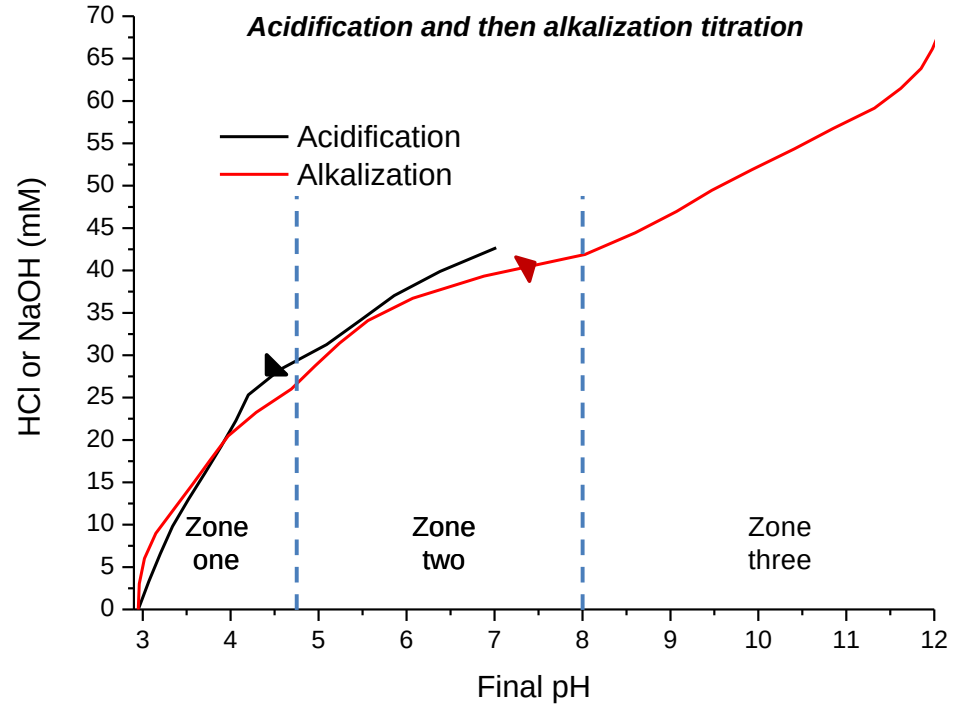

Figure4.1. Titration curve of acidification-alkalization with HCl and NaOH 0.5 M. Sodium caseinate concentration 25 g/L.

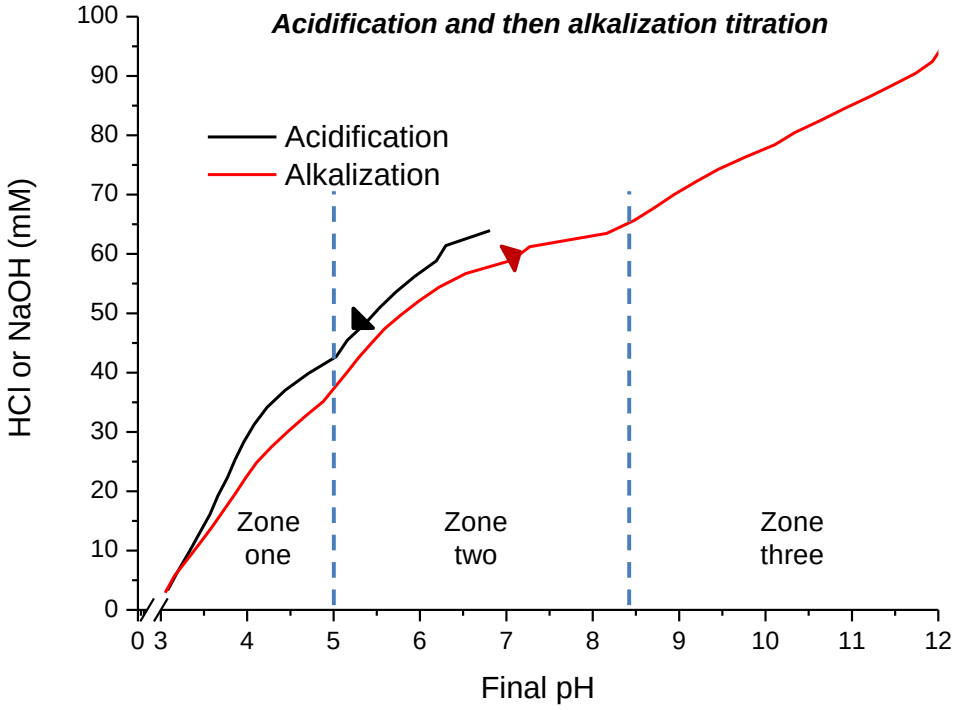

Figure4.2. Titration curve of acidification-alkalization with HCl and NaOH 0.5 M. Sodium caseinate concentration 50 g/L.

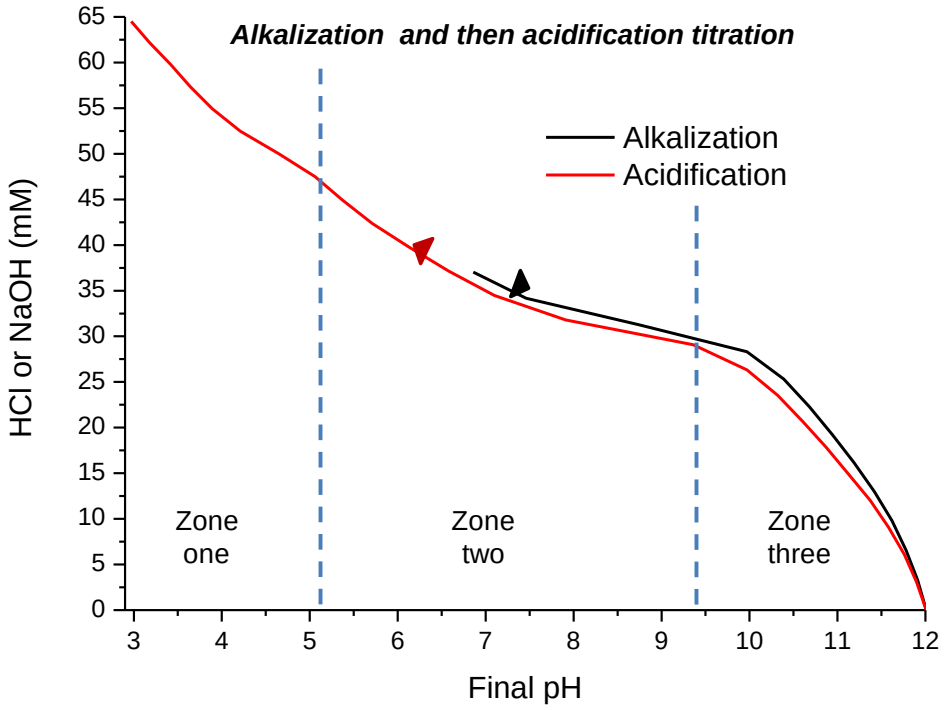

Figure4.3. Titration curve of alkalization and then acidification with NaOH and HCl 0.5 M. Sodium caseinate concentration 25 g/L.

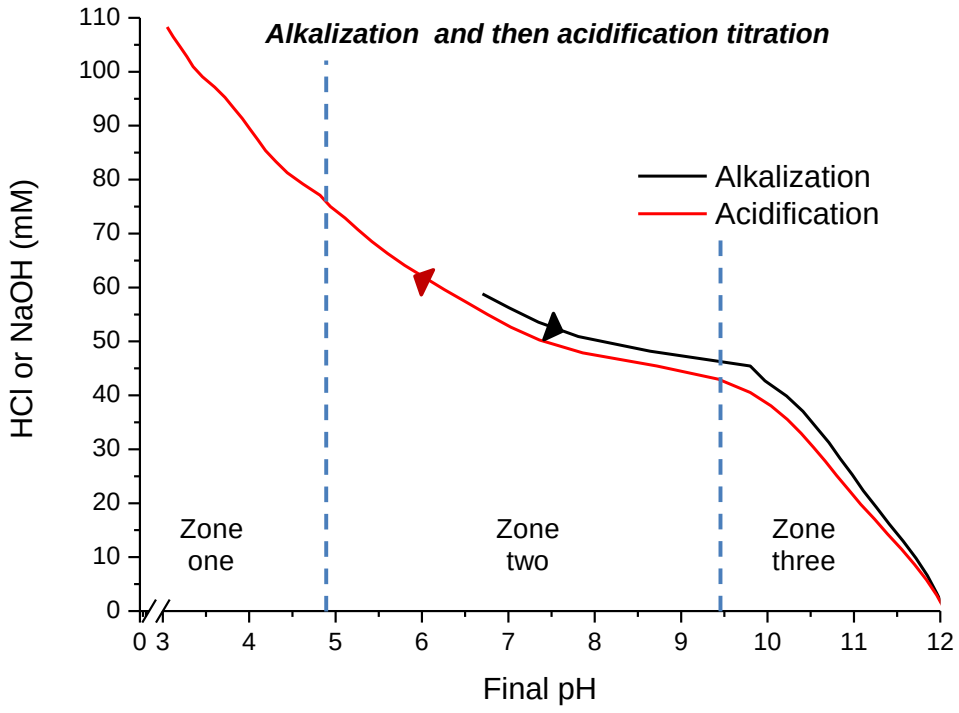

Figure4.4. Titration curve of alkalization-acidification with NaOH and HCl 0.5 M. Sodium caseinate concentration 50 g/L.

The forward and back titration curves for the acidification-alkalization and alkalization-acidification show differences which are more pronounced for the

acidification-alkalization titration than in the reverse mode. These differences in the titration curves are known as hysteresis and similar behaviour has been reported by Lucey *et al.* [4], Salaün *et al.* [1] and Al-Dabbas *et al.* [5] for the titration of cow's milk.

In the case of the sodium caseinate solutions, the hysteresis occurs because of the interaction of the acid or alkali titrant with the amino acids that constitute the protein molecules Maher *et al.* [6] explained that the contribution of proteins in the hysteresis is because some of them can be denatured at a specific pH, making some ionizable residual groups accessible for the back titration.

Three zones can be distinguished for the different titration curves and they are related to the amino acid compositions of the caseins. The range of the three zones is slightly different for each of the four systems, specifically depending on whether the titration was acidification-alkalization or alkalization-acidification. The differences normally occur because of the interactions between titratable amino acid groups and the titrant, inaccessibility of some amino acids due to the protein conformation and the physicochemical environment in which the protein molecules are located [1].

According to Cannan [7] the dissociation of proteins may be expected to occur in three regions around the pH values 4, 7 and 10-12, respectively. She states that the first zone is below pH 6 and can be associated with the dissociation of carboxyl groups (α-carboxyl, aspartic and glutamic acid), the zone between pH 6 and 8.5 are primarily imidazole groups and the last zone above pH 8.5 is related to amino groups (α-amino and lysine), tyrosine, cysteine and arginine.

In sodium caseinate solution titration curves, despite being a mixture of four proteins with different amino acids composition, the three zones can be readily distinguished. The first zone(pH 3-5) is related to the terminal α-carboxyl residues, aspartic acid and glutamic acid, which have pKa values [7] around 3.5, 4 and 4.6 respectively. The second zone (pH 5-9.5) is associated with the amino acids histidine and phosphoserine and their pKa values are approximately 6.5 and 6 respectively. The last zone represents the amino acids lysine, cysteine and tyrosine with pKa values of 10.5, 10, and 9.7 respectively.

The buffer capacity of sodium caseinate was evaluated using the titration data and the results are shown in Figures 4.5- 4.8.

Buffering capacity curves from acidification followed by alkalization, for both sodium caseinate solution concentrations, are very similar (see Figures 4.5 and 4.6). The three zones are located at similar pH values and distinguishing peaks can be seen. The first peak detected on decreasing pH from the original solution pH (pH around 4.8-5.3) is due to the proportion of the phosphoserine and histidine residues[1]. The second peak (pH 3.7-4.1) is related to the amino acid group α-carboxyl in aspartic and glutamic acid. During the alkalization titration for the 25 g/L sodium caseinate solution an additional peak was detected at basic pH (8.5-9.2). This peak is related to the residual group tyrosine.

For the 50 g/L sodium caseinate solution, the number of peaks that are evident during acidification and alkalization increase (Figure 4.6). The two additional peaks, at basic pH are associated with α-amino, lysine and cysteine. This difference is most likely a result of the higher concentration and therefore the increased number of each residual group enhancing possible detection. The same behaviour occurred during the acidification process where more peaks were detected at 50 g/L of sodium caseinate concentration than at 25 g/L. Salaün *et al.* [1] showed a similar trend in their results with regard to the number of peaks detected for the buffering capacity as the concentration of casein micelles was augmented.

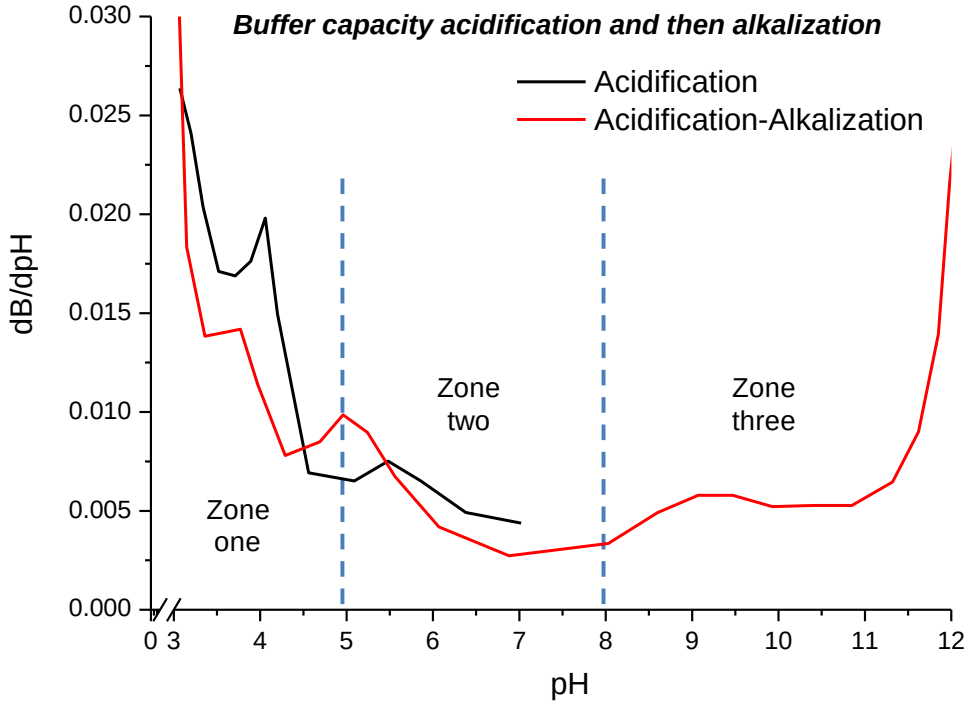

Figure4.5. Buffering capacity of acidification-alkalization with HCl and NaOH 0.5 M. Sodium caseinate concentration 25 g/L.

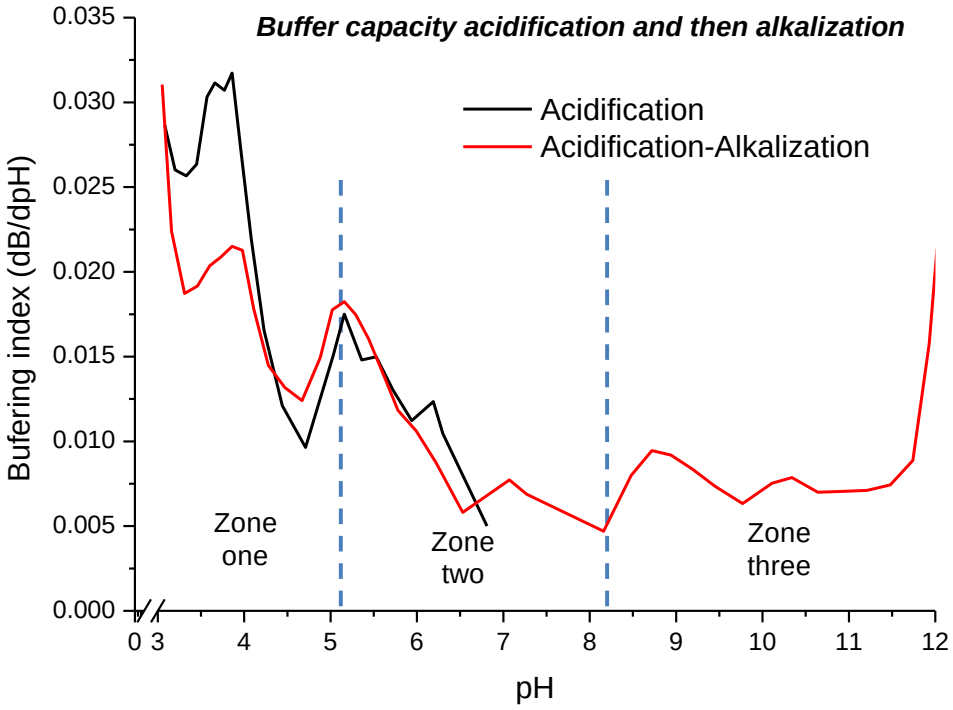

Figure4.6. Buffering capacity of acidification and then alkalization with HCl and NaOH 0.5 M. Sodium caseinate concentration 50 g/L.

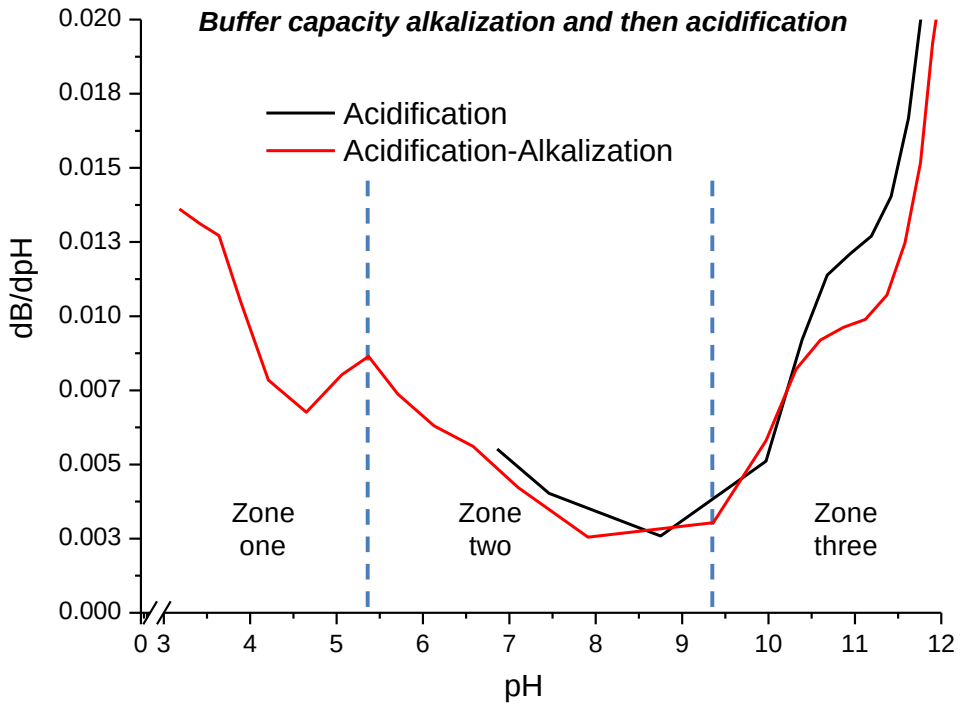

Figure4.7. Buffering capacity of alkalization and then acidification with NaOH and HCl 0.5 M. Sodium caseinate concentration 25 g/L.

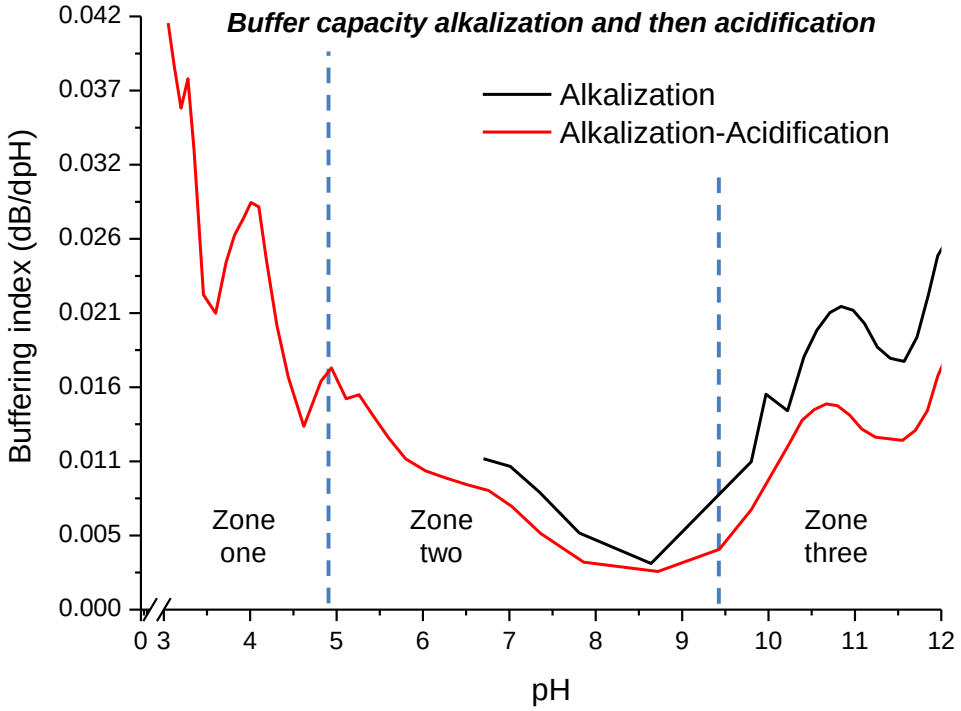

Figure4.8. Buffering capacity of alkalization and then acidification with NaOH and HCl 0.5 M. Sodium caseinate concentration 50 g/L.

Al-Dabbas *et al.* [5], using different dairy products to evaluate the buffering capacity, also found that the relatively high buffering capacity depends on the protein content

of the products. They explained that the increase in the buffering capacity is due to the buffering effect of amino acid groups that constitute the protein molecules.

The curves of buffering capacity obtained by alkalization followed by acidification titration for the two sodium caseinate solution concentrations are shown in Figures 4.7 and 4.8. They have similarities with more peaks and higher buffering capacity for the sodium caseinate concentration at 50 g/L than at 25 g/L. Moving from the original pH to the basic pH, one peak is differentiated at pH around 10.5 (zone three) that corresponds to the lysine residual group. According to the amino acid composition of the caseins [8], lysine forms a high proportion in the primary structure of the caseins.

During the acidification titration from pH 12 to pH 3 the curves are very similar to the acidification-alkalization from pH 3 to pH 12 (Figures 4.5 and 4.6), they show the same number of peaks around the same pH values for each zone at specific sodium caseinate concentrations.

The absence or minimum concentration of colloidal calcium phosphate (CCP) in the sodium caseinate solutions studied can be confirmed, because the first peak is present during the whole acidification-alkalization titration process.

Lucey *et al.* [4] explained that the presence of CCP in milk can be detected using its buffering capacity curves. They showed that the curves obtained were dissimilar for the entire acidification-alkalization process. They found a peak at pH around 5.1 when the titration was acidification, but when the milk was back titrated the peak was displaced to a pH value of about 6.3. The two different peaks are related to the solubilization and formation of CCP respectively. Also, they affirmed that the peaks that are associated with protein residues or salts present in milk are unchanged by the titration sequence.

The results in Figures 4.1-4.8 show that the changes and zones on the titration curves and the buffer capacity of sodium caseinate are function of the amino-acid composition. Despite that the amino-acid composition is known for each casein proteins, an accurate prediction of the buffer capacity property of sodium caseinate is not possible because this depends on the protein conformation. If the casein molecules are totally or partially unfolded, it is possible that titration curves and the

buffer capacity of sodium caseinate are different. Additionally, the existence of trace contaminants, which could have affected the buffer capacity, also have an effect on the titration and buffer capacity of the sample investigated. Because of that, the titration of sodium caseinate was necessary to have accurate information about its buffer capacity.

4.2.2 Buffer capacity of sodium caseinate with different buffer solutions

When emulsions are formulated with protein it is common to use a buffer solution as the aqueous phase. Thus, the final pH of the emulsion depends on whether the protein or the buffer controls the pH of the system particularly at low ionic strength buffer solutions. Because of the extreme sensitivity of protein conformation and properties to the pH and ionic strength of the aqueous environment, it is critical to understand what is controlling and defining the final pH of the protein-buffer solution.

The titration and buffering capacity curves of sodium caseinate solutions showed that the volume of titrant and buffering capacity are a function of the sodium caseinate concentration. The capacity of a buffer solution to act as a buffer and control the final pH of a system, after adding substances that tend to change the solution pH, not only depend on it and the concentration of the additives, but also on how narrow the difference is between the pH required and the pKa or pKb of the buffer[9, 10]

In order to investigate the effect of the ionic strength and pH on the final pH of buffer-sodium caseinate systems, different buffer solutions were prepared (see Appendix A3) to which sodium caseinate was added. Specific ratios of masses of sodium caseinate and buffer (mP/mB) were used in order to match the formulation of the concentrated emulsions from 30 to 70 wt% of oil and 1 wt% of sodium caseinate. The choice of 1 wt% of sodium caseinate was made because stable emulsions are formulated with this concentration of protein as will be shown later. Additionally, in emulsion formulation it is fundamental to optimise (minimise) the quantity of emulsifier to be used. Table 4.1 shows the relation between the emulsion oil concentration (wt%) and the ratio mP/mB (dimensionless).

Table 4.1 Protein mass-buffer mass ratios for different oil concentration emulsions.

Oil concentration (wt%)	Ratio (mP/mB)
70	0.034
65	0.029
60	0.025
55	0.022
50	0.020
40	0.016
30	0.014

Three different buffer pH values were investigated (around 4.5, 5.0 and 10.4) and the ionic strength range evaluated was between 5 and 80 mM, except for pH 10.4 where 160 mM buffer concentration was also used. Acetate and carbonate buffers were used for the pH values 4.5-5 and 10.4 respectively. The final pH of the buffer-sodium caseinate systems and their difference compared with the buffer pH (|ΔpH|) are reported. The results are shown in Figures 4.9- 4.11.

For all the buffer solutions studied at different ionic strengths, the general trend is a decrease in the control of the final pH by the sodium caseinate when the mP/mB ratio is reduced. This is a consequence of the high concentration of hydronium (H^+) or hydroxide (OH^-) ions released by the acid or base buffer solutions respectively, which counteract the buffer capacity of sodium caseinate.

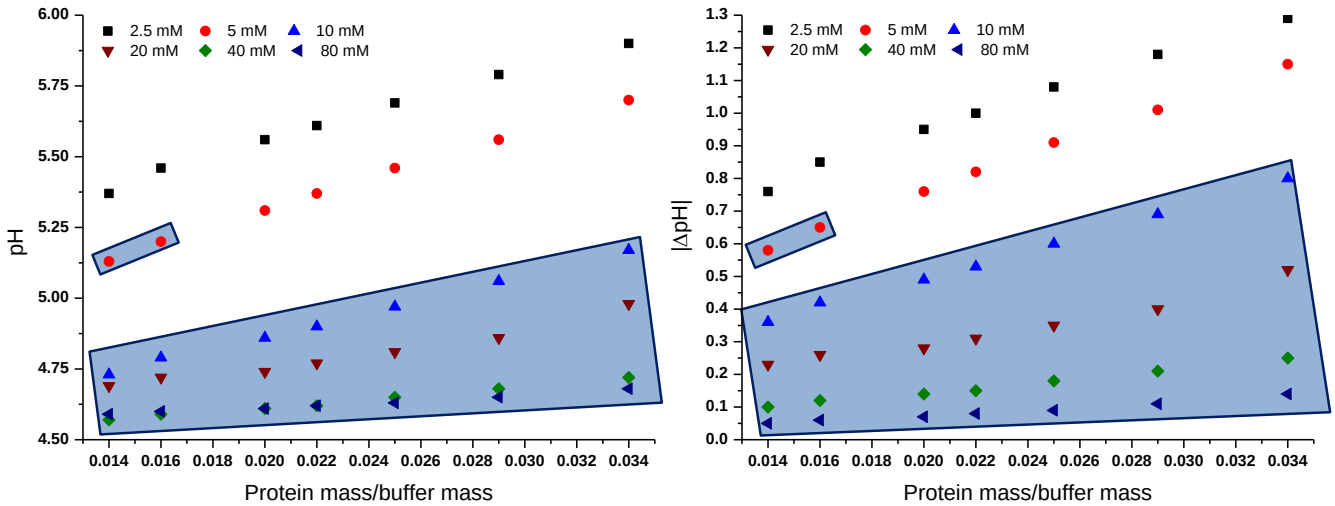

Figure4.9. Final solution pH buffer-sodium caseinate systems (left) and pH difference between the final solution pH and the pH of the original buffers (right) at different ionic strengths and ratios. Acetate buffer at pH around the isoelectric point of sodium caseinate (4.6-5).

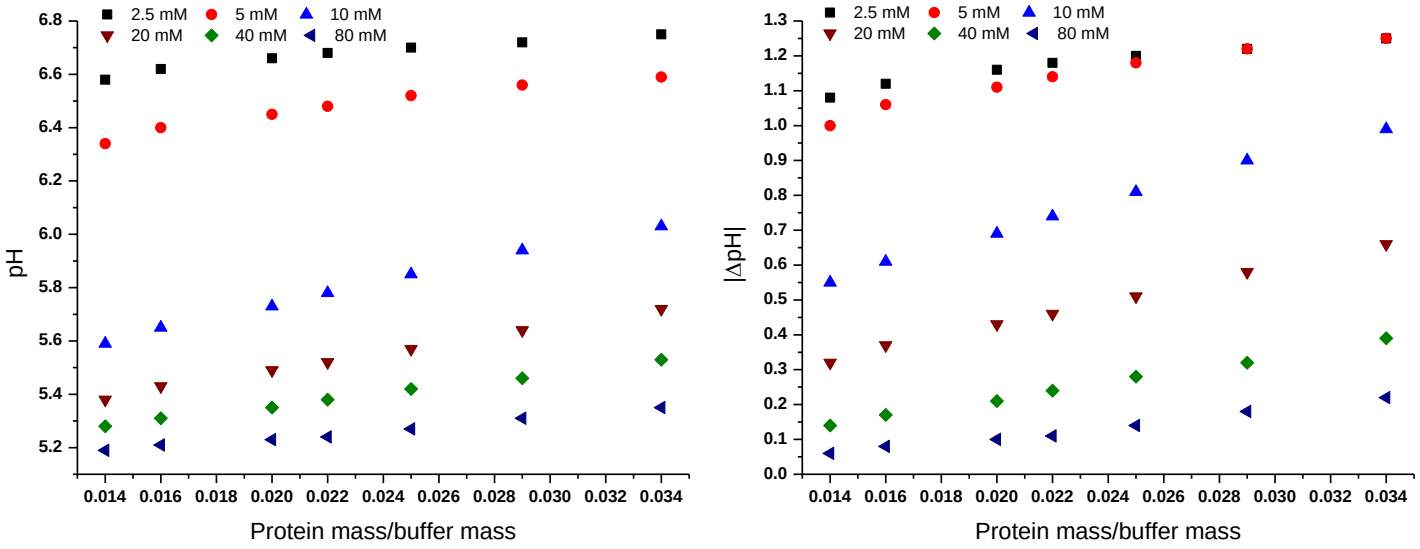

Figure4.10. Final pH systems buffer-sodium caseinate (left) and pH difference between the final solution pH and the pH of the original buffers (right) at different ionic strengths and ratios. Acetate buffer at pH around 5.

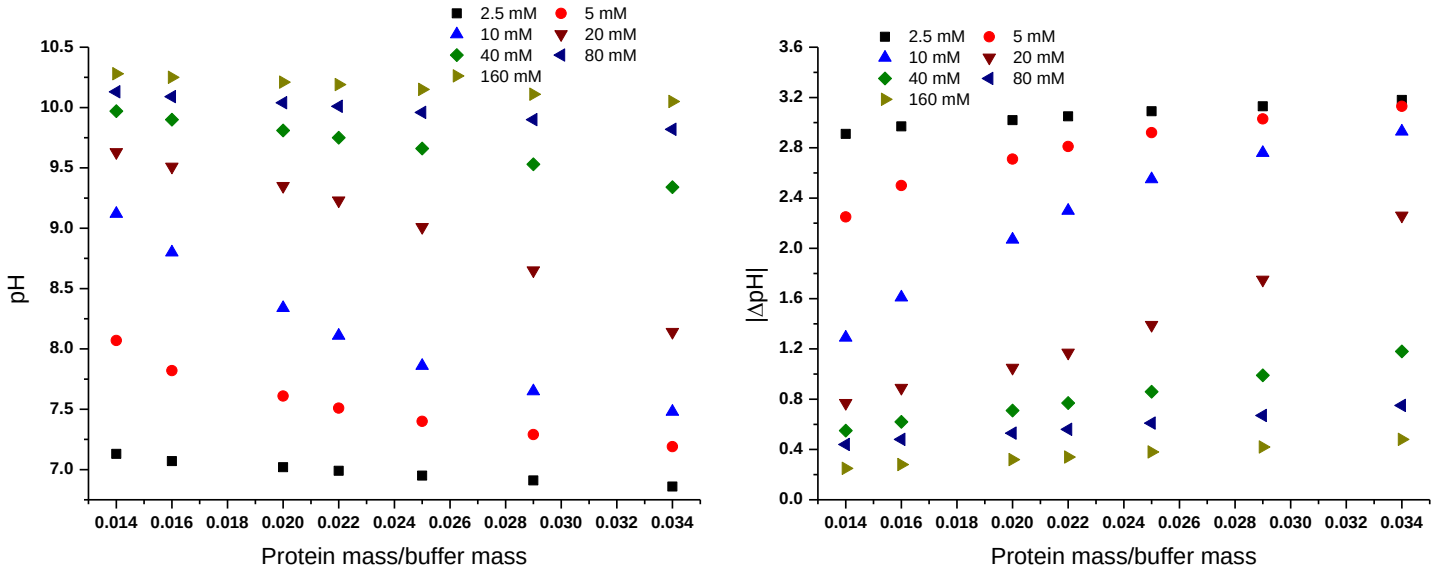

Figure4.11. Final pH systems buffer-sodium caseinate (left) and pH difference between the final solution pH and the pH of the original buffers (right) at different ionic strengths and ratios. Carbonate buffer at pH around 10.4.

For buffers at pH values around 4.5, the reduction in the capacity of the sodium caseinate to control the final pH can be observed as an upward trend as the ratio mP/mB increases (see Figure 4.9 left). Moreover, the slope of the lines decline slightly as the ionic strength of the buffer solution is augmented, being practically the

same slope for ionic strengths of 40 and 80 mM. For a specific ionic strength, the reduction in the sodium caseinate capacity to control the final pH is because of the dilution of the sodium caseinate solution as the mP/mB ratio decreases. As a consequence, the final pH of the system is practically the same pH of the buffer solution. These results are in agreement with the results showed in the previous section, where the buffering capacity of sodium caseinate is higher as its concentration increases.

When the ionic strength of a buffer solution increases, for a particular mP/mB ratio, sodium caseinate loses the capacity to control the final pH of the system. In Figure 4.9 (right) the trend to zero for |ΔpH| as the ionic strength of the buffer solution increases is evident. Lloret *et al.[10]*, using phosphate buffer to evaluate the effects of buffer composition in the detection of protein-protein interactions, reported that the buffer capacity of phosphate buffer increases when the component used for its formulation also increases.

In Figure 4.9 (left and right) the blue shadow region is used to depict when sodium caseinate precipitation occurred. For the systems studied, the precipitation of the sodium caseinate was observed for pH values up to 5.2 when a buffer solution of around pH 4.5 was used to prepare the samples. Figure 4.12 shows the precipitation of sodium caseinate in some of the systems investigated.

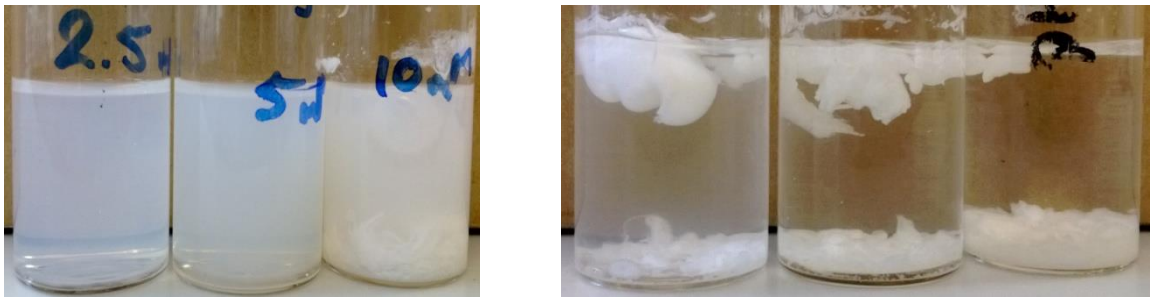

Figure4.12. Photographs of sodium caseinate-buffer solutions ratio a mP/mB ratio of 0.034. Left (from left to right) ionic strengths of 2.5, 5 and 10 mM; right (from left to right) ionic strengths of 20, 40 and 80 mM. Acetate buffer at pH around 4.5.

Precipitation of sodium caseinate occurs because its isoelectric point (4.6-5.0) is achieved in systems at ionic strengths of 10, 20, 40 and 80 mM. Precipitation takes place since the electrostatic repulsion between the protein molecules is not sufficiently strong to overcome the van der Waals and hydrophilic attractive interactions, as HadjSadok *et al.* [11] referred to in their characterisation of sodium caseinate as a function of different physicochemical parameters. Systems at ionic strengths of 2.5 and 5 mM (Figure 4.12 left) show turbidity whilst for those at an ionic strength 5 mM and mP/mB ratios of 0.014 and 0.016, precipitation of sodium caseinate occurs due to the final solution pH values being 5.2 and 5.1 respectively. The turbidity arises due to the solution pH approaching to the isoelectric point of the sodium caseinate, decreasing the electrostatic repulsion and allowing protein aggregation to occur without precipitation. The systems where the sodium caseinate precipitated, i.e. blue zone in the graphs, cannot be used in the formulation of stable emulsions, a result confirmed by experiment whereby no emulsions could be formed.

For solutions prepared using buffers with pH near the isoelectric point a similar trend was observed; as the ratio mP/mB increases for the ionic strengths from 10 mM to 80 mM (see Figure 4.9 left) the pH increases; the trend almost levels out for ionic strengths of 2.5 and 5 mM. This levelling out behaviour suggests that the sodium caseinate is able to control the final pH of the systems for the different mP/mB ratios studied.

Sodium caseinate precipitation did not occur for any of the solutions prepared using a buffer system near pH~5. Nevertheless, aggregation of sodium caseinate was observed for some of the solutions, being opaque, where the final pH was close to 5 (Figure 4.13).

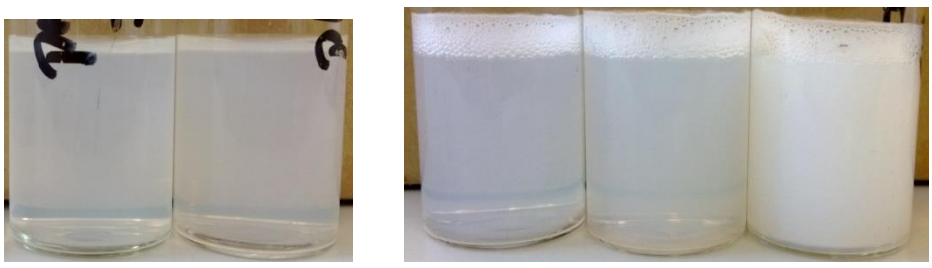

Figure4.13. Photographs of sodium caseinate-buffer solutions ratio a mP/mB ratio of 0.034. Left (from left to right) ionic strengths of 5 and 10 mM; right (from left to right) ionic strengths of 20, 40 and 80 mM. Acetate buffer at pH around 5.

Sodium caseinate-buffer solutions, prepared using a pH buffer of 10.4, show as expected a negative slope for the graph pH vs. mP/mB (Figure 4.11 left). This is because the final pH is lower than that of the buffer solution pH. A buffer solution at ionic strength 160 mM was used in order to evaluate the reduction of |ΔpH| for the mP/mB ratio of 0.034.

A general downward trend is observed as the mP/mB ratio increases, being more strongly evident for the buffer solutions at ionic strengths between 5 mM and 40 mM. For the buffer solutions at ionic strengths of 2.5, 80 and 160 mM, the final pH values are very similar for all mP/mB ratios studied. At an ionic strength of 2.5 mM the final pH was controlled by sodium caseinate, while the contrary happened at ionic strengths of 80 and 160 mM, i.e. the buffer solution controlled the final pH.

The appearance for all the systems studied for the buffer pH ~ 10.4 was similar. There was no evidence for casein aggregation. At pH values above 7, casein molecules have a high negative charge, causing a strong electrostatic repulsion between the molecules resulting in the presence of individual casein molecules [11].

Figure4.14. Photographs of sodium caseinate-buffer solutions for the mP/mB ratio of 0.034. Left (from left to right) ionic strengths of 2.5, 5 and 10 mM; right (from left to right) ionic strengths of 20, 40 and 80 mM. Carbonate buffer at pH around 10.4.

For the three buffer solutions investigated, |ΔpH| increases proportionally with the mP/mB ratio and decreases as the ionic strength increases. |ΔpH| values were noticeably higher for the pH 10.4 buffer system in comparison with the buffer solutions at pH values 4.5 and 5. The range of |ΔpH| for the different buffer solutions evaluated, at ionic strengths from 2.5 to 80 mM, were 0.05-1.29, 0.06-1.25 and 0.44-3.18 at pH values 4.5, 5 and 10.5 respectively. The big difference in the final pH for the buffer at pH 10.4 is due to the buffering capacity of sodium caseinate being

higher at pH values between 4.5 and 5 than at pH 10.4 (see Figures 4.5 and 4.6). This trend was similar for all the ionic strengths evaluated. The highest |ΔpH| values were for the three buffer systems are 1.29, 1.25 and 3.18 at pH 4.5, 5 and 10.4 respectively; corresponding to systems at an ionic strength of 2.5 mM and a mP/mB ratio of 0.034. At this ionic strength the low buffering capacity of the buffer solutions was expected, because the concentrations of the buffer components are very low [10].

4.3 Conclusions

Titration of sodium caseinate solutions, using hydrochloride acid or sodium hydroxide, presents three zones that are related to the amino-acid composition of the constituent proteins of the sodium caseinate. The first zone (pH 3-5) is related to the α-carboxyl residues, aspartic and glutamic acids. The second zone (pH 5-9.5) is associated with the histidine and phosphoserine amino-acids. The third zone (pH 9.5-12) is related to the amino-acids lysine, cysteine and tyrosine.

A peak in the pH range of 4.8-5.3 was detected during the acidification-alkalization titration indicating the absence of colloidal calcium phosphate. However, an evaluation of the purity of the sodium caseinate used can confirm this result.

At low solution ionic strengths sodium caseinate has a strong buffer capacity for initial solution pH ranges around 4.5-5 and 10.2-11. The highest buffer index of sodium caseinate occurs in the first range (4.5-5). The buffer capacity of sodium caseinate increases and can control the final pH of the sodium caseinate-buffer solution when the ionic strength of the buffer solution decreases or the protein mass-buffer mass ratio (mP/mB) increases.

Precipitation of sodium caseinate occurs when the pH value of the acetate buffer is near the isoelectric point and the ionic strength is above 10 mM for all mP/mB ratios studied. Sodium caseinate is also precipitated when the ionic strength in the acetate buffer is 5 mM and the mP/mB ratio is below 0.16.

The information about the buffer capacity of sodium caseinate is essential to formulate emulsions when low ionic strength values are required and the final pH of the system needs to be controlled.

4.4 References

1. Salaün, F., B. Mietton, and F. Gaucheron, *Buffering capacity of dairy products.* International Dairy Journal, 2005. **15**(2): p. 95-109.

2. Chiriac, V. and G. Balea, *Buffer Index and Buffer Capacity for a Simple Buffer Solution.* Journal of Chemical Education, 1997. **74**(8): p. 937.

3. Lutchman, D., et al., *Evaluation of the buffering capacity of powdered cow's, goat's and soy milk and non-prescription antacids in the treatment of non-ulcer dyspepsia.* South African Medical Journal (SAMJ), 2006. **96**(1): p. 57-61.

4. Lucey, J.A., et al., *Effect of acidification and neutralization of milk on some physico-chemical properties of casein micelles.* International Dairy Journal, 1996. **6**(3): p. 257-272.

5. Al-Dabbas, M.M., K. Al-Ismail, and B.M. Al-Abdullah, *Effect of Chemical Composition on the Buffering Capacity of Selected Dairy Products.* Jordan Journal of Agricultural Sciences, 2011. **7**(4): p. 690-70.

6. Maher M. Al-Dabbas, K.A.-I., Basem M. Al-Abdullah, *Effect of Chemical Composition on the Buffering Capacity of Selected Dairy Products.* Jordan Journal of Agricultural Sciences, 2011. **7**(4): p. 690-700.

7. Cannan, R.K., *The Acid-Base Titration of Proteins.* Chemical Reviews, 1942. **30**(3): p. 395-412.

8. Jensen, R., *Handbook of Milk Composition*, ed. S.L. Taylor1995, San Diego: Academic Press. 919.

9. Urbansky, E.T. and M.R. Schock, *Understanding, Deriving, and Computing Buffer Capacity.* Journal of Chemical Education, 2000. **77**(12): p. 1640.

10. Lloret N, F.R., Møller TC, Rieben NI, Upadhyay S, De Vico L, Jensen JH, Nygård J, Martinez KL., *Effects of buffer composition and dilution on nanowire field-effect biosensors.* Nanotechnology, 2013. **24**(3): p. 1-9.

11. HadjSadok, A., et al., *Characterisation of sodium caseinate as a function of ionic strength, pH and temperature using static and dynamic light scattering.* Food Hydrocolloids, 2008. **22**(8): p. 1460-1466.

Chapter 5 Stability of concentrated emulsions

5.1 Introduction

Concentrated emulsions are dispersed systems where the volumetric fraction of the droplets is between 0.5 and 0.7 without droplet deformation. The non-deformation of the droplets depends on droplet size and droplet size distribution [1]. The high proportion of the dispersed phase in concentrated emulsions reduces the space between droplets and as a consequence, the droplet interactions increase thereby controlling emulsion properties such as stability and rheology. Electrostatic, steric, entropic and van der Waals forces are the most important interactions between droplets to consider in emulsions; the first three are repulsive and the last is attractive. All these forces affect the stability of the emulsions.

Salager [2] explains that the destabilisation process comprises different steps that can be classified as: approach between drops; interdrop film drainage; flocculation and coalescence. The kinetics of the approach between the droplets and the interdrop film drainage depends on droplet size, the physicochemical properties of the continuous phase and type of emulsifier used. The drainage of the continuous phase between droplets is controlled by the disjoining pressure, which is a force that results in an increase in the thickness of the liquid film between close contact droplets opposing the drainage generated by the capillary pressure [3].

The coalescence process happens if the protective stabilising layer at the interface around droplets is not strong enough to prevent their combination producing even bigger droplets after inter-droplet flocculation. Using a protein as the emulsifier can produce two well-known flocculation processes, bridging and depletion, which depend on the proportion of the oil phase and the protein used.

In this chapter the results of an investigation of the stability of concentrated sodium caseinate emulsions is reported. The stability of the systems was studied using static light scattering (SLS) with a monitoring time of six weeks. The microscopic technique used to study the arrangement of the droplets in the emulsions was Cryo-SEM

5.2 Results and discussion

The stability of the concentrated emulsions was investigated as a function of oil concentration, aqueous phase pH, ionic strength, droplet size and droplet size distribution. For the formulation of the emulsions the non-polar phase used was soy bean oil and the concentration of sodium caseinate was 1 wt%. A homogeniser or a blender was used to produce the emulsions with different droplet size distributions and a Mastersizer 2000, from Malvern Instruments, was used to determine these distributions. The volume-based distribution was used, where the volume size distribution was calculated by the software from the intensity of light diffracted at each angle using Mie theory. For some comparisons the Sauter mean diameter ($D_{3,2}$) was employed, which is the mean diameter with the same ratio of volume to surface area as the entire group of droplets. The uncertainty of the data was calculated according to the procedure displayed in Appendix A1, the standard deviations for the droplet size distributions were between 0 and 0.08.

5.2.1 Oil concentration

The droplet size distributions of the fresh concentrated emulsions formed upon varying the soy bean oil concentration from 40 to 70 wt% are shown in Figure 5.1. The emulsification of the systems was achieved using a jet homogeniser at a pressure of 10 Bar and five passes through.

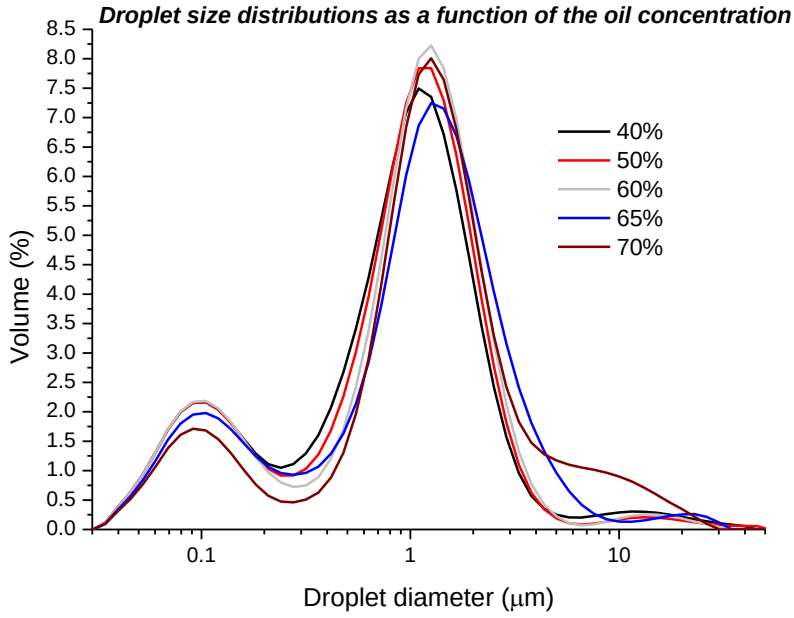

Figure 5.1 Droplet size distributions of concentrated emulsions between 40 and 70 wt% soy bean oil and 1 wt% sodium caseinate (jet homogeniser 10 Bar). Phosphate buffer pH 7 and ionic strength 0.5 mM.

The lognormal form of the droplet size distributions is very similar. The distributions are bimodal with a wide distribution of the small droplet sizes and a moderately narrow distribution for the large sizes. The bimodal distribution is due to caseins in an aqueous environment typically existing as a mixture of casein monomers and casein aggregations [4]. Thus the first mode is approximately between 0.035 and 0.36 μm and is associated with casein aggregation; while the second mode represents the oil droplets at the system.

As the oil concentration increases there is a gradual displacement of the curves to larger droplets and the second distribution becomes wider, especially for high oil concentrations (65 and 70 wt%) (see Figure 5.1). This behaviour is associated with the fact that casein monomers are not sufficient to keep the same droplet size distribution when the oil concentration is raised.

The droplet size distributions for all systems were remeasured after six weeks in order to detect changes in droplet distribution, due to destabilisation. The visual appearance of the emulsions did not appear to change during this time. The droplet size distributions for the concentrated emulsions at 40 and 65 wt% are given in Figures 5.2 and 5.3 as representative of the observed behaviour.

Both droplet size distributions show similar behaviour, with a slight increase in the diameters of the droplets. The increase in the droplet diameters is more marked for the small diameters, between 0.2 and 0.5 μm, than for the diameters above 10 μm. These changes in the distribution of droplet size suggest that two destabilisation processes are occurring during the ageing of the emulsion. The first is coalescence and the second is flocculation.

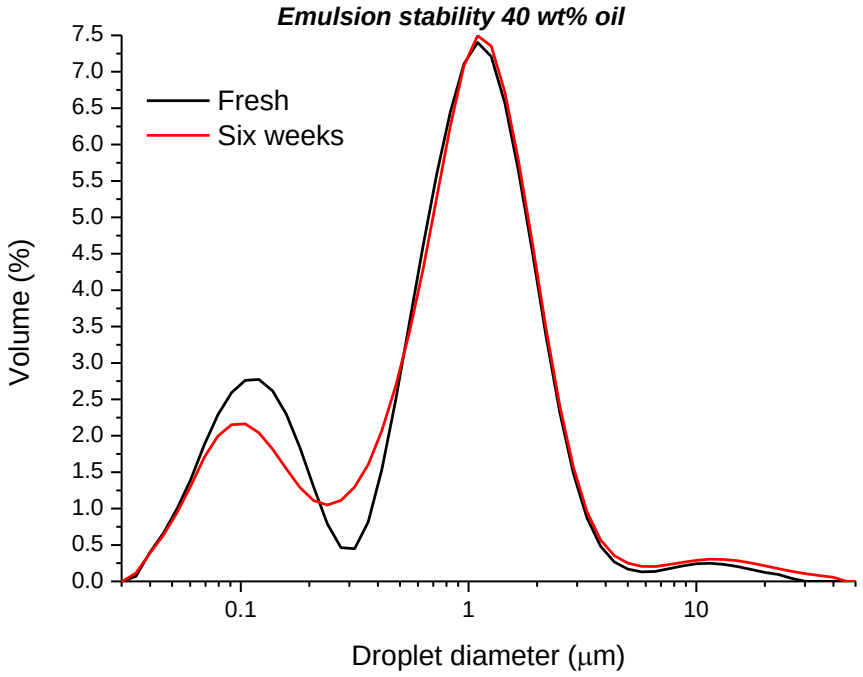

Figure 5.2 Droplet size distributions of fresh and six weeks concentrated emulsions 40 wt% soy bean oil and 1 wt% sodium caseinate. Phosphate buffer pH 7 and ionic strength 0.5 mM.

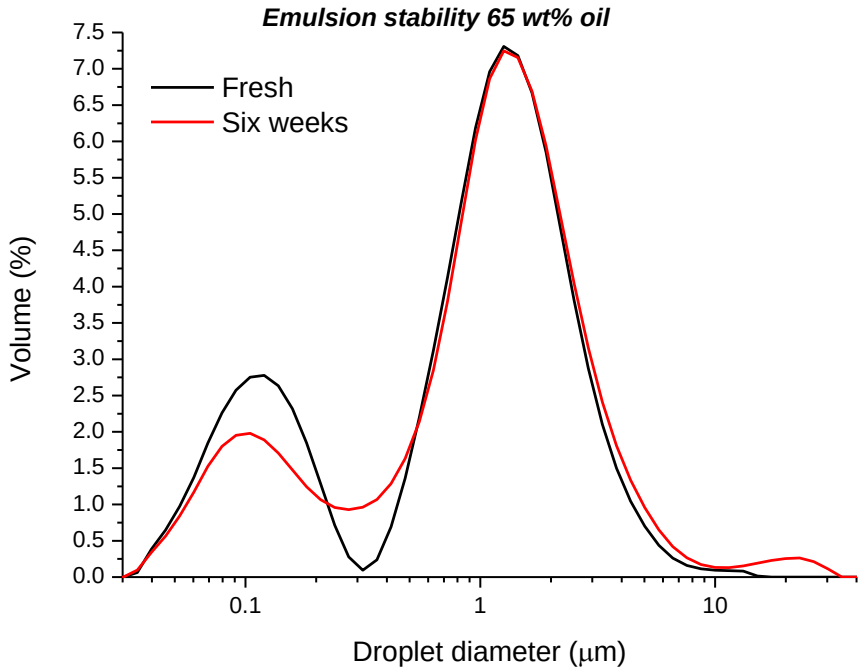

Figure 5.3 Droplet size distributions of fresh and six weeks concentrated emulsions 65 wt% soy bean oil and 1 wt% sodium caseinate. Phosphate buffer pH 7 and ionic strength 0.5 mM.

Research by Dickinson [5] confirmed that caseins have excellent coalescence stability, but that they are vulnerable to different kinds of flocculation. Two flocculation processes that occur frequently in emulsions made with macromolecules

are bridging and depletion flocculation and they depend on the oil/emulsifier ratio. Dickinson [6] states that when the ratio of oil to protein is more than 40:1, sodium caseinate surface coverage becomes significantly reduced and bridging flocculation can occur. As a consequence, for the concentrated emulsions investigated here, bridging flocculation occurs because the oil/protein ratios used are between 40 and 70.

Cryo-SEM was used to visualise the structure of concentrated 60 wt% soy bean oil emulsions with a pH 7 phosphate buffer (ionic strength 0.5 mM). (See Figure 5.4).

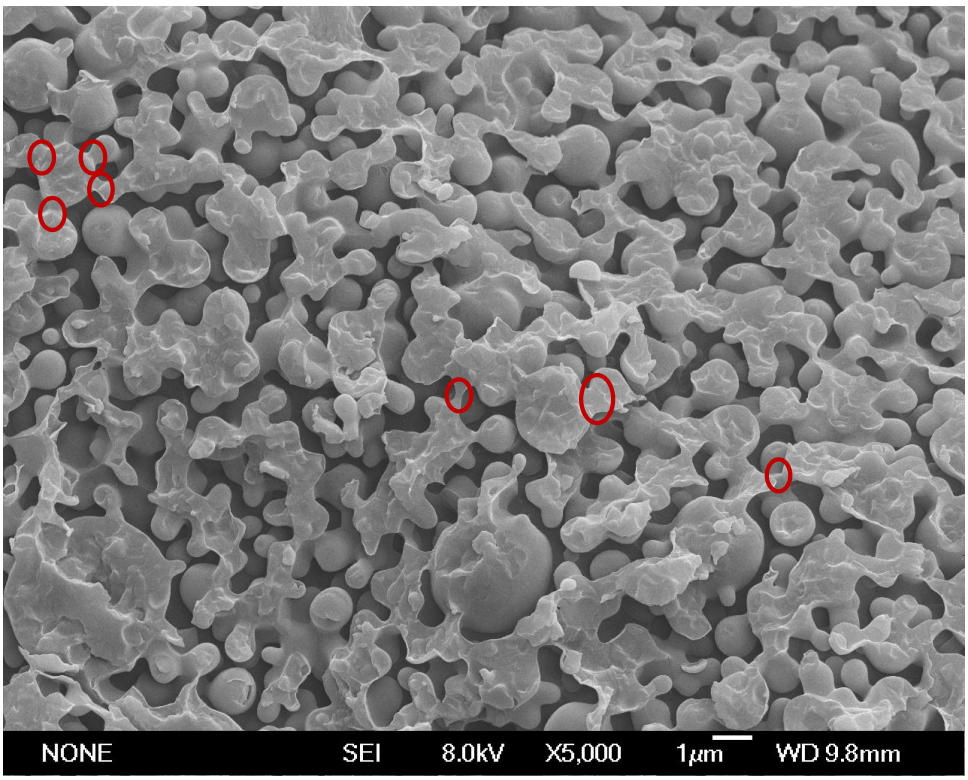

Figure 5.4 Cryo-SEM image of a fresh emulsion 60 wt% soy bean oil (x5,000). Phosphate buffer pH 7 and ionic strength 0.5 mM. The circles highlight the bridges between droplets.

Figure 5.4 shows that droplets keep their spherical shape, but there are many aggregates that are associated with the bridging flocculation. Some of the interconnections (bridging) are shown with a red circle in the Figure 5.4.

5.2.2 Droplet sizes

One of the most important parameters affecting emulsion properties is droplet size. Dickinson [6] states that to obtain good emulsion stability droplet sizes should be

about or below 1 μm. In order to investigate the effect of the size of the droplets in the stability of concentrated sodium caseinate emulsions, different concentrated emulsions were prepared using the jet homogeniser at 1, 2.5, 5 and 10 Bar and five passes through (see Figure 5.5).

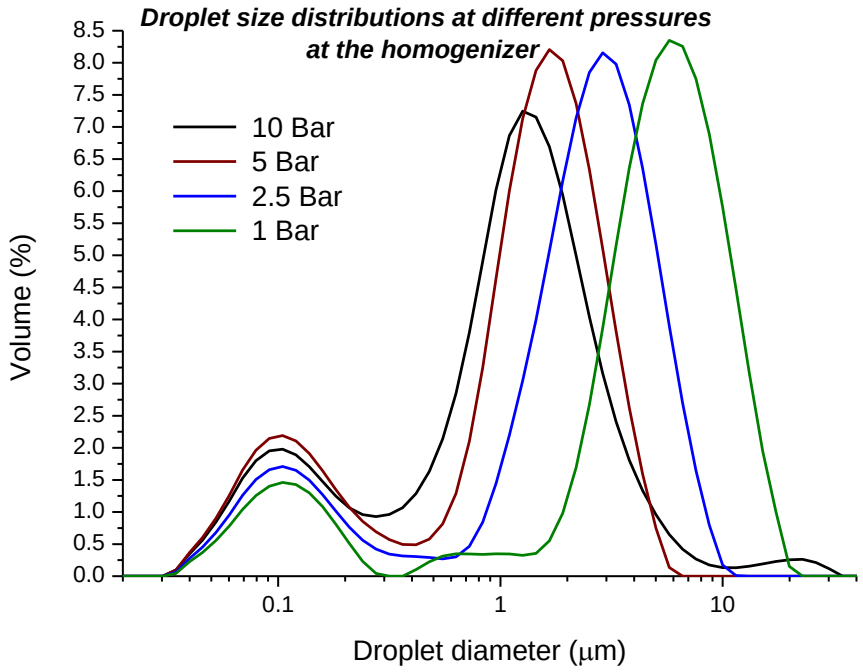

Figure 5.5 Droplet size distributions of concentrated emulsions at different pressure at the jet homogenizer, emulsions 65 wt% soy bean oil and 1 wt% sodium caseinate. Phosphate buffer pH 7 and ionic strength 0.5mM.

The lognormal forms of the droplet size distributions are very similar with the systems prepared at 10 Bar and different oil concentrations (Fig 5.1), i.e., the distributions are bimodal with one distribution at the low end of the range and the other at the higher end. The mode contains the casein aggregations (size diameters between 30 and 300 nm) and this mode increases when the pressure applied to make the emulsions is increased. The second mode, which corresponds to the droplet sizes, is displaced to larger size diameters as the pressure applied for the homogenisation process decreases. This behaviour was expected due to a reduction in the energy used to produce the droplets. Two emulsions made at different pressures (1 and 5 bar) are shown in Figure 5.6.

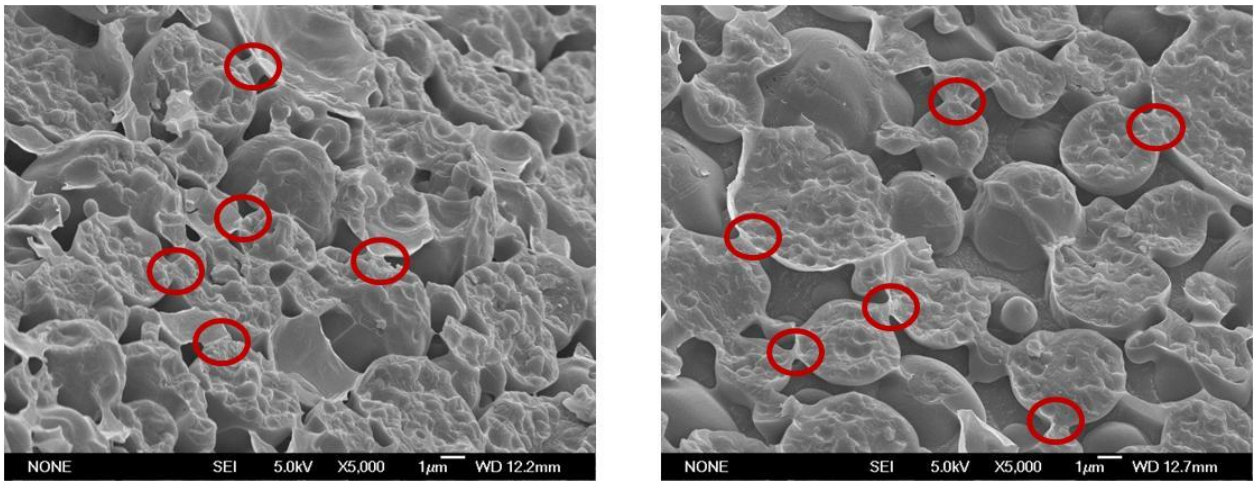

Figure 5.6 Cryo-SEM images: pressure of emulsification 1 bar (left) and pressure of emulsification 5 bar (right). Emulsion 65 wt% soy bean oil (x5,000). Phosphate buffer pH 7 and ionic strength 0.5 mM.

Figure 5.6 shows a clear difference between the droplets for the emulsions made at 1 and 5 Bar. At 1 Bar the shape of the droplets are spherical and it is easy to distinguish between them. Also, the proportion of the continuous phase is significant, allowing separation between droplets. On the contrary, at 5 Bar the shape of the droplets is not spherical and it is difficult to discriminate between them. The proportion of continuous phase is minimal, which reduces the separation of droplets causing their deformation. For both systems it is clear that the bridging flocculation occurs due to the low protein concentration, this was referred to earlier.

Increasing the pressure during the emulsification process also increases the heterogeneity of the droplets. In Figure 5.5 it can be seen that the volume percentage of the droplet diameters located in the valley, which separates the two modes, goes up as the pressure increases. Dalgleish [7] says this is a consequence of the high pressure applied during the emulsification process that can alter the structure of the proteins resulting in their total or partial unfolding. As a consequence, the proteins have more interfacial activity, decreasing the tension between the phases and producing droplets with smaller sizes. Similar results were reported by Kenta *et al* [8] who made emulsions using milk powder as the emulsifier and varying the pressure from 20 to 60 MPa.

After three days the emulsions made at 1, 2.5 and 5 Bar showed separation (Figure 5.7), while those prepared at 10 Bar were stable.

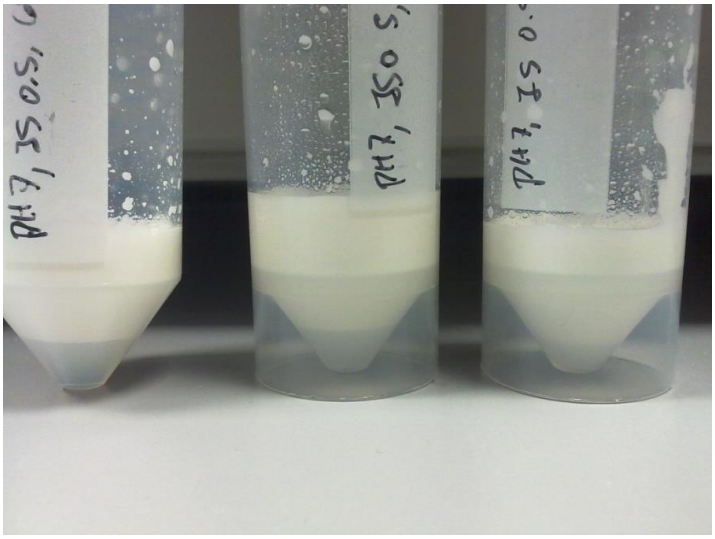

Figure 5.7 Appearance of the emulsions three days after the emulsification at 1, 2.5 and 5 bar of pressure. Concentrated emulsions 65 wt% soy bean oil and 1 wt% sodium caseinate. Phosphate buffer pH 7 and ionic strength 0.5 mM.

In Figure 5.7 it can be seen that the emulsions have become destabilised in a process known as creaming. In the creaming process the oil droplets ascend to the top of the container with the remainder occupied by the continuous phase. This process occurs due to the gravitational force, the density difference between the phases and the droplet sizes. Many models have been developed to calculate the creaming rate for dilute or moderately concentrated emulsions [1]. Despite that models have been used to dilute emulsions, a qualitative analysis can be done for concentrated emulsions using Stokes law equation:

$$\upsilon = \frac{2r^2(\Delta\rho)g}{9\eta_0} \qquad (5.1)$$

where r is the radius of the oil droplets, $\Delta\rho$ is the difference in the densities of the dispersed and continuous phases, g is acceleration due to gravity, and η_0 is the viscosity of the continuous phase. It can be seen in Figure 5.7 that the amount of separated volume of the continuous phase depends on the sizes of the droplets, being the largest creaming volume for the big droplets. This is because the rate of creaming depends on the size of the droplets, i.e. decreasing the size of the droplets retards the creaming process. This relationship agrees with Equation 5.1. The Sauter mean diameters ($D_{3,2}$) for emulsions prepared at different pressures are

shown in Table 5.1. For these systems once they are shaken, the droplets can be redispersed in a homogenous appearance showing the partial reversibility of the process.

Table 5.1. Sauter mean diameters for emulsions made at different pressures. Emulsion 65 wt% and 1 wt% sodium caseinate. Phosphate buffer pH 7 and ionic strength 0.5 mM.

Pressure at the homogeniser (Bar)	$D_{3,2}$ (μm)
5	0.37 ± 0.01
2.5	0.50 ± 0.01
1	0.67 ± 0.01

In order to evaluate any variation in the droplet sizes after six weeks, the droplet size distribution was measured and the results can be seen in Figures 5.8, 5.9 and 5.10. Depending on the pressure applied for the emulsification process of the systems, there is a gradual increase in the fraction of small droplets as the pressure employed increases. At 5 Bar of pressure the increase in the small droplet fractions is the highest, followed by formulation at 2.5 Bar. On the contrary, at 1 Bar of pressure there is a slight rise in proportion of big droplets.

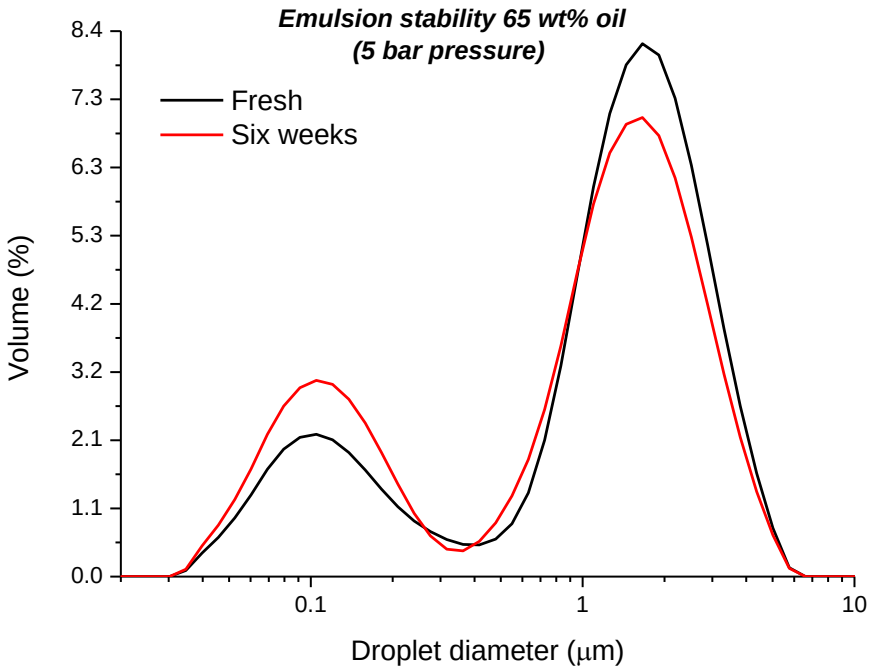

Figure 5.8 Droplet size distributions of fresh and six weeks concentrated emulsions 65 wt% soy bean oil and 1 wt% sodium caseinate (Pressure 5 bar). Phosphate buffer pH 7 and ionic strength 0.5 mM.

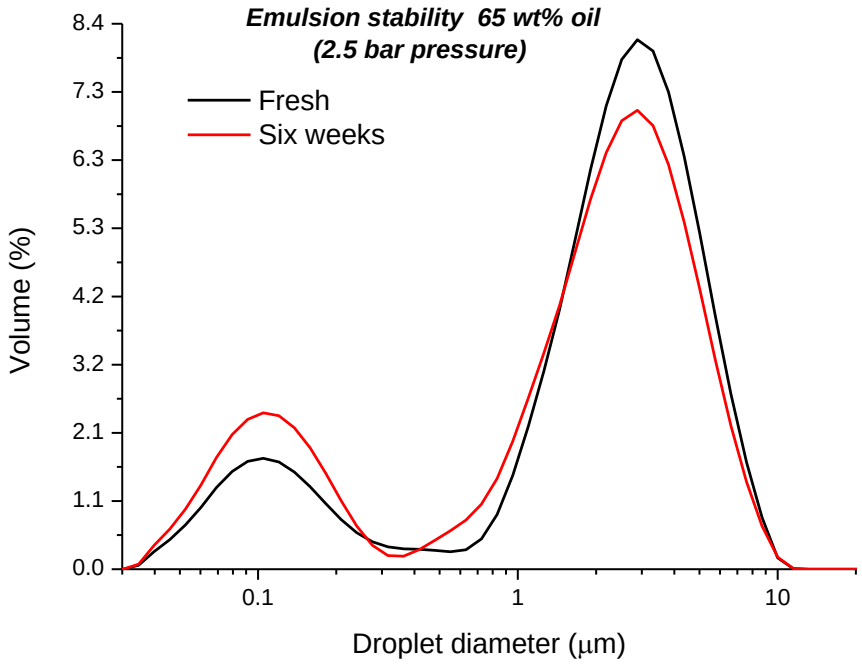

Figure 5.9 Droplet size distributions of fresh and six weeks concentrated emulsions 65 wt% soy bean oil and 1 wt% sodium caseinate (Pressure 2.5 bar). Phosphate buffer pH 7 and ionic strength 0.5 mM.

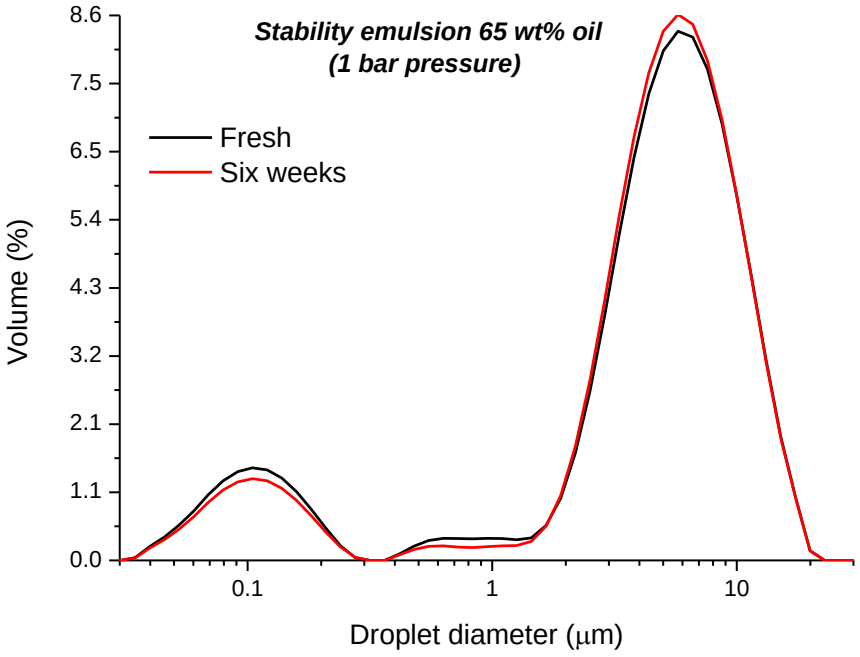

Figure 5.10 Droplet size distributions of fresh and six weeks concentrated emulsions 65 wt% soybean oil and 1 wt% sodium caseinate (Pressure 1 bar). Phosphate buffer pH 7 and ionic strength 0.5 mM.

The increase in the proportion of small droplets after six weeks, for the emulsions made at 2.5 and 5 Bar, could be a consequence of the disruptive effect of the pressure on the aggregate of caseins. Floury *et al.* [9], in their research about the effect of high-pressure homogenisation on droplet size and rheological properties of emulsions with whey protein, explained that high pressure emulsification can affect the intra-molecular electrostatic and hydrophobic interactions. Thus it is possible that during the emulsification process of a system at high pressure, some of the casein aggregates are destroyed and after that several of them are able to be aggregated again. Salaün *et al*. [10] refers to this phenomenon on the casein micelles present in milk during high-pressure treatment.

Applying low pressure during the emulsification process cannot achieve the energy necessary to weaken the interactions that keep the caseins aggregated. As a result, the droplet size distribution is almost the same after six weeks, see Figure 5.10.

In order to evaluate the droplet arrangement before and after the creaming process, Cryo-SEM was used on two different samples: one for the top of the concentrated emulsion cream and the second one from the system after being shaken past ageing. The differences in the arrangements can be seen in Figures 5.11.

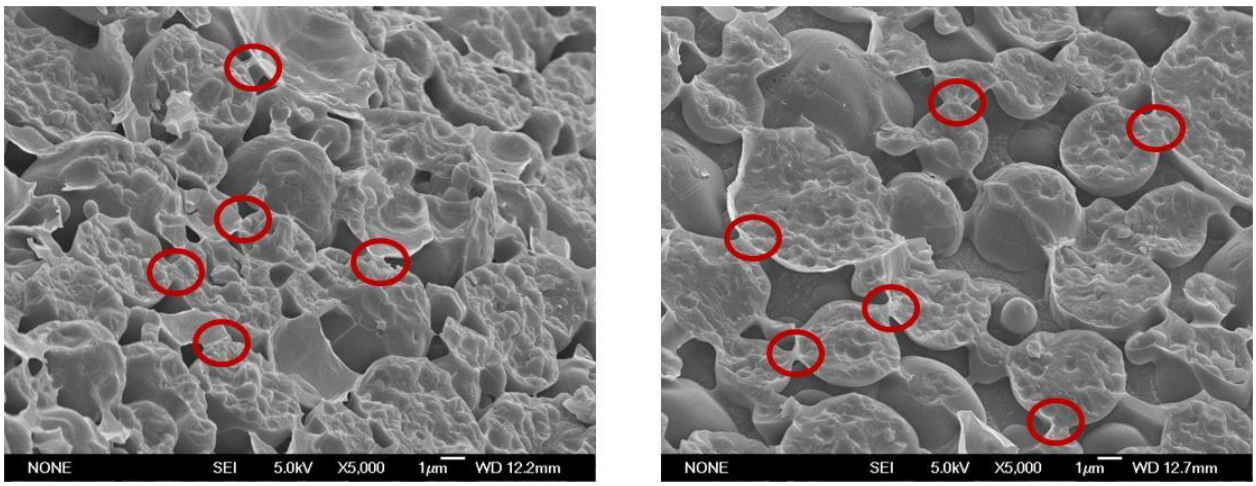

Figure 5.11 Cryo-SEM images: sample taken from the cream (left) and the sample took after shaking (right). Emulsion 65 wt% soy bean oil (x5,000). Phosphate buffer pH 7 and ionic strength 0.5 mM.

It can be noted that in the cream (Figure 5.11 left) the droplets are aggregated, reducing the volume of the continuous phase between them. When the system is

shaken, the droplets are redispersed and the space between them increases (see Figure 5.11 right). Similar to the previous systems shown, bridging flocculation between the droplets can be seen in Figure 5.11 and some of the bridges are highlighted with circles.

5.2.2 Droplet size distribution

Another parameter that affects the stability of concentrated emulsions is the breadth of the droplet distribution and in particular the proportion of smaller to larger droplet sizes. Seven emulsions were evaluated varying the proportion of fine droplets (10 Bar) to coarse droplets (blender) from zero to one. The droplet size distributions are shown in Figure 5.12.

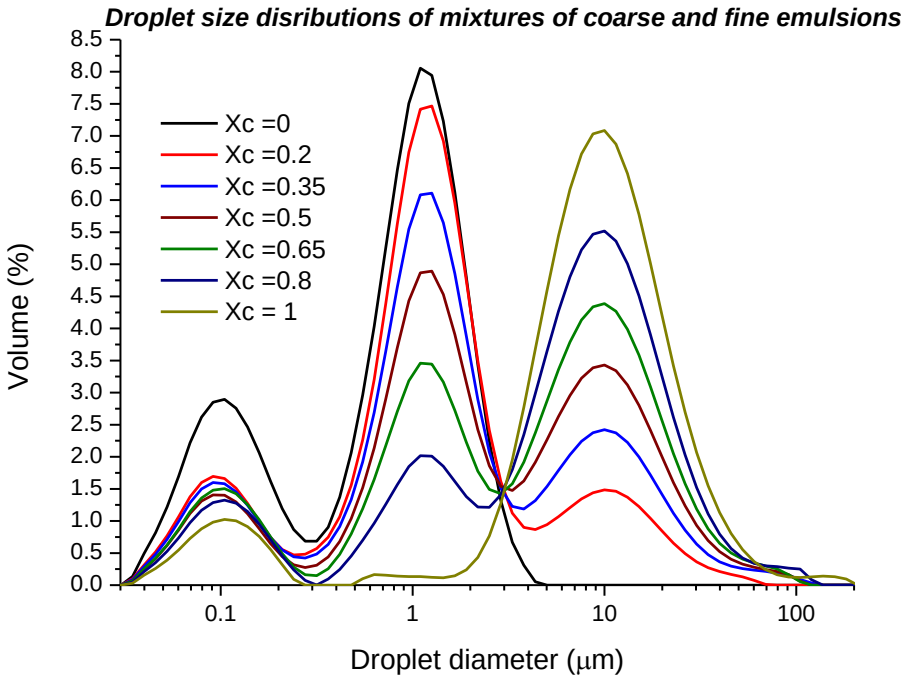

Figure 5.12 Droplet size distributions of emulsions made with a homogeniser at 10 bar of pressure (fine), blender (coarse) and mixtures of them. Systems 65 wt% soy bean oil and 1 wt% sodium caseinate. Phosphate buffer pH 7 and ionic strength 0.5 mM. X_C is the coarse fraction in the mixture.

Polymodal droplet size distributions can be distinguished for all systems, being bimodal for the original emulsions made at 10 Bar of pressure (Xc = 0) and blender (Xc = 1) and trimodal for the rest of the mixed systems. Casein aggregations are related to the first mode (about 30 and 300 nm) as was mentioned earlier.

The droplet size distributions show the effect of high pressure during formulation in the separation of the casein aggregations; and the formation of small droplets. It can be seen in Figure 5.12 that for emulsions made at 10 Bar that droplet sizes oscillate between 200 and 400 nm. For the emulsions made with the blender, as the fraction of coarse droplets increases, the droplets in that range are reduced to zero.

After two days some of the systems had become unstable showing creaming (Figure 5.13). The creaming rate is a function of the fraction of coarse droplets in the systems. In systems with coarse fractions from 0 to 0.5 the appearance was homogenous without any phase separation. On the contrary, the systems with coarse fractions of 0.65, 0.8 and 1 were heterogeneous showing a direct relationship between the volume of the continuous phase separated and the fraction of the coarse droplets. Table 5.2 shows the Sauter mean diameter for the different systems studied.

Figure 5.13 Appearance of the emulsions two days after the emulsification coarse fractions (right to left): 0, 0.2, 0.35, 0.5, 0.65, 0.8 and 1. Concentrated emulsions 65 wt% soybean oil and 1 wt% sodium caseinate. Phosphate buffer pH 7 and ionic strength 0.5 mM.

Table 5.2. Sauter mean diameters for emulsions made with different proportions of coarse droplets. Emulsions 65 wt% and 1 wt% sodium caseinate. Phosphate buffer pH 7 and ionic strength 0.5 mM

Fraction of coarse droplets (Xc)	$D_{3,2}$ (μm)
0	0.30 ± 0.01
0.2	0.43 ± 0.01
0.35	0.47 ± 0.02
0.5	0.56 ± 0.01
0.65	0.57 ± 0.01
0.8	0.67 ± 0.01
1	0.98 ± 0.01

It is clear that the fraction of the coarse drops increases the Sauter diameter and the creaming rate, producing the separation of the continuous phase as the droplets rise to the top of the system container.

Figure 5.14 shows the Cryo-SEM images of two emulsions with coarse fractions 0.2 and 0.8. The images for both systems are in agreement with their droplet size distributions shown in Figure 5.12. The emulsion with a coarse fraction of 0.2 shows a high proportion of droplets around 1 μm, while the emulsion with a coarse fraction of 0.8 has the highest droplet proportion around 10 μm. In the emulsion with a coarse fraction of 0.2, there is a strong interconnection between the droplets (bridging flocculation) and it is difficult to differentiate the small droplets made at 10 Bar pressure. Additionally, the space between droplets is reduced in comparison with the emulsion with 0.8 of coarse droplets.

In the systems with coarse fractions of 0.2, 0.35 and 0.5, the proportion of the emulsion made at 10 Bar (small droplets) essentially becomes the continuous phase for these systems (see Figure 5.14 left). Thus, the viscosity of the continuous phases increases, slowing down the motion of the big droplets to the top of the container and avoiding the creaming process.

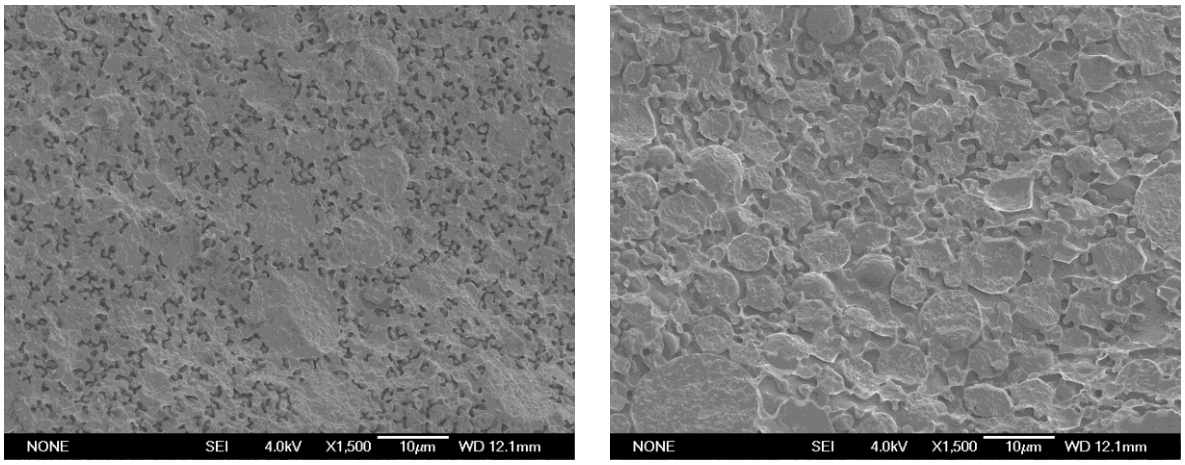

Figure 5.14 Cryo-SEM images: emulsion coarse fraction 0.2 (left) and emulsion coarse fraction 0.8 (right). Emulsion 65 wt% soy bean oil (x1500). Phosphate buffer pH 7 and ionic strength 0.5 mM.

In the emulsion with a coarse fraction of 0.8, bridging flocculation is also present; however, there is a large separation between the droplets. The big droplets and the reduced number of connections between them facilitate the migration of the droplets to the top of the container, enhancing the creaming process.

Six weeks after the emulsions were prepared, the droplet size distributions were evaluated in order to determine the type of destabilisation that had occurred. Figures 5.15 and 5.16 show a representative sample of the droplet size distributions for the fresh emulsions and six weeks later at coarse fractions of 0.2 and 0.8 respectively.

The droplet size distribution for the emulsion with a coarse fraction of 0.2 (Figure 5.15) confirms that applying high pressure for the emulsification process produces disaggregation of the caseins. This process is reversible because after some days they re-aggregate. Similar results were shown in Figures 5.8 and 5.9. Additionally, the increases seen in the size region of the small droplets can be associated with their flocculation via bridging as can be seen in Figure 5.14 left. The emulsions with coarse fractions of 0, 0.35 and 0.5 showed a similar behaviour.

Figure 5.16 shows practically the same size droplet distributions for the fresh emulsions and those for six weeks later. This result provides support for the idea that for the systems studied here, the only destabilisation process is creaming without changes in the droplet sizes. Moreover, the casein layer around the droplets is strong enough to prevent coalescence and Ostwald ripening despite the combination of small and big droplets in the system. The small droplet size region is unchanged, which supports the idea that the change capacity to casein aggregation, and in particular the ability to alter the conformation of the proteins, is a function of the pressure applied during the homogenisation process [8]. Similar results were obtained with the emulsions at 0.65 and 1 fraction of coarse droplets.

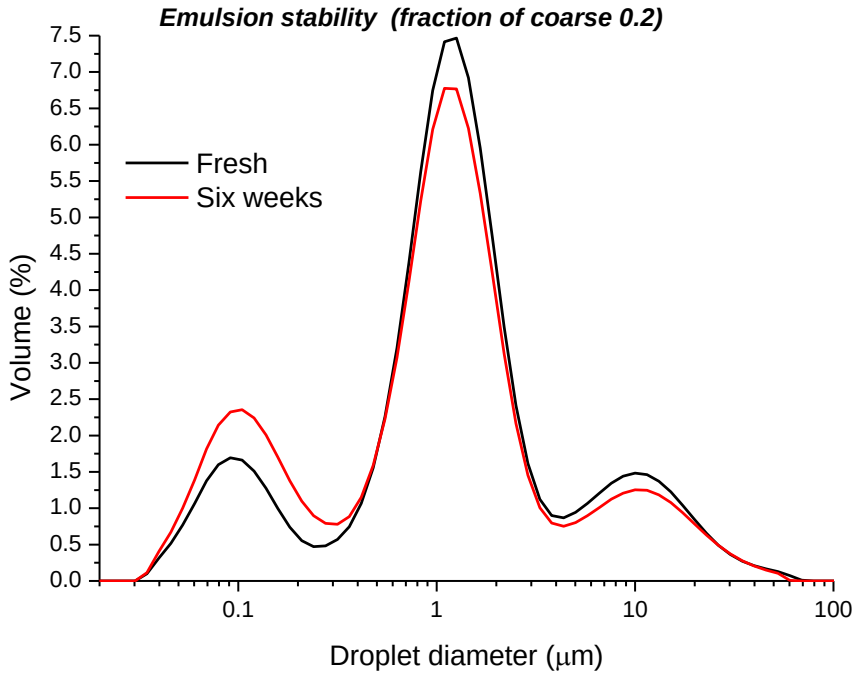

Figure 5.15 Droplet size distributions of emulsion coarse fraction 0.2. Systems 65 wt% soy bean oil and 1 wt% sodium caseinate. Phosphate buffer pH 7 and ionic strength 0.5 mM

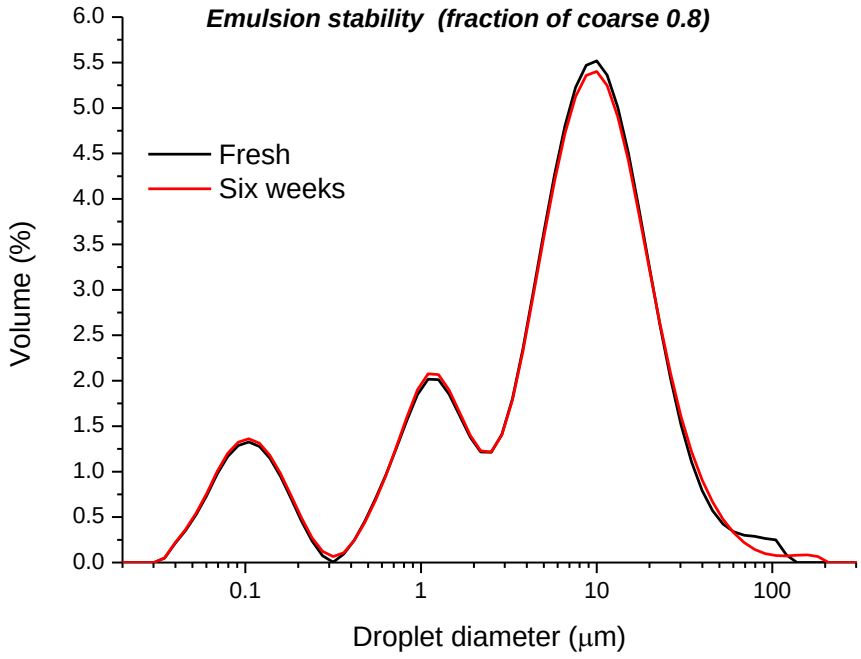

Figure 5.16 Droplet size distributions of emulsion coarse fraction 0.8. Systems 65 wt% soy bean oil and 1 wt% sodium caseinate. Phosphate buffer pH 7 and ionic strength 0.5 mM.

5.2.3 pH of the continuous phase

Emulsion stability is extremely susceptible to pH changes when proteins are used as an emulsifier. Flocculation and coalescence are attributed to attractive interactions between droplets, and these destabilisation processes occur under conditions where the electrostatic repulsion is low (isoelectric point). On the contrary, using pH values far from the isoelectric point of the proteins guarantees stable emulsions that are not subject to flocculation and future coalescence. The stability is due to the high electrostatic repulsion between droplets generated by the charge of the protein molecules [5, 11].

Emulsions were made at different pH values and their droplet size distributions were measured for the fresh system and again six weeks later. Emulsions at pH values around the isoelectric point were achieved using the buffering capacity of sodium caseinate (see Figures 5.17- 5.19).

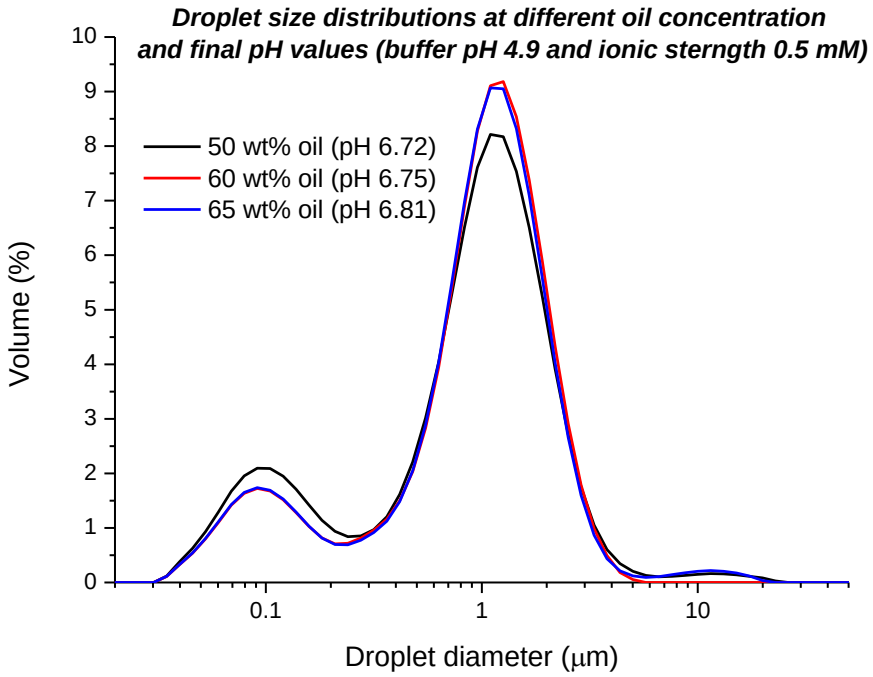

Figure 5.17 Droplet size distributions of emulsion with different oil concentrations. Final pH values 6.72 (50 wt%), 6.75 (60 wt%) and 6.81 (65 wt%). Acetate buffer pH 4.9 and ionic strength 0.5 mM.

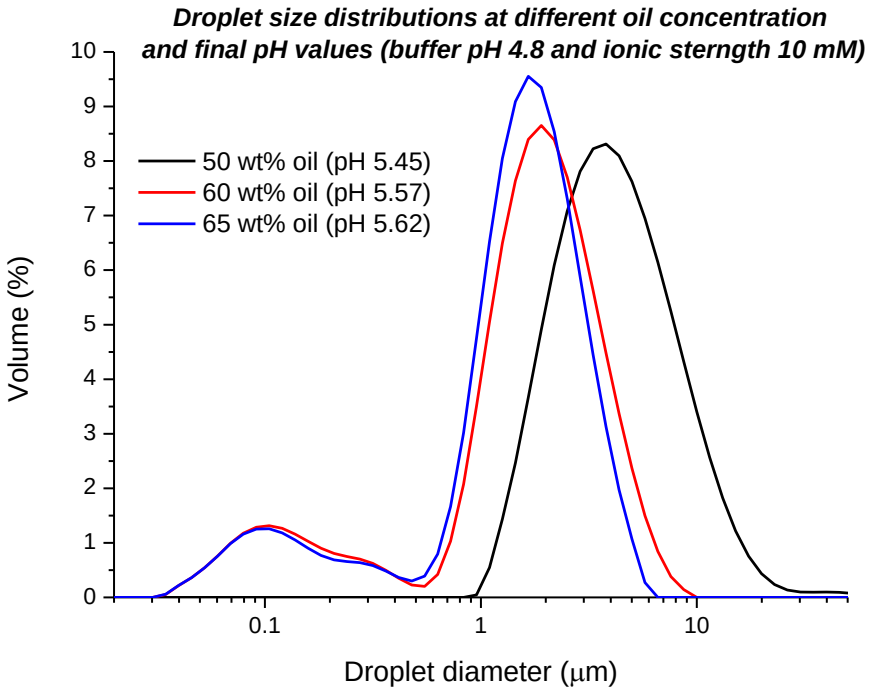

Figure 5.18 Droplet size distributions of emulsion with different oil concentrations. Final pH values 5.45 (50 wt%), 5.57 (60 wt%) and 5.62 (65 wt%). Acetate buffer pH 4.8 and ionic strength 10 mM.

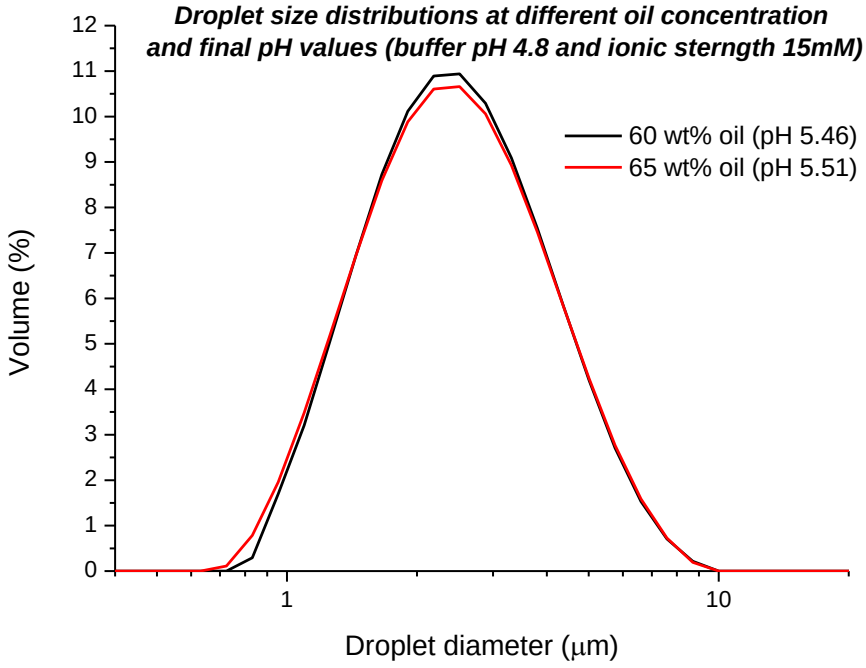

Figure 5.19 Droplet size distributions of emulsion with different oil concentrations. Final pH values 5.46 (60 wt%) and 5.51 (65 wt%). Acetate buffer pH 4.8 and ionic strength 15 mM.

Figures 5.17- 5.19 show that the droplet size distributions of emulsions can be changed when the buffering capacity of sodium caseinate is used for the formulation of the emulsions. These results are in agreement with those given in Chapter 4, where the capacity of sodium caseinate to control the final pH depends on the ionic strength and the mP/mB ratio.

Figure 5.17 shows that the droplet size distributions were similar for the systems studied, with a small mode related to the casein aggregation and the other associated with droplets of oil. The proportion of the samples corresponding to the second mode are very similar for the emulsions with 60 and 65 wt% of oil, while for 50 wt% this value is reduced because of the oil concentration. The final pH for all the concentrations was above 6.7 and the |ΔpH| values were 1.82, 1.85 and 1.9, for the oil concentrations of 50, 60 and 65 wt% respectively. It is clear that the final pH of the systems was controlled by the sodium caseinate.

Marked variations in the droplet size distributions can be observed when the pH buffered to 4.8 with an ionic strength of 10 mM (see Figure 5.18). Despite using the same input energy to produce the emulsions, a bimodal distribution was obtained for oil concentrations of 60 and 65 wt% and a monomodal distribution for 50 wt%. For emulsions at 60 and 65 wt% oil, the first mode is wider than for the entire first mode obtained for all the bimodal emulsions studied. The wide distribution in the first mode is related to aggregation of protein molecules. Chi *et al.* [12], in their review of the physical stability of proteins in aqueous solutions, explained that when protein solutions are close to the isoelectric point aggregation happens because of strong protein-protein interactions. At 50 wt% oil, the monomodal distribution is associated with the extensive aggregation of caseins that reduces the number of casein monomer molecules that can be adsorbed at the interface. As a consequence, the quantities of agents that can act as an emulsifier are reduced, thereby increasing the droplet sizes. McClements [11] reported that when the emulsifier is limiting, the droplet size is controlled by the emulsifier and not by the energy input during the emulsification process.

For these systems, the turbidity of the aqueous phase increases as the oil concentration decreases. The reduction of the oil concentration is associated with a decrease in the ratio of protein mass to buffer mass (mP/mB), resulting in a final pH

of the systems around the pH of the buffer solution. When the pH of the buffer solution is near the isoelectric point and sodium caseinate is added at small mP\mB, the final pH is approached to the isoelectric point encouraging the aggregation of the caseins (see Figure 4.20). HadjSadok *et al. [13]* reported the same behaviour when they changed the pH of sodium caseinate solutions between 8 and 4.5.

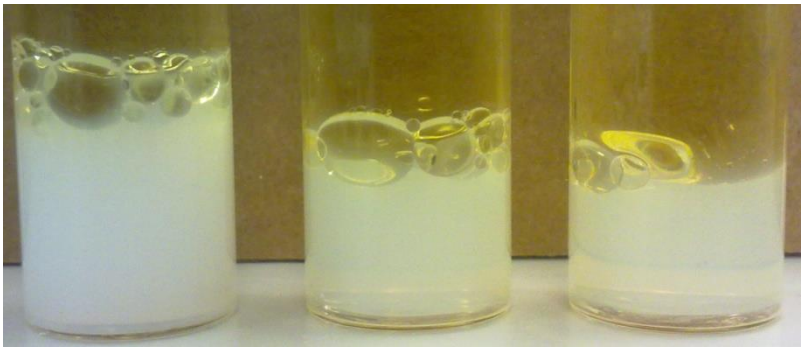

Figure 5.20 Changes in the turbidity of the aqueous phases for systems before emulsification at oil concentrations of 50, 60 and 65 wt%. (right to left). Final pH values (right to left) 5.45, 5.57 and 5.62. Acetate buffer pH 4.8 and ionic strength 10 mM.

When a buffer solution at pH 4.8 with ionic strength 15 mM was used to formulate the emulsions, only two monomodal emulsions could be made for oil concentrations of 60 and 65 wt%. The reason for the monomodal distribution and the increase in the droplet sizes was explained previously, being essentially a consequence of the reduction in the number of protein monomers that can act as emulsifying agents. At oil concentrations of 50 wt% no emulsions could be prepared because the final pH of the system was 5.28 and some precipitation of the sodium caseinate occurred. Turbidity in the systems was also observed as a function of oil concentration, decreasing from 50 to 65 wt% of oil (see Figure 5.21).

Figure 5.21 Changes in the turbidity of the aqueous phases for systems before emulsification at oil concentrations of 50, 60 and 65 wt%. (right to left). Final pH values (right to left) 5.28, 5.46 and 5.51. Acetate buffer pH 4.8 and ionic strength 15 mM.

The stability of the emulsions formulated with buffer solutions at pH 4.8 and different ionic strengths was evaluated (see Figures 5.22 - 5.24). Figure 5.22 shows the droplet size distribution for one of the emulsions formulated at pH 4.8 and an ionic strength 0.5 mM. For the three emulsions formulated, using the same buffer, the final pH of the systems was about 6.7 and the droplet size distributions were similar after six weeks. The systems were visually stable without apparent creaming.

Systems with a wide size distribution in the first mode, with oil concentrations of 60 and 65 wt%, were also stable against creaming when the buffer used was at pH 4.8 and an ionic strength of 10 mM. Figure 5.23 corresponds to one of the emulsions that showed the wide size distribution in the first mode. The droplet sizes distributions, for the fresh sample and six weeks later, were very similar regardless of the aggregation of the caseins that can be distinguished in the aqueous phase (see Figure 5.20).

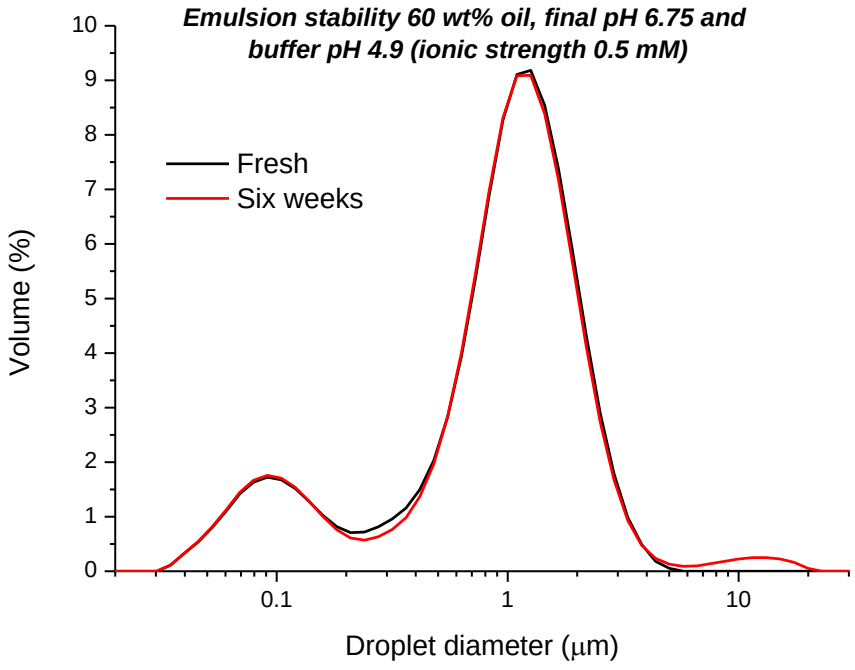

Figure 5.22 Droplet size distributions of fresh and six weeks concentrated emulsions 60 wt% soybean oil, 1 wt% sodium caseinate and final pH 6.75. Acetate buffer pH 4.9 and ionic strength 0.5 mM.

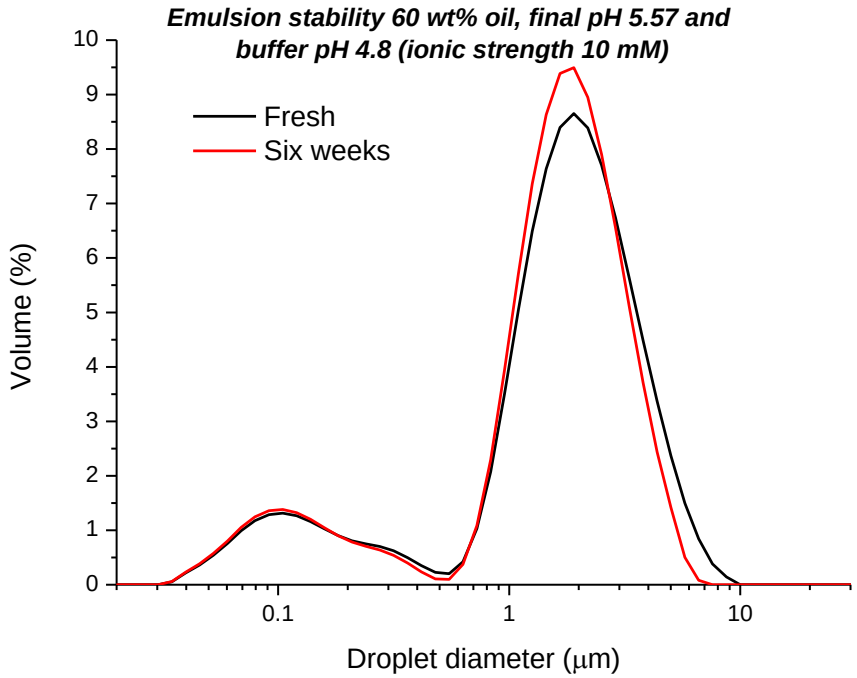

Figure 5.23 Droplet size distributions of fresh and six weeks concentrated emulsions 60 wt% soybean oil, 1 wt% sodium caseinate and final pH 5.57. Acetate buffer pH 4.8 and ionic strength 10 mM.

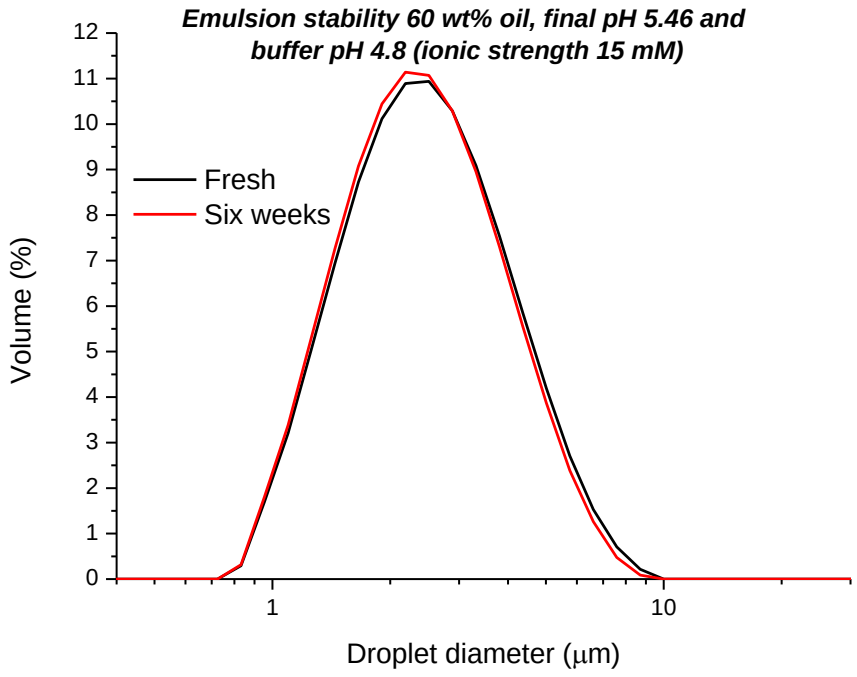

Figure 5.24 Droplet size distributions of fresh and six weeks concentrated emulsions 60 wt% soybean oil, 1 wt% sodium caseinate and final pH 5.46. Acetate buffer pH 4.8 and ionic strength 15 mM.

Emulsion separation was visually observed, after 2 weeks, for the emulsions whose droplet size distribution was monomodal. Figure 5.24 shows the droplet size

distribution of one of these emulsions; fresh and after the systems were shaken six weeks later. The monomodal distribution, for the systems studied, occurred in emulsions formulated with acetate buffer at pH 4.8 and ionic strengths 10 (50 wt% oil) and 15 mM (60 and 65 wt% oil).

Figure 5.25 shows Cryo-SEM images for two emulsions (60 wt% oil) formulated using a buffer solution at pH 4.8-4.9 having different ionic strengths. In the image of an emulsion prepared at an ionic strength of 0.5 mM the final pH was 6.75 (left) the sizes of the droplets are in accordance with the measured droplet size distribution (Figure 5.22) and their spherical shape can be distinguished. However, the droplets are associated with each and a network structure can be seen. The emulsion at pH 5.46 shows bigger droplet sizes, which also concur with its droplet size distribution (Figure 5.24), and their shape is not spherical. Additionally, there is complete interconnection between them.

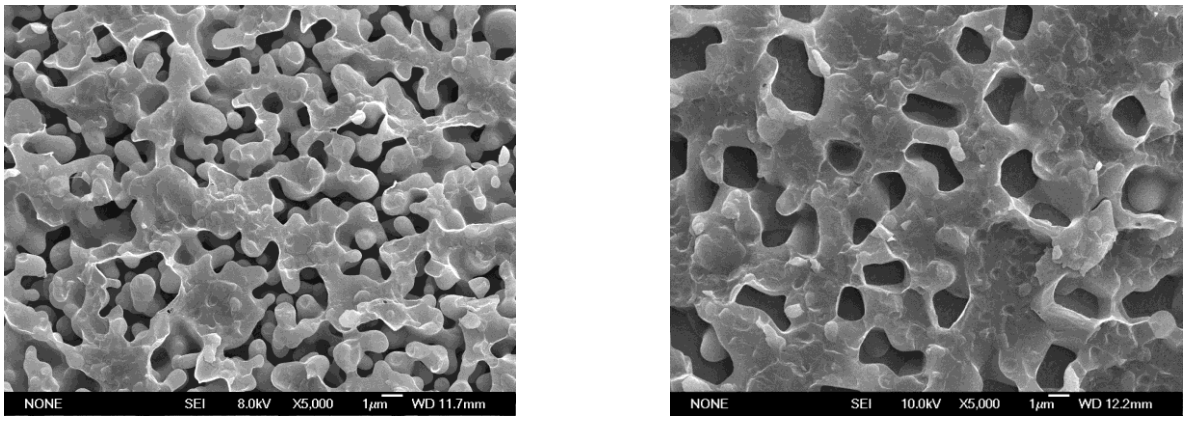

Figure 5.25 Cryo-SEM images: Acetate buffer at ionic strength 0.5mM and final pH 6.75 (left) and acetate buffer at ionic strength 15 mM and final pH 5.46 (right). Acetate buffer pH 4.8-4.9 and emulsions 60 wt% oil.

It is clear that the formulation of emulsions with sodium caseinate is extremely sensitive at pH around the isoelectric point. Different creaming rates and droplet size distributions can be obtained with small changes of pH values.

At the final pH of about 7, droplet size distributions are similar for all of the ionic strengths studied. Some results can be seen in earlier sections where final emulsions are not obtained by mixing emulsions with different droplet size

distributions. These systems showed a bimodal droplet size distribution with a small mode related to casein aggregation and a second that corresponds to oil droplets.

The stability and droplet size distribution were also evaluated for emulsions at pH values above neutral pH. The aqueous phases were clear without any sodium caseinate aggregation or precipitation (see Figure 5.26). This behaviour was expected, because at basic pH the casein molecules have a strong negative charge that produces electrostatic repulsions between them.

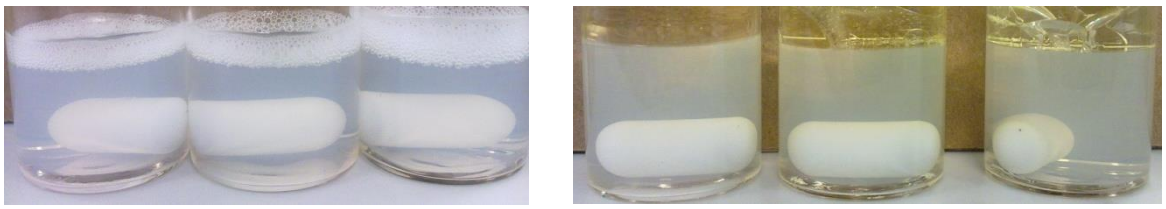

Figure 5.26 Aqueous phases systems at ionic strengths 0.5, 7 and 10 mM (left) and 20, 40 and 60 mM (right). Carbonate buffer pH 10.4.

Emulsions formulated at basic pH showed bimodal distributions similar to the droplet size distribution at pH values around 7 (see Figure 5.27).

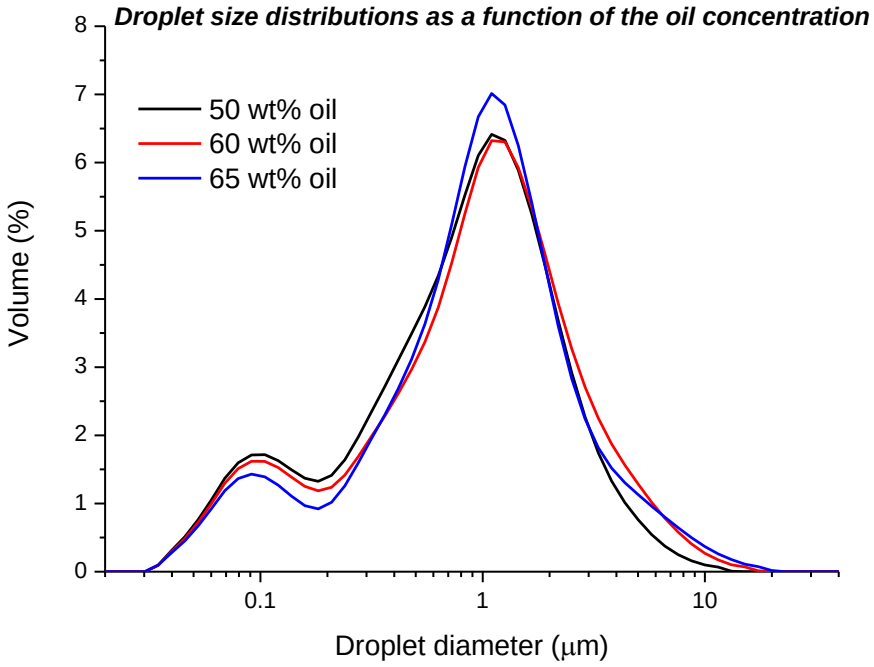

Figure 5.27 Droplet size distributions of emulsion with different oil concentrations. Final pH values 10. Carbonate buffer pH 10.2 and ionic strength 200 mM.

An ionic strength of 200 mM was used for the buffer solution, because at pH 10 the buffer solution is only able to control the final pH when the ionic strength is considerably higher (see Figure 4.11). The first mode, which is about 0.1 μm in diameter, represents the aggregation of casein molecules. The second mode, which is about 1 μm of diameter, represents the droplet sizes. An interesting feature for the droplet size distribution at basic pH is that the valley between the two modes is not as deep as the rest of the pH values. This distribution corresponds with an enlarged diversity of oil droplet sizes.

The destabilisation process mechanism was creaming. The droplet size distribution was measured both on the fresh sample and again six weeks later and their curves were practically unchanged. Figure 5.28 shows an example of the droplet size distributions for an emulsion with a final basic pH.

A comparison of droplet size distributions at different pH values and an ionic strength of 15 mM, is shown in Figure 5.29.

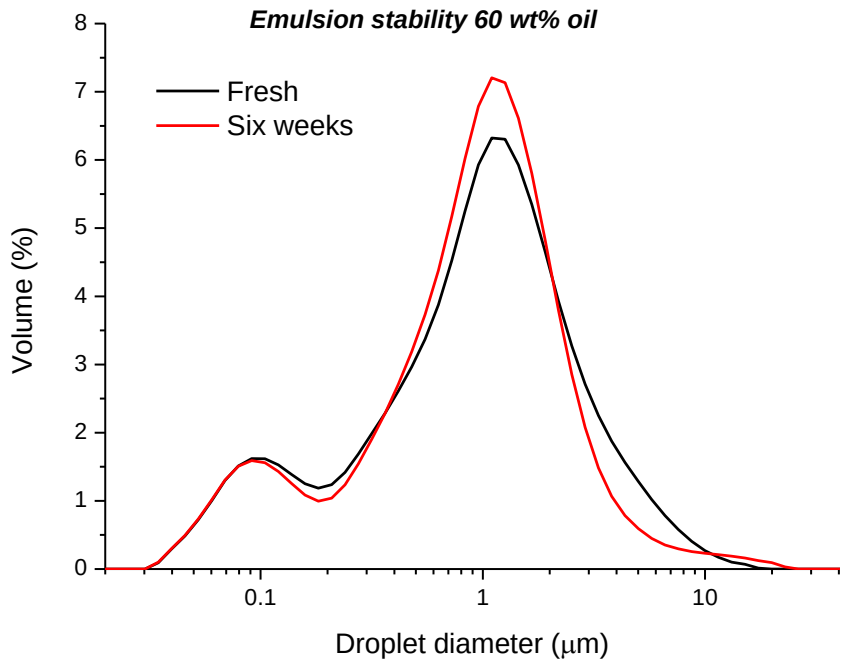

Figure 5.28 Droplet size distributions of fresh and six weeks concentrated emulsions 60 wt% soybean oil, 1 wt% sodium caseinate and final pH 10. Carbonate buffer pH 10.2 and ionic strength 200 mM.

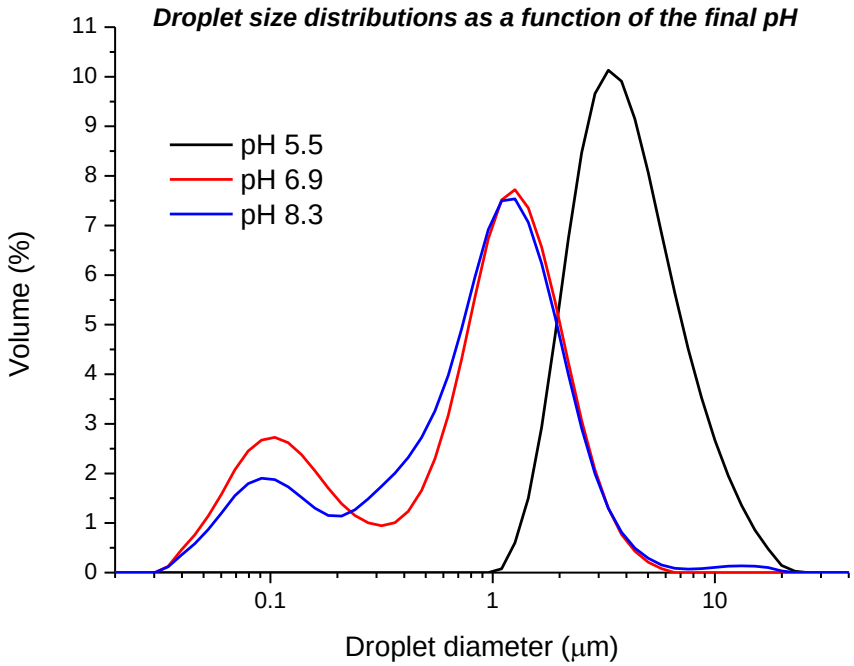

Figure 5.29 Droplet size distributions of emulsion with different pH values. Final pH values 5.5 (Acetate buffer), 6.9 (Phosphate buffer) and 8.3 (Carbonate buffer). Emulsions 60 wt% oil, 1 wt% protein and ionic strength 15 mM.

For basic emulsions formulated at pH between 8 and 10, their droplet size distributions were similar after six weeks with a curve shape as shown in Figure 5.28. Similar to the rest of the emulsions evaluated at different pH and ionic strength values, creaming was again the destabilisation process. Also, bridging flocculation was observed in the emulsions formulated at basic pH.

Figure 5.29 shows that there is a slight difference in the droplet size distribution at a basic and neutral pH. Both distributions are bimodal with the modes positioned around the same range of droplet diameters. On the other hand, emulsions formulated at pH 5.5 show a monomodal distribution with bigger droplet diameters. Comparing droplet size distributions, at low ionic strength (below 10 mM) and different pH values, was not possible because the final pH values tended towards neutral (see results from Chapter 4). For high ionic strengths, only emulsions at neutral and basic pH could be formulated. At pH around 5, sodium caseinate precipitated for all the systems formulated.

5.2.4 Ionic strength in the continuous phase

Ionic strength is also a factor that has a relevant effect on the stability of emulsions formulated with proteins, this is because electrostatic interactions between droplets can be modified changing the ionic strength in the continuous phase. The investigation of the effect of the ionic strength on the stability of emulsions with sodium caseinate was restricted only for neutral pH. Because in Chapter 4 the results showed that sodium caseinate was able to change the final pH of the systems when a low ionic strength was used. Consequently, keeping a constant pH and changing the ionic strength, in the low ionic strength range, was not possible. With variations of the ionic strength in the high range values, it was possible to keep a constant pH only with basic and neutral buffer solutions. At pH around 5 and with a high ionic strength, sodium caseinate precipitated and the production of emulsions was impossible.

Figure 5.30 shows the droplet size distributions for a neutral pH and different ionic strengths. The behaviour for different oil concentration changing the ionic strength was very similar for the emulsions studied. Bimodal curves were the droplet size distribution for all of them showing the modes as explained earlier.

Changing substantially the ionic strength in the emulsions does not produce variations in the droplet size distributions for the emulsions studied. It is well known in colloid systems that changes in the ionic strength influences the interactions between the colloids. When droplets or particles have charge, the thickness of the counter ions layers around each droplet or particle is severely affected by the ionic strength. Increasing the ionic strength produces a reduction in the thickness of the counter ions layers, producing van der Waals forces of attraction that overlap the electrostatic repulsions and droplets can be flocculated. However, using dilution during the static light scattering measurements can produce disruptions in some structures that have a role in the emulsion. Cryo-SEM images of two emulsions at different ionic strengths are shown in Figure 5.31.

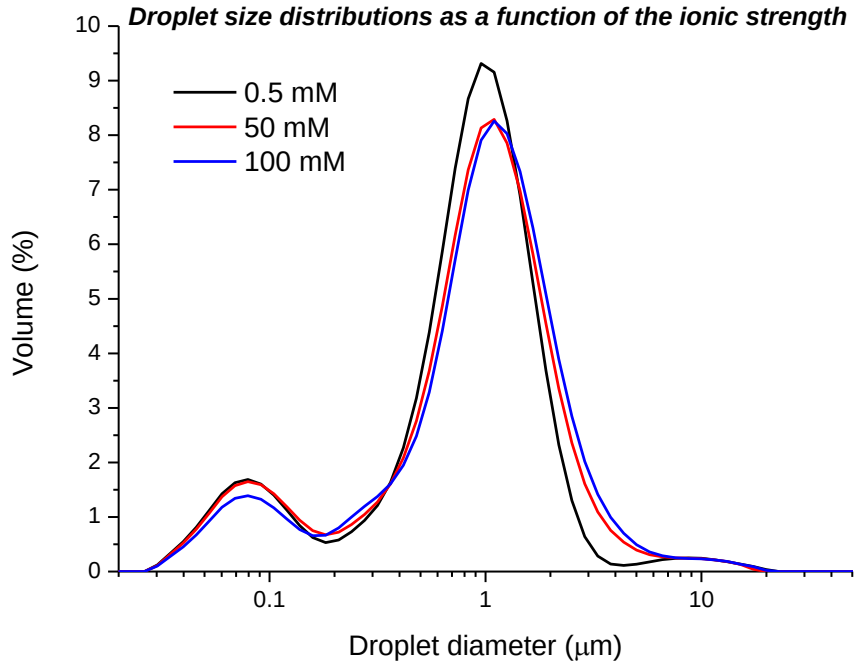

Figure 5.30 Droplet size distributions of emulsion 60 wt% oil with different buffer ionic strengths. Phosphate buffer pH 6.8.

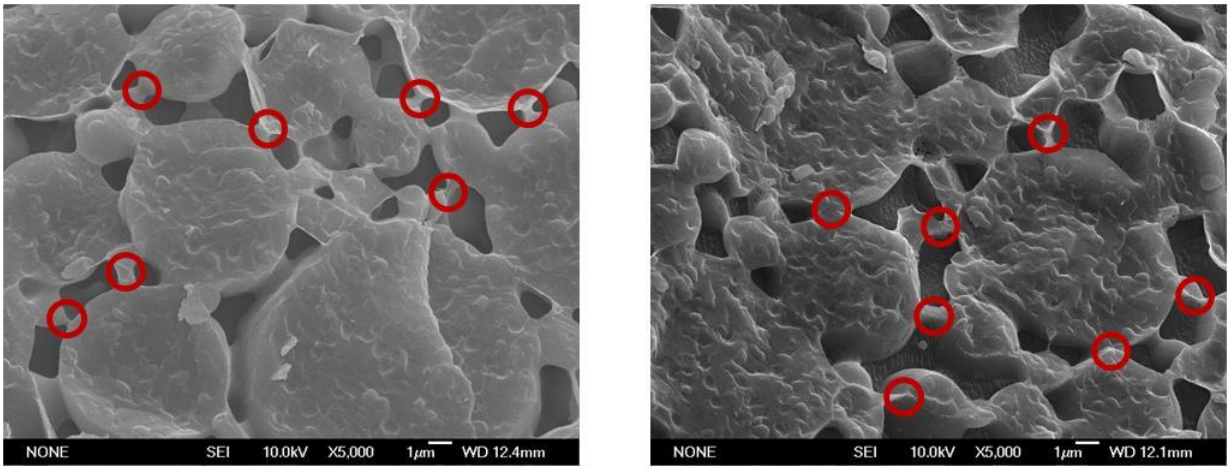

Figure 5.31 Cryo-SEM images: ionic strength 0.5 mM (left) and ionic strength 200 mM (right). Phosphate buffer pH 6.8 and emulsions 65 wt% oil. Emulsification process using low pressure in the homogenizer.

5.3 Conclusions

Despite the low content of emulsifier (1 wt% sodium caseinate) all emulsions investigated were stable during the investigation period and stable emulsions could be formed up to 72 wt% oil. Some emulsions disestablished by creaming process. However, ready redistribution could be achieved by gently shaking.

The droplet size distributions for emulsions formulated at basic and neutral pH, were bimodal with a small mode corresponding to aggregation of the casein molecules. Emulsions premiered at pH values near 5 displayed monomodal size distributions with droplet sizes being larger than the rest of the pH values and showed creaming after 3 days. Emulsions homogenised at 10 Bar were the most stable for all the pressures used at the homogeniser.

Bridging flocculation was observed for all prepared emulsions. This was because the concentration of sodium caseinate used was 1 wt% and molecules of caseins were not enough to cover all the oil droplets.

The stability of emulsions with broad droplet size distributions, obtained by mixing emulsions with different droplet sizes, depended on the fraction of small droplets. The stability of emulsions increased as the fraction of small droplets was also increased.

Changing the ionic strength did not produce any affect on the stability of the concentrated emulsions, although considerable changes were achieved for the π-A isotherms of sodium caseinate at the air-water interface and interfacial tension at oil-water interface. Hence, for similar charges in the ionic strength the stability of the emulsions depend more strongly on the droplet distribution than the changes of the interaction between them produced by varying the ionic strength.

5.4 References

1. *Emulsion Formation and Stability*, ed. T.F. Tadros2013: Wiley-VCH Verlag GmbH & Co. KGaA. 272

2. Briceño, M.I., *Rheology of suspensions and emulsions*, in *Pharmaceutical Emulsions and Suspensions*, F. Nielloud and G. Marti-Mestres, Editors. 2000, Marcel Dekker: NY, USA. p. 557–607.

3. Benkeblia, N., et al., *Variation of Fructooligosaccharides and their Metabolizing Enzymes in Onion Bulb (Allium cepa L. cv. Tenshin) During Long-term Storage.* Journal of Food Science, 2005. **70**(3): p. S208-S214.

4. Tan, H.L., *The Microstructure and Rheology of Complex Fluids Coantaining Na-Caseinate*, in *Chemistry* 2010, Victoria University of Wellington

5. Dickinson, E., *Structure formation in casein-based gels, foams, and emulsions.* Colloids and Surfaces A: Physicochemical and Engineering Aspects, 2006. **288**(1–3): p. 3-11.

6. Dickinson, E., *Properties of Emulsions Stabilized with Milk Proteins: Overview of Some Recent Developments.* Journal of Dairy Science, 1997. **80**(10): p. 2607-2619.

7. Dalgleish, D.G., *Conformations and structures of milk proteins adsorbed to oil-water interfaces.* Food Research International, 1996. **29**(5–6): p. 541-547.

8. Kenta, S., et al., *Sedimentation Field-Flow Fractionation as a Tool for the Study of Milk Protein-Stabilized Model Oil-in-Water Emulsions: Effect of Protein Concentration and Homogenization Pressure.* Journal of Liquid Chromatography & Related Technologies, 2012. **36**(3): p. 288-303.

9. Floury, J., A. Desrumaux, and J. Lardières, *Effect of high-pressure homogenization on droplet size distributions and rheological properties of model oil-in-water emulsions.* Innovative Food Science & Emerging Technologies, 2000. **1**(2): p. 127-134.

10. Salaün, F., B. Mietton, and F. Gaucheron, *Buffering capacity of dairy products.* International Dairy Journal, 2005. **15**(2): p. 95-109.

11. McClements, D.J., *Protein-stabilized emulsions.* Current Opinion in Colloid & Interface Science, 2004. **9**(5): p. 305-313.

12. Chi, E.Y., et al., *Physical Stability of Proteins in Aqueous Solution: Mechanism and Driving Forces in Nonnative Protein Aggregation.* Pharmaceutical Research, 2003. **20**(9): p. 1325-1336.

13. HadjSadok, A., et al., *Characterisation of sodium caseinate as a function of ionic strength, pH and temperature using static and dynamic light scattering.* Food Hydrocolloids, 2008. **22**(8): p. 1460-1466.

Chapter 6 Rheology of concentrated emulsions with sodium caseinate

6.1 Introduction

The rheology of emulsions is extremely important for theoretical and applied purposes. From a theoretical point of view, it is possible to elucidate information about the different interactions that occur in the system and the types of destabilisation mechanisms that can occur. From an applied perspective, the flow behaviour of emulsions is important in industries such as cosmetics, pharmaceuticals and food, where the texture and perception of the emulsion are imperative parts of the requirements for final product quality control. Rheological data also provides information for industries where emulsions need to be transported, specifically the amount of energy that must be supplied to move an emulsion between different locations. An example is the movement of heavy oil in the form of oil in water (O/W) based emulsions through pipelines.

The rheological behaviour of concentrated emulsions is completely different than that for dilute or semi-dilute systems. While in dilute or semi-dilute systems the interactions between droplets are practically absent and distortion of the hydrodynamics of the continuous phase around a droplet does not affect other droplets, in concentrated emulsions the interaction between droplets and the hydrodynamics of the thin film, which separates the droplets, controls the rheology of the systems.

Interactions between droplets, in O/W emulsions, depend entirely on the characteristics of the emulsifier and the physicochemistry of the continuous phase. When proteins are used as emulsifiers small changes in parameters such as pH, ionic strength and protein concentration generate considerable changes in the rheological response of the emulsions.

To my knowledge, few studies have investigated the rheology of concentrated emulsions with sodium caseinate, and it is acknowledged that part of this research is a continuation of work undertaken by Hui Lin Tan during her PhD thesis research at

Victoria University of Wellington [1]. Some studies have been completed with different proteins or concentrated emulsions with surfactants for applications in the oil and explosives industries. The objective of this part of the research was to investigate the effect of oil concentration, droplet size distribution, ionic strength and pH on the rheological behaviour of concentrated sodium caseinate emulsions. Emphasis is placed on the integration of the information obtained from the sodium caseinate monolayer structures at the different interfaces with the rheology of concentrated sodium caseinate emulsions.

6.2 Results and discussion

The rheology of the concentrated emulsions was investigated as a function of oil concentration, droplet size distribution, aqueous phase ionic strength and pH. For the formulation of the emulsions the non-polar phase used was soy bean oil and the concentration of the sodium caseinate was 1 wt%. Rheometry was conducted using the stress-controlled TA Instruments AR2000 rheometer using a plate-and-plate geometry with a plate diameter of 40 mm and a gap between the two plates of 1 mm. All the rheological measurements were conducted at 25°C. The rheological tests applied were: steady state, strain sweep, frequency sweep, creep-recovery and time dependence. For each test at least three runs were completed in order to ensure data reproducibility.

6.2.1 General behaviour

Before showing the effect of the different parameters evaluated, a description of the general behaviour of the systems studied is presented.

6.2.1.1 Flow behaviour

For the systems studied, with an oil concentration from 50 to 70 wt%, the steady state test was evaluated at a shear rate interval between $1x10^{-3}$ and 100 s^{-1}. Shear rates below $1x10^{-3}$ s^{-1} were not used, because the torque of the values associated with them was less than the 0.1 μN*m, which is the lowest limit of the equipment. On the other hand, constant pseudo-Newtonian flow behaviour was observed at shear rates of more than 100 s^{-1}.

In order to achieve a steady state condition for the shear rate used, different measurement point durations were evaluated for different oil concentrations. For emulsions with oil concentrations of 50 and 55 wt%, a steady state response was not achieved for low shear rates even when measured for up to 20 minutes. In contrast, for concentrations of 60 wt% and higher a steady state response was achieved within three minutes. Therefore, for the purpose of comparing the rheological behaviour of the emulsions studied and taking into consideration that the systems evaluated showed time dependent flow behaviour which will be explained later, the measurement time for all the systems studied was set at three minutes.

The 65 wt% soy bean oil and 1 wt% Na-Ca emulsion was used to demonstrate the general flow behaviour that was found for in the systems studied. The data shown in Figure 6.1 displays the variation of the shear stress as a function of shear rate.

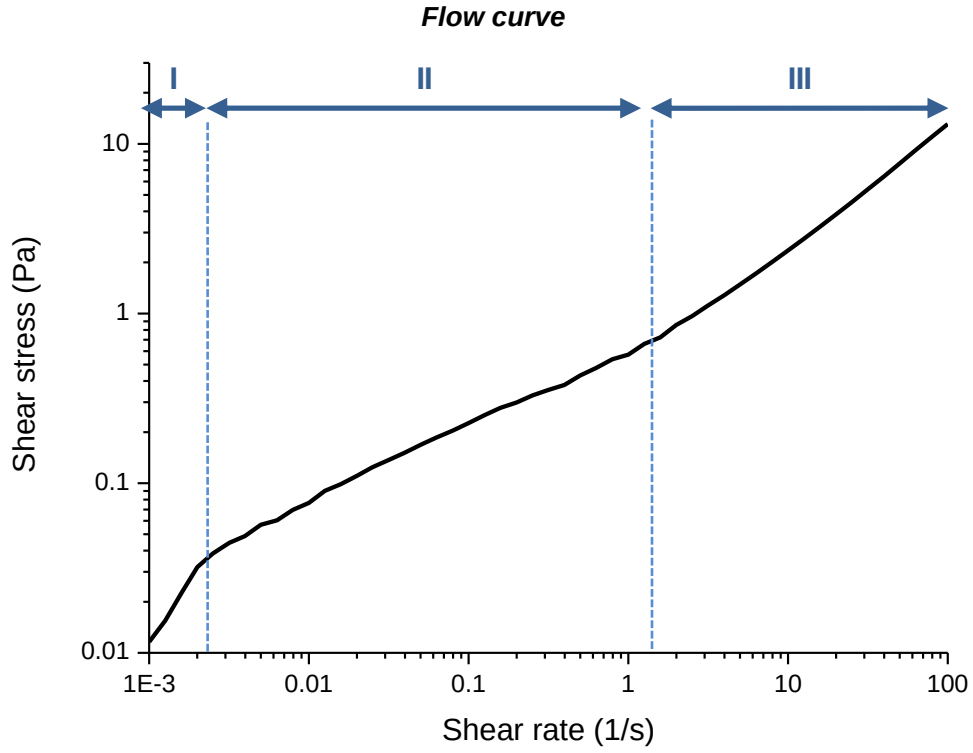

Figure 6.1 Steady state stress vs. shear rate curve for 65 wt% soy bean oil and 1 wt% sodium caseinate. Phosphate buffer solution at pH 6.8 and ionic strength 30 mM.

The flow curve shows shear-thinning behaviour and a yield point with three zones that can be easily distinguished in the curve, labelled I, II, and III in Figure 6.1. Hui Lin Tin [1], in a comprehensive study of concentrated emulsions with sodium caseinate, reported similar behaviour. In that investigation, however, the effect of pH,

ionic strength and droplet size distribution were not probed. Yield point and shear-thinning behaviour have been reported for some concentrated emulsions. Bellalta *et al.* [2] studied the rheological and microstructural characterisation of O/W emulsions with whey protein, and they found that all the systems investigated showed a yield point. At 60 wt% shear-thinning was apparent, whereas for oil concentrations of 50 wt% Newtonian behaviour was observed. Partal *et al.* [45] found shear-thinning behaviour and a yield point in their concentrated emulsions with oil concentrations between 60 and 80 wt% using sucrose palmitate as the emulsifier.

With regards to the three zones, their occurrence and placement depends on the interactions and structure between the droplets. Mason [3] explains that the capacity of a concentrated emulsion to flow depends on the balance of the external force (shear rate) and the forces generated by the droplet interactions. Also, the interaction between the droplets is responsible for the microstructure of concentrated emulsions [2, 4].

The first zone I, at very low shear rates, is associated with the domain where the structural forces dominate the external forces and shear banding and the system is resistant to flow, creating a high viscosity. Non-steady state conditions are sometimes achieved in this zone being typical of shear banding. Ovarlez *et al.* [5] explained that shear banding is produced when liquid-like (sheared) and solid-like (unsheared) bands co-exist in a homogenous shear stress field. Within the shear banding domain the systems do not flow until the critical shear rate ($\dot{\gamma}_c$) is achieved, at which point the systems attain a steady state condition and start to flow. Also, they note that shear banding is typical for thixotropic systems that show heterogeneous structures.

In the second zone II, which is located above $\dot{\gamma}_c$, the system starts to flow and the sample displays a typical shear-thinning behaviour until a second critical shear rate is reached. Masalova *et al.* [6], who took photographs at different shear rates and evaluated the droplet movement in the flow of the emulsions, explained that the flow in this zone is set by the mechanism of rolling of the droplets or aggregations . Because of the conformation of the droplets in the systems investigated, the second zone is more related to the rolling of an aggregation of droplets than the rolling of

individual ones. The Cryo-SEM images of the concentrated emulsions evaluated showed a large interconnection between the droplets that can produce aggregations (see Figures 5.4, 5.6 and 5.11).

Upon increasing the shear rate above the transition point between zones II and III, the system shows Newtonian behaviour that is associated with droplet deformation or break-up; with the transition shear rate sited between the zones II and III known as a secondary yield point [7]. The phenomenon of droplet deformation or droplet break is explained by Mason [3, 8] in their reviews of emulsion rheology. They comment that the occurrence of droplet deformation and droplet break are related to the shear rate applied, the elasticity of the emulsifier thin film, and the interfacial tension between the phases. The droplet deformation or droplet break explained by Mason [3] and Derkach [8] is unlikely to happen in the emulsions investigated because the sizes of the droplets are between 1 and 10 μm resulting in a high internal pressure in the droplets. An estimation of the pressure difference (ΔP) of the droplets at 1 and 10 μm was obtained using the Young-Laplace equation [9]:

$$\Delta P = \gamma \left(\frac{1}{R_1} + \frac{1}{R_2}\right) \qquad 6.1$$

where γ is the interfacial tension, and R_1 and R_2 are the radii of curvature. If the droplets are spherical, equation 6.1 is simplified as:

$$\Delta P = \frac{2\gamma}{R} \qquad 6.2$$

For the estimation of ΔP, it was assumed that the droplets were spherical with an interfacial tension of 7.25 mN/m. This interfacial tension was used according to the values reported in Figure 3.20. The pressure differences for 1 and 10 μm droplets are 14,500 and 1450 Pa respectively. The smaller the droplets the more difficult they are to deform due to this increasing pressure.

In order to investigate if there was any change in the droplet size distribution after the secondary yield point in the emulsions studied, droplet size distributions were compared before and after application of the steady state test to the systems. The shear rates evaluated were from $1x10^{-3}$ to 500 s^{-1}, and typical results for the

measured droplet size distribution are shown in Figure 6.2. The droplet size distributions are similar before and after shearing. However, a small peak was observed in the droplet size distribution, between 10 and 20 μm, after shear rates were applied. This peak could be associated with the well-known phenomenon of shear-induced aggregation of droplets referred to by Dickinson [10].

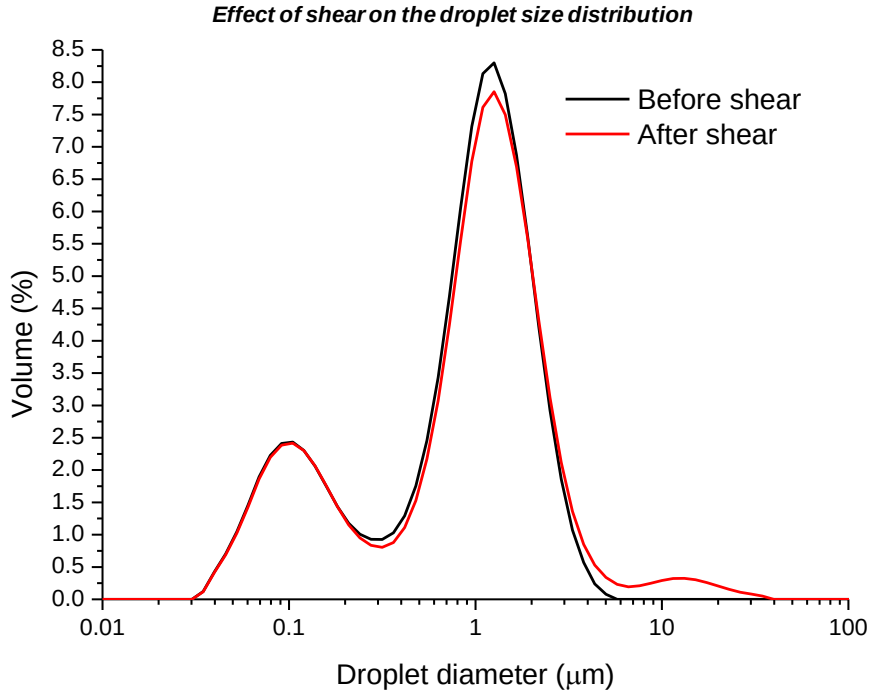

Figure 6.2 Droplet size distributions before and after shear for 65 wt% soy bean oil and 1 wt% sodium caseinate emulsion. Phosphate buffer solution at pH 6.8 and ionic strength 30 mM.

6.2.1.2 Time-dependent flow behaviour

For many fluids and dilute dispersed systems, viscosity is generally independent of time, being only a function of the shear rate and temperature. In concentrated emulsions, it is standard to observe time dependent rheological properties. This is because an increase in droplet numbers produces increased interaction between them, creating network structures that can be broken by shearing. These network structures then require time in which to reform. As a consequence, rheological properties of concentrated emulsions depend on the time and the shear rate that is applied.

In this research, two different test methods were used to corroborate the time dependent flow response of the concentrated emulsions studied. The time

dependent flow in the systems evaluated was detected when a steady state response was not achieved for a low shear rate. To investigate the time dependent flow behaviour, step and dynamic-mechanical analysis (DMA) tests were performed [11].

Step test

The step test consists of three intervals of shear rate: the reference interval (low-shear); the high shear; and the regeneration interval (low-shear). The reference interval provides information about the behaviour of the system when a low-shear rate is applied in order to be compared with the other two intervals. The high-shear interval is used to break down the internal structure of the sample. The regeneration interval is applied at the same shear rate as the reference interval to facilitate regeneration of the structure of the sample [11]. For the concentrated emulsions studied, the low and high shear rates applied were $5x10^{-3}$ and 100 s^{-1} respectively. The low shear rate used is located around the beginning of zone II in the flow curve (see Figure 6.1). At this point, changes in the emulsion structure occur since the imposed shear rate force overlaps with the interaction forces in the emulsion and the system flows. At high shear rate, the system is situated in zone III and the droplet aggregations are separated. Typical results for the step test are shown in Figure 6.3, which indicate clear differences in the emulsion viscosity when the step test is applied. At low shear rates the apparent viscosity gradually increases, while at a high shear rate it is practically constant. After applying a high shear rate and destroying the internal structure of the emulsion, the system progressively recovers its internal structure and the viscosity increases sharply. The dependence of the viscosity with time, when a constant shear rate is applied to a system is typical for thixotropic rheological behaviour [12].

Thixotropic behaviour is well-known in the food industry [13]. Some examples are reported by Peressini *et al* [14], Partal *et al* [15] and Bellalta *et al* [2], who investigated emulsions with oil concentrations above 50 wt% with different proteins or surfactants. Barnes [13] explained that thixotropic behaviour is a consequence of the finite time the system needs to change its microstructure and to return to its original structure when a shear rate is applied and then changed or removed. He mentions that the driving force for microstructural change, when a shear is applied to

the system, is the competition between the collapse due to flow stress, build-up due to in-flow collisions and Brownian motion.

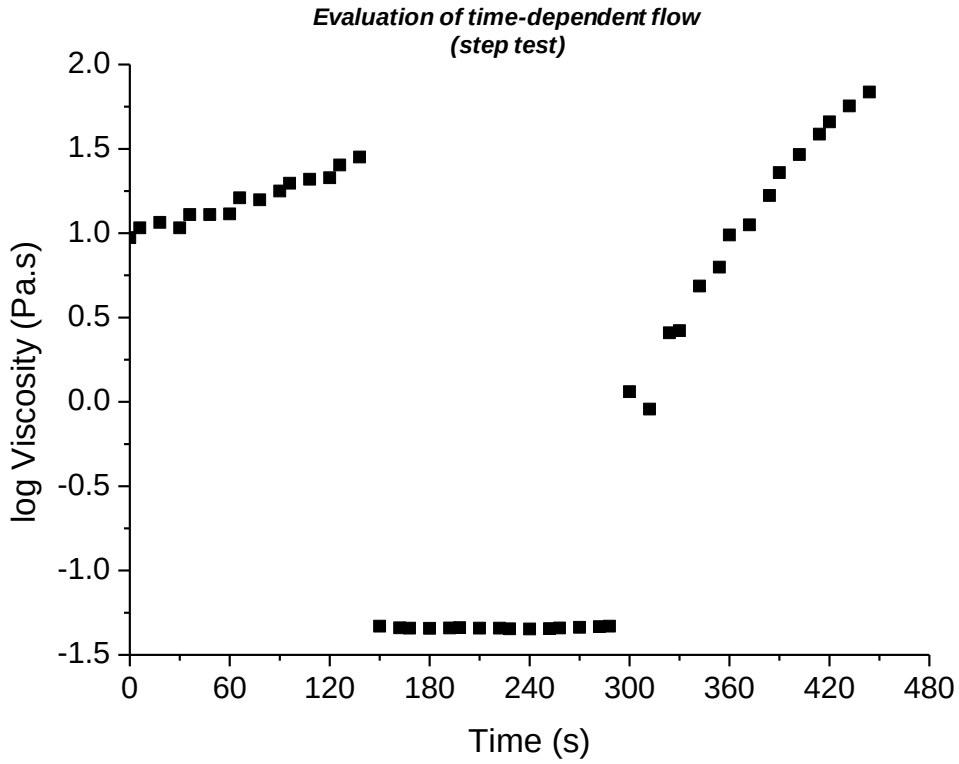

Figure 6.3 Step test for 65 wt% soy bean oil and 1 wt% sodium caseinate emulsion (0.005 and 100 s^{-1}). Phosphate buffer solution at pH 6.8 and ionic strength 30 mM.

In thixotropic systems, the viscosity depends on the shear rate used and the length of time it is applied [12]. If the apparent viscosity increases when a low shear rate is applied, the emulsion behaves as a rheopexic fluid [16].

Dynamic-mechanical analysis (DMA) test

The thixotropic behaviour of the emulsions studied was corroborated by the DMA test. This test is recommended to investigate time-dependent behaviour without chemical modification during measurement [11]. To perform the test, a constant strain and frequency are applied to a sample over a period of time and the variation of the storage (G') and loss (G'') moduli are obtained. It is essential for the application of the test, that the strain used is located before the cross over point between the storage and loss moduli. Figure 6.4 shows representative data for the variation of the storage modulus as a function of time for the DMA test. There is a marked increase of the storage modulus with time, being indicative that new strong

microstructural features are generated. The result validates the thixotropic nature of the emulsion, which substantiates the flow response depicted in Figure 6.1.

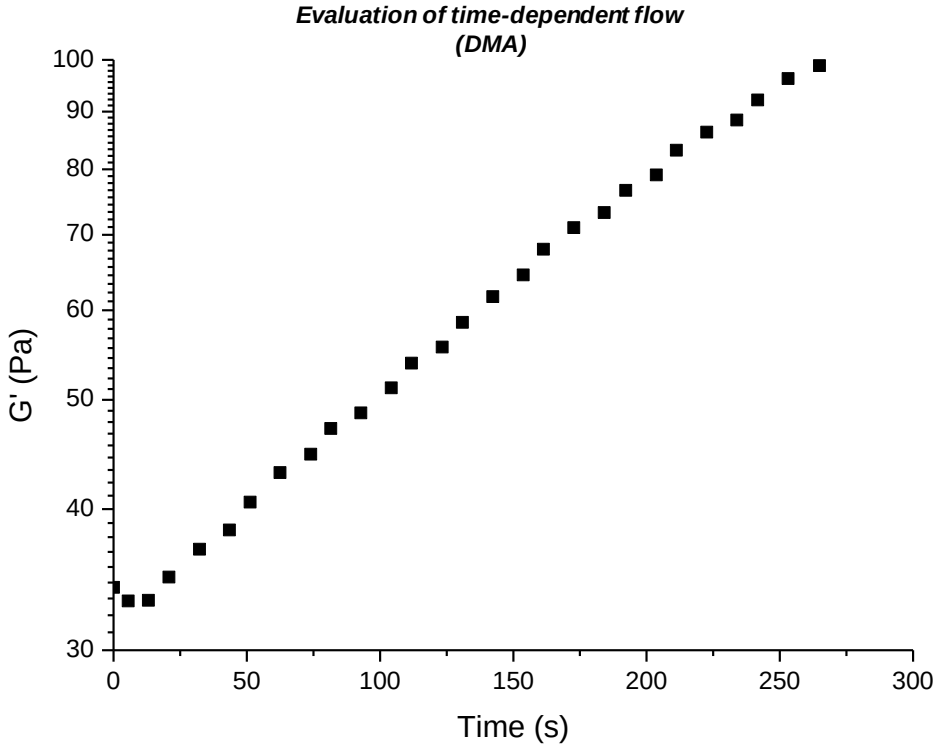

Figure 6.4 DMA test for 65 wt% soy bean oil and 1 wt% sodium caseinate emulsion (strain 2% and 1 Hz). Phosphate buffer solution at pH 6.8 and ionic strength 30 mM.

As seen from the results shown in Figures 6.3 and 6.4 and the images of the concentrated emulsions shown in the previous chapter (5.11 and 5.31), the rheological behaviours of the emulsions studied depend on their microstructures and the interactions between the droplets. Techniques that provide information about emulsion microstructures and interactions between droplets have to be used to evaluate the effect of parameters such as oil concentration, droplet size distribution, ionic strength and aqueous phase pH on the rheological properties of the emulsions. Norton *et al.* [17] confirmed that dynamic or oscillatory tests can be used to determine structural changes occurring in emulsions and the interactions between their droplets during shear. Therefore, the evaluation of the parameters mentioned earlier on the rheological properties of the emulsions will be analysed with emphasis on the dynamic tests.

6.2.2 Oil concentration

Internal phase content, or oil concentration in an O/W emulsion, together with droplet size and droplet size distribution, are the most important physical factors that affect the properties of emulsions [12]. Many studies have been undertaken to investigate the relationship between the dispersed phase concentration and the rheological properties of emulsions. However, many of them are with surfactants or polymers and involve less concentrated systems.

In this part of the research, a continuation of Tan's work [1], was done to evaluate the effect of the oil concentration on the rheological properties of sodium caseinate concentrated emulsions, undertaking steady state and dynamic tests. A greater emphasis was placed on the dynamic tests, as the main factor in the rheological properties of the concentrated emulsions is the interaction between droplets.

The emulsions studied were formulated with 1 wt% sodium caseinate and oil concentrations of 50, 55, 60 and 65 wt%. The continuous phase was a phosphate buffer at pH 6.8 and ionic strength 30 mM. For the emulsions used, three aspects are assumed: i) the droplet size distributions are essentially the same (see Figure 5.1) and ii) the adsorption of sodium caseinate at the oil-water interface is similar to that at the air-water interface, iii) the conformation of the sodium caseinate at the interface was considered as a constant, because the physicochemistry of the systems are fixed.

6.2.2.1 Flow behaviour

The steady state test was performed on the same conditions described in the sub-section 6.2.1.1. The flow curves obtained were similar to those shown in Figure 6.1, i.e., shear-thinning with a yield point and a secondary yield point. The summarised results of the estimated yield point using the Bingham model and the apparent viscosity (at shear rate of 0.1 s^{-1}) are given in Table 6.1. An example of the estimation of the yield point is shown in Appendix A4.

A shear rate of 0.1 s^{-1} was selected to compare the apparent viscosity because it was located in the region where the steady state condition was achieved for all the emulsions evaluated (Figure 6.1).

Table 6.1: Yield point and apparent viscosity.

Oil concentration (wt%)	τ_y ***(Pa)***	***Apparent viscosity (Pa.s)****
50	0.32 ± 0.06	21.54 ± 0.29
55	2.67 ± 0.20	42.7 ± 0.27
60	9.67 ± 0.40	108.3 ± 0.18
65	14.6 ± 0.85	144.2 ± 0.15

***The shear rate used to compare the apparent viscosity was 0.1 s^{-1}**

As shown Table 6.1, there is a dramatic increase in the yield point and viscosity of the emulsions when the oil concentration is increased. For the yield point estimation, the data generated by the steady state test in the zones I and II was fitted with the Bingham model. Despite the simplicity of this model, it can be used for comparative purposes. According to Barnes [18] a unique yield stress value is not possible because its value depends on the mathematical models and techniques used in its estimation. In the case of thixotropic behaviour, estimating yield stress is even more complicated because it is a function of structure and time Cheng [19] (1986), Maki *et al.* [20] and Ovarlez *et al.* [5].

The increment of the yield point and apparent viscosity, by increasing the oil concentration, is a consequence of the interaction between the droplets and the hydrodynamic forces [12].It is well known that the interactions between droplets are enlarged by decreasing the distance between them [21]. (See Equation 1.17) According to this equation and keeping constant the droplet diameter, a considerable decrease in the distance between droplets is expected upon increasing the fraction of the dispersed phase. As a consequence, the interactions between the droplets increase, thereby affecting the rheological properties of the emulsions.

The hydrodynamic forces also increase when the distance between the droplets decreases. In the case of the emulsions with protein molecules, the hydrodynamic forces are intensified because of the contribution of the electrical and steric components [17, 22].

In order to evaluate the arrangement of the droplets in the systems upon increasing the oil concentration, Cryo-SEM was used for emulsions with 60 and 65 wt% oil. Figure 6.5 shows a representative microstructure for emulsions with 60 and 65 wt%

oil. It can be seen in Figure 6.5 that there are different microstructures for the systems shown. A common feature is the interconnection between the droplets that are associated with bridging flocculation. For the system with 60 wt% of oil, the droplets keep their shape and a separation between them can be observed. However, for the emulsion with 65 wt% of oil, the droplets have an amorphous shape and the distance between them is reduced. By increasing the oil concentration the different arrangements of the droplets in the systems can produce different rheological responses.

Considering the model of the conformation of sodium caseinate at the air-water interface at pH 7 presented in Chapter 3, the adsorption of casein molecules at the droplet interface provides charge and thickness. By increasing the oil concentration the distance between the droplets is reduced and the draining of the continuous phase located in the film between them is promoted. However, the draining of the film is opposed by the repulsive electrostatic and steric forces, increasing the viscosity and yield point of the emulsions. Also, the increase in the apparent viscosity and yield point can be a consequence of the protein-protein interactions that occur when the distance between the droplets is reduced [23].

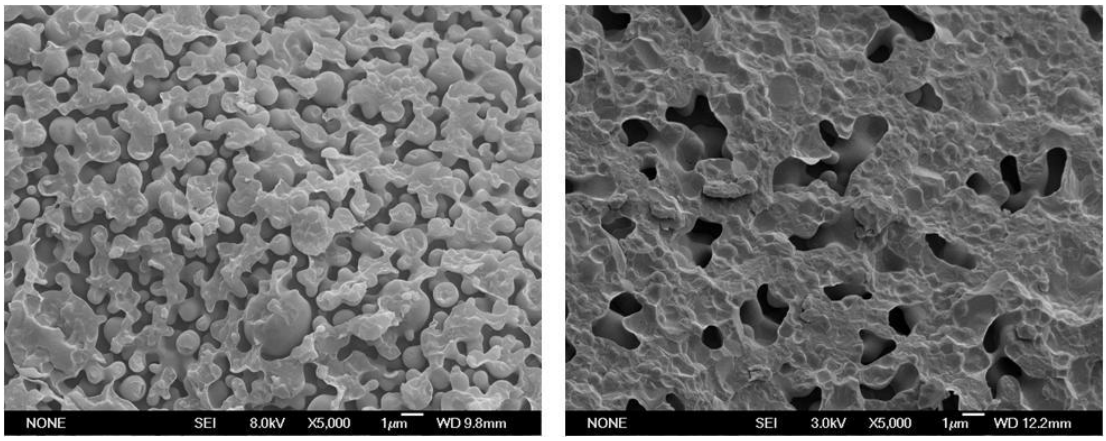

Figure 6.5 Cryo-SEM micrographs of 5000 magnification for concentrated emulsions with 60 wt% soy bean oil (left) and 65 wt% soy bean oil (right). Phosphate buffer solution at pH 6.8 and ionic strength 30 mM.

6.2.2.2 Dynamic tests

In order to evaluate the effect of the oil concentration on the viscoelastic behaviour of the emulsion, and to understand the interaction between the droplets, strain sweep, frequency sweep and creep-recovery tests were performed.

Strain Sweep

In Figure 6.6 different viscoelastic behaviours related to the oil concentration of the emulsions is shown. For the 50 wt% oil emulsion, the loss modulus is larger than the storage modulus for all the strains evaluated. However, for the high oil content emulsions the storage modulus is larger than the loss modulus when the strains are below 0.1. Also, the difference between the moduli depends on the concentration of the oil, increasing as the oil concentration rises. For example, comparing the differences for a strain of 0.01, the values are about 0.4, 7.8 and 70 Pa. These differences provide information about the viscous and elastic components in the emulsions, which can be related to the interactions between the droplets.

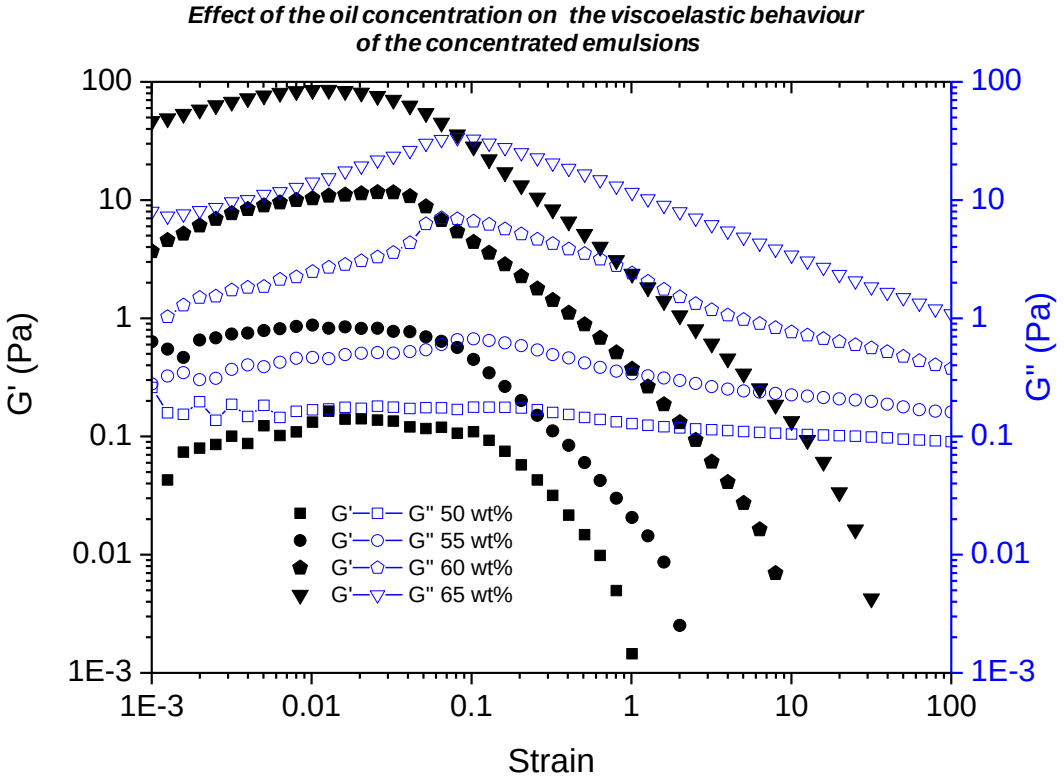

Figure 6.6 Representative curves of strain sweep test for the storage and loss moduli (frequency 1 Hz). Concentrated emulsions with different oil concentrations, soy bean oil and 1 wt% sodium caseinate. Phosphate buffer solution at pH 6.8 and ionic strength 30 mM.

The linear viscoelastic range (LVE), associated with near constancy of the moduli as a function of strain, is present only for some emulsions and this depends on the oil concentration. Figure 6.6 shows that for an oil concentration of 55 wt% a pseudo LVE can be detected before the cross over point is achieved. When the oil concentration increases, the values of G' and G" rise slightly. The storage modulus

increases until a peak is reached and after that it falls before the cross over point. These results are clearly a consequence of the rheopexic behaviour of the systems studied as explained earlier.

The strain sweep data shows that an increase in the oil concentration considerably augments the elastic component of the emulsions. This is a consequence of a large interaction between droplets and strong hydrodynamic forces in the system. Similar results have been reported [14, 24-26] which were associated with the formation of a droplet network.

An additional method to study the interaction between droplets is the evaluation of the torque applied to the emulsions at a specific strain. In Figure 6.7 the torque versus strain for the four concentrated emulsions studied is displayed. It is clear that on increasing the oil concentration a larger torque is required to produce a particular deformation (strain). This result corroborates the results shown in Figure 6.6, where increasing the oil concentration confers a larger elastic portion to the system, resulting from increasing the droplet interactions. Melnyk *et al.* [27] used a similar technique to evaluate the aggregation of gluten protein molecules with different salts. They studied the aggregation of gluten using a high shear-based technique in the presence of different electrolytes from the Hofmeister series. They reported an increasing torque as the salt concentration increased and concluded that this is because of the aggregation of gluten protein molecules generated from increasing interactions between the protein molecules.

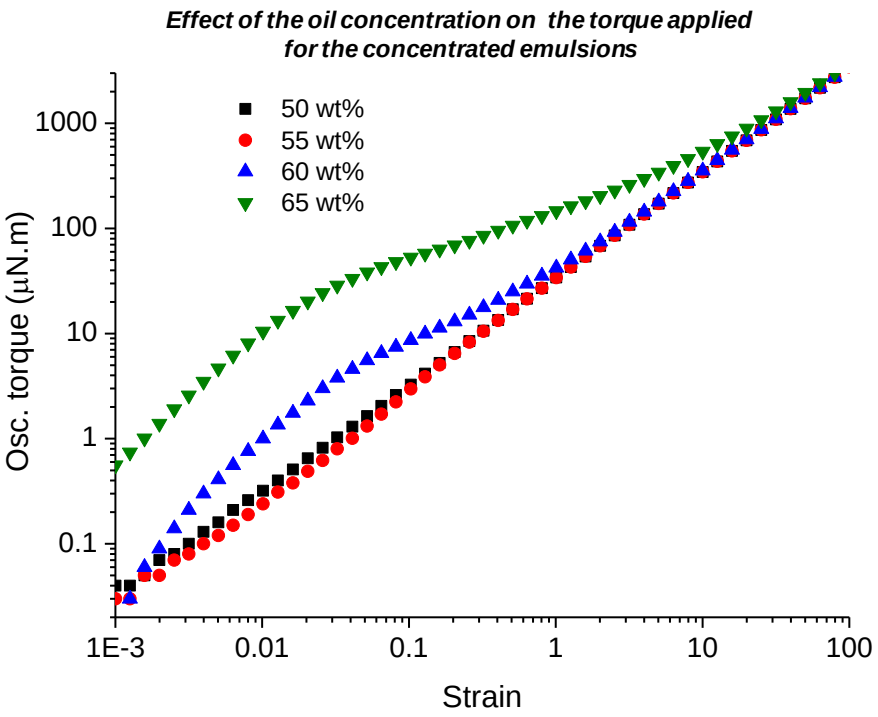

Figure 6.7 Representative curves of torque versus strain (Frequency 1 Hz). Concentrated emulsions with different oil concentrations, soy bean oil and 1 wt% sodium caseinate. Phosphate buffer solution at pH 6.8 and ionic strength 30 mM.

Frequency sweep

Frequency sweep tests were also performed for the emulsions studied, with frequencies from 0.1 to 10 Hz and an oscillatory shear of constant amplitude 2% (see Figure 6.8). The emulsion with 50 wt% was not included for the frequency test because of its viscous behaviour in the strain sweep test.

As can be seen from Figure 6.8, increasing the oil concentration increases the storage and loss moduli, demonstrating the same trend shown in Figure 6.5. The storage modulus is higher than the loss modulus for the emulsions with 60 and 65 wt% of oil for the range of frequencies studied. Furthermore, the loss and storage moduli for both concentrations are almost parallel. For the emulsion with 55 wt% of oil, the storage modulus is higher than the loss modulus until a frequency of about 9 Hz where the cross over point is achieved. All the emulsions have a mostly elastic gel-like behaviour with both storage and loss moduli increasing with the oil concentration. A general feature is the small but progressive increase of the storage modulus with the frequency. This behaviour is again related to the rheopexic

behaviour of the emulsions. Tang *et al.* [24], who studied the rheological and microstructural properties of concentrated emulsions with soy protein, suggested that the increase of the storage modulus of the applied frequency is due to the gel-like network that consists of physical cross-links. A similar relationship was reported by Peressini *et al.* [14] who studied the rheological characterisation of traditional and light mayonnaises.

The quantification of the interaction between droplets can be estimated using Bohlin's theory. According to this theory of flow, there is a correlation between the rheology and microstructure of concentrated colloidal systems such as emulsions, suspensions and polymer solutions. He explained that a concentrated emulsion can be modelled as a network of rheological elements that interact for creating system structures [28]. Bohlin developed different mathematical equations which are applied to the data obtained from different tests. In dynamic tests, for example; creep or frequency sweep, the equation proposed is [29]:

$$G' = A\omega^{1/z} \qquad 6.3$$

where ω [Hz] is the frequency, A [Pa] is a constant related to the magnitude of the interactions between droplets, and z [dimensionless] is the coordination number that provides information about the level of the interactions.

On the basis of this theory, the storage modulus data, for frequency sweep tests (Figure 6.8), were fitted using equation 6.3 and the results are shown in Table 6.2 and an example is shown in Appendix A4. A significant increase in the value of A is observed upon increasing the oil concentration in the emulsions. Considering the meaning of A for the Bohlin's equation, it is clear that the interactions between droplets are strongly dependent on the concentration of the dispersed phase. A high degree of interaction between droplets is associated with strong microstructures, which justify the significant increase of the storage modulus values with oil concentration (see Figures 6.6 and 6.8). While a small variation in z, the coordination number is seen, A dominates, indicating that the increasing strength of the interactions dominates as opposed to the number of interactions between droplets.

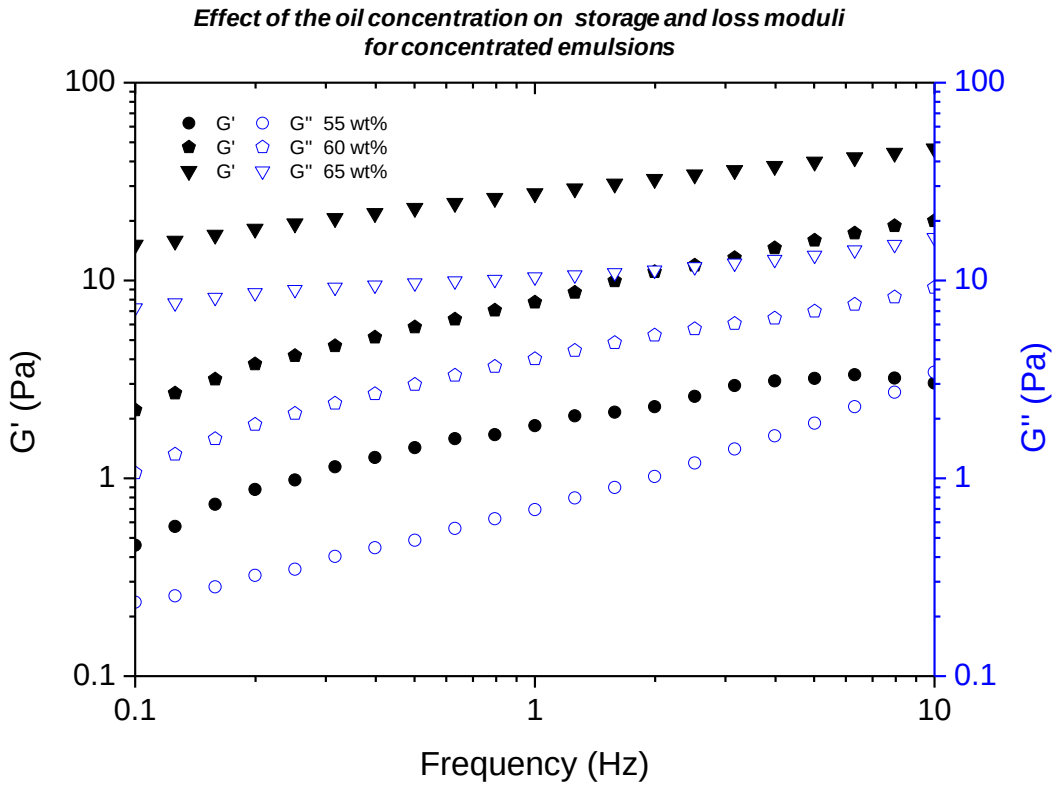

Figure 6.8 Representative curves of storage and loss moduli as functions of frequency (strain 2 %). Concentrated emulsions with different oil concentrations, soy bean oil and 1 wt% sodium caseinate. Phosphate buffer solution at pH 6.8 and ionic strength 30 mM.

Table 6.2: Bohlin's parameters, A and z of concentrated emulsions.

Oil concentration [%wt]	***A [Pa]***	***z [dimensionless]***
55	*1.76 ± 0.05*	2.79 ± 0.16
60	*7.83 ± 0.10*	2.34 ± 0.04
65	27.20 ± 0.01	4.20 ± 0.04

The numerical values of A, estimated using the Bohlin's equation, agree completely with Tardos' equation (1.17), where increasing the oil concentration favours interactions between droplets. The reported shear-thinning behaviour shown in section 6.2.2.1 for the emulsions evaluated is corroborated by the inverse of the coordination number, which is related to the flow behaviour index in the power law, being less than one for the emulsions studied.

Creep-recovery test

Quantification of the elastic and viscous proportions of a sample can be determined from creep-recovery test data. This test is suitable to evaluate dispersed systems or polymer solutions showing physical-chemical network forces [11]. The creep and recovery test basically consists of applying a constant shear stress for a specific time to a sample to produce a deformation. Subsequently, the shear stress is removed and the sample is allowed to recover during a period of time similar to the deformation time, with the first step known as the creep phase and the second as the recovery phase [30]. Data generated during a creep-recovery test allows the calculation of parameters such as the permissible maximum deformation and the elastic and viscous percentages [31].

In order to determine the elastic and viscous portions of a sample, the applied torque or stress should conform to the LVE range. When a comparison between different systems is required, choosing a torque or stress that lies within the LVE range for all the samples is often unfeasible. With the purpose of setting an appropriate torque to perform the creep-recovery test for the emulsions evaluated, strain sweep results (Figure 6.5) were displayed as a function of the applied torque (see Figure 6.9).

In Figure 6.9 there is a marked rise in the torque applied to reach the cross over point when the oil concentration is increased. This result confirms the relationship between the oil concentration and droplet interactions. By increasing the oil concentration the microstructures are more stable, providing an elastic-like behaviour to the systems. Consequently, more force is needed to destroy the structure and make the system flow.

Choosing an appropriate torque that allows comparison between emulsions with different oil concentrations is not simple. Figure 6.9 shows that there is a large difference between the torque applied to emulsions up to 60 wt% compared with the emulsion with 65 wt% oil. A torque of 1 μN.m was used to perform creep-recovery tests because this was located before the cross over point for the emulsions with 55, 60 and 65 wt% oil. The total time set was three minutes. The data for the creep and recovery tests for the different emulsions is shown in Figure 6.10. The deformation (strain) and viscoelastic behaviour of the emulsions used directly depends on the oil

concentration. The maximum deformation is significantly decreased when the oil concentration increases from about 400 (50 wt% oil) to $2.6x10^{-3}$ (65 wt% oil). These results are consistent with the results in the strain and frequency sweep tests, and the application of Bohlin's equation. Also, the results in Figure 6.7 show that for a constant torque the strain produced on the samples depends on the oil concentration.

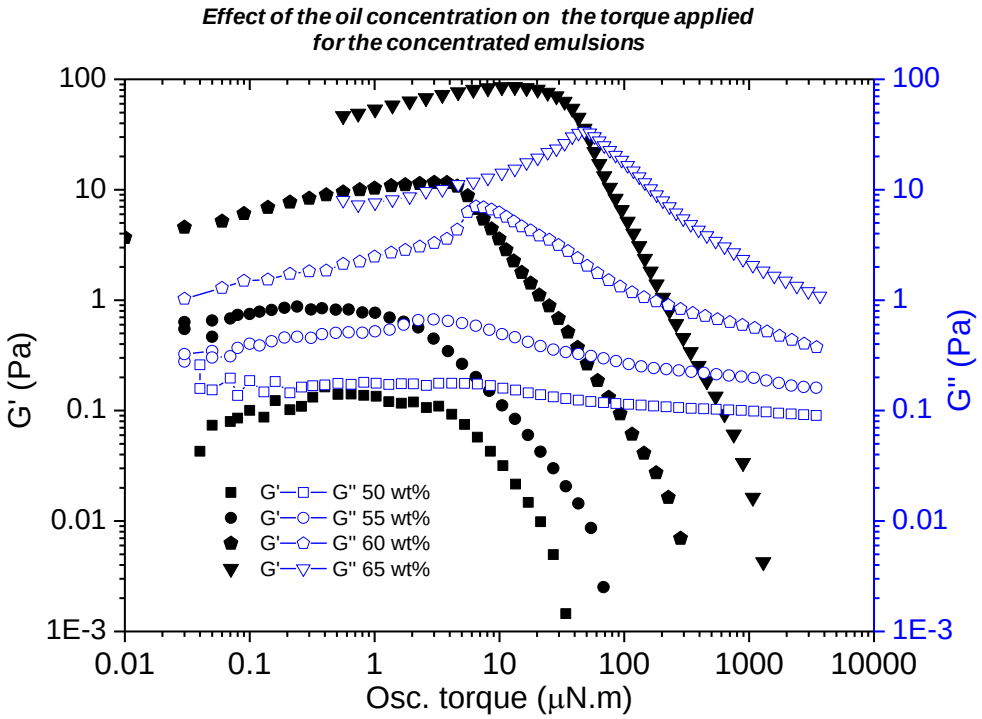

Figure 6.9 Torque sweep test (frequency 1 Hz). Concentrated emulsions with different oil concentrations, soy bean oil and 1 wt% sodium caseinate. Phosphate buffer solution at pH 6.8 and ionic strength 30 mM.

With the torque used (1 μN.m) for the creep-recovery test, only the emulsion with 65 wt% oil shows viscoelastic behaviour, i.e., the system has elastic and viscous components; 0.14 and 0.86 respectively. Emulsions with oil concentrations of 50 or 55 wt% have an ideal viscous behaviour when a constant torque is applied and a linear relationship between deformation and time can be observed. After removing the torque, recovery does not occur because the systems do not have an elastic component [11]. The emulsion with 60 wt% oil shows a quasi-viscous behaviour without any recovery after removing the torque applied.

From an examination of Figure 6.10, it is clear that using the creep-recovery test to quantitatively estimate the viscoelastic components of emulsions with different oil concentrations, by applying a constant torque, cannot be achieved because of the

dissimilarity in the interaction between the droplets and hydrodynamic forces. However, qualitative information related to the structure of emulsions and the interaction between their droplets can be obtained by applying a constant torque as will be explained later.

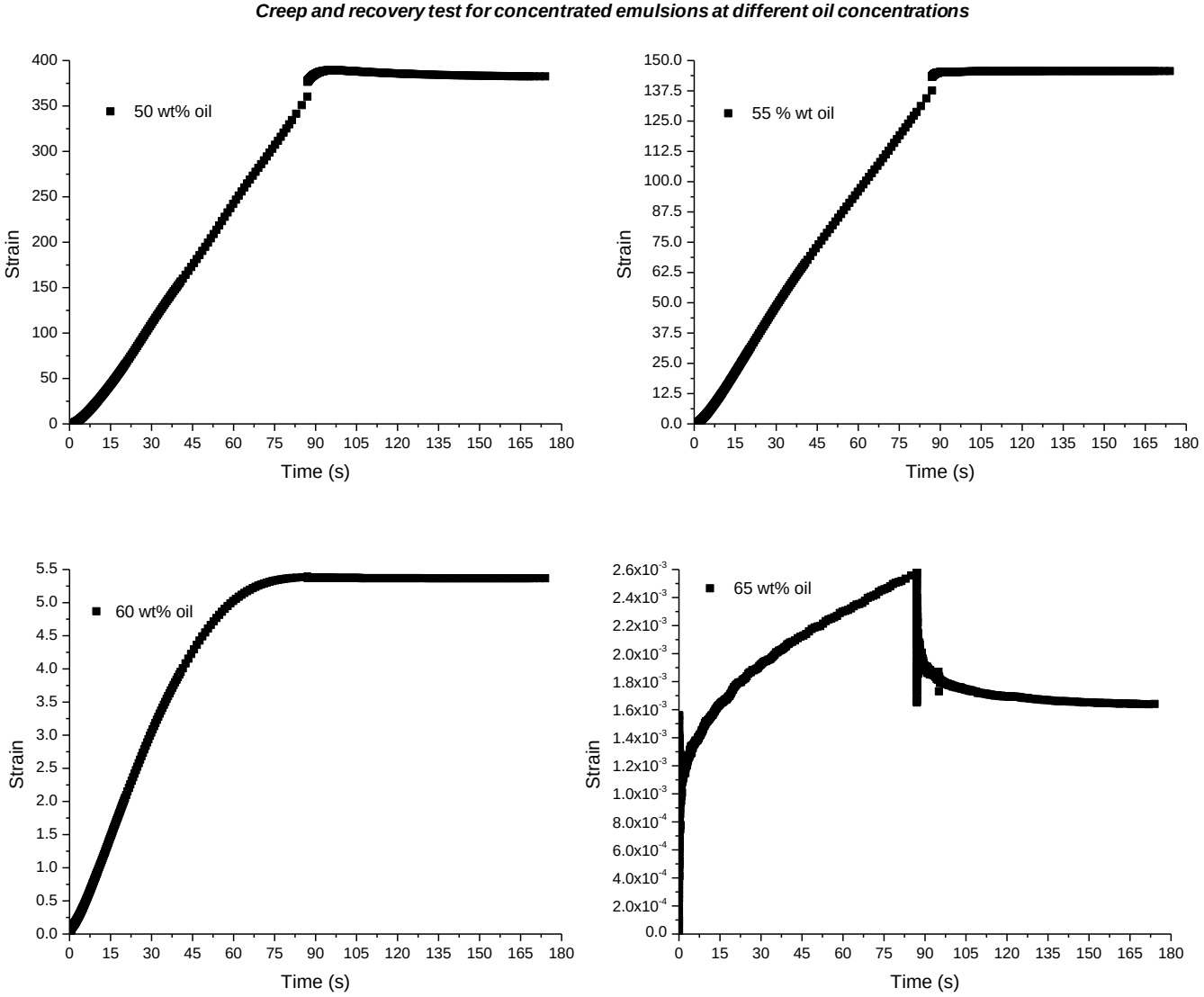

Figure 6.10 Creep and recovery curves (torque 1 μN.m). Concentrated emulsions with different oil concentrations, soy bean oil and 1 wt% sodium caseinate. Phosphate buffer solution at pH 6.8 and ionic strength 30 mm.

6.2.3 Droplet size and droplet size distribution

As well as the dispersed phase concentration, droplet size distribution has a strong influence on emulsion rheology [32]. Although many studies have been performed in an attempt to understand the effect of droplet size and droplet size distribution on the

rheological properties of concentrated emulsions, a full explanation is still not clear [33]. Also to my knowledge, no research has been published on concentrated emulsions with sodium caseinate that specifically considers these aspects.

Concentrated emulsions with 70 wt% oil and 1 wt% sodium caseinate were formulated. A homogeniser was used to make the base emulsions at two different pressures (1 and 5 Bar) and two different droplet size distributions. The different size distributions have Sauter mean diameters of 0.9 and 0.4 μm respectively. The droplet size distribution with the biggest droplets is referred to as coarse (1 Bar), while the droplet size distribution with the smallest droplets is referred to as fine (5 Bar). By mixing these two emulsions at fractions of the fine sample of 0.75, 0.5 and 0.25, five droplet size distributions were obtained. (See Figure 6.11).

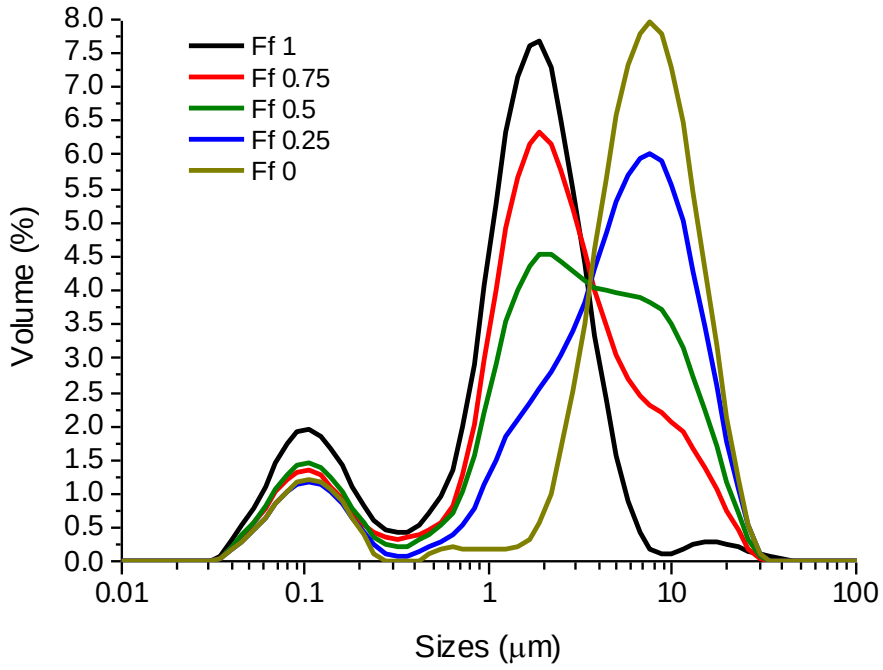

Figure 6.11 Droplet size distributions of concentrated emulsions 70 wt% soy bean oil and 1 wt% sodium caseinate with different fine droplet fractions. Phosphate buffer solution at pH 7 and ionic strength 50 mM.

For all the emulsions studied (Figure 6.11) there is a population of aggregates having a size of 0.1 μm. As was explained in Chapter 5, this population is related to casein aggregation. The emulsions that were homogenised at 1 Bar (Ff 0) and 5 Bar (Ff 1) show narrow droplet size distributions. The combination of both base

distributions produced a wide droplet size distribution, moving from a high (Ff 0.75) to a low (Ff 0.25) volumetric percentage of the fine emulsion.

6.2.3.1 Flow behaviour

The steady state test was performed for the emulsions with different droplet fractions; the flow behaviour for the systems investigated was the same described in section 6.2.1.1, i.e., shear thinning with a yield point. In Table 6.3 the results for the steady state test are summarised. There is a strong effect of droplet size distribution on the yield point and apparent viscosity. The general trend is that both parameters decrease as the fraction of fine droplets is reduced.

Table 6.3: Values of yield point using Bingham model and apparent viscosity for emulsions at different fine fractions.

Fine fraction	τ_y ***(Pa)***	***Apparent viscosity (Pa.s)****
1	16.2 ± 1.2	176.8 ± 0.2
0.75	12.1 ± 1.4	145.5 ± 0.4
0.5	13.0 ± 0.8	86.5 ± 0.3
0.25	7.2 ± 0.3	65.4 ± 0.5
0	1.3 ± 0.2	7.5 ± 0.4

***The shear rate used to compare the apparent viscosity was 0.1 s^{-1}**

The results given in Table 6.3 will be discussed from two perspectives: considering those with similar oil droplet size distribution breadth but different droplet sizes (emulsions Ff 1 and Ff 0); and those with a significant polydispersity of droplet size distribution (Ff 0.25, 0.5, 075). There is a large difference in the yield point and viscosity values for the emulsions with fine (Ff 1) and coarse (Ff 0) droplet sizes. This result was expected because similar results have been widely reported for concentrated emulsions [16, 32-34]. However, a fundamental aspect of this research is to connect this result with the sodium caseinate conformation at the air-water interface.

With regards to the viscosity results, Derkach [8], in his review of the rheology of emulsions states that for fractions of the dispersed phase in the range 0.6-0.75, the size of the droplets strongly affects the viscosity of the emulsions. Pal [33] reported a similar result in his study of the effect of droplet size on the rheology of emulsions.

He proposes that there are two potential reasons why when decreasing the droplet size, the emulsion's viscosity increases sharply: i) a decrease in the separation of the droplets; and ii) an increase in the effective volume fraction ($\emptyset_{\text{eff}}$) of the droplets.

With regard to the separation between the droplets, it is well known that the distance between droplets affects the interaction between them [21]. The distance between droplets and droplet size are related according to Equation 1.17. This equation shows that for a constant value of φ, there is a direct relationship between droplet size and the distance between them.

The interactions between droplets, when the distance between them is reduced, can be described thermodynamically as follows [35]. For stable emulsions, when two droplets are separated by a thin film and achieve equilibrium, there are two antagonistic forces acting between their interfaces: the disjoining and the capillary pressures. The disjoining pressure is a net force, which acts perpendicular to the film surface, and is produced by the contribution of electrostatic, van der Waals, hydrophobic, and steric forces [22]. This force tends to separate the droplets by thickening the film. By way of comparison, with the capillary pressure the difference between the droplet and the continuous phase pressure tends to reduce the distance between them by thinning the film [35].

The influence of the effective volume fraction ($\emptyset_{\text{eff}}$) of the droplets is related to the thickness of the emulsifier and the radius of the droplet, with this effect becoming significant when the droplet size is small. According to Romero *et al.* [36], the equation of the effective volume fraction is ($\emptyset_{\text{eff}}$) is:

$$\emptyset_{eff} = \emptyset\left(1 + {}^{\delta}/_{R}\right)^{3} \quad 6.4$$

where R is the radius of the droplets, $\emptyset$ is the volume fraction and δ the thickness of the adsorbed emulsifier layer. Equation 6.4 shows the large impact of droplet size on the effective volume fraction. Increasing the effective volume fractions dramatically increases the viscosity of the emulsion.

In concentrated emulsions, the droplet size also affects the hydrodynamics of the system. When a shear flow is applied, the emulsion droplets are submitted to two

contrary effects: hydrodynamic and interfacial stress [21]. The hydrodynamic stress tends to elongate the droplets, while the interfacial stress produces an opposite effect. These two stresses are linked by the capillary number (N_{Ca}) as follows:

$$N_{Ca} = \eta_c \dot{\gamma} / (\sigma / R) \quad 6.5$$

where η_c is the continuous phase viscosity, $\dot{\gamma}$ is the shear rate, R is the droplet radius and σ is the interfacial tension. Large droplet deformation is associated with big droplets, increasing the capillary number and reducing the viscosity [37]. Additionally, the capacity of the droplet to elongate, without breaking, is a consequence of the elasticity of the interface generated by the emulsifier.

Assuming that for the emulsions, the adsorption of the casein molecules at the interface follows the model developed in Chapter 3, a dramatic increase in the viscosity when reducing the droplet size is expected. According to this model, at pH 7 sodium caseinate molecules have a portion of their hydrophilic amino acid residual groups immersed in the water phase and a net negative charge. Therefore, the adsorption of the casein molecules at the droplet interface generates steric and electrostatic forces. These forces contribute to the positive disjoining pressure and prevent film rupture between droplets. Sodium caseinate monolayers also show a high elasticity at the air-water interface (Figure 3.6), which confers a considerable elongation capacity to the droplets when a hydrodynamic stress is applied. All these properties make a noticeable contribution to the emulsion viscosity and the viscosity value is magnified when the droplet size is reduced.

The polydispersity of the droplet size distribution did not show any effect on the yield point for the emulsions with fine fractions from 1 to 0.5. This result suggests that the fine droplets dominate the systems until the fraction of fine is 0.5. From 0.5 to 0 fraction of fine, a big difference in the yield point is observed (see Table 6.3).

A marked difference in the apparent viscosity with the droplet size distribution is observed in the results in Table 6.3. Decreases in the viscosity values of the emulsions are observed when the fine fraction is reduced. Ramirez *et al.* [32], in their research into droplet size distribution bimodality and its effect on O/W emulsion viscosity reported similar results for their concentrated emulsions with 70 vol% of oil

phase. They emphasise that the reduction of the viscosity depends on the droplet size distribution of the mixed base emulsions. They showed that factors such as the ratio of the average diameter, polydispersity and separation or overlapping of the size distribution have different rheological responses. Pal [33] also investigated the effect on the droplet size distribution on the rheological properties of concentrated emulsions. He found that some of the mixtures showed lower viscosity and storage modulus than for the base emulsions. Pal explained that this behaviour is related to the lubrication effect of fine droplets, i.e., fine droplets substituted for coarse droplets increasing the separation between the big droplets and thereby reducing the viscosity of the emulsion.

For the concentrated emulsions studied here, the lubricant effect is very unlikely. This is because for the sodium caseinate concentration used (1 wt %), the droplets show bridging flocculation (Figures 5.11 and 5.31), which could hinder the lubricant role of small droplets. However, it is possible that the small droplets become part of the continuous phase (Figure 6.12), increasing the distance between the big droplets, which reduces emulsion viscosity.

Figure 6.12 shows different emulsion microstructures for systems with 65 wt% of oil. While the oil concentration used here is not the same as that used in the rheological experiments, the micrographs give some understanding of the arrangement of the different droplet sizes and size distributions.

In Figure 6.12 representative microstructures for emulsions with fine fractions 1 (fine), 0.75, 0.25 and 0 (coarse) are shown. It can be seen that the shape of the droplets, the arrangement of the droplets in the systems and the separation between droplets are completely different. In coarse and fine fraction 0.25 emulsions, a clear shape of the droplets can be observed. For the Ff 0.25 emulsion, the fine droplets look as though they are a part of the continuous phase and are increasing the separation between droplets. In the coarse emulsion the shape of the droplets is perfectly defined, but the arrangement between them reduces the inter-droplet separation. For fine and fine fraction 0.75 emulsions, the shape of the droplets is not well defined. The separations between the dispersed phases are narrower for the fine emulsion than for Ff 0.75.

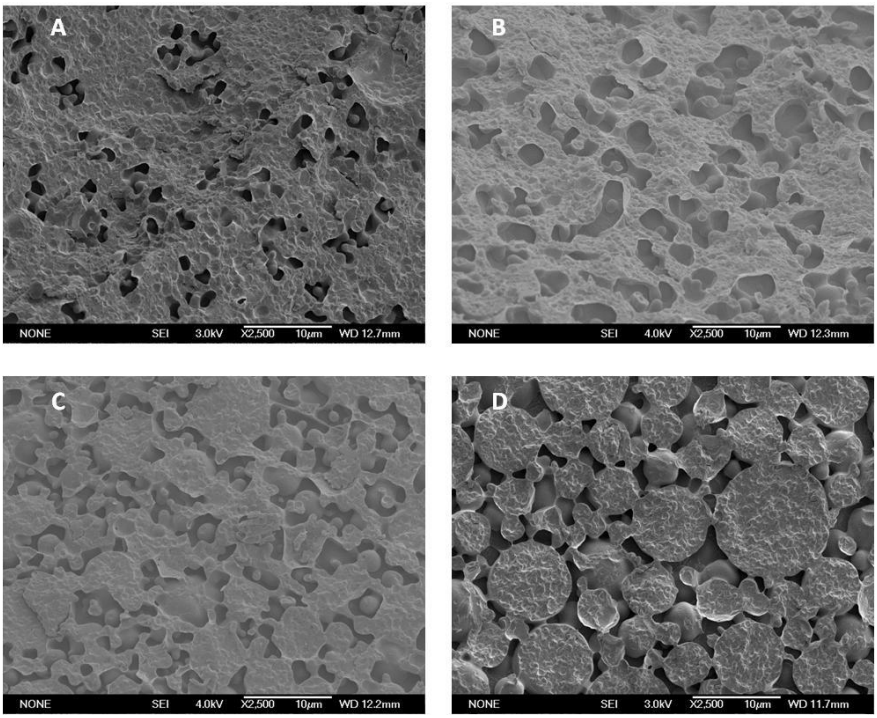

Figure 6.12 Cryo-SEM micrographs of 2500 magnification for concentrated emulsions with 65 wt% soy bean and with fine fractions of 1 (A), 0.25 (B), 0.75 (C) and 0 (D). Phosphate buffer solution at pH 7 and ionic strength 50 mM.

6.2.3.2 Dynamic tests

Dynamic tests were also performed to study the viscoelastic behaviour of the emulsions and the interaction between their droplets.

Strain sweep

Strain sweep tests were performed for the different emulsions and the result is shown in Figure 6.13. The different emulsions evaluated show elastic-like behaviour over a large range of strain and the strain value for the cross over point depends on the fine fraction, being about 0.16 and 0.07 for fine and coarse emulsions respectively. The slight increase of G' with the applied strains, before the cross over point, is related to the rheopexic behaviour of the emulsions as confirmed previously. It is clear that emulsions with the smallest droplet sizes show the largest storage modulus, there being a significant difference with the other emulsions. However, it is also evident that the large droplets dominate the system with even the Ff 0.75 being more similar to Ff0 than Ff1.

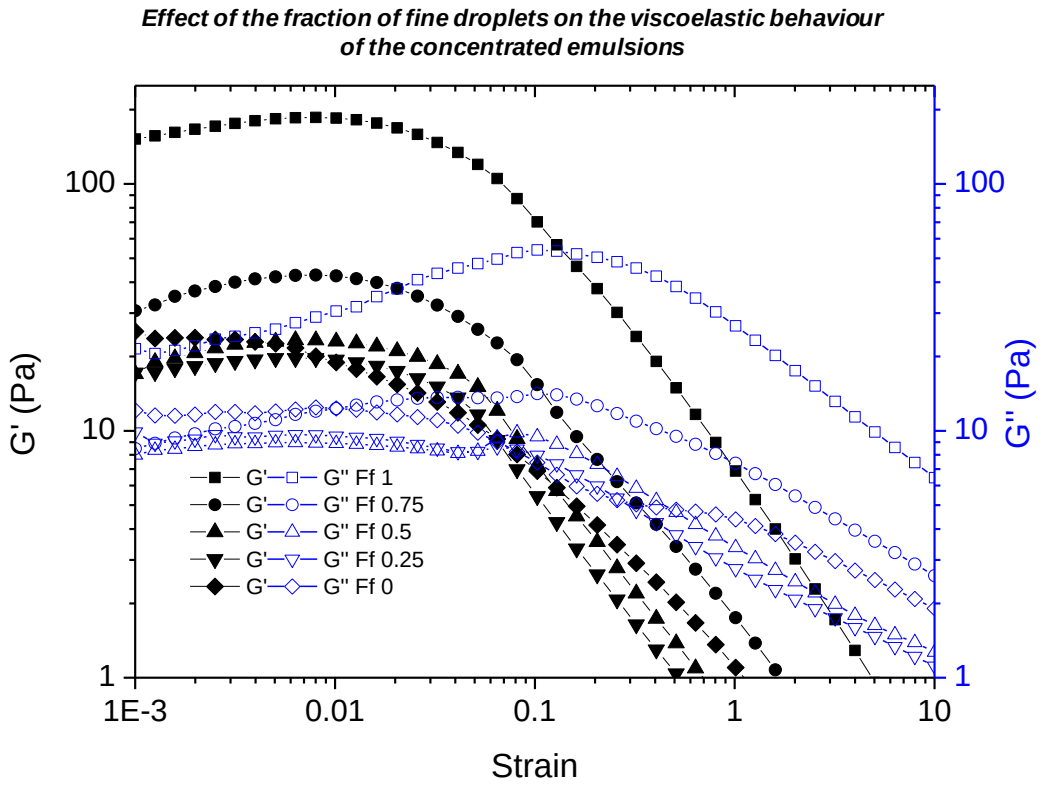

Figure 6.13 Representative log-log plots of strain amplitude dependence of the storage and loss moduli, G' and G'' at 1 Hz, for 70 wt% soy bean oil, 1 wt% sodium caseinate emulsions at different fine fractions. Phosphate buffer solution at pH 7 and ionic strength 50 mM.

The large storage modulus for the fine emulsion confers a gel-like appearance to the system, and the coarse emulsion and emulsions with fine fractions spread when they are released on a surface. On the contrary, the fine emulsion keeps its shape once this system is placed on a surface, with this behaviour typical for gel systems (see Figure 6.14). This visual result suggests different arrangements and interactions between the droplets for the emulsions investigated (Figure 6.12).

Figure 6.14 Appearance of emulsions 70 wt% soy bean oil and 1 wt% sodium caseinate. From left to right fine fractions: 0, 0.25, 0.5, 0.75 and 1. Phosphate buffer solution at pH 7 and ionic strength 50 mM.

A marked reduction of the viscoelastic properties of the concentrated emulsions is observed when the droplet size increases (Figure 6.13). For instance, when the strain is 0.01 the storage moduli for the fine and coarse emulsions are 185 and 19

Pa respectively. This result confirms the important role of the size of the droplets on the rheological properties of concentrated emulsions.

Widening the droplet size distribution (Figure 6.13) also reduces the viscoelastic behaviour of the concentrated emulsions investigated. In order to compare the effect of the droplet size distribution on the storage modulus for the emulsions at different fine fractions, the storage modulus data are displayed versus the strain, see Figure 6.15.

Figure 6.15 shows the noticeable influence of broadening the droplet size distribution towards larger droplet sizes on the elastic component for the concentrated emulsions. The addition of a small proportion of coarse droplets in the mixture, for example 0.25, already significantly decreases the storage modulus of the emulsion. Bigger differences are obtained for the storage modulus as the coarse proportion is increased. These results can be understood as an increase in the emulsion continuous phase, considering the fine droplets as part of this phase, when coarse droplets are added to the mixture of a constant dispersed concentration. That is, the large droplets alone define the dispersed phase and they move and interact through a continuous phase of smaller droplets. Hence the new droplet configuration increases the distance between the coarse droplets and a decrease in the droplet interactions is expected, reducing the elastic components of the concentrated emulsions.

It is important to highlight that the effect of droplet size distribution on the viscoelastic properties of concentrated emulsions has an important application in properties such as texture, appearance and transportation.

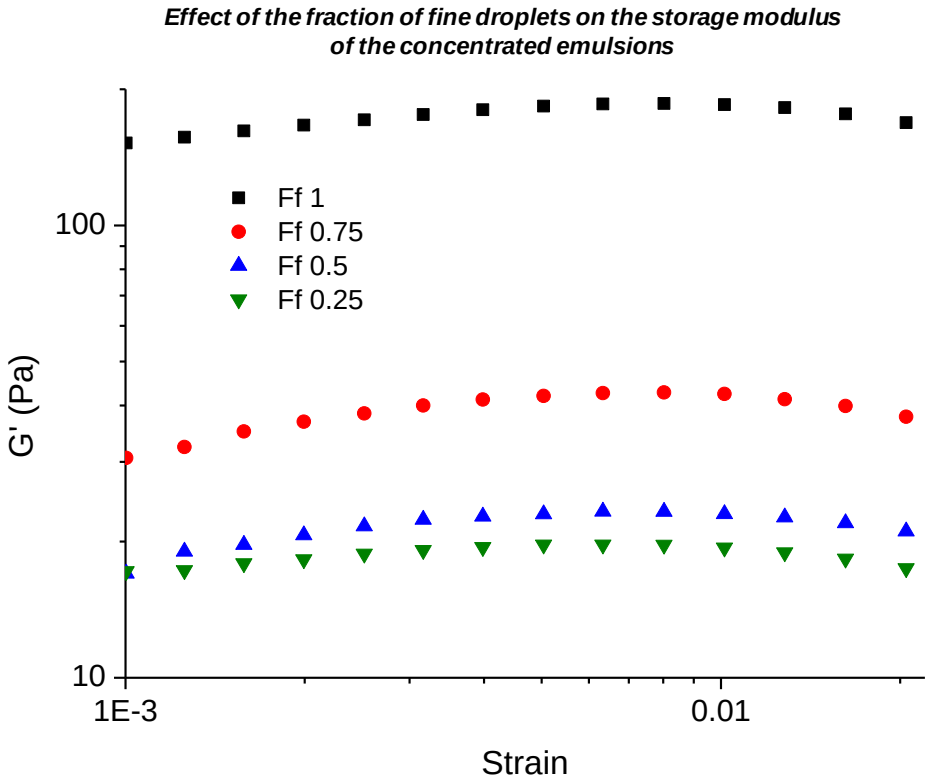

Figure 6.15 Storage modulus as a function of strain, for various emulsions at different fine fractions (1 Hz). Emulsion with 70 wt% soy bean oil and 1 wt% sodium caseinate. Phosphate buffer solution at pH 7 and ionic strength 50 mM.

Creep-recovery test

Creep-recovery tests were performed for the different emulsions. The time used for creep and recovery was as outlined in Section 6.2.2.2. The applied torque was 1.5 μN.m and it was located before the cross over point for different emulsions (see Figure 6.16).

The data for creep-recovery tests for the emulsions investigated is shown in Figure 6.17 where the emulsions demonstrate different responses when a constant torque is applied and then removed. The data for the emulsion with a fine fraction of 0.25 displays a quasi-ideal viscous behaviour, while the remaining emulsions show viscoelastic behaviour with a well-defined elastic and viscous proportion. The lowest deformation was for the fine emulsion (Ff 1), while the largest deformation was for the emulsion with a fine fraction of 0.25.

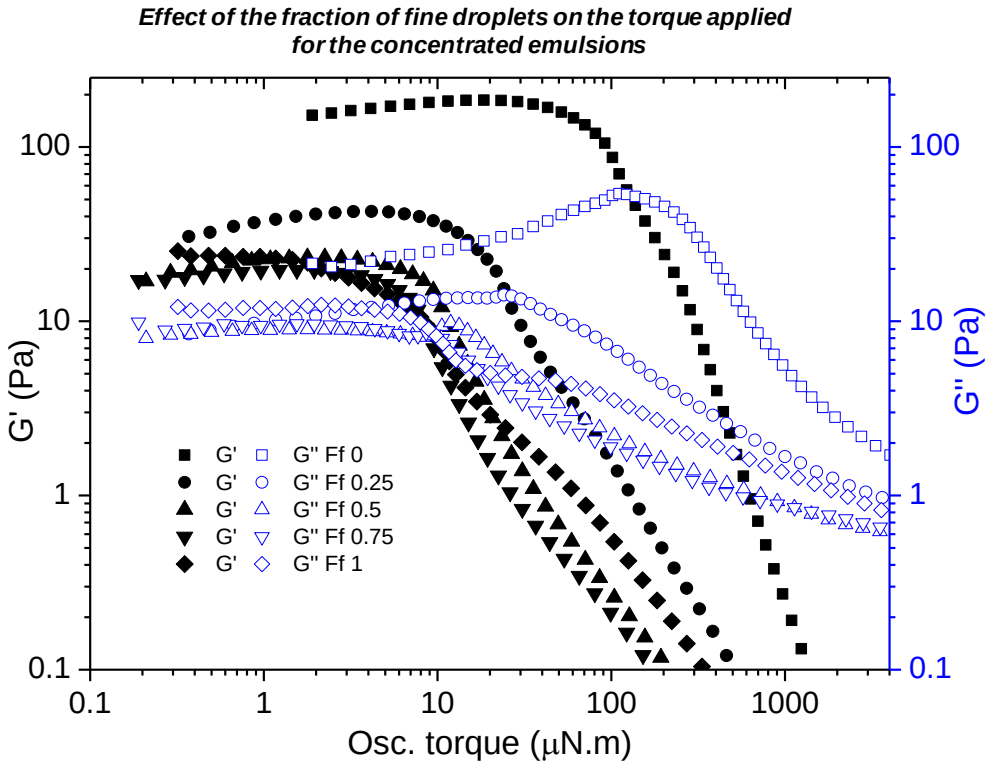

Figure 6.16 Torque sweep test (frequency 1 Hz) for 70 wt% soy bean oil, 1 wt% sodium caseinate emulsions at different fine fractions. Phosphate buffer solution at pH 7 and ionic strength 50 mM.

By applying a constant torque the different creep-recovery responses obtained are related to the diverse interactions and structures of the emulsions evaluated. These parameters can be correlated to the viscous and elastic components in the system. The values of deformation and the elastic and viscous proportions of the emulsions at different fine fractions are shown in Table 6.4.

Table 6.4: Viscoelastic parameters from the creep and recovery test.

Fine fraction	***Maximum deformation***	***Elastic percentage (%)***	***Viscous percentage (%)***
1	7.39×10^{-4}	52	48
0.75	1.26×10^{-2}	37	63
0.5	5.3×10^{-2}	18	82
0.25	1.09	2	98
0	4.5×10^{-2}	29	71

In Table 6.4, a general trend is a decrease in the elastic portion of the samples when the fine fraction of droplets is reduced. An exception to this trend was the coarse emulsion, confirming the notion of the smaller droplets mediating the characteristics of the emulsion. While the droplet sizes of the fine and coarse emulsions are

different, the breadth of the droplet size distributions related specifically to the oil droplets are the same (Figure 6.11). Thus, the increase in the elastic portion of the coarse emulsion is associated with the arrangement of the droplets in the system, which may be similar to the fine emulsion. With respect to the results for the emulsion with a 0.25 fraction of fine droplets it is possible that the droplet arrangement does not offer much resistance to the applied torque. When Pal [33] mixed different proportions of emulsions with droplet sizes of 5 and 18 μm he achieved similar results when comparing the storage modulus. He found the lowest storage modulus at a volume fraction of fine around 0.35.

The dynamic results obtained suggest that for a constant proportion of the dispersed phase in the concentrated emulsions, the droplet size and its distribution have a big influence on their viscoelastic properties. Therefore any rheological equations that only consider the dispersed phase concentration cannot accurately estimate rheological information. Thus, a test has to be performed to obtain the real rheological information required for a concentrated emulsion.

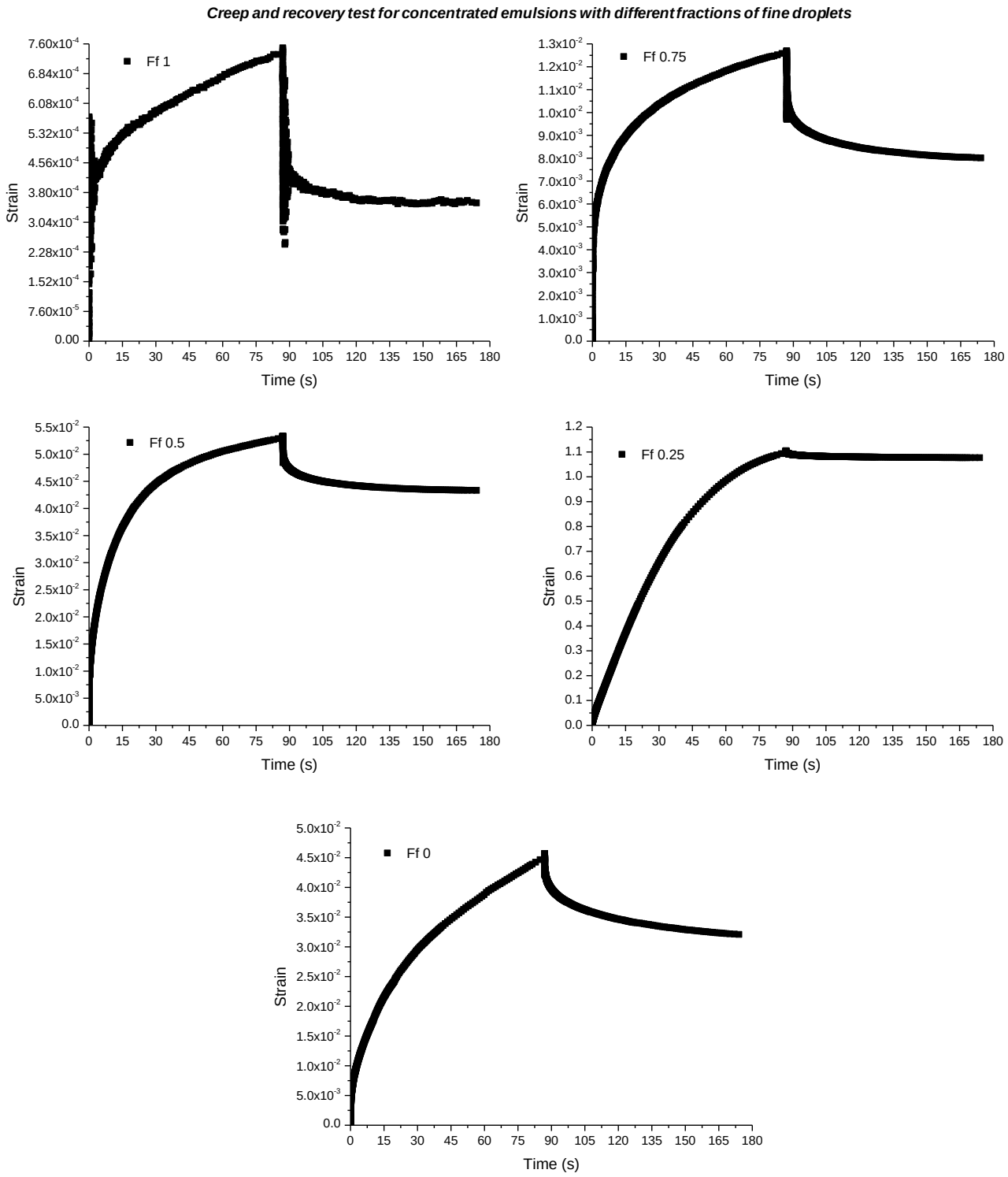

Figure 6.17 Creep and recovery curves for 70 wt% soy bean oil, 1 wt% sodium caseinate and different fine fractions. Phosphate buffer solution at pH 7 and ionic strength 50 mM.

6.2.4 Ionic strength

Proteins are very vulnerable to any physicochemical changes within the systems in which they are located. Changes in the protein conformation and properties are produced by the modification of parameters such as ionic strength and pH [38]. The aim of this section is to evaluate the effects of ionic strength on the rheological properties of sodium caseinate concentrated emulsions, using the results obtained for the different interfaces outlined in Chapter 3. The system studied was a concentrated emulsion with 1 wt% sodium caseinate and oil concentration of 65 wt%; the aqueous phase was a phosphate buffer at pH 6.8 with different ionic strengths.

The rheological properties were evaluated by steady state and dynamic tests. It is important to note that for the analysis of the results, the droplet sizes of the systems were assumed to be constant. This is a reasonable assumption given the droplet size distributions shown in Figure 6.18.

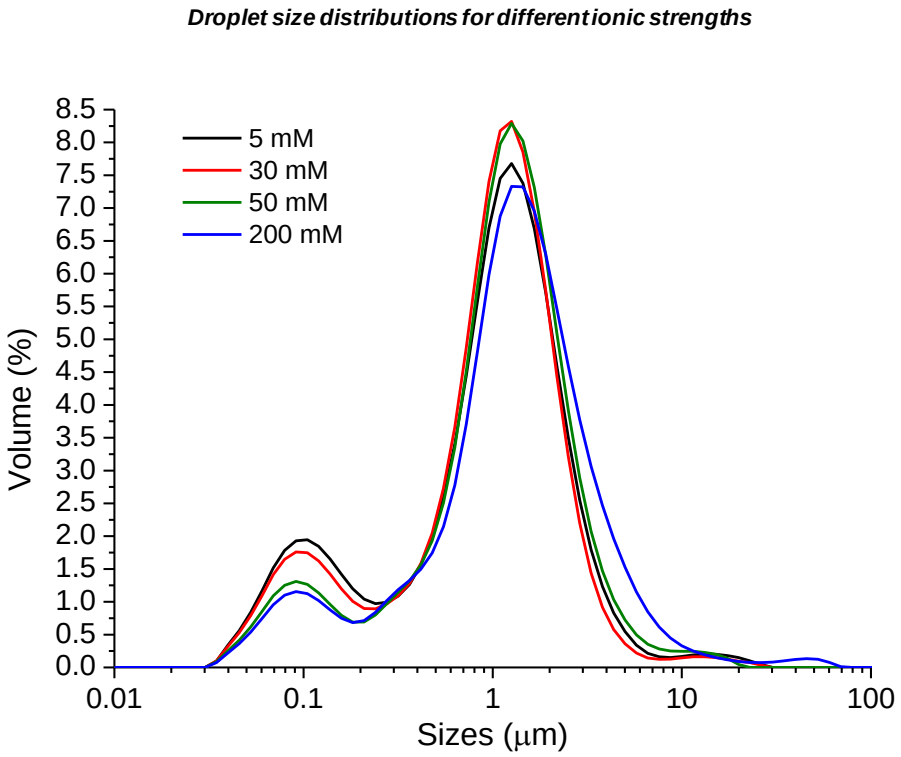

Figure 6.18 Droplet size distributions of concentrated emulsions 65 wt% soybean oil and 1 wt% sodium caseinate with different ionic strengths. Phosphate buffer solution at pH 6.8.

6.2.4.1 Steady state test

The steady state test was performed as a function of ionic strength (see Figure 6.19). All the samples show shear-thinning behaviour with a yield point. In Table 6.5 the yield point, Herschel-Bulkley model parameters and apparent viscosity values as a function of ionic strength are presented. Appendix A4 shows how the data were fitted by the model.

Table 6.5: Values of yield stress and apparent viscosity as a function of the ionic strength

Ionic strength (mM)	τ_y ***(Pa)***	K	n	***Apparent viscosity (Pa.s)****
5	0.12 ± 0.01	0.696 ± 0.009	0.70 ± 0.003	3.19 ± 0.16
30	0.12 ± 0.01	0.384 ± 0.008	0.762 ± 0.005	2.26 ± 0.29
50	0.11 ± 0.02	0.25 ± 0.009	0.817 ± 0.008	1.58 ± 0.24
200	0.07 ± 0.01	0.169 ± 0.005	0.836 ± 0.007	1.15 ±0.16

***The values of apparent viscosity corresponded at shear rate 0.1 s^{-1}**

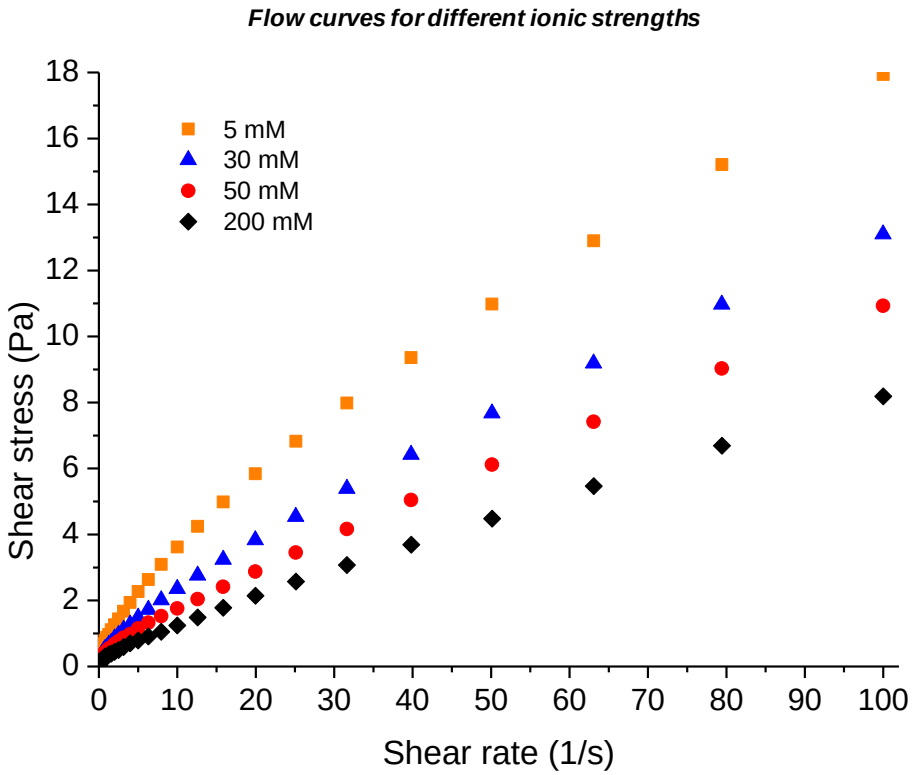

Figure 6.19 Stress vs. shear rate curves for 65 wt% soy bean oil, 1 wt% sodium caseinate and different ionic strengths. Phosphate buffer solution at pH 6.8.

The Herschel-Bulkley model fitted the data adequately with an adjusted R square about 1 and standard errors below 0.02. There is a slight decrease of the yield point

values when the ionic strength is increased. As the oil concentration and droplet size distributions are constant, a similar droplet arrangement should be expected for the different systems. Thus, the small difference between the yield point results is most likely a consequence of the interactions between the droplets, which are produced by the different conformations of the casein molecules at the interface by changing the ionic strength.

The rheological parameters for the Herschel-Bulkley model, K and n, showed clear decreasing and increasing trends respectively as the ionic strength was augmented. According to Estevez [39], a decrease in the flow coefficient or consistency index (K) indicates that the viscosity of the systems is reduced; a rise in the Herschel-Bulkley index or flow behaviour index (n) is related to a reduction in the pseudo-plastic behaviour of the system. Hence, the trend for the K parameter concurs with the decreasing of the apparent viscosity of the systems.

The observed decrease of apparent viscosity, when increasing the ionic strength, is associated with the surface phenomena that are created by the adsorption of the casein molecules at the interface. This is because physical factors such as droplet size distribution and oil concentration are constant. The subphase phenomena are a consequence of the short distance between droplets and the adsorption of ionisable emulsifier, such as proteins [40].

Salager *et al.*[41] explained that surface phenomena can be static or dynamic. They explained that static phenomena are related to the equilibrium between van der Waals attraction forces and electrostatic and steric repulsion forces. Dynamic phenomena occur when a liquid is displaced parallel or tangentially with respect to a surface, i.e., when a shear is applied to the system. A dynamic phenomenon that considerably affects the viscoelastic properties of concentrated emulsions, when the droplets are charged, is known as the electroviscous effect.

Salager *et al.*[41] explained that there are two electroviscous effects. The primary electroviscous effect occurs when the counterions in the diffuse layers are dragged by the movement of the liquid located between two interface charges, producing a charge delocalisation. As a consequence a flow potential is generated, which resists

the movement of the counterions displaced, restricting the flow of the interfacial liquid and increasing the viscosity of the system.

With regards to the second electroviscous effect, Tardos [42] and McKenna [40] explained that this is produced when the double layers of charged interfaces contribute to an increase in the effective diameter of the droplets, increasing steeply the viscosity of the system because of a reduction in the droplet volume fraction (see Equation 6.4).

Hao [43] presented an equation for the electroviscous effect in dilute suspensions, as follows:

$$\eta = \eta_m \left\{1 + 2.5\phi \left[1 + \frac{1}{\sigma \eta_{m r^2}} \left(\frac{\zeta \varepsilon_m}{2\pi}\right)^2\right]\right\} \quad 6.6$$

where η represents the apparent viscosity of the suspension, η_m is the viscosity of the continuous phase, ϕ volume fraction, σ is the conductivity of the suspension, r is the radius of the particle, ζ is the zeta potential of the particle and ε_m is the dielectric constant of the continuous phase. Even though this equation was developed for dilute suspensions, it has been used for qualitative prediction in concentrated emulsions [44]. According to the conformation of the casein molecules at the interfaces, upon increasing the ionic strength reported here (see Section 3.2.4), at a low ionic strength and pH 7 a long fraction of the casein molecules, the hydrophilic residual groups, are immersed in the aqueous phase. This increases the thickness of the layer around the droplets in the emulsions. On the contrary, at high ionic strength and pH 7 the solubility of the residual groups is reduced, forcing them to migrate to the interface, which reduces the thickness of the layer around the droplets. Also, the variation in the thickness of the double layer, upon changing the concentration of the ions in the aqueous phase (see Equation 1.6), contributes to the hydrodynamic radius of the droplets. Therefore by combining the different conformations of the casein molecules (by changing the ionic strength) with both electroviscous effects and Equation 6.6, it is clear that the ionic strength has an effect on the apparent viscosity of sodium caseinate concentrated emulsions (See Table 6.5).

Some examples of the electroviscous effect on the viscosity of concentrated emulsions have been reported in research into crude oil. Plegue *et al.* [44] in their investigation into the viscosity and colloid properties of concentrated crude oil-in-water emulsions found that a decrease of the emulsion viscosity by adding sodium chloride could be associated with a decrease in the electroviscous effects as the ionic strength increased. For their investigation, a crude oil volume fraction of 0.6 was used with two different heavy crudes and the emulsifier used was the natural surfactants present in the oil. They explained that many equations have developed to quantify the electroviscous effect in dilute suspensions and these cannot be applied to concentrated emulsions.

However, the dramatic influence of the electroviscous effect on the viscosity of concentrated dispersion has been demonstrated experimentally. Romero *et al.* [36] investigated the viscoelastic properties and stability of highly concentrated bitumen in water emulsions. For their investigation, they used a volume fraction of bitumen of 0.8 and nonylphenol-ethoxylate as the emulsifier. They found that an increase in the ionic strength produced a decrease in the viscoelastic properties. Also, they found that by increasing the ionic strength they were able to reduce the absorbed layer thickness, decreasing the electroviscous effects on the rheological properties of the emulsions.

6.2.4.1 Dynamic test

The results shown in Table 6.5 are a consequence of droplet interactions, which are generated by the different conformations of the casein molecules at the interface. Hence, dynamic rheological tests were performed to evaluate the viscoelastic properties of the emulsions and to gain information about the interactions between the droplets.

Strain sweep

The results in Figure 6.20 show the viscoelastic behaviour of the emulsions studied at different ionic strengths. It can be seen that the emulsions have a large elastic proportion when varying the strain where the elastic modulus is greater than the viscous modulus. There is a slight increase in G' with the applied strain before the

cross over point; this behaviour was outlined earlier in the discussion about the time-dependence of the concentrated emulsions studied.

As can be seen from Figure 6.20, there is a general decrease in the viscoelastic components of the emulsions as the ionic strength is increased. However, for the systems at ionic strengths of 50 and 200 mM the values of G' and G'' are very similar.

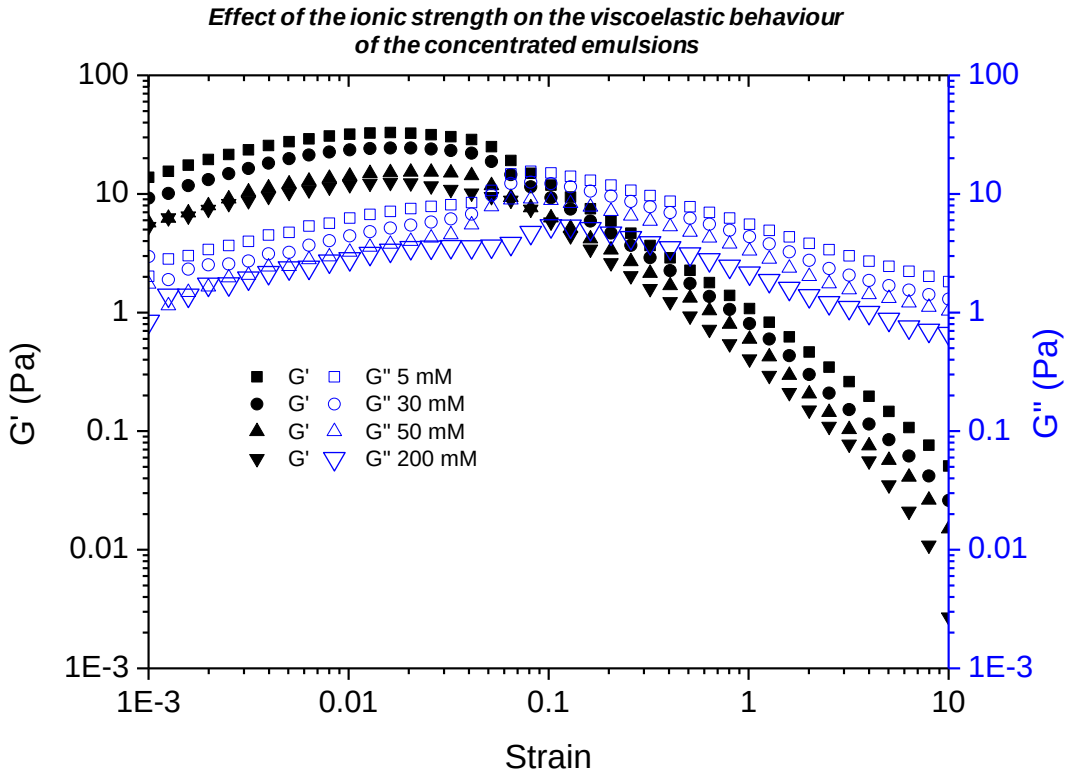

Figure 6.20 Representative log-log plots of strain amplitude dependence of the storage and loss moduli, G' and G'' at 1 Hz, for 65 wt% soy bean oil, 1 wt% sodium caseinate and different ionic strength. Phosphate buffer solution at pH 6.8.

The results shown in Figure 6.20 can also be associated with the electroviscous effects. According to Dickinson *et al.* [45] casein molecules have a large capacity to hold water molecules. At low ionic strengths, the flow of the continuous phase located between two interfaces is resisted by the flow potential generated by the delocalisation of the charge when a strain is applied. This occurs because the low concentration of ions assists the solubility of the hydrophilic part of the casein molecules holding the aqueous phase. When a shear is applied to the emulsion, the hydrophilic parts of the protein molecules attempt to keep the water molecules and ions opposing the shear. As a consequence the viscosity of the system increases, being the contribution of the first electroviscous effect.

The linear disordered chain structure of the casein molecules and the thickness of the double layer, due to the low ionic strength, contribute to an increase in the effective diameter of the droplets. Both factors reduce the droplet volume fraction and increase the viscosity of the system, being the addition of the second electroviscous effect.

Tardos [46] reported similar results, using electrostatically stabilised dispersions and unstable dispersion systems that were weakly flocculated. He inferred that the increase of the viscoelastic parameters G' and G'', on decreasing the ionic strength, was because of the change in the electroviscous effect.

Frequency sweep

In order to investigate the interaction between the droplets generated by the ionic strength, the data for the frequency sweep was used to estimate the parameters of Bohlin's equation. The frequency sweep data is displayed in Figure 6.21. This data shows that the elastic component is higher than the viscous component in the frequencies evaluated, without a cross over point for any of the systems used. The general trend is a decrease in G' and G" as the ionic strength is increased, being consequential with the strain sweep results. The data for the storage modulus was a good fit with Bohlin's equation (see Table 6.6).

The storage modulus data are fit well using Bohlin's equation, and the coefficient of determination for the systems is about one. The parameter associated with the magnitude of the interaction between droplets (A) decreases as the ionic strength is increased. This trend confirms the results of the strain sweep tests. With regards to the coordination number (z), this is almost constant for the different systems, indicating a similar grade of interactions. The results in Table 6.6 can be understood if the interactions between the droplets are very similar in the systems, but their magnitude depends on the conformation of the casein molecules at the interface generated by the ionic strength.

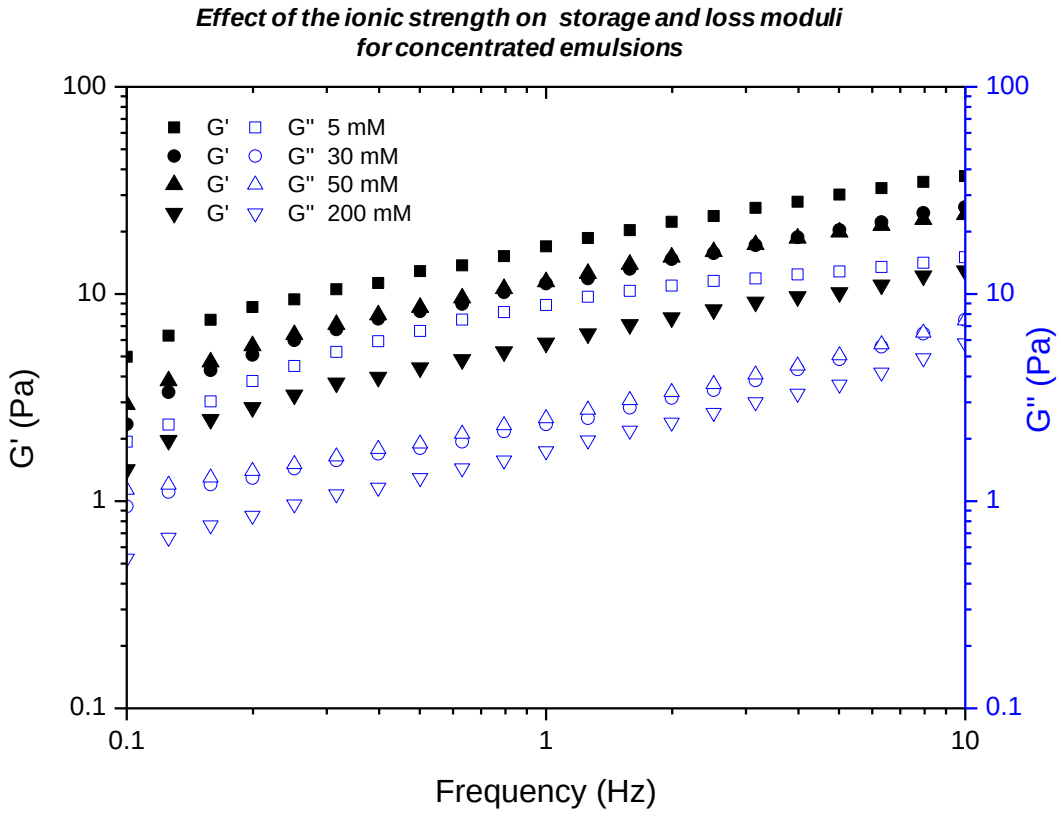

Figure 6.21 Representative curves of storage and loss moduli as functions of frequency (strain 2 %). Concentrated emulsions with different ionic strengths, soy bean oil and 1 wt% sodium caseinate. Phosphate buffer solution at pH 6.8.

Table 6.6: Bohlin's parameters, A and z for different ionic strengths.

Ion strength [mM]	*A [Pa]*	*z [dimensionless]*
5	16.4 ± 0.2	2.69 ± 0.06
30	10.6 ± 0.2	2.46 ± 0.06
50	11.0 ± 0.2	2.75 ± 0.08
200	5.64 ± 0.01	2.65 ± 0.07

Creep-recovery test

Quantification of the viscoelastic components of the emulsions was evaluated at different ionic strengths using creep-recovery tests. Before doing the tests, the torque was set to 1 μN.m using the strain sweep results for G' and G'' as a function of the oscillation torque (Figure 6.22). It can be seen from Figure 6.22 that there is a displacement in the applied torque range to the left as the ionic strength increases.

This result suggests that the interactions between the droplets are weakened by increasing the ionic strength.

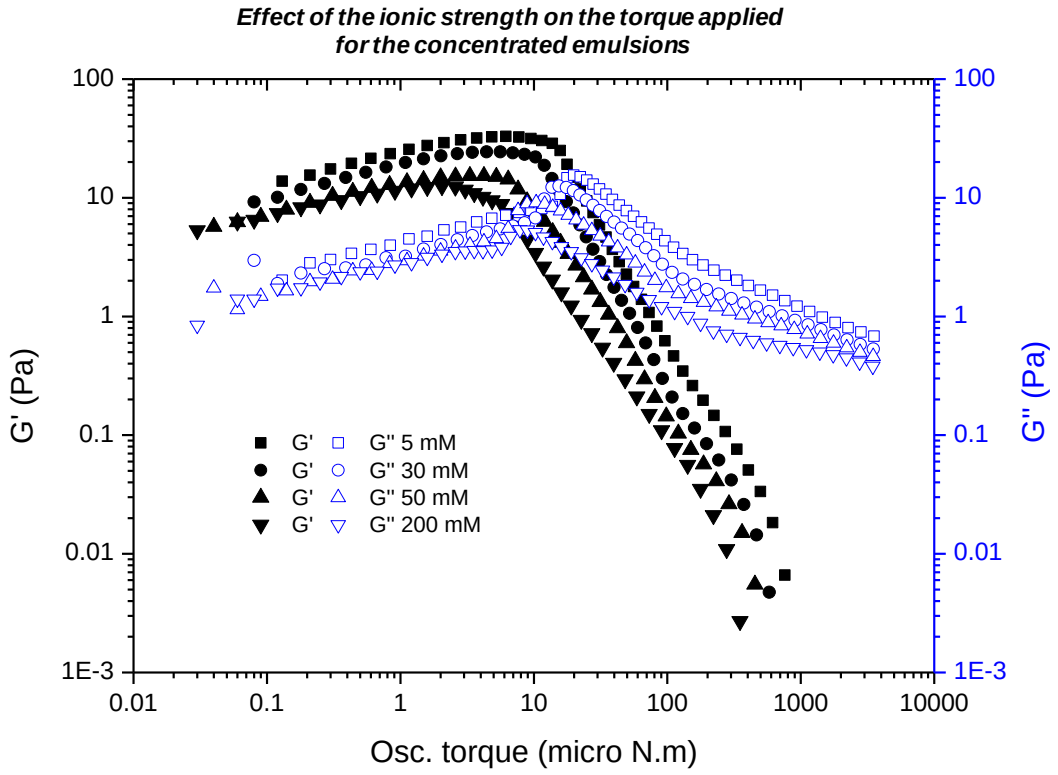

Figure 6.22 Representative log-log plot of the oscillation torque of the storage and loss moduli, G' and G'' at 1 Hz, for 65 wt% soy bean oil, 1 wt% sodium caseinate and different ionic strength. Phosphate buffer solution at pH 6.8.

According to the creep and recovery test results shown in Figure 6.23, all the systems evaluated have viscous and elastic components for the applied torque. The deformation capacity of the systems increases as the ionic strength is augmented. This trend agrees with the results shown for the strain and frequency sweep tests. Table 6.7 displays the results for the creep-recovery test. There is general tendency for a reduction in the elastic component of the systems as the ionic strength is increased (Table 6.7). This result, as well as the maximum deformation trend, agrees with the reduction in the flow behaviour index (n) for the Herschel-Bulkley equation as the ionic strength was increased, indicating a decrease of the pseudo-plastic behaviour of the systems.

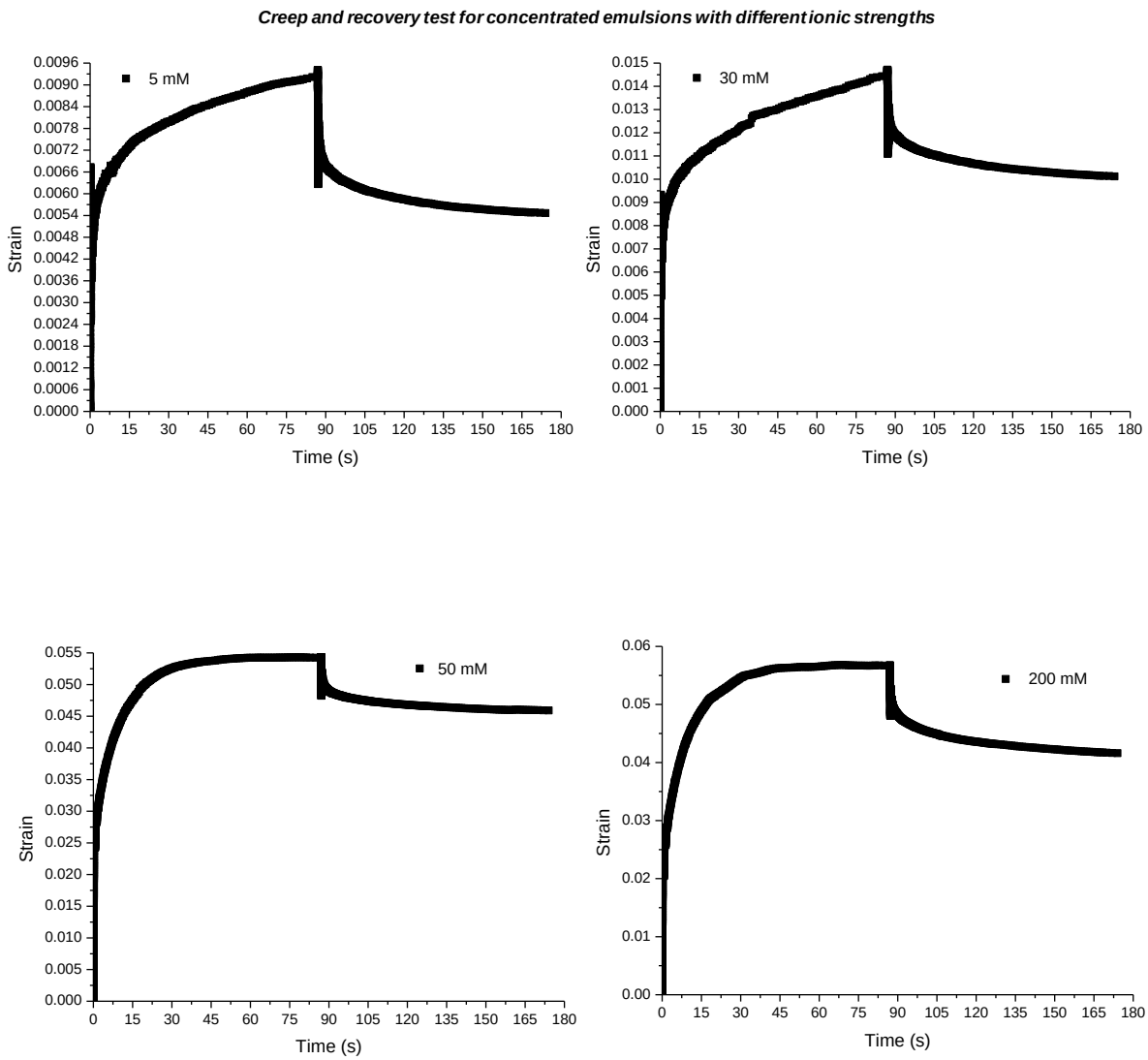

Figure 6.23 Creep and recovery curves for 65 wt% soy bean oil, 1 wt% sodium caseinate and different ionic strength. Phosphate buffer solution at pH 6.8.

The deformation values for the different emulsions investigated (Table 6.7) also agree with parameter A of Bohlin's equation. This is because strong interactions between droplets impede large deformation in the emulsions.

The results for the creep-recovery test, shown in Figure 6.23 and Table 6.7, can be related to the sodium caseinate conformation at the air-water interface in two features. Firstly, according to the information from the Langmuir monolayer of sodium caseinate, at a low ionic strength the hydrophilic part of the protein molecules is immersed in the subphase with a high interaction with the water molecules. Consequently, if the same conformation of the protein molecules is kept

on the interface of the droplets in the emulsion, the first electroviscous effect occurs and increases the elastic portion of the system. Secondly, considering the DLVO theory [47] the thickness of the double layer increases as the ionic strength is reduced. An increase in the double layer augments the effective volume fraction of the droplet, which contributes to the second electroviscous effect.

Table 6.7: Parameters viscoelastic from the creep and recovery test. Concentrated emulsions 65 wt% soy bean oil and 1 wt% sodium caseinate. Phosphate buffer solution at pH 6.8

Ionic strength (mM)	***Maximum deformation***	***Elastic percentage (%)***	***Viscous percentage (%)***
5	$9.25x10^{-3}$	41	59
30	$1.46x10^{-2}$	30	70
50	$5.42x10^{-2}$	15	85
200	$5.67x10^{-2}$	27	73

6.2.5 pH effect

The conformation of sodium caseinate at the air-water and oil-water interfaces is strongly affected by variation of the pH of the aqueous phase (Figures 3.4 and 3.22). Hence as for ionic strength, it is expected that the rheology of the systems investigated here will depend on their pH.

Three systems were evaluated with an oil concentration of 60 wt% and 1 wt% sodium caseinate. The aqueous phases were acetate, phosphate and carbonate buffers with pH values of 5.4, 6.8 and 8.6 respectively, while the ionic strength was 15 mM for all the buffers. The ionic strength of 15 mM and oil concentration 60% was used in order to prevent sodium caseinate precipitation at acidic pH value because of the buffering capacity of sodium caseinate (see Chapter 4). It is important to note that the droplet size distributions were not the same for the systems investigated, as can be seen in Figure 6.24. It was not possible to produce similar size distribution emulsions with different pH values with buffer solutions at ionic strength 15 mM.

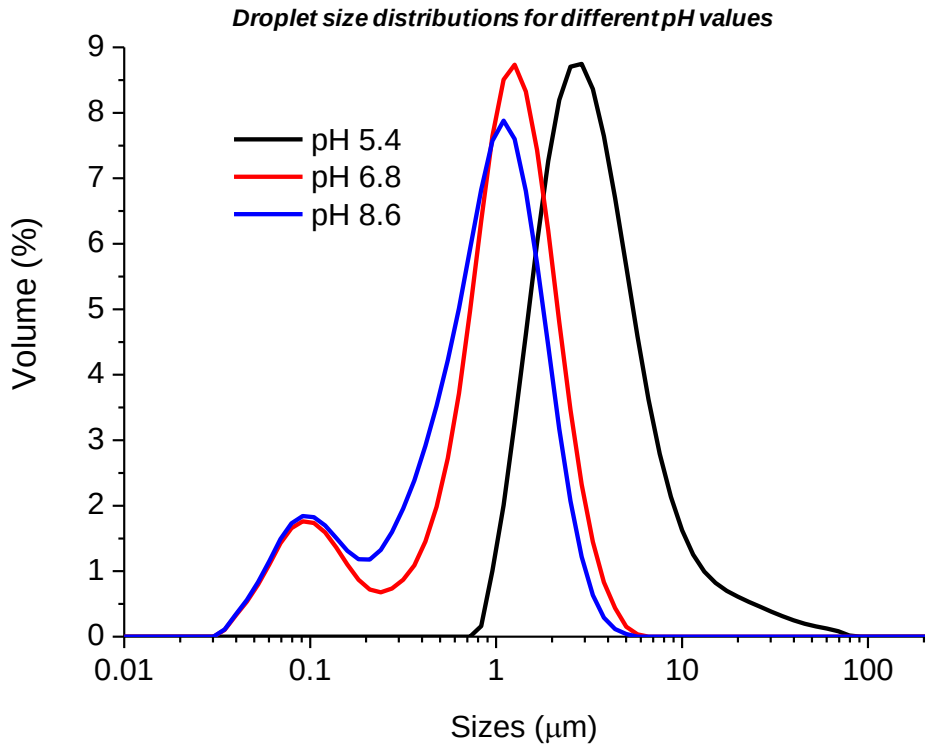

6.24 Droplet size distributions of emulsion with different pH values. Final pH values 5.4 (Acetate buffer), 6.8 (Phosphate buffer) and 8.6 (Carbonate buffer). Emulsions 60 wt% oil, 1 wt% protein and ionic strength 15 mM.

It can be seen from Figure 6.24 that at pH values 6.8 and 8.6 the droplet size distributions are similar. However, at pH 5.4 the droplet size distribution is monomodal with the biggest sized droplets. As was discussed in Chapter 4, the difference in the droplet size distribution for pH 5.4 is a consequence of sodium caseinate aggregation without precipitation. According to the results obtained in this research, for sodium caseinate at the air-water and oil-water interface, the large droplet size distribution for the emulsion at pH 5.4 could be because of aggregation of the caseins molecules. This aggregation reduces the number of individual molecules that are able to sit at the oil-water interface and decreases the interfacial tension. As a consequence, protein aggregates cover a lower interfacial surface area and produce bigger droplets than the individual protein molecules. Dickinson *et al.* [45], in their research with emulsions 40 vol% oil and 2 wt% of β-casein, reported big droplet size at pH near the isoelectric point and they suggested that it was because some droplets were flocculated.

For pH values of 6.8 and 8.6, the similar droplet size distribution can be a consequence of the large number of individual molecules present, since electrostatic repulsion prevents aggregation and the proteins cover more interfacial area thereby generating smaller droplets. Considering the droplet size distributions for the systems studied, an appropriate comparison of the rheological behaviour is not possible due to the dissimilarity between them. Nevertheless, the rheological results conform to the outcomes obtained for sodium caseinate at the air-water and oil-water interfaces.

The microstructure of the emulsions at the different pH values was also investigated by using Cryo-SEM and the representative micrographs are shown in Figure 6.25. The images show that the size distributions are polydisperse for all the systems, as expected from the light scattering data (Figure 6.24). For all the systems there is interconnection between the droplets, which is related to the bridging flocculation mentioned earlier. For pH values of 6.8 and 8.6, oil droplets are spherical and there is separation between them. In the system with a pH of 5.4 the droplets do not have defined forms and their sizes are the biggest. The different microstructures are related to the interaction between the caseins molecules as the pH is changed, which produces different droplet size distributions that affect the rheological responses of the systems.

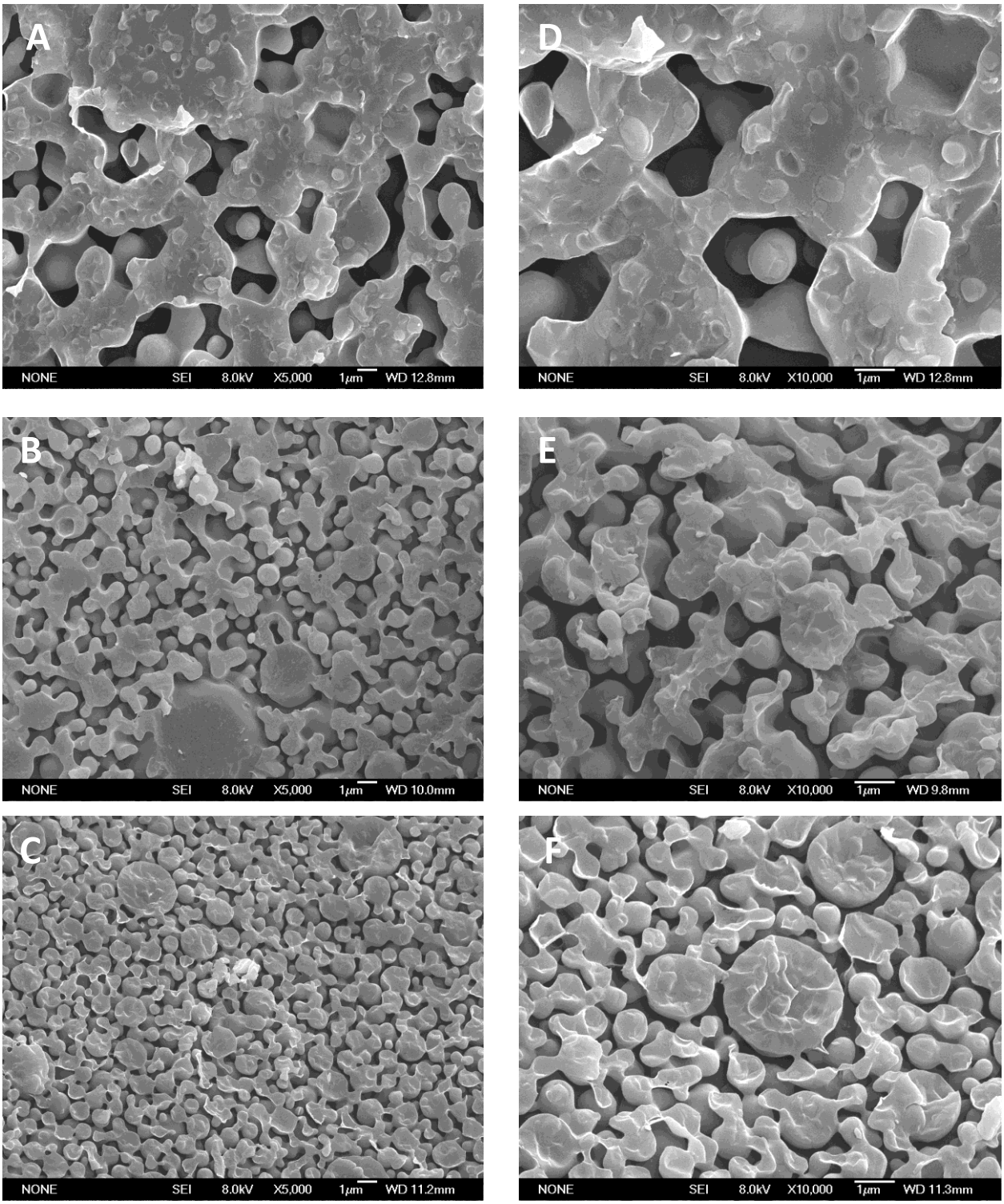

Figure 6.25 Cryo-SEM micrographs of 5000 magnification pH 5.4 (A), pH 6.8 (B) and pH 8.6 (C) and 10000 magnification pH 5.4 (D), pH 6.8 (E) and pH 8.6 (F), for concentrated emulsions with 60 wt% soy bean and different pH values. Buffer solutions at pH and ionic strength 15 mM.

6.2.5.1 Steady state

The flow behaviour for the three pH values used was similar to all other concentrated emulsions studied, i.e. shear-thinning with a yield stress. Table 6.8 gives the yield point and apparent viscosity for the pH values evaluated.

Table 6.8: Values of yield point using Bingham model and apparent viscosity for sample at pH values.

pH	τ_y ***(Pa)***	***Apparent viscosity (Pa.s)****
5.4	4.7 ± 0.4	54.7
6.8	3.3 ± 0.4	28.4
8.6	6.4 ± 0.7	60.8

***The* shear rate used to compare the apparent viscosity was 0.1 s^{-1}**

The Bingham model was used to estimate the yield point for the emulsions evaluated. The highest yield point and apparent viscosity for the systems evaluated was at pH 8.6. In accordance to the model suggested here, for the conformation of caseins at the air-water interface, at pH 8.6 the casein molecules have a long proportion of charged amino-acid residual groups. Therefore, if the same conformation of casein molecules is maintained at the droplet interface, the hydrophilic portion of the protein molecules sits in the water phase resulting in the two electroviscous effects becoming dominant.

At pH 5.4 the lowest yield point and apparent viscosity should be expected, this is because the droplets have the biggest size (see Figure 6.24 and 6.25). However, when proteins are used as emulsifiers, physicochemistry parameters have to be considered. Lam *et al.* [38], in their review of the emulsifying properties of food proteins, using a structure-function approach, showed that pH values have a big impact on the properties of an emulsion. They emphasised that at the isoelectric point, attraction between droplets produces flocculation and the formation of a three-dimensional network. Consequently, the values of viscosity and yield point at the pH 5.4 are more related to the interaction between droplets and generation of the network than the effect of the droplet size (see Figure 6.25). Similar results were reported by Dickinson *et al.* [45] and Chen *et al.* [48] who used milk proteins such as, α_{s1}-casein, β-casein and sodium caseinate to produce emulsions of 40 and 30 vol%

respectively, having high viscosity and elastic components for emulsions formulated close to the isoelectric point.

The lowest values of viscosity and yield point occurred for the emulsion at pH 6.8. This is a direct consequence of the conformation of the protein molecules at the interface. Considering the similar droplet size distribution at pH values 6.8 and 8.6 (Figure 6.24), the only difference between both systems is the protein conformation at the interface due to the change in hydrophobicity of the casein molecules. According to the model obtained by the study of the sodium caseinate at the air-water interface presented in Chapter 3, at pH 8.6 casein molecules are more hydrophilic than at pH 6.8. As a consequence, at neutral pH a proportion of the protein molecules will be located in the water phase generating interactions between the protein and water molecules which are not as strong as for basic pH, where the casein molecules are more hydrophilic. This difference in the interaction between the protein molecules and water might be the cause for the difference in the viscosity of the emulsions at different pH values.

6.2.5.2 Dynamic tests

The microstructures of the samples shown in Figure 6.25 and the different conformations of the sodium caseinate at the interfaces by changing pH, suggest different viscoelastic properties of the concentrated emulsions at diverse pH values. In order to evaluate the elastic and viscous component of the systems studied, strain sweep, frequency sweep and creep-recovery tests were performed.

Strain sweep test

Figure 6.26 shows the strain development of G' and G'' for concentrated sodium caseinate emulsions formed at different pH conditions. All the systems show an elastic-like behaviour, i.e., a storage modulus larger than a viscous modulus, until a strain of about 0.1 where all of them achieve the cross over point . The shape of the G' curves, where a LVE is not present, corroborates the time-dependent behaviour of the systems.

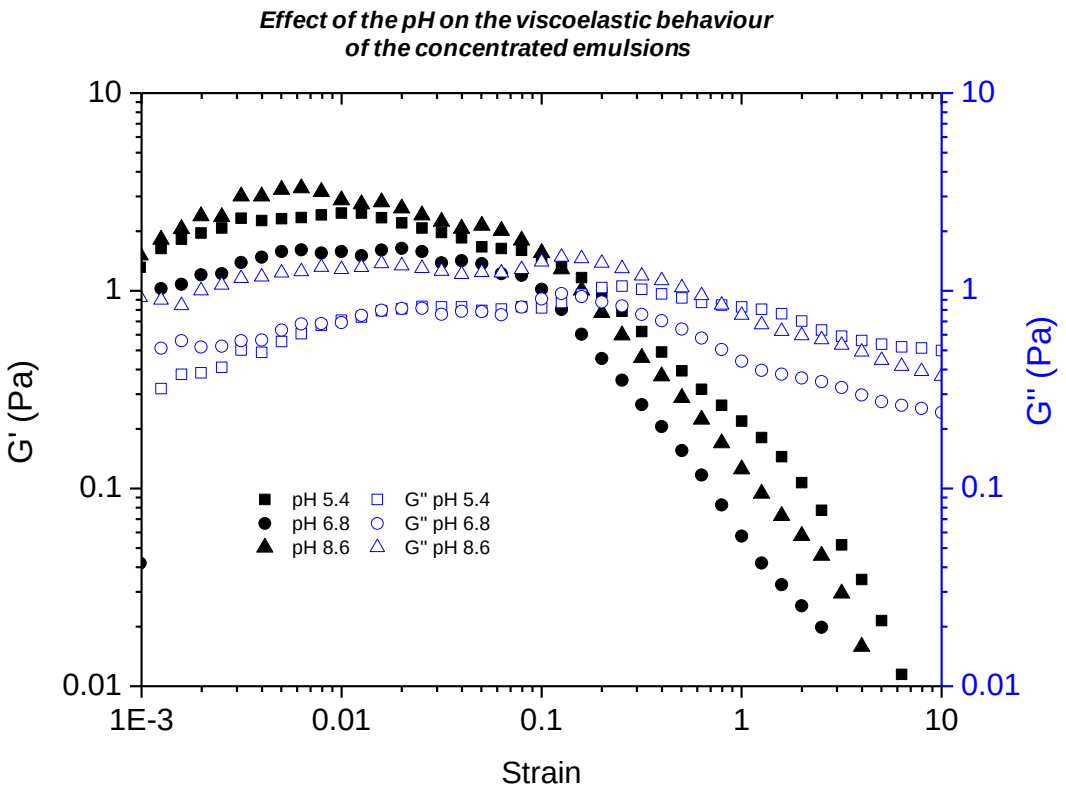

Figure 6.26 Representative log-log plots of strain amplitude dependence of the storage and loss moduli, G' and G" at 1 Hz, for 60 wt% soy bean oil and 1 wt% sodium caseinate emulsions. Acetate (pH 5.4), phosphate (pH 6.8) and carbonate (pH 8.6) buffers at ionic strength 15 mM.

As displayed in Figure 6.26 the storage modulus for the emulsions at pH values 5.4 and 8.6 are relatively similar. Considering the difference in the droplet size distributions for both emulsions (Figure 6.24), it is possible that the similarities in the storage modulus respond to two different interactions: interaction casein molecules-aqueous phase and the interaction between the casein molecules themselves. In accordance with the conformation of the casein molecules at the air-water interface, at pH 8.6 a long portion of the amino-acid residual groups are hydrophilic. The large number of amino-acid residual groups with charge increases the interaction between this part of the protein and the water, generating the electroviscous effect as explained previously. For emulsions at pH 5.4, close to the isoelectric point, a strong attraction between the droplets occurs producing the network structure shown in Figure 6.25. For emulsions at pH 6.8, considering it has similar droplet size distribution as the emulsion at pH 8.6, the lowest storage modulus can be related to the reduced interaction of the casein molecules with the aqueous phase compared with the system at pH 8.6.

Frequency sweep test

For the emulsions at different pH values, parameters for Bohlin's equation were calculated (Table 6.9), using the frequency sweep data show in Figure 6.27.

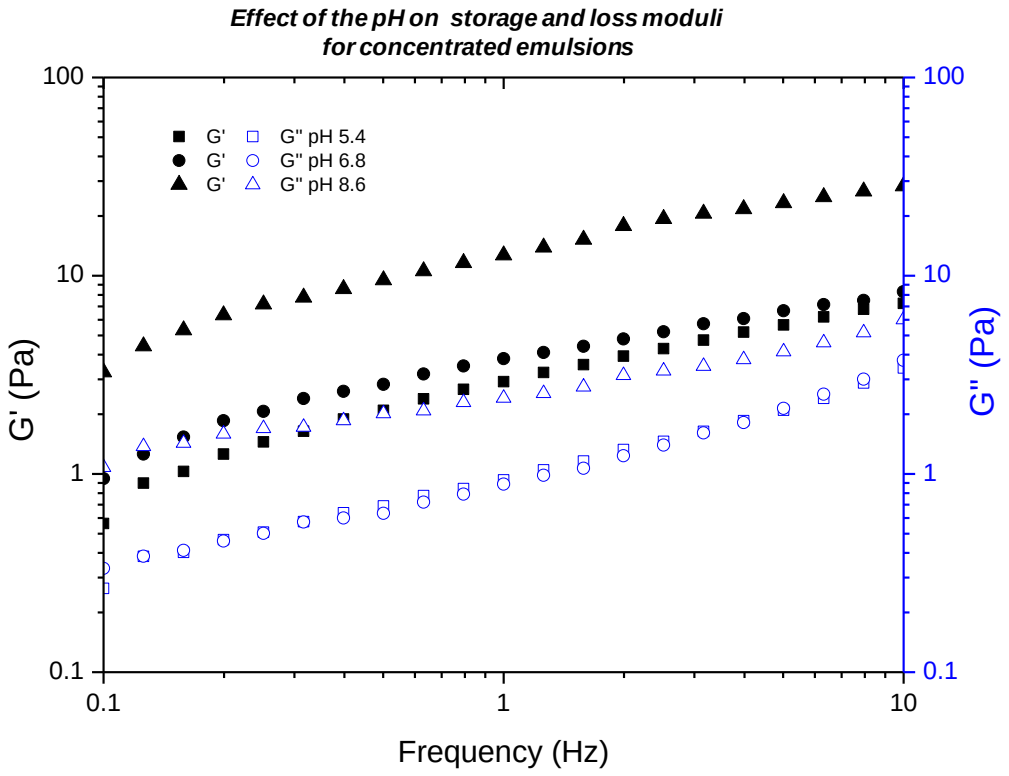

Figure 6.27 Representative curves of storage and loss moduli as functions of frequency (strain 1 %). Concentrated emulsions with 60 wt% soy bean oil and 1 wt% sodium caseinate. Acetate (pH 5.4), phosphate (pH 6.8) and carbonate (pH 8.6) buffers at ionic strength 15 mM.

Figure 6.27 shows that for all the applied frequencies the emulsions have an elastic-like behaviour. The emulsion at pH 8.6 showed the highest elastic modulus values, confirming its large elastic component. For the emulsions at pH values of 5.4 and 8.6 there was a switch in their storage modulus trend compared with their results for the strain sweep.

In Table 6.9 the numerical values of the parameters A and z for Bohlin's equation are given. Comparing the A values for the emulsions at pH 6.8 and 8.6, it can be seen that these correspond with the conformation of the casein molecules at the interface, producing different interactions between the casein molecules and the aqueous phase. This interaction affects the electroviscous phenomenon, which in turn influences the apparent viscosity and elasticity of the systems, as was discussed

earlier. Consequently, the parameter A is also related to the electroviscous effect, if it is associated with the capacity of the aqueous phase to flow. The comparison of the A values for the emulsions at pH values of 5.4 and 8.6, confirms the larger storage modulus for the emulsion at pH 8.6 obtained in the dynamic tests.

With regards to the z parameter, it was almost the same for the emulsions at pH values 6.8 and 8.6. This could be because the type of interactions in the systems is the same, but the magnitude depends on the interaction of the casein molecules-with the aqueous phase. With the system at pH 5.4, the difference could be associated with a different interaction in the system.

Table 6.9: Bohlin's parameters, A and z for different pH values.

pH	***A [Pa]***	***z [dimensionless]***
5.4	2.81 ± 0.04	2.33 ± 0.05
6.8	3.6 1 ± 0.06	2.69 ± 0.07
8.6	12.51 ± 0.24	2.64 ± 0.08

Creep-recovery test

The elastic and viscous components of the three emulsions were estimated by the creep-recovery test with a torque applied of 0.3 μN.m (see Figure 6.28). It can be seen that all the systems showed elastic and viscous components. The largest deformation was for the emulsion at pH 5.4, followed by the systems at pH values of 6.8 and 8.6. The trend for this result concurs with the A values obtained from Bohlin's equation (Table 6.9), which can be easily related to the conformation of the sodium caseinate at the interface for the pH values evaluated and the microstructure of the samples. The results for the elastic and viscous components in the samples can be seen in Table 6.10.

Table 6.10: Parameters viscoelastic from the creep and recovery test at different pH values.

pH	***Maximum deformation***	***Elastic percentage (%)***	***Viscous percentage (%)***
5.4	$1.3x10^{-1}$	88	12
6.8	$3.2x10^{-2}$	66	34
8.6	$2.3x10^{-2}$	66	34

As can be seen in Table 6.10, the emulsion at pH 5.4 has the highest elastic component. This high elastic component in the system can be a consequence of its microstructure network (Figure 6.25), which is produced by the strong attraction between the droplets. As a consequence, the emulsion has a large capacity to recover its microstructure once a stress or torque is removed. For the emulsions at pH values of 6.8 and 8.6, they show similar elastic and viscous components.

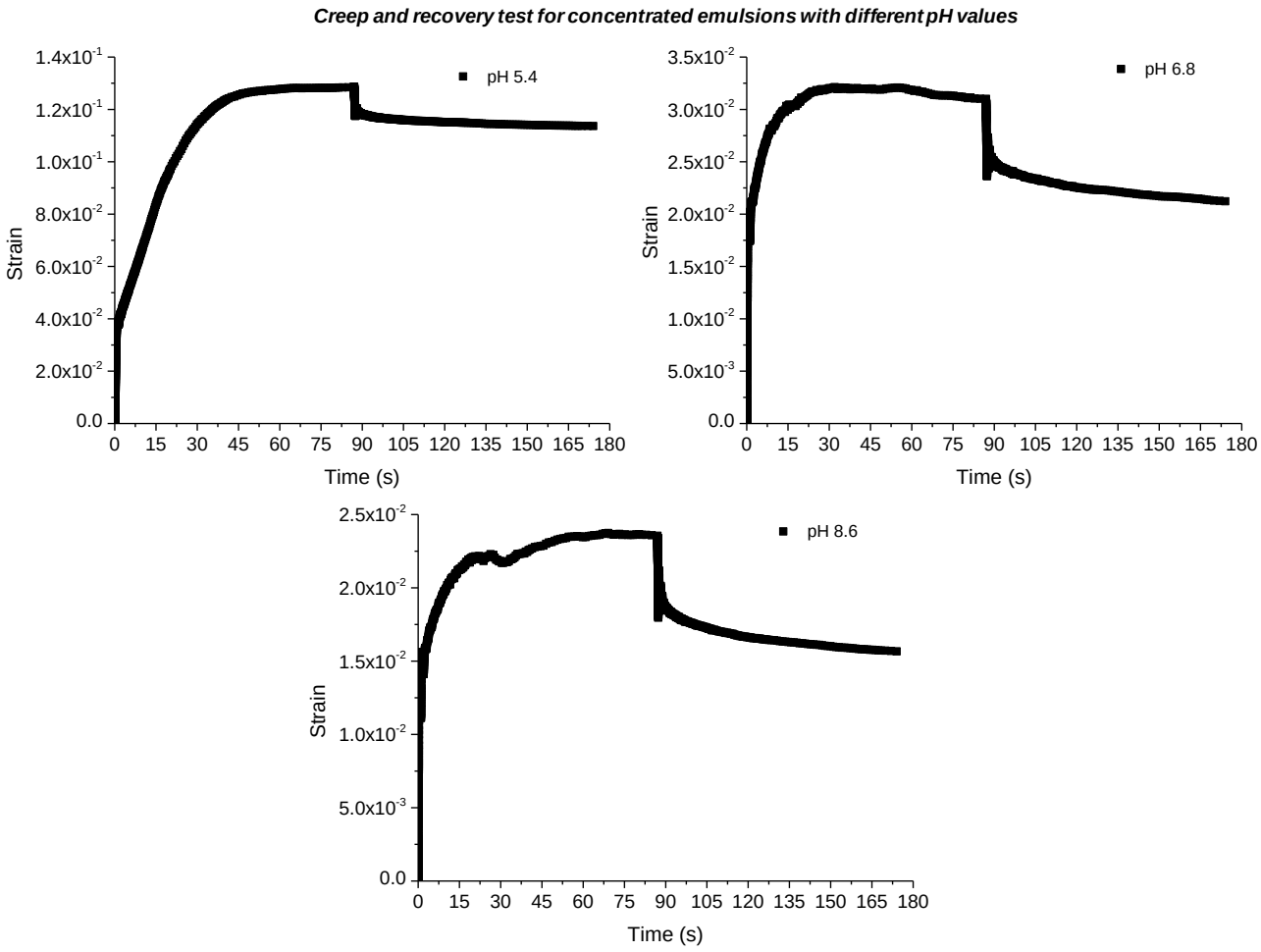

Figure 6.28 Creep and recovery curves for concentrated emulsions with 60 wt% soy bean oil and 1 wt% sodium caseinate. Acetate (pH 5.4), phosphate (pH 6.8) and carbonate (pH 8.6) buffers at ionic strength 15 mM.

However, they showed different deformation capacities that completely agree with their droplet interactions as was mentioned earlier.

Some researchers have shown the effect of pH on the rheological properties of emulsions. Chen *et al.* [48] studied the rheology of sodium caseinate solutions and emulsions with sodium caseinate when acidification was produced by glucone-δ-lactone (GDL). They used different pH values around the isoelectric point, reporting

different rheological behaviours and three-dimensional gel network formation for the pH near isoelectric point. Dickinson *et al.* [45] investigated the stability of casein emulsions changing pH and ionic strength. They used sodium caseinate, α_{s1}-casein and β-casein for the emulsion formulations; they found differences in the rheological behaviour and droplet size distribution.

According to the results shown here, there is a clear connection between the conformation of sodium caseinate at the different interfaces (air-water and oil-water) and the rheological properties of sodium caseinate concentrated emulsions at different pH values. Interactions between the casein molecules and the aqueous phase and between the casein molecules themselves are produced and altered by changing the pH of the aqueous phase. The magnitude of these interactions affects the rheological properties of the concentrated emulsions by electrostatic responses (electroviscous effect) or microstructures of the systems.

6.3 Conclusions

The steady state flow response of concentrated sodium caseinate emulsions is dominated by shear thinning following a yield point andthree distinct flow zones are identified. In the first zone, at a very low shear rate, the forces within the structure itself dominate over the external forces. In the second zone, above the yield point, the emulsions start to flow until a second critical shear rate is reached. In the third zone, the aggregate of droplets are broken. The yield point is a function of the oil concentration, droplet size, droplet size distribution, ionic strength and pH. As rheopexic systems, the emulsions also have atime dependent flow behaviour.

Raising the oil concentration increases the yield point and the apparent viscosity of the concentrated emulsions. The viscoelastic components also increase with the oil concentration. The storage modulus is higher than the viscous modulus for emulsions with oil concentration above 55 wt%. The approach between the droplets as the oil concentration increases generates emulsions with a high elastic component and low capacity for deformation. This is because the interactions between the droplets are increased, which can be quantified according to Bohlin's equation.

In emulsions with different droplet sizes but with a similar breadth of the droplet size distribution, those with smaller droplet size show higher apparent viscosity, yield point and viscoelastic components, but they have a low capacity to be deformed. This behaviour is associated with the increase in the interactions of the droplets and hydrodynamic forces.

For emulsions with a wide droplet size distribution, made by mixing emulsions with different droplet sizes, decreasing the proportion of small droplets decreases the apparent viscosity and viscoelastic components and increases the capacity for deformation. However, the yield point is almost constant. The decrease in the apparent viscosity of the emulsions is associated with the incorporation of small droplets as a part of the continuous phase.

For emulsions with the same oil concentration and droplet size distribution, increasing the ionic strength decreases the apparent viscosity and viscoelastic components, and increases the capacity for deformation. This behaviour is a consequence of the reduction of the electroviscous effect in the system, due to the sodium caseinate molecules changing their conformation at the interface in response to the change in the local electric field. According to the model developed here, increasing the ionic strength reduces the solubility of the hydrophilic parts of the molecules and they migrate to the interface, increasing the effective droplet volume fraction. Moreover, increasing the ionic strength decreases the double layer thickness. Both factors reduce the electroviscous effect of the concentrated emulsions.

Concentrated sodium caseinate emulsions formulated at pH 6.8 have lower apparent viscosity and viscoelastic components than emulsions formulated at pH 8.6 even though the emulsions have the same oil concentration and a similar droplet size distribution. That is the rheological properties of these emulsions depend on the conformation of the casein molecules at the interface. At pH 8.6 the casein molecules have larger hydrophilic portions and a stronger negative charge than at pH 6.8, generating more interactions between the aqueous phase and the hydrophilic components of the proteins. As a consequence, the electroviscous effect increases by increasing the double layer thickness and reducing the effective droplet volume fraction. For pH 5.4 a similar droplet size distribution as that for the systems

at pH 6.8 and 8.6 could not be formulated. However, these emulsions show a high elastic component related to the network produced by the interactions between the droplets.

6.4 References

1. Tan, H.L., *The Microstructure and Rheology of Complex Fluids Coantaining Na-Caseinate*, in *Chemistry* 2010, Victoria University of Wellington

2. Bellalta, P., et al., *Rheological and microstructural characterization of WPI-stabilized O/W emulsions exhibiting time-dependent flow behavior.* LWT - Food Science and Technology, 2012. **46**(2): p. 375-381.

3. Mason, T.G., *New fundamental concepts in emulsion rheology.* Current Opinion in Colloid & Interface Science, 1999. **4**(3): p. 231-238.

4. Derkach, S.R., *Rheology on the Way from Dilute to Concentrated Emulsions.* International Review of Chemical Engineering (I.RE.Ch.E.), 2010. **2**(3): p. 465-472.

5. Ovarlez, G., et al., *On the existence of a simple yield stress fluid behavior.* Journal of Non-Newtonian Fluid Mechanics, 2013. **193**(0): p. 68-79.

6. Masalova, I. and A.Y. Malkin, *Peculiarities of rheological properties and flow of highly concentrated emulsions: The role of concentration and droplet size.* Colloid Journal, 2007. **69**(2): p. 185-197.

7. Foudazi, R., *Models for structure-rheology of highly concentrated emulsions.* CPUT Theses Dissertations, 2009: p. 102.

8. Derkach, S.R., *Rheology of emulsions.* Advances in Colloid and Interface Science, 2009. **151**(1-2): p. 1-23.

9. Schramm, L.L., *Emulsions, foams, and suspensions: fundamentals and applications*2006: John Wiley & Sons.

10. Dickinson, E., *Milk protein interfacial layers and the relationship to emulsion stability and rheology.* Colloids and Surfaces B: Biointerfaces, 2001. **20**(3): p. 197-210.

11. Mezger, T.G., *The Rheology Handbook*. 3 ed2011: Vincentz Network.

12. Briceño, M.I., *Rheology of suspensions and emulsions*, in *Pharmaceutical Emulsions and Suspensions*, F. Nielloud and G. Marti-Mestres, Editors. 2000, Marcel Dekker: NY, USA. p. 557–607.

13. Barnes, H.A., *Thixotropy—a review.* Journal of Non-Newtonian Fluid Mechanics, 1997. **70**(1–2): p. 1-33.

14. Peressini, D., A. Sensidoni, and B. de Cindio, *Rheological characterization of traditional and light mayonnaises.* Journal of Food Engineering, 1998. **35**(4): p. 409-417.

15. Partal, P., et al., *Comportamiento reológico no estacionario de emulsiones aceite en agua estabilizadas con un palmitato de sacarosa.%B 1997.* Grasas y Aceites, 1997. **48**(6): p. 425-436.

16. Malkin, A., et al., *Effect of droplet size on the rheological properties of highly-concentrated w/o emulsions.* Rheologica Acta, 2004. **43**(6): p. 584-591.

17. *Practical Food Rheology*. An Interpretive Approach, ed. I.T. Norton, F. Spyropoulos, and P. Cox2011: Wiley-Blackwell.

18. Barnes, H., *The 'Yield stress myth?' paper - 21 years on.* Applied Rheology, 2007. **17**(4): p. 1-5.

19. Cheng, D.C.H., *Yield stress: A time-dependent property and how to measure it.* Rheologica Acta, 1986. **25**(5): p. 542-554.

20. Maki, K.L. and Y. Renardy, *The dynamics of a viscoelastic fluid which displays thixotropic yield stress behavior.* Journal of Non-Newtonian Fluid Mechanics, 2012. **181–182**(0): p. 30-50.

21. Pal, R., *Shear Viscosity Behavior of Emulsions of Two Immiscible Liquids.* Journal of Colloid and Interface Science, 2000. **225**(2): p. 359-366.

22. Tabakova, S.S. and K.D. Danov, *Effect of disjoining pressure on the drainage and relaxation dynamics of liquid films with mobile interfaces.* Journal of Colloid and Interface Science, 2009. **336**(1): p. 273-284.

23. Gladwell, N., R.R. Rahalkar, and P. Richmond, *Influence of disperse phase concentration upon the viscoelastic behaviour of emulsions.* Rheologica Acta, 1986. **25**(1): p. 55-61.

24. Tang, C.-H. and F. Liu, *Cold, gel-like soy protein emulsions by microfluidization: Emulsion characteristics, rheological and microstructural properties, and gelling mechanism.* Food Hydrocolloids, 2013. **30**(1): p. 61-72.

25. Ma, Z. and J. Boye, *Advances in the Design and Production of Reduced-Fat and Reduced-Cholesterol Salad Dressing and Mayonnaise: A Review.* Food and Bioprocess Technology, 2013. **6**(3): p. 648-670.

26. Gunasekaran, S. and M.M. Ak, *Dynamic oscillatory shear testing of foods — selected applications.* Trends in Food Science & Technology, 2000. **11**(3): p. 115-127.

27. Melnyk, J.P., et al., *Effect of the Hofmeister series on gluten aggregation measured using a high shear-based technique.* Food Research International, 2011. **44**(4): p. 893-896.

28. Laverse, J., et al., *X-Ray Microtomography for Food Quality Analysis*, in *Food Industrial Processes - Methods and Equipment*, B. Valdez, Editor 2012 InTech.

29. Zaidel, D.N.A., I.S. Chronakis, and A.S. Meyer, *Stabilization of oil-in-water emulsions by enzyme catalyzed oxidative gelation of sugar beet pectin.* Food Hydrocolloids, 2013. **30**(1): p. 19-25.

30. Yilmaz, M.T., et al., *Characterization of O/W model system meat emulsions using shear creep and creep recovery tests based on mechanical simulation models and their correlation with texture profile analysis (TPA) parameters.* Journal of Food Engineering, 2012. **108**(2): p. 327-336.

31. Ghannam, M.T., *Creep–recovery experimental investigation of crude oil–polymer emulsions.* Journal of Applied Polymer Science, 2004. **92**(1): p. 226-237.

32. Ramirez, M., et al., *Drop size distribution and its effect on O/W emulsion viscosity.* Journal of dispersion science and technology, 2002. **23**((1-3)): p. 309-321.

33. Pal, R., *Effect of droplet size on the rheology of emulsions.* AIChE Journal, 1996. **42**(11): p. 3181-3190.

34. Romero, A., F. Cordobés, and A. Guerrero, *Influence of pH on linear viscoelasticity and droplet size distribution of highly concentrated O/W crayfish flour-based emulsions.* Food Hydrocolloids, 2009. **23**(2): p. 244-252.

35. Aveyard, R. and J.H. Clint, *Foam and thin film breakdown processes.* Current Opinion in Colloid & Interface Science, 1996. **1**(6): p. 764-770.

36. Romero, N., et al., *Viscoelastic properties and stability of highly concentrated bitumen in water emulsions.* Colloids and Surfaces A: Physicochemical and Engineering Aspects, 2002. **204**(1–3): p. 271-284.

37. Pal, R., *Rheology of Particulate Dispersions and Composites*2007: CRC Press, Taylor & Francis Group. 440.

38. Lam, R.S.H. and M.T. Nickerson, *Food proteins: A review on their emulsifying properties using a structure–function approach.* Food Chemistry, 2013. **141**(2): p. 975-984.

39. Estévez, A.M., B. Escobar, and M. Sepúlveda, *Physical and rheological characterization of seeds of three legume trees.* Idesia (Arica), 2012. **30**: p. 83-91.

40. *Texture in food Volume 1*. Semi-solid foods, ed. B.M. McKenna. Vol. 1. 2003: Woodhead Publishing. 448.

41. Salager, J.L., *Infleuencia de la formulacion sobre las propiedades de las espumas*, in *Cuadernos FIRP*, L. FIRP, Editor 1999, Universidad de los Andes Merida, Venezuela.

42. Tadros, T.F., *Fundamental principles of emulsion rheology and their applications.* Colloids and Surfaces A: Physicochemical and Engineering Aspects, 1994. **91**(0): p. 39-55.

43. Hao, T., *Electrorheological Fluids*. 1 ed. The Non-aqueous Suspensions2005: Elsevier Science. 578.

44. Plegue, T.H., et al., *Viscosity and colloidal properties of concentrated crude oil-in-water emulsions.* Journal of Colloid and Interface Science, 1986. **114**(1): p. 88-105.

45. Dickinson, E., M.G. Semenova, and A.S. Antipova, *Salt stability of casein emulsions.* Food Hydrocolloids, 1998. **12**(2): p. 227-235.

46. Tadros, T.F., *Use of viscoelastic measurements in studying interactions in concentrated dispersions.* Langmuir, 1990. **6**(1): p. 28-35.

47. *Emulsion Formation and Stability*, ed. T.F. Tadros2013: Wiley-VCH Verlag GmbH & Co. KGaA. 272

48. Chen, J., E. Dickinson, and M. Edwards, *Rheology of Acid-Induced Sodium Caseinate Stabilized Emulsion Gels.* Journal of Texture Studies, 1999. **30**(4): p. 377-396.

Chapter 7 Conclusions and Future Work

7.1 Conclusions

Sodium caseinate has been used extensively in the formulation of food and pharmaceutical emulsions and foams. However, a systematic investigation of its conformation at the air-water and oil-water interfaces upon changing ionic strength and pH has not been reported. The motivation of this research was essentially to understand the behaviour of sodium caseinate at an interface and use the information obtained to formulate concentrated emulsions. The resulting stability and rheological response of the emulsions were correlated with the behaviour of sodium caseinate at an interface. Different conformational states of sodium caseinate at the air-water interface could be realised by changing the ionic strength and pH values of the aqueous phase. The different conformations of the sodium caseinate at the air-water are associated with:

1. Alterations of the hydrophilic-hydrophobic character of the residual groups present in the casein molecules upon changing the pH of the aqueous phase. As the hydrophobicity of the amino-acid residual groups within the casein molecules is increased in response to pH changes, the interfacial area covered by the proteins is correspondingly increased. This behaviour was found to occur at pH values below the isoelectric point of sodium caseinate (4.6-5). On the other hand, enhancing the relative fraction of hydrophilic amino-acid residual groups reduces the interfacial area occupied by the casein molecules. This occurs because a long portion of the protein molecules is immersed in the aqueous phase. For the sodium caseinate this behaviour happens for basic pH conditions. Additionally, the elasticity of sodium casein monolayers at the air-water interface is a function of the aqueous phase pH. Around the isoelectric point, sodium caseinate monolayers display the highest elasticity because of the attraction between the casein molecules. At pH values far from the isoelectric point, the elasticity of the monolayer decreases due to electrostatic repulsion between the casein molecules.

2. The solubility of sodium caseinate is reduced by increasing the ion concentration of the aqueous phase. For the pH values evaluated an increase in the interfacial area covered by the caseins molecules was achieved when the ionic strength was increased. This behaviour is due to the reduction of the solubility of the hydrophilic residual groups in the casein molecules, which obliges them to migrate from the aqueous phase to the interface.

The results from the study of the sodium caseinate at the air-water interface were supported by the investigation of the oil-water interfacial tension of sodium caseinate, using the pendant drop technique. The interfacial tension decreased as the pH increased with this behaviour associated with the interaction between the hydrophilic portions of the casein molecules and the aqueous phase. Increasing the ionic strength decreases the interfacial tension for evaluated pH. This is related to the reduction in the solubility of the hydrophilic fractions of the casein molecules, which in turn increases the interfacial area occupied by the casein molecules. These results support those obtained for the air-water interface experiments, despite the differences in the geometry of the interface and the phases investigated. Thus, using the Langmuir monolayer at the air-water interface is an appropriate model for the oil-water interface in emulsions prepared with sodium caseinate.

Protein molecules have the capacity to behave as an acid or base depending on the subphase pH. Hence, the buffer capacity of sodium caseinate was investigated in order to aid in evaluating the behaviour of sodium caseinate solutions and sodium caseinate concentrated emulsions at very low ionic strengths (below 10 mM). For sodium caseinate, high buffer capacities are observed at pH values of 5 and 10.4. The capacity of sodium caseinate to control the final pH of the sodium caseinate-buffer solution increased when the buffer solutions had ionic strengths between 2.5 and 5 mM or the ratio of the protein mass to buffer mass (mP/mB) was increased. Also, precipitation of sodium caseinate occurred when the pH of the buffer solution was around the isoelectric point and the ionic strength was above 10 mM.

Concentrated emulsions were formulated using the buffer capacity of the sodium caseinate to control the final pH of the solution. The droplet size distributions for the emulsions formulated were bimodal, except emulsions at pH near 5 that were monomodal with droplet sizes bigger than the rest of the pH values. All the

emulsions demonstrated bridging flocculation and creaming. The creaming rate depends on the oil droplet size, being a direct relationship between the droplet size and the creaming rate. Thus, pH and ionic strength are not parameters that control the destabilization process of sodium caseinate concentrated emulsions. The stability of emulsions having wide droplet size distributions depends on the fraction of small droplets; increasing the stability as the fraction of small droplets is increased.

All emulsions show shear thinning behaviour with a yield point. The value of the yield point depends on the oil concentration, droplet size, droplet size distribution, pH and ionic strength. Emulsions with oil concentrations above 55 wt% are viscoelastic. The yield point and apparent viscosity increase as the oil concentration increases. For emulsions with wide droplet size distributions the viscoelastic properties (apparent viscosity and viscoelastic components) increases as the small size fraction increases, the yield points are almost constant when the fraction of small sized droplets decreases to ~50%. The increase in the yield point, apparent viscosity and viscoelastic components of the emulsions with pH and ionic strength is associated with the change in the conformation of the sodium caseinate molecules at the oil-water droplet interfaces. These rheological properties increase when the ionic strength decreases or the pH is increased. This trend is the result of the hydrophilic parts of the casein molecules having a high interaction with the water molecules in the aqueous phase and the increasing importance of the electroviscous effect in these systems.

Sodium caseinate has an excellent versatility to be used as an emulsifier for formulation of concentrated emulsions. The formulation of concentrated emulsions with different droplet size distributions, stability and rheological behaviours are able to be achieved by changing the physicochemical environment of the aqueous phase.

The rheological behaviour of the sodium caseinate concentrated emulsions is well described by the associated changes in the conformation of sodium caseinate at the hydrophilic/hydrophobic interface. This characteristic is very useful in the food or pharmaceutical industries to produce formulate emulsions with different textures and viscoelastic properties.

7.2 Future Work

The techniques used in this research to investigate the different conformations of sodium caseinate at the air-water and oil-water interfaces, to change ionic strength and pH values, were the Langmuir trough, surface potential and pendant drop. The integration of their results allowed a model of conformation of sodium caseinate at the interfaces to be developed. However, those techniques do not provide information about the thickness of the protein adsorbed and the visual microstructure of protein molecules assembly at the interfaces. Some techniques that can be used to measure the thickness of the monolayer and its variation by changing pH and ionic strength are: ellipsometry, atomic force microscopy (AFM) and low angle X-ray reflectivity. On the other hand, fluorescence and Brewster angle microscopes can be used to observe microstructures of monolayers at the air-water interface. An important extension to the investigation of sodium caseinate at the interfaces would be to use a technique to measure the thickness of the monolayer and another one to visualise the microstructure at the interfaces. The results obtained with these techniques would allow the models developed and proposed in this thesis work for sodium caseinate at the air-water and oil-water interfaces to be authenticated.

It is well known that ions have a considerable influence on the protein conformation due to the effect of salting-in and salting-out. These effects were studied originally by Hofmeister and much research has been published about this issue. In the evaluation of the conformation of sodium caseinate at the interfaces, diverse buffer solutions were used to achieve different pH values. It would be interesting to investigate the effect of different ions in solution, with the same pH and ionic strength, as used to investigate the conformation of sodium caseinate at the interface. Subsequently, the same ions can be used to formulate concentrated emulsions and evaluate their effect on the properties of the emulsions. The information acquired from this additional investigation would extend the characterisation of sodium caseinate as an emulsifier.

For the study of the sodium caseinate at the oil-water interface, the measurement time for the pendant drop technique was set to 20 minutes without waiting for the equilibrium to be achieved. Despite the objective of this research being to use the oil-water interface to compare the results with those obtained in the air-water interface

when ionic strength and pH were changed; it would be useful to do a complete study of the kinetics of adsortion of sodium caseinate at the oil-water interface by changing the parameters investigated to provide more complete information about the behaviour of sodium caseinate at the oil-water interface

Another parameter that is crucial to the formulation of emulsions that could have been investigated was the condensed non-polar phase. Thus, it would be interesting to evaluate the conformation of sodium caseinate at the interface with different non-polar phases using aliphatic, aromatic and vegetable oils with different fatty acid compositions. After that it would be valuable to formulated sodium caseinate concentrated emulsions with the same non-polar phases and look for possible correlations. This additional investigation would produce results that could be applied within the food and pharmaceutical industries where different non-polar phases are used.

The electroviscous phenomenon of sodium caseinate concentrated emulsions has a significant effect on the observed rheological properties of the emulsions. Also, there was a clear relationship between the electroviscous effect on the emulsions and the sodium caseinate conformation at the interface in the model developed. Thus, because the electroviscous effect is typical for long polymers or proteins with linear conformation, as is the case of caseins, it would be interesting to use different proteins with linear and non-linear structures and evaluate the electroviscous effect of the rheology of their concentrated emulsions.

The additional work suggested will be useful in more fully characterising the behaviour and response of sodium caseinate at the air-water and oil-water interfaces and thereby to ensure greater understanding of its function as an emulsifier.

Appendix A1 Calculation of data uncertainty

In this appendix, the methodology used to determine the uncertainty of all the experimental data obtained in this research is described, and an example is outlined.

The calculation of uncertainty was approximated via the t-Student distribution with two degrees of freedom (n-1), and assuming that the data are independent and normally distributed. The reason why the t-Student is used is because the sample size is small (n=3) and the central limit theorem cannot be applied to use the normal distribution.

The results were stated using the 95% confidence interval as follows:

$$X_m \mp t \times \left({}^{s_m}/_{\sqrt{n}} \right) \qquad (1)$$

where X_m is the arithmetic media for sample m, t is the percentile for a 5% significance level in a t-Student distribution with two degrees of freedom, s_m is the standard deviation for sample m and n is the number of observations (n = 3). The confidence level used for the data was 95% which corresponds to the percentiles 4.3027 in a t-Student distribution. The second term in the expression (1) is the margin of error and quantifies the error of the data.

Figure 1 shows three isotherms for a sodium caseinate monolayer for a specific system and Table 1 displays some of the resulting isotherms data and the parameters required to determine the uncertainty of the data.

Figure 2 shows the surface pressure average values including its related 95% confidence interval, for each area evaluated to obtain the isotherm for sodium caseinate at the air/water interface. The minimum and maximum standard deviations obtained for the example used were 0.01 and 0.34 mN/m respectively.

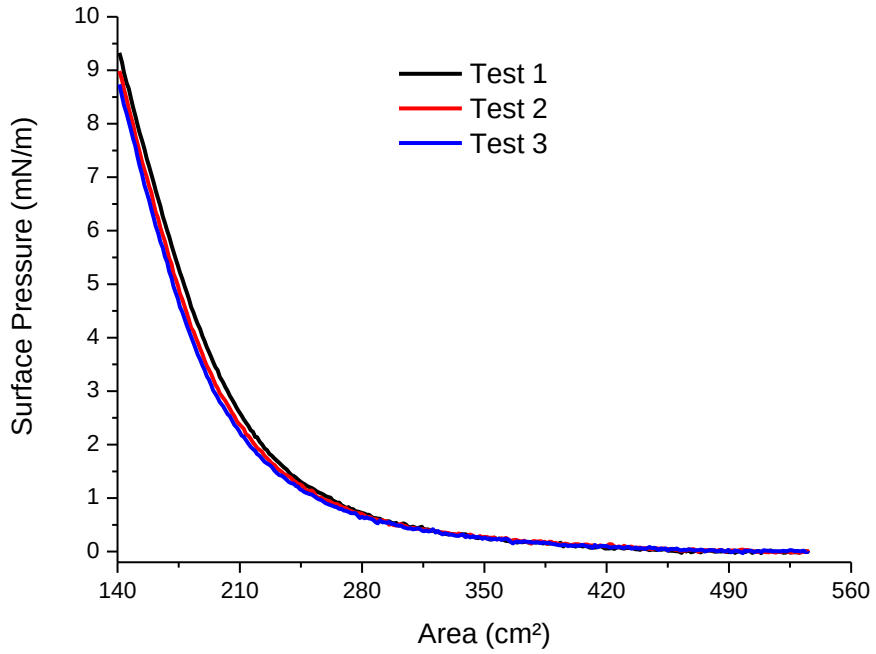

Fig.1. π-A isotherms for sodium caseinate spread at the air/water interface. Subphase: phosphate buffer, pH 7 and ionic strength 45 mM.

Table 1. Data of area and surface pressure (S.P.) from the isotherms in Fig.1 used to calculate the different parameters required to obtain the uncertainty of the results.

Area [cm²]	**S.P. (1) [mN/m]**	**S.P. (2) [mN/m]**	**S.P. (3) [mN/m]**	X_m **[mN/m]**	S_m **[mN/m]**	**[E] [mN/m]**	X_m**+ E [mN/m]**	X_m**- E [mN/m]**
535	-0.01	-0.02	0.00	-0.01	0.01	0.03	0.02	-0.04
500	0.01	0.03	0.01	0.02	0.01	0.03	0.05	-0.01
400	0.12	0.13	0.10	0.12	0.01	0.03	0.15	0.09
300	0.48	0.51	0.49	0.49	0.01	0.03	0.52	0.46
200	3.17	2.88	2.72	2.92	0.22	0.56	3.48	2.36
145	8.77	8.46	8.20	8.47	0.28	0.71	9.18	7.76
141	9.33	8.99	8.74	9.02	0.30	0.73	9.75	8.28

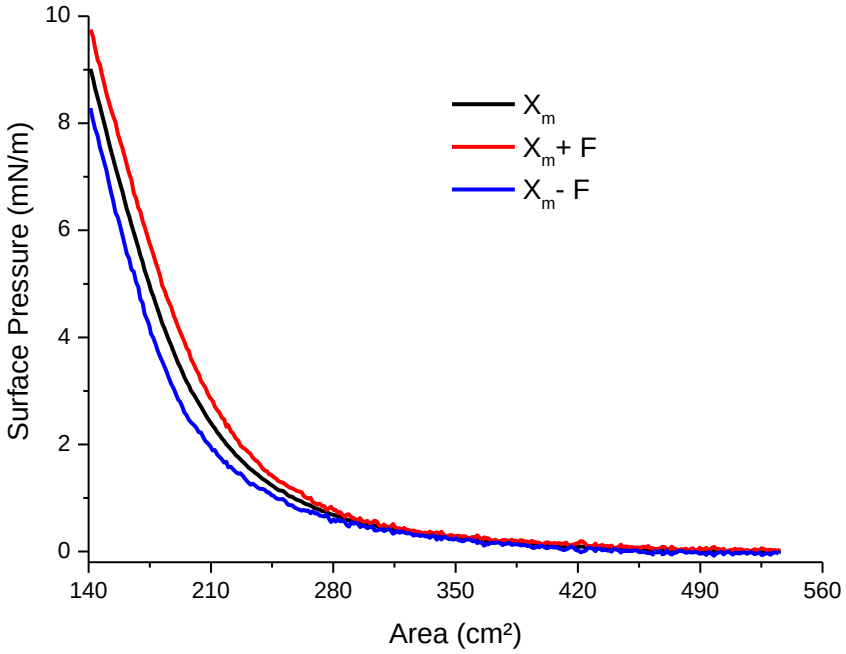

Fig.2. Surface pressure average values including they related 95% interval of confidence over three samples.

Appendix A2 Estimation of phase transition points for sodium caseinate isotherms at the air/water interface

The methodology used to estimate the transition points between the LE-LC and LC-S phases of the sodium caseinate isotherms at the air/water interface was the same reported by Rodriguez et al[(1)]. They fitted the data for each phase to a line, according to a viral equation applied to the π-A isotherm, and the point of intersection of two consecutive lines estimates the transition point. The end of the gas phase was set as the interfacial area where the surface pressure is equal to 0.1 mN/m.

Figure 1 shows the isotherm for the data generated by the software NIMA 702.

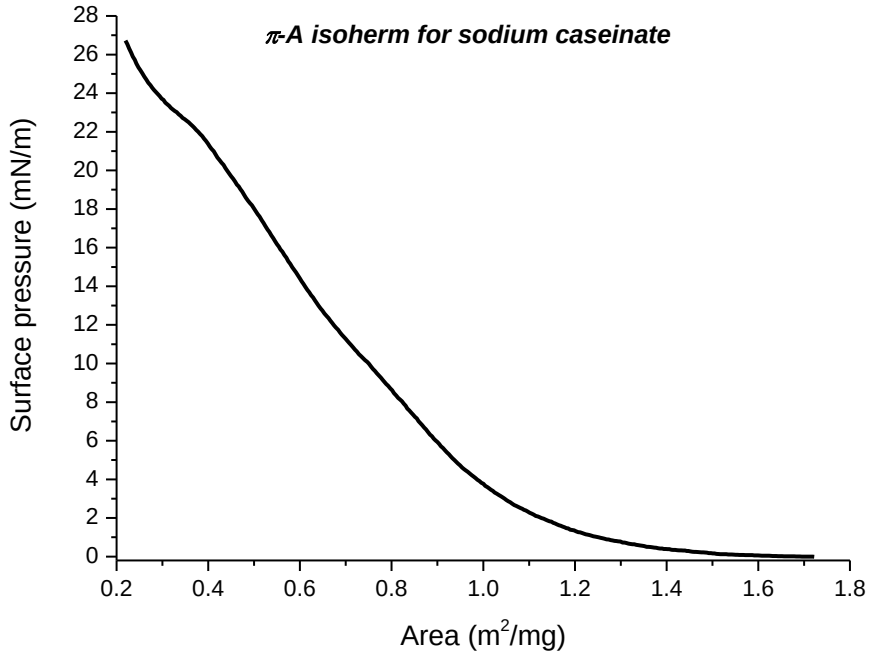

Figure 1. π-A isotherms for sodium caseinate spread at the air/water interface: subphase pH 6.7, phosphate buffer. Ionic strength: 63mM, 0.031 mg of sodium caseinate present at the interface.

(1) Rodriguez, J.M. et al. Food Hydrocolloids 13 (1999) 401-408

The graph estimation of the phases was done tracing the line that fits the experimental points using the method of least squares of Excel with coefficient of

determination (R^2) not below 0.91. Figure 2 shows the line for each phase, Table 1 shows the adjusted equation and coefficient of determination for each line, and Table 2 displays the transition points for the isotherm.

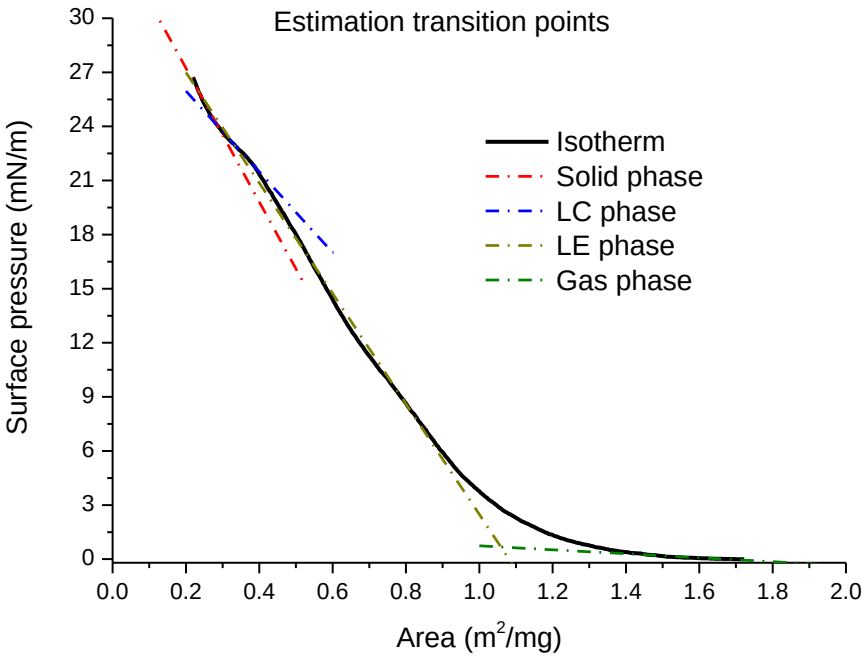

Figure 2. π-A isotherms for sodium caseinate spread at the air/water interface and lines of the different phases: subphase pH 6.7, phosphate buffer. Ionic strength: 63mM, 0.031 mg of sodium caseinate present at the interface.

Table 1 Equation adjusted for each phase and coefficient of determination for the isotherm in Figure 2.

Phases	***Equation of the line****	***R^2***
Liquid-expanded	Y= -30.635X+33.119	0.99
Liquid-condensed	Y= -22.4X+30.422	0.99
Solid	Y= -37.071X+34.643	0.98

*Y and X represent the surface pressure (mN/m) and the area (m^2/mg) respectively.

Table 2 Phase transition points for the isotherm in Figure 2.

Phase Transition	***Area (m^2/mg)***	***Surface pressure (mN/m)***
End of gas phase	1.54	0.10
LE-LC	0.33	23.08
LC-S	0.28	23.98

Appendix A3 Changing ionic strength in buffer solutions

Generally, changes in the ionic strength of an aqueous solution are achieved by adding electrolytes (salts). In systems where protein molecules are present, incorporating electrolytes affects the properties of proteins because of their high sensitivity to the electrolyte ions.

In this research, it could be seen that changes in the ionic strength not only significantly affected the conformation of sodium caseinate at the air-water and oil-water interface, but also the rheological properties of concentrated emulsions with sodium caseinate. As a consequence, a procedure was developed to change the ionic strength in a buffer solution using only the buffer components. Changes in the ionic strength, for the different buffers solutions used, were achieved by combining the chemical equations of the buffer components, the equation to calculate the pH of a buffer system (Henderson-Hasselbalch equation) and the ionic strength equation. The chemical equations for the buffer components used were:

- Acetate buffer

$$CH_3COONa \rightarrow CH_3COO^- + Na^+ \quad (1)$$

$$CH_3COOH \rightleftarrows CH_3COO^- + H^+ \qquad \boldsymbol{pK_{a1} = 4.76} \quad (2)$$

- Phosphate buffer

$$Na_2HPO_4 \rightarrow 2Na^+ + {HPO_4}^{-2} \quad (3)$$

$$KH_2PO_4 \rightarrow K^+ + {H_2PO_4}^- \quad (4)$$

$${H_2PO_4}^- \rightleftarrows H^+ + {HPO_4}^{-2} \qquad \boldsymbol{pK_{a2} = 7.20} \quad (5)$$

$${HPO_4}^{-2} \rightleftarrows H^+ + {PO_4}^{-3} \qquad \boldsymbol{pK_{a3} = 12.34} \quad (6)$$

- Carbonate buffer

$$Na_2CO_3 \rightarrow 2Na^+ + {CO_3}^{-2} \quad (7)$$

$$NaHCO_3 \rightarrow Na^+ + {HCO_3}^- \quad (8)$$

$${HCO_3}^- \rightleftarrows H^+ + {CO_3}^{-2} \qquad \boldsymbol{pK_{a2} = 10.33} \quad (9)$$

An example of how changes in the ionic strength for a buffer solution can be achieved without adding additional salt is given for the acetate buffer system.

In addition to equations 1 and 2 (the chemical equations of the buffer components), the follow equations were used:

- For the pH of the buffer solution (Henderson-Hasselbalch)

$$pH = pK_a + log\left(\frac{[A^-]}{[HA]}\right) \qquad (10)$$

where pK_a is the acid dissociation constant, $[A^-]$ and $[HA]$ are molar concentrations of the conjugate base and an undissociated weak acid respectively.

- For the ionic strength (ideal solutions)

$$I = \frac{1}{2}\sum_{i=1}^{n} C_i Z_i^2 \qquad (11)$$

where Ci is the molar concentration of ion i and Z_i is the number charge of ion i.

- For the equilibrium of the weak acid (Equation 2)

$$K_a = \frac{[H^+][CH_3COO^-]}{[CH_3COOH]} \qquad (12)$$

In this example, the acid and salt molar solution concentrations needed to be prepared for the buffer solution are represented as Ca and Cs respectively.

The ionic strength of the buffer system is given by (using Equations 1 and 2):

$$I = \frac{1}{2}([H^+](+1)^2 + [CH_3COO^-](-1)^2 + [Na^+](+1)^2) \qquad (13)$$

According to the stoichiometry of equations 1 and 2 $[Na^+] = [CH_3COONa]$ and $[H^+] = [CH_3COOH]$, but the $[CH_3COO^-]$ comes from both the acid and the salt and it has to be considered. Rewriting equation 12 and taking into consideration the contribution of the $[CH_3COO^-]$ from the salt, the Le Châtelier principle has to be used.

	CH_3COOH	$\rightleftarrows$	CH_3COO^-	+	H^+
Initial condition	Caf		Csf		0
Change	$-X$		X		X
Equilibrium	$Caf - X$		$Csf + X$		X

Now equation 12 is:

$$K_a = \frac{[Csf+X][X]}{[Caf-X]} \qquad (14)$$

where X is the molar concentration of the acid dissociated in the buffer system and the sub-index f represents the concentration of all the species in the buffer solution.

The volume of acid and salt used to prepare the buffer solution are identified as Va and Vs respectively, and they can be related to the final buffer volume (Vf) by

$$Vf = Va + Vs \qquad (15)$$

assuming that the volumes are additive.

The concentration of the chemical species in the buffer system can be written as a function of the initial concentration of the buffer components, the volumes required for its preparation and the buffer volume. Thus, some of the equations will need to be rewritten.

Equations 10, 13 and 14 can be modified as follow:

$$pH = pK_a + log\left(\frac{{}^{CsVs}/_{Vf}}{{}^{CaVa}/_{Vf}}\right) \qquad (16)$$

Ionic strength is now:

$$I = \frac{1}{2}\left(X(+1)^2 + \left(X + \frac{VsCs}{Vf}\right)(-1)^2 + \left(\frac{VsCs}{Vf}\right)(+1)^2\right) \quad (17)$$

Dissociation of the weak acid is given by:

$$K_a = \frac{X^2 + X\left(\frac{VsCs}{Vf}\right)}{\left[\left(\frac{VaCa}{Vf}\right) - X\right]} \qquad (18)$$

The unknown variables are: Cs, Ca, Vs, Va and X. However, concentrations of the acid and salt solutions are defined to be same in order to simplify the calculation, then equation 16 becomes:

$$pH = pK_a + log\left(\frac{Vs}{Va}\right) \qquad (19)$$

The defined variables are: K_a, I, pH and Vf.

Once the I, pH and Vf are chosen, SOLVER, an Excel tool to solve complex linear and non-linear simultaneous equations, is used to calculate Cs, Ca, Vs, Va and X, using equations 15, 17, 18 and 19. The restriction in the use of SOLVER for this application is that all the unknown variables have to be positive.

Appendix A4 Fitting rheological data with different models

In this appendix, the methods used to fit the rheological data with Bingham, Bohlin and Herschel-Bulkley models are described. An example is given to show how the data fitted with each model. For all the models the data were fitted using the fitting tool of OriginPro 8.5.

Bingham model

The yield point ($\boldsymbol{\tau_y}$) was estimated using the Bingham model, according to the equation:

$$\tau = \tau_y + \eta_{pl}\dot{\gamma} \qquad 1$$

where τ is shear stress, η_{pl} is the plastic viscosity and $\dot{\gamma}$ is the shear rate.

Figure 1 shows an example for the estimation of the yield point using equation 1. The black points represent the data for zones I and II of the flow curve, while the red line is related to the model equation. The table attached displays the parameters for the data fitted, where y, a, b and x correspond to τ, τ_y, η_{pl} and $\dot{\gamma}$ respectively. The coefficients of determination (R^2) obtained to estimate the yield points using the Bingham model were not below 0.86.

Bohlin model

The quantification of the interaction between droplets was estimated using Bohlin's model:

$$G' = A\omega^{1/z} \qquad 2$$

where ω is the frequency, A is a constant related to the magnitude of the interactions between droplets, and z is the coordination number that provides information about the level of the interactions.

Figure 2 shows an example for the estimation of A and z to quantify the interaction between droplets using equation 2. The black points represent the storage modulus

of the frequency sweep test, while the red line is related to the fitting of the model equation. The table attached displays the parameters for the data fitted, where y, A, x and b correspond to G', A, ω and z respectively. The coefficients of determination (R^2) obtained to estimate the parameters A and z using the Bohlin model were not below 0.93.

Herschel-Bulkley model

The yield stress (τ_y) and Herschel-Bulkley index (p) were estimated using Herschel-Bulkley model:

$$\tau = \tau_y + \kappa.\dot{\gamma}^p \qquad 3$$

where τ is shear stress, κ is the flow coefficient, $\dot{\gamma}$ is the shear rate and p is the Herschel-Bulkley index. The Herschel-Bulkley index is used to describe the flow as shear-thinning (p <1), shear-thickening (p >1) or Bingham behaviour (p =1).

Figure 3 displays an example for the estimation of τ_y, p and κ. The black points represent the data for the flow curve, while the red line is related to the model equation. The table attached displays the parameters for the data fitted, where y, y^0, a, b and x correspond to τ, τ_y, κ, p and $\dot{\gamma}$ respectively. The coefficients of determination (R^2) obtained using the Bohlin model were not below 0.99.

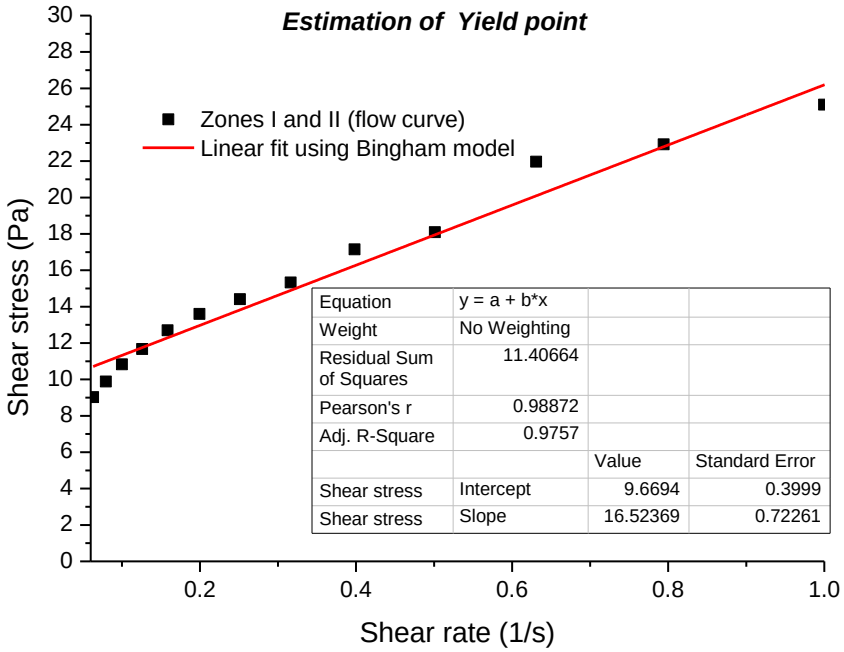

Figure 1 Estimation of yield point using Bingham model in zones I and II of the steady state stress vs. shear rate curve for 60 wt% soy bean oil and 1 wt% sodium caseinate. Phosphate buffer solution at pH 6.8 and ionic strength 30 mM.

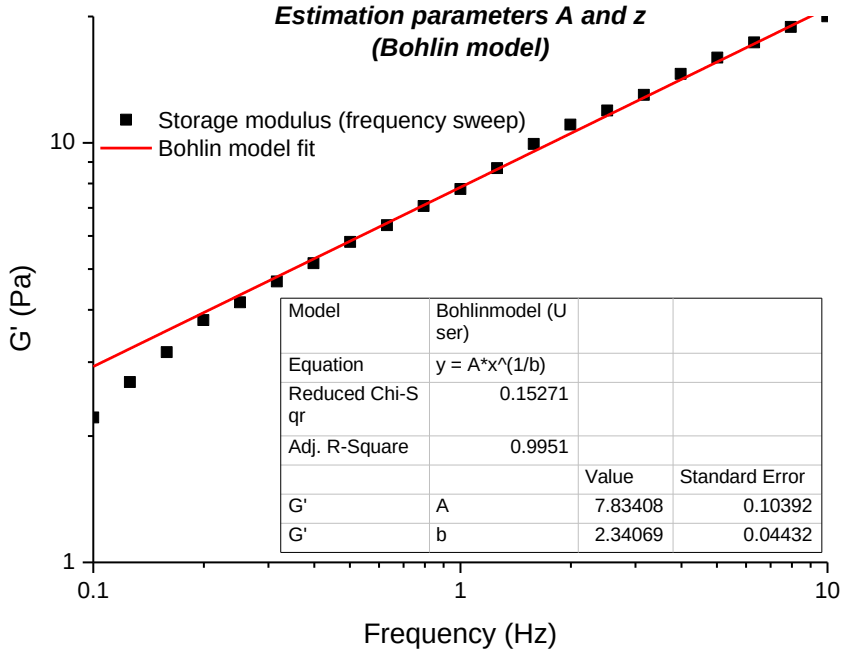

Figure 2 Estimation of parameters A and z using Bohlin model curve of storage modulus, as functions of frequency (strain 2 %), emulsion 60 wt% soy bean oil and 1 wt% sodium caseinate. Phosphate buffer solution at pH 6.8 and ionic strength 30 mM.

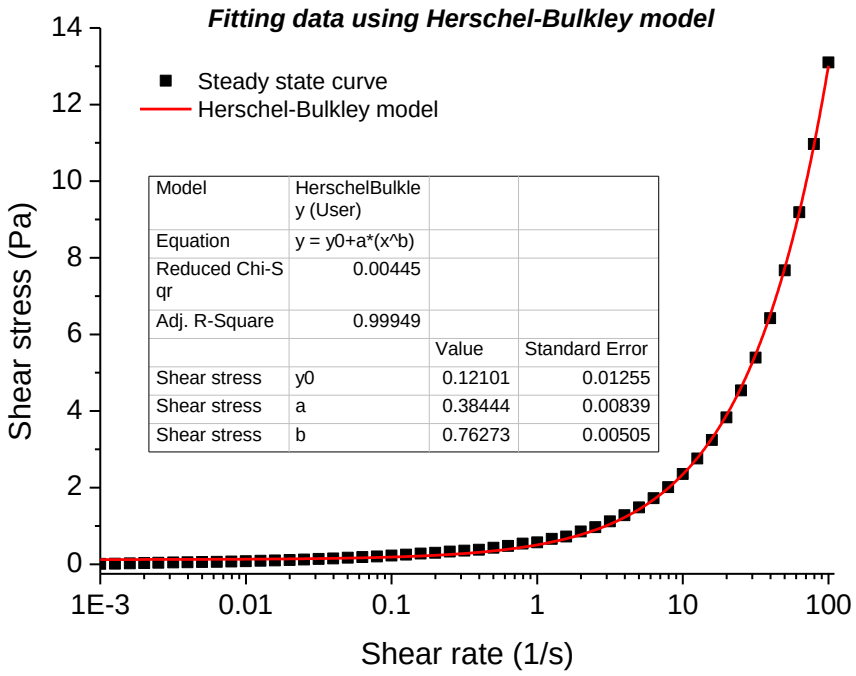

Figure 2 Estimation of yield point and the Herschel-Bulkley index using Herschel-Bulkley model, stress vs. shear *rate curve for 65 wt% soy bean oil and 1 wt% sodium caseinate. Phosphate buffer solution at pH 6.8 and ionic strength 30 mM.*